Pulsed plasma chemical functionalization of solid surfaces

Barwick, David C.

PULSED PLASMA CHEMICAL FUNCTIONALIZATION OF SOLID SURFACES

David C. Barwick B.Sc. M.Sc. (Dunelm)

Ph.D. Thesis

Department of Chemistry

University of Durham

September 2004

TABLE OF CONTENTS

DECLARATION

STATEMENT OF COPYRIGHT

The work described in this thesis was undertaken in the Department of Chemistry at the University of Durham between October 2001 and September 2004. It is the original work of the author except where otherwise acknowledged.

ACKNOWLEDGEMENTS

I would like to express my thanks to Professor Jas Pal Badyal, for supervision and funding throughout the course of my Ph.D. I would also like to thank Dr. Wayne Schofield for his advice, encouragement and the numerous reflectometry measurements he performed.

Thanks go to Dr. Declan Teare for the SPR experiments, James McGettrick for cross-sectioning the microscopic beads and to everyone in Lab 98, past and present for making my three years there so productive and enjoyable.

I should like to acknowledge the technical assistance of Dr. Andy Beeby with the fluorescence microscopy images; the Newcastle University Hospital Biomedical Electron Microscopy Unit with the SEM images; Peter and Malcolm the glassblowers; and George, Kelvin and Barry in the electronics workshop.

ABSTRACT

Pulsed plasma polymerization provides a highly efficient, single step, solventless method of surface functionalization. These surfaces can then be further derivatized for particular applications. The motivation underlying this work is to utilise this technique for a variety of applications to improve on existing methods of surface treatment. This approach is substrate independent and not hindered by geometry and in most cases the number of reactions stages required reach the desired product can be noticeably reduced.

Applications for surface coatings produced in this research cover a wide area for example a single step method of manufacturing a thermally responsive coating for cell culture has been developed. Previous preparative methods have required three of more steps to produce the desired surface which comprises poly(n-isopropylacrylamide) and although attempts have been made employing plasma polymerization, the depositions were carried out under continuous wave conditions, resulting in irreversible adsorption of proteins at temperatures above that of the lower critical solution temperature. A significant increase in structural retention and a lesser degree of cross-linking resulting from the use of pulsed conditions in this work has eliminated this major drawback.

The versatility of pulsed plasma chemical functionalization has also been exemplified by the surface immobilization of various initiating groups that can be further deployed to grow polymer brushes from the surface by a variety of well-established methods including atom transfer radical polymerization. This method has found to be suitable for a wide range of substrates such as silicon, polytetrafluoretylene and polystyrene beads. The formation of block copolymers and microscopic polymeric arrays has also been possible.

Plasma polymer coatings generated from nitrogen-containing precursors have allowed the surface attachment of a Palladium catalyst, which in turn facilitates the electrodeless deposition of transition metals. Previously, catalysts could not be adhered to a substrate in less than four or five individual steps. The approach adopted here achieved the desired results in just two reaction stages.

For my friends and family.

Chapter 1 Plasmas

1.1: Introduction

Plasma assisted vapour deposition is now widely used in the automotive, aerospace and biomedical industries. This has arisen from the trend to switch from wet to dry processing using lower temperatures. Plasma deposition is also frequently used in the production of microelectronics for sensors and dielectric films, where deposition of thin films is required.

Plasmas or gas discharges are present in many forms ranging from natural occurrences, namely solar wind and lightning, to man-made applications such as fluorescent tubes and neon signs. Plasmas are the main constituent of stars and hence constitute more than 99.9% by mass of the known universe. The term plasma was first used by Langmuir in 1928 and is energetically the fourth state of matter[1], the other three being solids, liquids and gases, Figure 1.1.

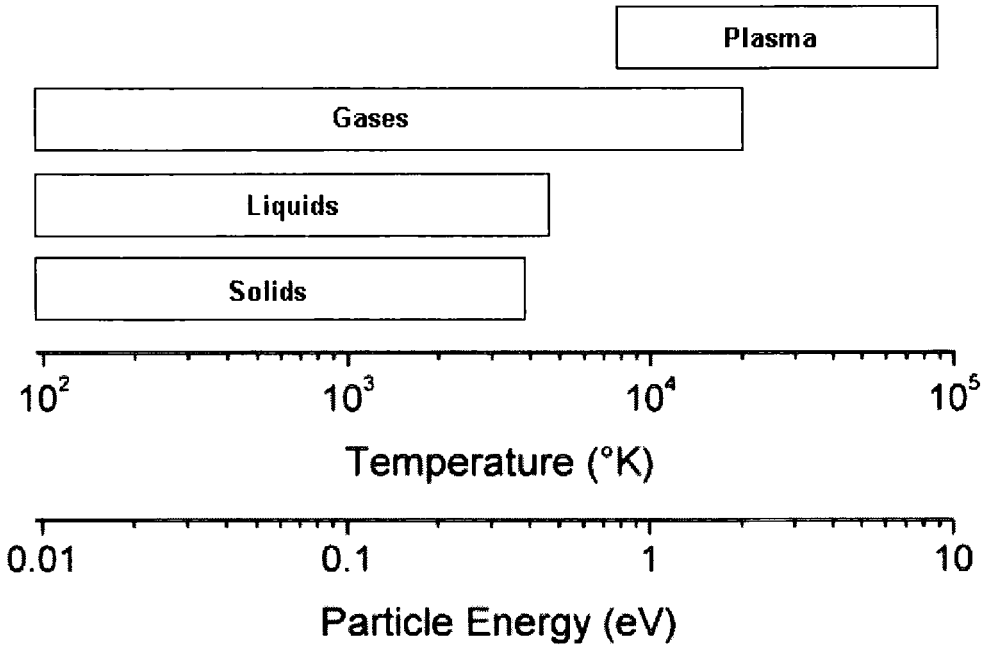

Figure 1.1: State of matter versus temperature, showing why the plasma state is referred to as "the fourth state of matter".

A plasma can be described as a "quasi-neutral gas of neutral and charged particles characterized by a collective behaviour"[2]. Hence it consists of ions, electrons, radicals and electromagnetic radiation. To remain "quasi-neutral", a plasma must contain equal amounts of oppositely charged species. To satisfy this condition; the distance over which an imbalance of charge can exist must be less than the size of the plasma[3]. This distance, λ_d (The Debye length, which is the distance of which an imbalance of charge can occur) can be described by Equation 1.1:

$$\lambda_d = \sqrt{\varepsilon_0 K T_e / ne^2} \qquad (1.1)$$

Where

- ε_0 = *permittivity of free space*
- K = *Boltzmann constant*
- n = *electron density*
- e = *charge on electron*
- T_e = *electron temperature*

1.2: Classification of Plasmas

Plasmas can be categorized as either equilibrium plasmas or non-equilibrium plasmas[4]. This classification depends on the relationship between the mean electron energy and the energy of the remaining species in the plasma i.e. ions and radicals.

1.2.1 Equilibrium plasmas

Equilibrium plasmas occur when electron temperature is equal to gas temperature e.g. in plasma jets and plasma arcs. Equilibrium plasma generation requires temperatures in excess of 20,000 °K, making it unsuitable for chemical deposition. Plasmas of this type can be successfully deployed to process inorganic materials and simple-structure organic compounds[5], but

polymers and complex materials cannot be treated under these conditions as they would rapidly degrade.

1.2.2 Non-Equilibrium Plasmas

Non-equilibrium or *cold* plasmas have average electron energies of 1-10 eV and electron densities in the range of 10^9 - 10^{12} cm^{-3}. There is a lack of equilibrium between electron temperature T_e and gas temperature T_g, with ratios of T_e/T_g in the range of 10-100[4]. Hence the electron temperature is far in excess of the gas temperature; this is a result of the mass of the electrons in the plasma being insignificant compared to that of molecules and ions present. Non-equilibrium plasmas can be generated at temperatures around 300 °K as this is the temperature of the neutral species present. The electrons acquire a large amount of kinetic energy when subjected to an electric field and this energy is sufficiently high to break molecular bonds, allowing non-equilibrium or glow discharge plasmas to be an effective method of chemical modification where thermally sensitive species are involved. Figure 1.2 details electron density and energy of glow discharges compared to other examples of plasmas.

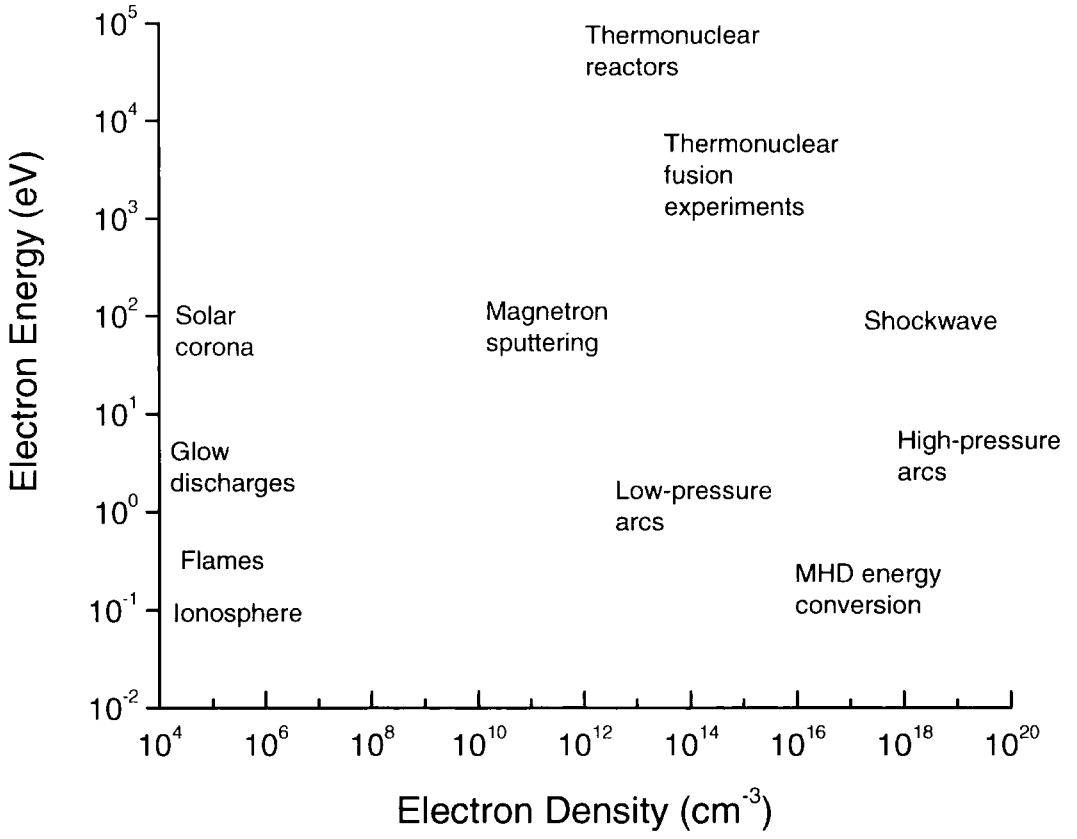

Figure 1.2: Categorization of plasmas according to electron density and energy[2].

1.3 Plasma Generation

A plasma glow discharge can be generated by applying an electric field to a gas. Typical glow discharges are often generated within a glass reactor connected to a vacuum pump to keep gas flow and pressure at the desired values. The electric field is supplied to the gas from an external circuit consisting of a voltage source in series with a ballast impedance, which limits the flow of current through the plasma. This results in a decrease in the potential difference between the anode and cathode when current is increased.

The plasma glow discharge is initiated from free electrons, which collide with atoms and molecules until kinetic energy is in excess of ionization energy. Plasmas are chiefly obtained from gaseous species, but they can be generated from solids and liquid, providing sufficient energy is applied to

cause vaporization. Gas plasmas can be initiated and sustained by using radio frequency (RF)[6], direct current (DC) or microwaves.

The main advantage of plasma deposition is that reactions can occur at lower temperatures than that required for thermal reactions at thermodynamic equilibrium. Hence films can be grown from surfaces that would not have the stability to accept the coatings at higher temperatures.

The chemical processes that occur in cold plasmas are controlled by the discharge energy of the DC, RF etc. and not by the temperature of the surface or the gas. Hence they can be described as non-thermal, non-equilibrium processes, resulting in cold plasmas effectively generating chemically reactive species at lower temperatures.

Loss processes can also take place. Electrons and ions can be lost to the surfaces of the reactor via diffusion processes or by recombination with one another. Neutral atoms and radicals can also be lost by recombination caused by homogeneous reactions in the gas phase or by reacting with the reactor surfaces. Providing the electron creation rate balances the electron loss rate, the plasma can be sustained.

1.4 Plasma Properties

1.4.1 Plasma Potential

The potential of a plasma is more positive than the negative surface with which it is in contact. This arises from the higher degree of mobility of electrons compared to positively charged ions[7]. Once an electric field has been initiated, the more mobile electrons leave the plasma, leading to a build-up of positive potential. This potential will continue to rise until the flux of electrons and positively charged species leaving the plasma is equal, resulting in the plasma being *quasi-neutral.*

1.4.2 Electron Energy

Electrons within a plasma have energies in the order of 1-10 eV. The energy of electrons is related to their temperature by the kinetic theory of gases, Equation 1.2.

$$\varepsilon = \frac{3}{2} KT \qquad (1.2)$$

where ε is the average electron energy, K the Boltzman constant and T the temperature (in degrees Kelvin). Hence an electron possessing energy of 1 eV (1.6 x 10^{-19} J) will have a temperature of 11,600 K and a distribution of electrons with a mean energy of 1eV will have a temperature of 7739 K. However as the mass of electrons is insignificant compared to that of molecules and ions present, the temperature of a non-equilibrium plasma will not vary noticeably from that of ambient conditions.

A certain fraction of electrons possess energies significantly higher than the average electron energy and this causes the ionization that occurs in glow discharge plasmas[8].

1.4.3 Plasma Sheath

A potential difference between the plasma and any surface it is in contact with will occur in a narrow region at the plasma's edge[9] called the "plasma sheath". This area has a negative potential and hence a lower density of electrons in comparison to the bulk of the plasma. This reduced electron density results in the plasma sheath area appearing darker. This is ascribed to a reduced excitation of gas species.

1.5: Plasma Reactions[2, 10]

Two classes of reactions occur within a plasma reactor:

1.5.1: Homogeneous reactions occur due to inelastic collisions between heavy species and electrons:

1.5.1.1 Excitation

An electron collision results in the excited state of atoms (A) or molecules (M):

$$e + A \rightarrow e + A^*$$
$$e + AB \rightarrow e + AB^*$$

These excited atoms/molecules return to their ground states, emitting energy as electromagnetic radiation, which results in the uv or visible emission of the plasma. Electromagnetic radiation is also the result of recombination between two particles of opposite charges.

1.5.1.2 Dissociative ionization

Low energy electrons attach themselves to electronegative gas molecules e.g.

$$CF_4 + e \rightarrow CF_3 + F + e \rightarrow CF_3 + F^-$$

1.5.1.3 Dissociation

An electron collision with a molecule causes dissociation :

$$e + A_2 \rightarrow 2A + e$$

1.5.1.4 Ionization

Electron impact results in positive, negative, atomic or molecular ions:

$e + A_2 \rightarrow A_2+ + 2e$

$e + A_2 \rightarrow A_2^-$

$e + AB \rightarrow A^+ + B + 2e$

Collisions can also occur between molecules, atoms, radicals and ions which can give rise to ion recombination, charge transfer, reactant transfer, disproportionation and radical recombination processes;

1.5.2: Heterogeneous Reactions are those that arise from interactions between a solid surface and a plasma:

1.5.2.1 Adsorption

Molecules (M), radicals (R) or monomers (M) from the plasma are adsorbed by the surface they are in contact with:

$M(g) + Surface \rightarrow M(s)$

$R(g) + Surface \rightarrow R(s)$

Where g and s denote gas and solid respectively.

1.5.2.2 Recombination

Atoms or radicals (R) from the plasma react with pre-adsorbed species to form other compounds (M):

$R(s) + R_1 \rightarrow Surface + M$

1.5.2.3 Metastable De-excitation

An excited metastable ion can be returned to its ground state via a collision with the surface.

$A^* + Surface \rightarrow A$

1.5.2.4 Sputtering

An ion collides with the surface and the momentum exchange results in the ejection of an atom from the surface into the gas phase. Typical ion energies in sputtering reactions would fall around 20 – 30 eV.

Inert, non-polymerizing gases such as argon, tetrafluoromethane and helium are commonly used for this treatment and it allows the formation of reactive sites on a surface[11]. This is one of the earliest applications of plasmas in materials processing[12, 13] which allows modifications to surface characteristics without changing bulk properties. Surface activation reactions are able to adjust properties such as adhesion, crosslinking, wetting and compatibility e.g. with biomaterials[14, 15, 16]. A commonly-employed example of this procedure is the use of an argon plasma to remove fluorine atoms from polytetrafluoroethylene (Teflon), leaving reactive carbon sites, which in turn, results in greater adhesion between the substrate and any subsequently deposited monolayers.

Sputtered atoms can condense back into the solid phase upon colliding with any surface in the plasma chamber. Hence this process can be used in the semiconductor industry to deposit thin metal films onto silicon.

1.5.2.5 Etching

Plasma Etching is largely chemical in action. This process involves a glow discharge plasma being employed to generate reactive species, which diffuse to the surface in contact with the plasma and form volatile products which can then desorb from the surface into the gas phase.

A typical reaction would be:

$$CF_4 \mapsto F,\ CF,\ CF_2,\ CF_3,\ etc.$$

$$Si(s) + 4F \mapsto SiF_4(g)$$

This leads to the production of microstructures with large depth to width ratios[17]. This process is predominantly used for the development of integrated circuits where trenches in silicon for the storage of charge need to be ~0.2 μm

wide and ~4 μm deep. Cavities with this depth-to-width ratio are not obtainable using conventional wet chemistry processes.

1.6 Plasma Polymerization

Radicals within the plasma react with adsorbed radicals to form a polymer (P):

$$R(g) + R(s) \rightarrow P(s)$$

Additionally this can occur between two radicals already adsorbed on the surface. Hence plasma polymerization can be described as the formation of polymeric materials from the plasma state of monomers of the reactive species created in the plasma state[18, 19, 20]. The ionisation of gas is the essential step in plasma generation, but in a low pressure plasma, the amount of ions is small compared with that of neutral species.

Conventional polymerization does not yield high molecular weight materials from vacuum and the products can therefore not be recognised as polymers. Plasma polymerization is the only exception where polymeric materials can be deposited from a vacuum.

1.6.1 Mechanism of Plasma Polymerization[21]

Plasma polymerisation takes place over several reaction steps:

- Initiation – attributable to free radicals produced by collisions of electrons and ions with the monomer or by dissociation of the monomer absorbed on the surface due to electron collisions.
- Propagation – the formation of a polymeric chain by interactions of surface free radicals with gas phase or absorbed monomer molecules.
- Termination – reaction at the surface which closes the polymer chain
- Re-initiation – Chain fragments can be reconverted into radicals via further collisions with electrons.

The mechanism of plasma polymerization can be described by Figure 1.3, where *M* denotes a monomer molecule, subjected to plasma excitation that can proceed to form radicals and various products, denoted with subscripts Y and Z to distinguish differences in size between them.

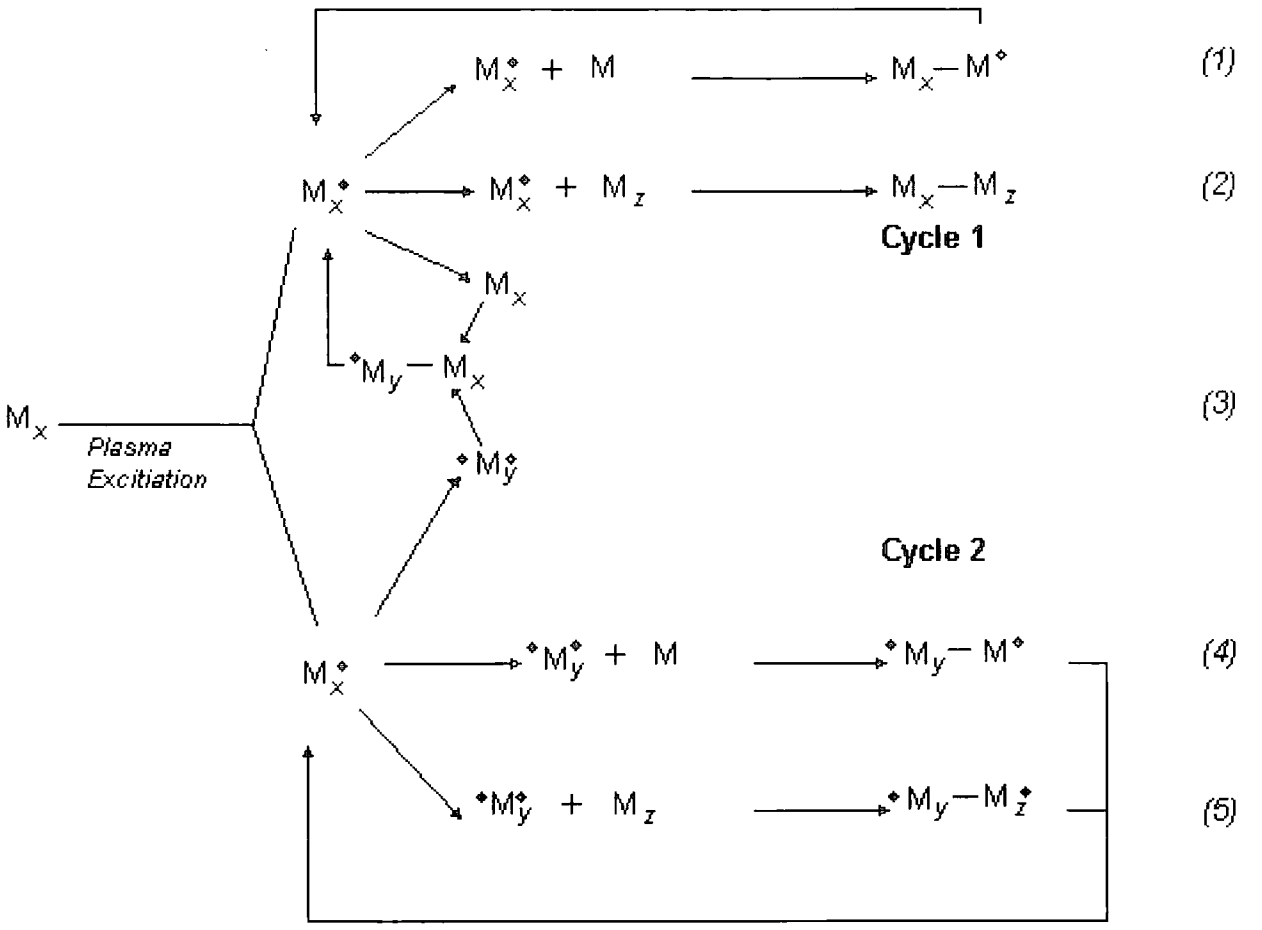

Figure 1.3: Yasuda's Mechanism of Plasma Polymerization[22].

A key aspect of the polymer generation mechanism is the reactions which result in an increase of molecular size. For example when a reactive species collides with a monomer molecule, this constitutes a propagation reaction in chain growth. Figure 1.3 demonstrates two main cycles which lead to rapid step growth. Cycle 1 involves the repeated activation of reaction products from monofunctional activated species and the subsequent repeating reactions of these species. Cycle 2 involves multifunctional activated species. It is the activated species such as free radicals that are responsible for the

chain-growth polymerization. Reaction (3) can be described as a cross cycle reaction.

Following plasma ignition, the gas phase is changed from being the vapour of an organic monomer to a complex mixture of neutral, ionized and radical species. The reactor walls and any substrates placed in the reactor become involved in the reaction, allowing polymer-forming intermediates to originate from a solid surface, resulting in the formation of polymer layers on a substrate. The net polymerization is a result of the balance between ablation and etching processes, which can be described by the CAP model[10, 23, 24, 25] (Competitive Ablation Polymerization), Figure 1.4.

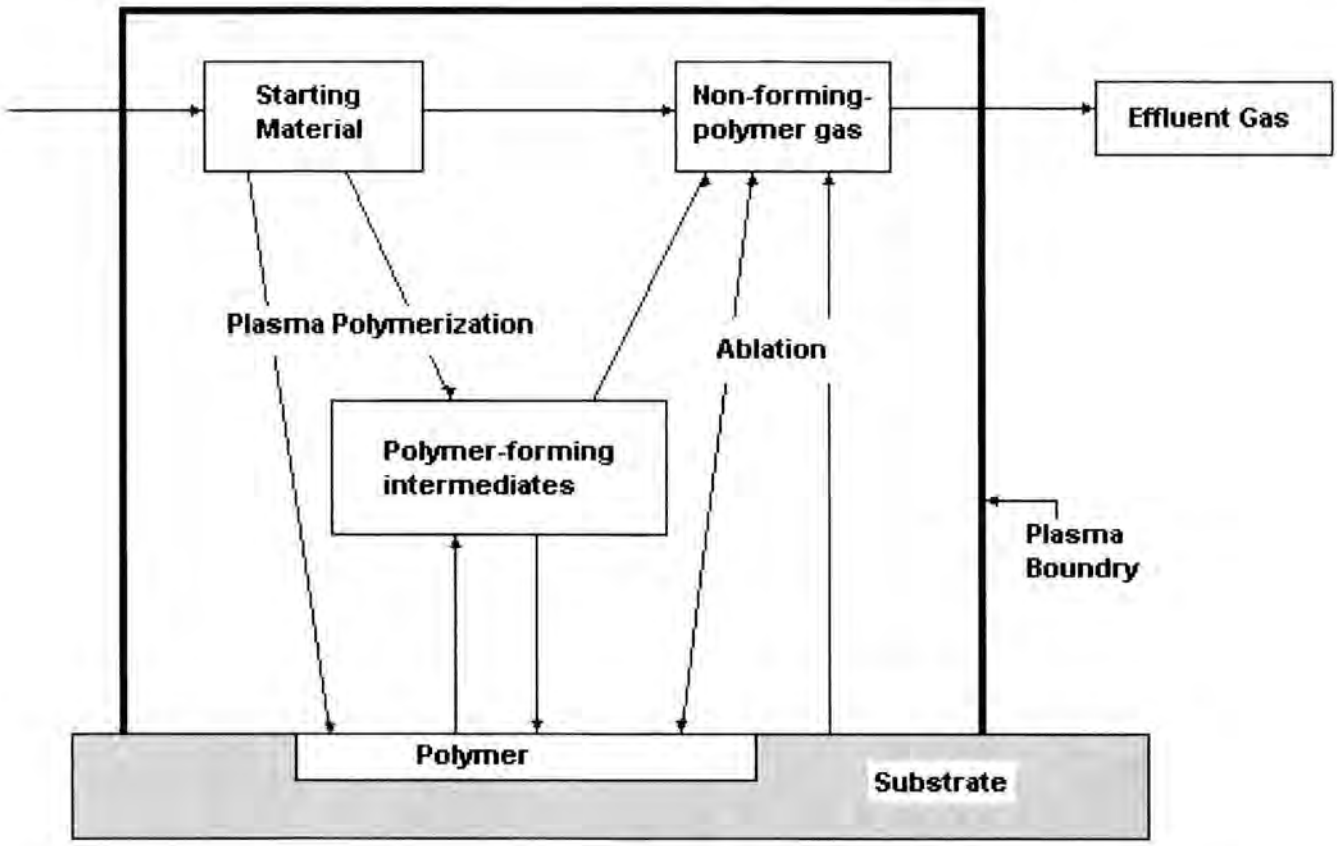

Figure 1.4: Competitive Ablation Polymerization[26].

Plasma polymer films are normally physically and chemically different to conventional polymers due to the fact that conventional polymerization centres on a molecular process compared to polymerization in a plasma, which is an atomic process[27, 28]. When analysing a steady-state flow system,

the most convenient approach is to work with mass flow rates as opposed to molecular ones. Hence for a fixed vapour pressure and reactor geometry, the characterisation of the plasma requires that the power density be quantified. This is defined as W/F_M, where F_M is the mass flow rate and W the discharge power; hence power density represents input energy per unit mass of monomer.

Mass flow rate can be determined if the assumption is made that the gas in the plasma reactor behaves as an ideal one.

$$m = \frac{MV}{RT} P \qquad \textbf{(1.3)}$$

Where m is the mass of gas in the reactor, M is the molecular weight of the gas, V is the volume of the reactor chamber, R is the universal gas constant, T is gas temperature and P is gas pressure.

For a reactor which is continually fed monomer vapour at mass flow rate F_M, if the outlet of the reactor to the pump is then closed at time $t = 0$, leaving inlet to the monomer open, F_M changes with pressure according to Equation 1.4

$$F_m = \frac{dm}{dt} = \frac{MV}{RT}\frac{dP}{dt}\Big|_{t=0} \qquad \textbf{(1.4)}$$

Plasma polymers are normally highly branched and cross-linked, have no discernable repeat units and the precursor need not have to contain a functional group for plasma polymerisation to occur.

1.6.2 Advantages of Plasma Polymerization

Plasma polymerization offers several benefits making it more practical than other methods of surface modification such as silane-silica[29] and thiol-gold[30, 31, 32, 33].

- Equipment required is commercially available and easy to use;
- Surface deposition is uniform;
- An extensive range of precursors can be used leading to an extensive range of surface functionalities;
- Plasma-produced films are coherent and adhere to a wide range of substrates including polymers, glass and metal surfaces;
- Surface deposition is geometry independent – complex shapes can be plasma treated;
- Film thickness is controllable to the nanometre range;
- Plasma processing will not alter the bulk properties of the substrate;
- Plasma-polymerized films are defect free;
- Plasma processes are solvent free and require small amounts of precursor – technique is economical;
- Technique is environmentally friendly relative to wet chemical methods.

1.7: Plasma Reactors

Figure 1.5 outlines the design of a typical radio-frequency plasma reactor used to coat surfaces with plasma polymers:

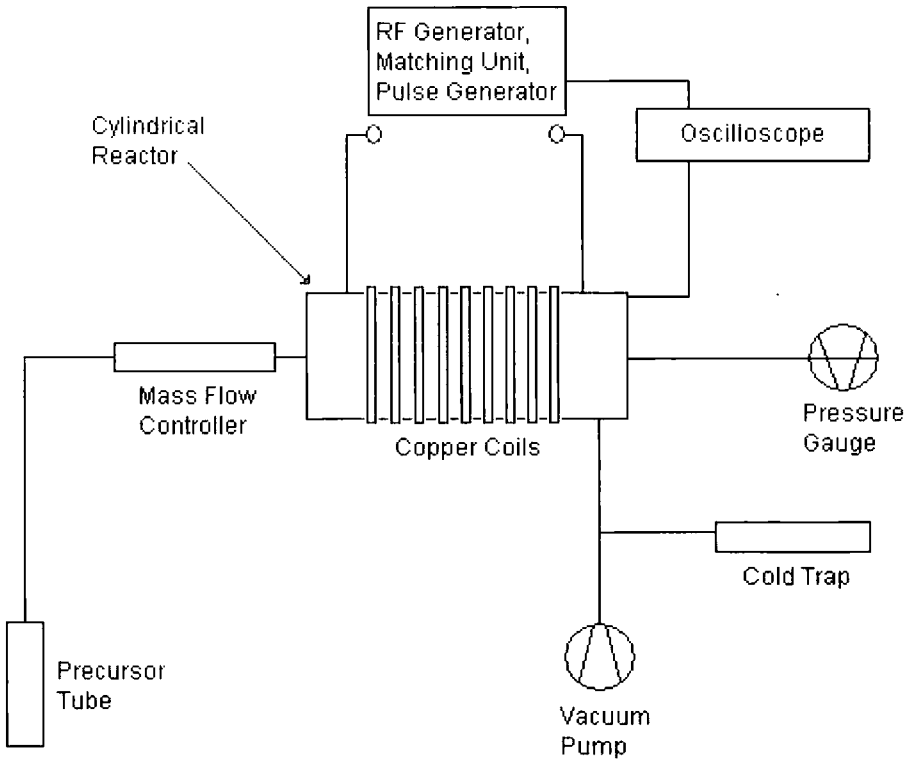

Figure 1.5: Schematic of a plasma reactor.

- Monomer tube – contains the monomer in its liquid/solid state.
- Mass flow controller – controls the flow of precursor to the reactor.
- Cold Trap - cooled by liquid nitrogen, which freezes and contains all vapour that passes through the reactor, preventing it from reaching the vacuum pump.
- Vacuum pump – ensures reactor operates at pressures between 10^{-4} and 10 torr.
- RF Source – connected to the copper coils that are wound around the tubular reactor to ignite the plasma. The radio frequency is set at 13.56 MHz and designed to operate at a constant output impedance of 50 Ω.

- Matching Unit – to reduce the reflective power pf the plasma hence protecting the power source.
- Pulse Unit – to pulse the plasma, hence reducing peak power.
- Oscilloscope – to monitor plasma output.

RF plasmas can be generated with the electrodes outside the reactor, hence reducing contamination. RF plasmas can operate efficiently at atmospheric pressure, but the reactor has to be housed in a Faraday cage to contain the electromagnetic radiation emitted, preventing interference. For plasma experiments, generators with a fixed frequency of 13.56 MHz and adjustable power are employed. In addition to the generator, a matching network is also used to transform the impedance of the generator to that of the load. The impedances must be matched to allow an efficient coupling of power to the discharge.

Low pressure regimes are often required for the deposition of films. This is to allow the ions to traverse the region between the glow discharge and the target substrate without losing significant amounts of kinetic energy, giving the species sufficient time to react before being pumped through the reactor into the cold trap.

1.7.1 Leak Rate

To avoid contamination of the reaction chamber from the atmosphere, it is crucial to determine a leak rate, analogous to a molecular flow rate. The following steps are involved:

- The reaction chamber is pumped down to base pressure and isolated from the vacuum pump;
- The rise in pressure with time is recorded;
- Outgassing from the pressure gauge and chamber walls is considered to be negligible.

The leak (flow) rate is calculated as follows:

$$Q_m = \frac{dP}{dt} / RT \qquad (1.6)$$

Where Q_m is molecular flow rate, dP is change in pressure, dt is change in time, R; the molar gas constant and T is temperature. For the equipment used in this work, an acceptable leak rate to minimise contamination[34] is considered to be less than 2 x 10^{-9} mol s^{-1}. This corresponds to the rise in pressure from 0.04 mBar to 0.06 mBar, transpiring in no less than 5 minutes.

1.8 Pulsed Plasma Polymerization

An additional feature of the plasma reactor used in this work is a pulse generator, allowing the discharge to be pulsed. Experiments carried out under continuous wave conditions, where the plasma is sustained by a continuous supply of power to the system, result in a high degree of fragmentation of the precursor molecules[35]. This occurs extensively, even if low powers are used, and the polymeric films that arise often have very little resemblance to the monomer used to form them. This results in a restriction of monomers available if the film properties are to be controlled. One strategy to overcome this is to pulse the power applied to the system[36, 37, 38, 39].

1.8.1 Pulsed Plasma Parameters

The radio frequency power applied to the system in a pulsed plasma operation is modulated at a much lower frequency than the conventional applied radio frequency used in the continuous wave operation. The parameters that can be adjusted in the pulsed operation are therefore plasma "on time", t_{on}, plasma "off time" t_{off} and the peak power applied by the RF generator, P_0, figure 1.6.

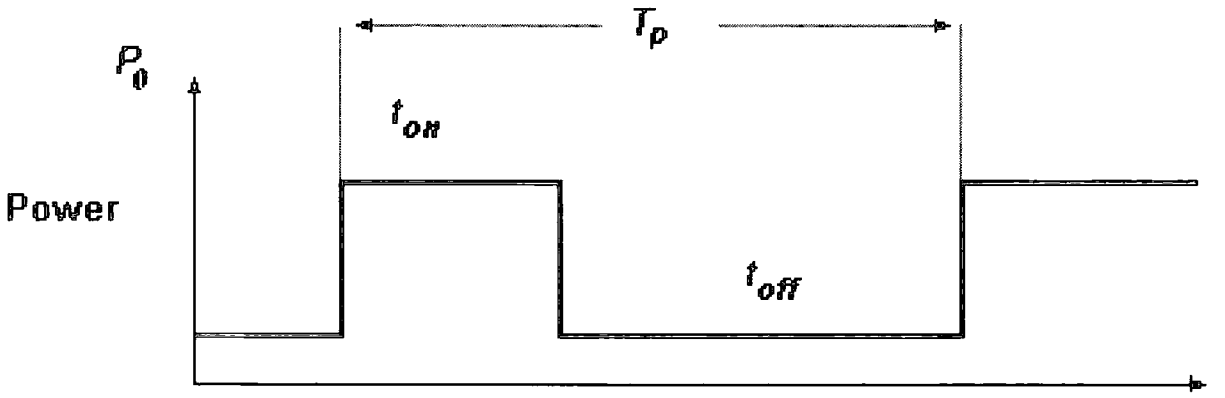

Figure 1.6: Schematic showing relationship between pulsing parameters.

T_p is the pulse period, so $1/T_p$ is the pulse frequency. The pulse duty cycle can be described as $t_{on}/(t_{on} + t_{off})$ which can be used to determine the average power delivered to the system:

$$P_{av} = P_0 \times \frac{t_{on}}{(t_{on} + t_{off})} \qquad (1.7)$$

The average power applied to the plasma and the the pulse frequency can be adjusted by changing the duration of t_{on} and t_{off}.

1.8.2 Experimental Modifications for Pulsed Operations

The RF applied to the plasma can be pulsed by controlling the RF generator with a pulsed DC analogue voltage obtained from a pulse generator. By attaching an oscilloscope to the pulse generator, it is possible to monitor the frequency and duty cycle whilst at the same time monitoring the plasma's response via its pulse amplitude.

1.8.3 Effects of Pulse Parameters on Plasma Processes

Before any reactions can occur, the plasma must be ignited. When an RF field is applied across a gas, the charged particles gain energy. Electrons within the gas oscillate and collide with gas molecules, resulting in the production of

excited neutral or ionized particles leading to breakdown of the gas. The time duration before this can occur is dependent on the power applied in addition to the ionization and pressure of the gas. Once breakdown has occurred and the discharge initiated, the pulse width and duty cycle govern how much the discharge resembles that of a continuous wave plasma. Once the power to the discharge is removed i.e. during the "plasma off" phase, electron density within the gas diminishes. The length of time required for this to occur is dependent on the gas. Electron energy relaxation times for many gases investigated[40, 41, 42] are in the order of microseconds for the gas pressures used. Previous work[43, 44] has shown that pulsed plasma depositions offer some of the following advantages over continuous wave operations:

- A reduced heat load on the reactor and the substrate due to a time-averaged decline of electron bombardment of surrounding surfaces. The ions and electrons dissipate following the commencement of the pulse "off time". Hence thin films can easily be deposited without degrading the substrate or any layers deposited previously;
- A reduction in UV emission from the plasma attributable to the decay of ion and electron energy leads to less cross-linking and hence higher structural retention of the monomer's functional groups;
- Greater degree of control of dissociation of parent gas. High power, short pulses at a low duty cycle give rise to complete dissociation of the precursor gas with the heat load on the reactor at a minimum;
- The dissipation of ions and electrons during the "plasma off" times results in a greater degree of residual free radicals within the plasma, giving rise to higher structural retention of functional groups and hence a greater degree of film chemistry controllability. In mechanistic terms, this marked enhancement in selectivity is a consequence of low levels of precursor fragmentation occurring during the short duty cycle on-period combined with conventional polymerization reaction pathways predominating within the much longer pulsed plasma off-period.

Examples of well-defined molecularly tailored substrates produced by this method include perfluoroalkyl[45], epoxide[46], anhydride[47], carboxylic acid,[48] cyano,[49] and amine[50] functionalized surfaces.

References

[1] Langmuir, I., *Phys. Rev.*, 33, **1929**, 954.

[2] Grill, A. *Cold Plasmas in Technology,* IEEE Press, **1994.**

[3] Franklin, R., *Plasma Phenomena in Gas Discharges,* Ch 1, **1976**, Clarendon Press, Oxford.

[4] Dresvin, S. V.; Donskoi, A. V.; Goldfarb, V. M.; Klubnikin, V. S., *Physics and Technology of Low Temperature Plasmas,* **1977**, Iowa University Press: Ames.

[5] Haaland, P. D.; Clarson, S. J., *Trends in Polymer Science,* **1993.**

[6] Chandrakar, K., *J. Phys. D: Appl. Phys.*, 11, **1978**, 1809.

[7] Hollaghan, J. R.; Bell, A. T., *Techniques and Applications of Plasma Chemistry*, Wiley, New York, **1974.**

[8] Rossnagel, S. M., *Thin Film Processes II,* Academic Press, London, **1991,** 21.

[9] Chen, F. F.; *Introduction to Plasma Physics,* Plenum Press, New York, **1974.**

[10] Moruzzi, J. L.; Kiermasz, A.; Eccleston W., *Plasma Phys.,* 24, **1982,** 605.

[11] Beauchamp, J. L.; Buttrill, S. E.; *J. Chem. Phys.,* 48, **1968**, 1783.

[12] Vessen, J. L.; Cuomo, J. J.; Vossen, J. L.; Kern, W. *Thin Film Processes,* , Academic Press, New York, **1978.**

[13] Inagaki, N., *Plasma Surface Modification and Plasma Polymerization,* Technomic, **1996.**

[14] Kramer, P. W.; Yeh, Y.; Yasuda, H.; *J. Membrane. Sci.*, 1, **1989**, 46.

[15] Yasuda, H., *Plasma Polymerization,* Academic Press, Orlando, **1985.**

[16] Inagaki, N.; Tasaka, S.; Ohkubo, J.; Chuma, H.; Okazaki, S.; Saruta, T.; Masui, M.; Takeuchi, M., *Plasma Polymerization and Plasma Interaction with Polymeric Materials,* Wiley, New York, **1990**.

[17] Pearton, S. L.; Ren, F., *J. Mater. Sci.*, 5, **1994**, 1.

[18] Matsuyama, H.; Kariya, A.; Teramoto, M., *J. Appl. Polym. Sci.,* 51, **1994,** 689.

[19] Mattson, B.; Stenberg, B.; *J. Appl. Polym. Sci.,* 50, **1993,** 1247.

[20] Clark, D. T., *J. Vac. Sci. Technol.,* A4, **1986,** 1049.

[21] Shepsis, L. V.; Pedrow, P. D.; Mahalingam, R.; Osman, M. A., *Thin Solid Films,* 11, **2001,** 285.

[22] Yasuda, H.; Hsu, T., *Surf. Sci.,* 76, **1978,** 232.

[23] Yasuda, H.; Hsu, T., *J. Polym. Sci., Polym. Chem.,* 16, **1978,** 415.

[24] Masuoka, T.; Yasuda, H., *J. Polym. Sci., Polym. Chem.,* 19, **1981**, 2937.

[25] Masuoka, T.; Yasuda, H., *J. Polym. Sci., Polym. Chem.*, 20, **1982**, 2633.

[26] Oehrlein, G. S., *Surf. Sci.,* 386, **1997**, 222.

[27] Yasuda, H.; Hirotsu, T., *J. Appl. Polym. Sci.,* 22, **1978**, 1195.

[28] Yasuda, H.; Hirotsu, T., *J. Polym. Sci., Polym. Chem.,* 16, **1978**, 743.

[29] Schick, G. A.; Sun, Z, Q., *Langmuir,* 10, **1994**, 3105.

[30] Wilbur, J. L.; Kumar, A.; Kim, E.; Whitesides, G. M., *Adv. Mater.*, 6, **1994**, 600.

[31] Huck, W. T. S.; Yan, L.; Stock, A.; Haag, S.; Whitesides, G. M., *Langmuir,* 15, **1999**, 6862.

[32] Yan, L.; Marzolin, C.; Tefort, A.; Whitesides, G.M., *Langmuir*, 13, **1997**, 6704.

[33] Yan, L, Zhao, X.; Whitseides, G. M., *J. Am. Chem. Soc.*, 120, **1998**, 6179.

[34] Enrich, C. D.; Basford, J. A., *J. Vac. Sci. Technol. A.,* 10, **1992**, 1.

[35] Lopez, G. P.; Ratner, B. D.; Rapoza, R. J. ; Horbett, T. A., *Macromolecules*, 26, **1993**, 3247.

[36] Hynes, A.; Badyal, J. P.S., *Chem. Mater.*, 10, **1998**, 2177.

[37] Han, L.M.; Timmons, R.B.; Bagdal, D., *Chem. Mater.* 10, **1998**, 1422.

[38] Savage, C. R.; Timmons, R. B., *Chem. Mater.* 3, **1991**, 575.

[39] Lau, K.K.S.; Gleason, K.K.; *J. Phys. Chem. B.*, 102, **1998**, 5977.

[40] Haydon, S. C.; Plumb, I. C., *J. Phys. D: Appl. Phys.*, 11, **1978,** 1721.

[41] Yasuda, H.; Hsu, T., *J. Polym. Sci. Polym. Chem. Ed.,* 15, **1977,** 81.

[42] Timmons, R. B.; Savage, C. R.; Lin, J. W., *Chem. Mater.,* 3, **1991,** 575.

[43] Timmons, R. B., *Surf. Coat. Aust.* 36, **1999,** 10.

[44] Wang, J.H.; Chen, X.; Chen, J. J.; Calderon, J. G.; Timmons, R. B. *Plasmas and Polymers*, 2, **1996,** 245.

[45] Coulson, S. R.; Woodward, I. S.; Brewer, S. A.; Willis, C.; Badyal, J. P. S. *Chem. Mater.*, 12, **2000**, 2031.

[46] Tarducci, C.; Brewer, S. A.; Willis, C.; Badyal, J. P. S. *Chem. Mater.*, 12, **2000**, 1884.

[47] Ryan, M. E.; Hynes, A. M.; Badyal, J. P. S., *Chem. Mater.*, 8, **1996**, 37.

[48] Hutton, S. J.; Crowther, J. M.; Badyal, J. P. S., *Chem. Mater.*, 12, **2000**, 2282.

[49] Tarducci, C.; Schofield, W. C. E.; Brewer, S.; Willis, C.; Badyal, J. P. S. *Chem. Mater.* 13, **2001**, 1800.

[50] Rimsch, C. L.; Chem, X. L.; Panchalingham, V.; Savage, C. R.; Wang, J. H.; Eberhart, R. C.; Timmons, R. B., *Abstr. Pap. Am. Chem. Soc. Poly.*, 209, **1995**, 141.

Chapter 2: Analytical Techniques

2.1: X-ray Photoelectron Spectroscopy

Photoelectron spectroscopy is a technique used to measure ionization energies of molecules when electrons are ejected from different orbitals – *The Photoelectric Effect.* This information is used to infer orbital energies by ionization of the sample by photons. This can be achieved using UV radiation and is referred to as Ultra Violet Photo Electron Spectroscopy (UPS)

The energy of an incident photon ($h\nu$) must be equal to ionization or binding energy (E_b) and kinetic energy (E_k) of the ejected electron (the photoelectron)[1].

$$E_b = h\nu - E_k \qquad (2.1)$$

A photoelectron may originate from a number of orbitals, each requiring a different binding energy; hence a series of values of kinetic energy will be obtained.

Photoelectronic spectra are interpreted in terms of an approximation known as Koopman's theorem[2], which states that binding energy is equal to the orbital energy of the photoelectron. Hence the binding energies can be said to describe the sequence of atomic or molecular orbitals quantitatively, allowing the binding energy to be identified from the orbital it originated from. However the theorem ignores the fact that the remaining electrons rearrange their distribution following ionization of the sample. Ejection of an electron can also leave an ion in a vibrationally excited state, resulting in a fraction of the photon energy not appearing as kinetic energy of the photoelectron.

In addition to valence electrons which provide bonding for a system, each atom, with the exception of hydrogen, possesses core electrons not involved with bonding. In *X-ray photoelectron spectroscopy (XPS)*, the energy of the incident

photon is so high (hv ~ 1500 eV, compared to UPS, ~ 20 eV) that electrons can be ejected from the inner cores of atoms[3]. The process involves primary excitation of the sample by irradiation with a source of monochromatic x-rays, which leads to photoemission of core electrons. Emitted electrons are characterized by their inelastic mean free path, which is governed by their kinetic energy.

Core ionization energies are characteristic of the individual atom as opposed to the overall molecule, hence XPS yields binding energies of core electrons characteristic of the elements present in a compound or alloy, allowing qualitative chemical analysis. Detection of K-shell ionization energy values (and values corresponding to other inner shells) indicates the presence of the corresponding element. All ionization energies measured by XPS are one-electron ionization energies.

Since energy levels are quantized, photoelectrons have an energy distribution consisting of a series of discrete bands that reflects the shell structure of the atoms in the sample. The experimental determination of this distribution by kinetic energy analysis of the photoelectrons produced by x-ray exposure is termed *XPS*.

The XPS (also referred to as electronic spectroscopy for chemical analysis, ESCA) technique is restricted to surface layers because even though X-rays may penetrate into the bulk sample, only photoelectrons generated within a 2-5 nanometer depth of the surface have a finite probability of escaping from the material without changing their state of motion[4]. These electrons originate the XPS signal, whereas electrons that have changed their state of motion contribute to the background.

The kinetic energy (E_k) of the emitted core electrons can be determined using Equation 2.2.

$$E_k = h\nu - E_b - \Phi \qquad \textbf{(2.2)}$$

Where

$h\nu$ = X-ray energy

E_b = binding energy of the photo emitted electron

Φ = spectrometer work function

The work function Φ is a characteristic of the spectrometer and can thus be measured experimentally.

After the ejection of a core electron, the electronic system is left in a highly excited and short-lived state which can be deactivated by X-ray fluorescence (XRF) or emission of an Auger electron[5]. In XRF, the vacancy is filled by an outer electron, the excess energy emitted as an X-ray photon. In Auger emission, the excess energy is transferred to another electron, which is in turn ejected from the atom[6]. In order to be emitted, the photoelectron must have sufficient energy to overcome the binding energy. Auger electrons can also be recorded and are distinguishable from conventional "XPS electrons" by the use of different excitation wavelengths since the kinetic energy of Auger electrons is independent of the exciting photon energy.

The photoelectron can also interact with other electrons when departing the atom. For example, it may excite a valence electron to an unfilled (conduction band) state and lose an amount of kinetic energy equal to the excitation energy. This is called a *shake-up* process[7]. Similarly, the departing photoelectron might transfer sufficient energy to a valence electron to remove it entirely from the atom, hence more than one electron is ejected at the time of photo-ionization – a shake-off process. This can result in broad structures of high binding energies in a spectrum, Figure 2.1. Shake-up peaks are positioned at the lower kinetic energy side of the main peaks and are normally indicative of a polymeric system that contains some unsaturation e.g. aromatic groups[8,9]. For instance shake-up peaks are a common occurrence in materials such as polystyrene.

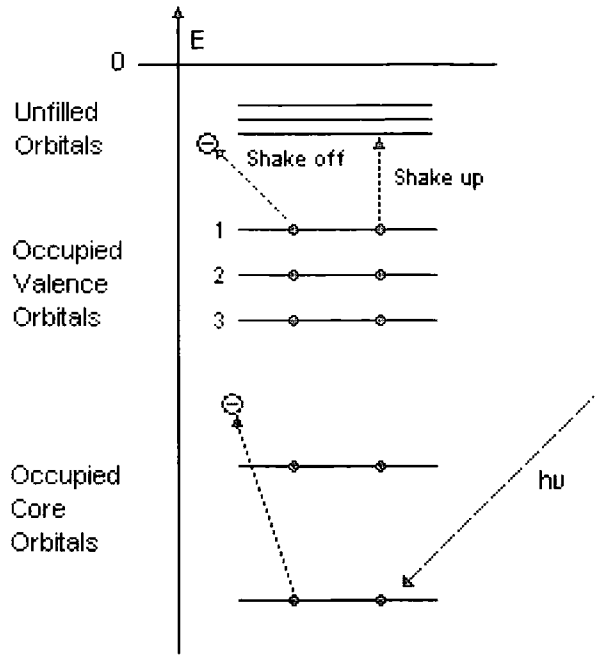

Figure 2.1: The origin of shake-up and shake-off peaks in XPS spectra.

The formation of an ion by photoemission results in a further redistribution of the electrons surrounding the target atom, which affects the final-state energy. This process is called electronic relaxation[10] and has both an intra-atomic and an extra-atomic component, and is governed by the polarizabilities of the atoms involved. The presence of chemical bonding, and hence neighbouring atoms, leads to binding energy shifts which yield information on ligands present and oxidation states[11]. Furthermore, the intensity of the peaks is linked to the relative concentration of the element within the sampled region, resulting in the measurement of the relative areas of the photoelectron peaks allowing the composition of the sample to be determined. Atomic sensitivity factors (ASF) which account for instrumental factors must be defined for each element, Table 2.1. Equation 2.3 allows the relative concentrations *C(i)* of the elements present at the surface to be obtained from XPS experimental intensities *I(i)*. Values are expressed as atomic percentages[12].

$$C_{(i)} = \frac{(I_{(i)} / ASF_{(i)})}{(\Sigma_j I_{(j)} / ASF_{(j)})} \qquad \textbf{(2.3)}$$

Table 2.1: Sensitivity factors of elements analysed in this work.

Element	**Sensitivity Factor**
Carbon	1.00
Oxygen	0.42
Nitrogen	0.69
Silicon	1.03
Chlorine	0.37
Bromine	0.26
Sulphur	0.46
Palladium	0.09
Nickel	1.0 (estimated)
Copper	1.0 (estimated)
Boron	0.20 (estimated)

XPS is well suited for studying thin films due to the fact that electrons can only leave the surface from depths within 2 - 5 nm, despite the fact that x-rays penetrate much further, Figure 2.2.

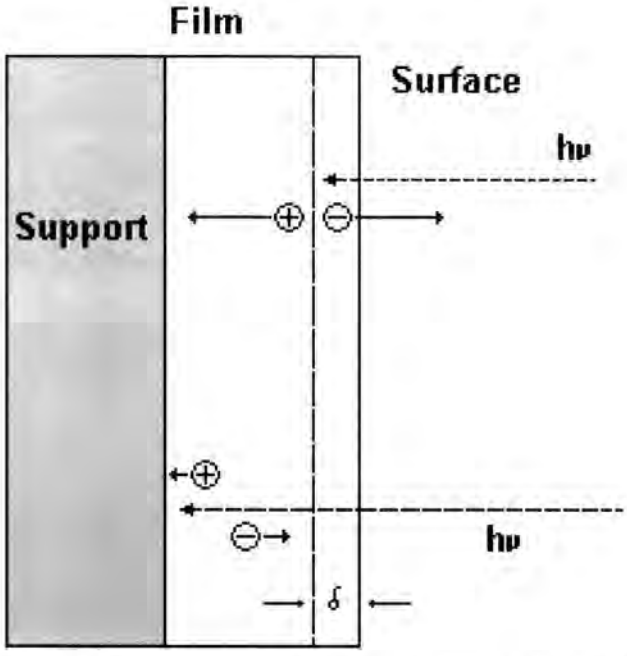

Figure 2.2: Behaviour of detached electrons in the bulk and at the surface of a film.

2.1.1 Experimental Set-up

XPS instruments consist of the following elements:

X-ray source

Any material used to emit x-rays must be able to produce electrons of sufficient energy from the sample to gain a large spectral window. The width of emission must, however be low enough to obtain a clear spectra. X-ray sources commonly consist of a double-sided anode coated with MgK_α (1253.6 eV[13]) or AlK_α (1486.6 eV), which ensure both good resolution and sensitivity. The anode is typically cooled by a flow of water, passing alongside and incandescent filaments are situated either side of it in order to excite electrons on whichever side of the anode is used. Electrons produced by the filament are accelerated by a 8 kV potential passed through the anode. Since the photoelectron energy depends on x-ray energy, the excitation source must be monochromatic.

Electrostatic Analyser

Photoelectrons emitted from the sample are focused into the analyser by a lens. Only electrons of particular energy values are detected at any one time. In order to obtain a clear spectrum, a double-focusing electrostatic analyser[14] is required that can provide a constant resolution for any peak in the spectra. Once electrons enter the analyser, having passed through electrostatically charged plates, their intensity is recorded by a channeltron. This consists of lead silicate glass, which electrically conducts and produces secondary electron emission. The input end of the channeltron is at zero or low voltage, whereas the output end is at a high positive voltage. When electrons enter the device, collisions with the walls occur, resulting in the emission of secondary electrons.

The emitted electron signal is plotted as a spectrum of binding energies. Spectral information is collected from a depth of 2-20 atomic layers, depending on the material studied. A schematic of an XPS machine is shown in Figure 2.3

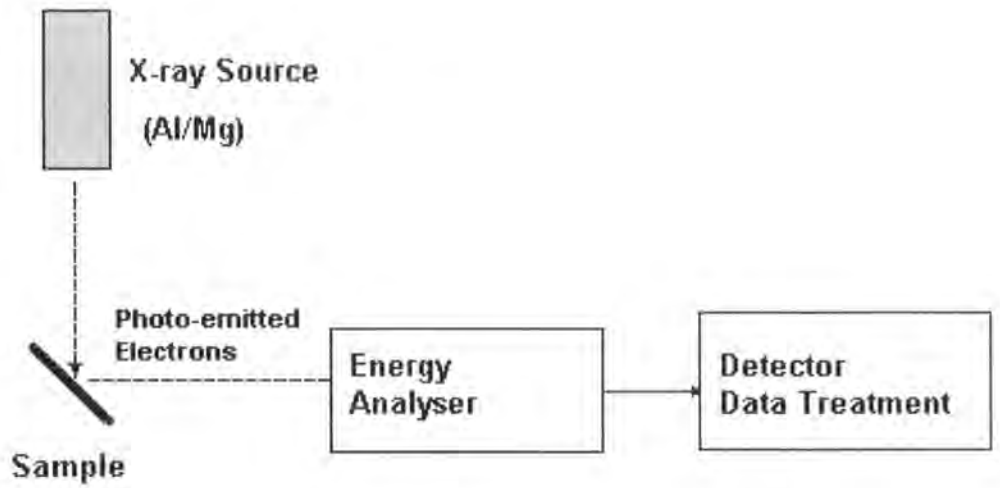

Figure 2.3: Block diagram of a typical XPS spectrometer.

The analysis and detection of photoelectrons requires that the sample be placed in a high-vacuum chamber (~10^{-10} mbar). This is to avoid interactions between electrons and gas molecules and to prevent any molecules being adsorbed on the surface of the sample. Diffusion pumps are typically used to achieve the

vacuum, however they must be cooled continually to avoid any back-pumping of oil into the UHV chamber.

2.1.2 Sample Analysis

Curve fitting is carried out using Marquardt minimization computer software, which details each component of a complex envelope as a Gaussian-Lorentzian function[15]:

$$\frac{F(E)}{H} = m\exp[-4\ln(2x^2)] + (1-m)/(1+4x^2) \qquad \textbf{(2.4)}$$

$$x = (E - E_0)^2 / (FWHM)^2 \qquad \textbf{(2.5)}$$

Where $F(E)$ = intensity at energy E, H = peak height, E_0 = peak centre, $FWHM$ = full width at half maximum and m = mixing ratio (1= pure Gaussian, 0 = pure Lorentzian). Asymmetry is incorporated with a tail function:

$$T(E) = \exp\left(\frac{-k}{A}\,|\,E - E_0\,|\right) \qquad \textbf{(2.6)}$$

Where A = asymmetry parameter and k = constant derivatized by A and $FWHM$. The tail function can be introduced into the Gaussian Lorentzian function to yield function Y, which defines peak shape:

$$Y(E) = F(E) + [H - F(E)]T(E) \qquad \textbf{(2.7)}$$

Hence the envelope is attributable to five parameters (*H, FWHM, E_0, m and A*) which are entered as initial values in the curve fitting program.

By obtaining knowledge of chemical shifts from literature sources[16], number, position and area ratio of component peaks can be acquired. This, in turn, allows peaks to be fitted to coincide with the data obtained during XPS experiments.

2.2: Fourier Transform Infrared Spectroscopy

Fourier transform infrared (FTIR) spectroscopy is a very fast method of measuring the vibrations of functional groups and highly polar bonds. Thus these chemical "fingerprints" are made up of the vibrational features of the sample's components[17].

In all types of absorption spectroscopy, intensity is directly proportional the number of molecules sampled. A simple relationship between the intensity of the transmitted (I) and incident radiation (I_0) and the amount of sample in the beam (either concentration or thickness) exists and is referred to as the Beer-Lambert law[18], Equations 2.8, 2.9.

$$I = I_0 \exp(-\varepsilon c l) \qquad \textbf{(2.8)}$$

Or in the logarithmic form

$$\log\left(\frac{I_0}{I}\right) = \varepsilon c l \qquad \textbf{(2.9)}$$

Where in both cases *c* is the concentration, *l* is the cell thickness and ε is the frequency dependent extinction coefficient. The Beer-Lambert law can hence be described as the foundation for all quantitative infrared spectroscopy.

For every vibrational transition there is a series of accompanying rotational levels. These movements require energy in the <100 cm^{-1} region of the electromagnetic spectrum and although they may appear as discrete lines in gas phase spectra, intramolecular collisions and interactions in liquids and solids cause broadening of the lines into a continuum, so that their fine structure is not observed. Molecular species with energy differences between their various vibrational/rotational levels in the appropriate region will be in a position to absorb incoming infra-red radiation[19].

In order for absorption of infra-red radiation to occur, the vibrational movement of the molecule under observation must have associated with it a fluctuating electric dipole moment. This requires that the charge distribution around the molecule must not be symmetrical. The strength of the dipole moment is determined by the magnitude of the charge difference and the distance between the centres of charge. As the molecule bends and stretches, the changing dipole moment establishes an electric field. When the alternating electric field of the electromagnetic radiation matches in frequency one of the natural oscillatory frequencies of the molecule, interaction between the two fields may occur, resulting in resonant energy transfer and a change in amplitude of the motion. An example of a functional group that exhibits a strong dipole moment in the ground state is the carbonyl group.

Traditional infrared techniques experience difficulties due to the "one wavenumber at a time" nature of data acquisition. This leads to either a poor signal to noise ratio in a spectrum or large amounts of time required to obtain a high quality spectrum. A large signal to noise ratio leads to inherent errors and the time constraints prohibit in-situ work. These problems can be overcome using Fourier transform infrared spectroscopy (FTIR) which is based on the interferometer originally designed by Michelson[20] and a mathematical procedure developed by Fourier that converts response from the time to the frequency domain.

FTIR can be applied to the analysis of solids, liquids, and gases and is based on the excitation of molecular vibrations by the adsorption of photons in

the spectral region of 0.75 – 2.5 μm (near infrared), 2.5 – 50 μm (medium infrared) and 50 – 1000 μm (far infrared). This is the so called "fingerprint" region where most single and double bonds absorb, and where the most useful chemical information exists.

2.2.1: Infrared Sources[21]

The source of infrared radiation normally consists of inert solid materials heated to incandescence (1500 and 2000 K) by an electric current. Materials suitable for this purpose include the oxides of zirconium, yttrium and thorium and silicon carbide. Heated ceramic sources can also be employed.

2.2.2: Infrared Detectors[22]

The infrared detector is a device utilized to measure the infrared energy of radiation emitted from the source which has passed through the spectrometer, hence translating radiation energy to electrical energy to generate a spectrum. Two types of detector are available, *thermal detectors* and *selective detectors*.

A pyroelectric detector is a common example of a *thermal detector*. It consists of a thin pyroelectric crystal e.g. deuterated triglycine sulphate (DTGS). When this crystal is polarized in an electric field, it retains a residual electrical polarization after the field is removed, which is sensitive to temperature fluctuations. Electrodes on the faces of the crystal collect charge, hence acting as a capacitor across which a voltage is generated; the amount of which is sensitive to changes in temperature. The pyroelectric detector operates at room temperature and possesses a flat wavelength response ranging from far infrared to near infrared. It is well suited to infrared spectrometers due to its capability of handling frequencies up to several thousand hertz.

A common type of *selective detector* is the photoconductive cell, which has a very rapid response and high selectivity. An example of this type of cell is the mercury cadmium telluride detector (MCT), which needs to be cooled by liquid nitrogen. The photoconductive cells show an increase in electrical conductivity when exposed to infrared radiation. Detectors utilize photon energy to promote

bound electrons in the detector metal to free states, which results in electrical conduction.

2.2.3: The FTIR Spectrometer[23]

The FTIR spectrometer works by the following principles: a parallel beam of polychromatic radiation is emitted from the source to the Michelson interferometer and two mirrors, Figure 2.4. The beam splitter is a plate of an infrared transparent material such as potassium bromide coated to reflect 50% of the radiation that falls onto it. Hence the radiation is split between the two mirrors, reflected and recombined to a single beam at the beam splitter. The relative path lengths between the two mirrors and the beam splitter govern whether there is constructive or destructive interference. If mirror 2 is moved closer to the beam splitter, radiation is detected at alternating intensities. As the distance of the moving mirror from the beam splitter is changed, different wavelengths of radiation are in-phase and out-of-phase at a frequency that depends upon both the rate at which the mirror moves and the frequency of radiation. The detectors are sufficiently fast to cope with time domain signal changes from the modulation in the interferometer.

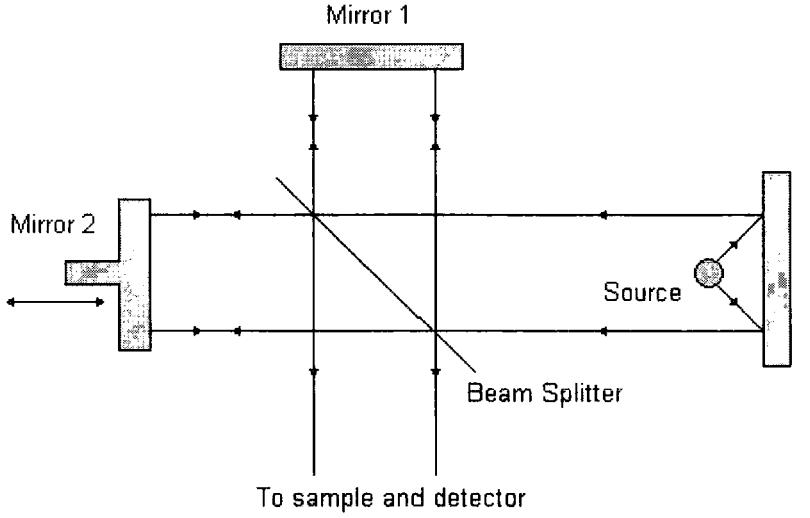

Figure 2.4: The interferometer unit of a FTIR spectrometer.

If the recombined beam is passed through a sample before reaching the detector, absorptions in the sample will appear as gaps in the frequency distribution. The complex pattern of overlaid sinusoidal waves of light (in the time domain) is known as an interferogram. The obtained interferogram can be converted to a spectrum by means of a Fourier Transformation.

Hence FTIR spectrometers record the interaction of IR radiation with experimental samples, measuring the frequencies at which the samples absorb radiation and the intensities of the absorptions. Determining these frequencies allows identification of the sample's chemical makeup, since the wavelength of light absorbed is characteristic of the chemical bond. By interpretation of the infrared absorption spectrum, the chemical bonds in a molecule can be determined.

Molecular bonds vibrate at various frequencies depending on the elements present and the type of bonds. For any given bond, there are several specific frequencies at which it can vibrate. According to quantum mechanics, these frequencies correspond to the ground state (lowest frequency) and several excited states (higher frequencies). The frequency of a molecular vibration increases when the chemical bond absorbs infrared radiation. For any given transition between two states the energy (determined by the wavelength) must equal the difference in energy between the two states (usually ground state (E_0) and the first excited state (E_1)).

2.2.4: Sampling Techniques

FTIR spectroscopy uses simple transmission sampling techniques. However, 'difficult' samples and experiments need specialized sampling accessories. The following techniques can be employed:

2.2.4.1: Attenuated Total Reflectance

Internal reflection spectroscopy or attenuated total reflection (ATR) is an important method for obtaining FTIR spectra of solids[24]. If a beam of monochromatic radiation traverses a prism so that it is internally reflected from its

back face, and the angle θ at which the infrared light impinges upon the interface between the ATR crystal (the dense medium) and the air (or water, buffer with or without proteins - the rare medium) is greater than the critical angle, then the light will totally internally reflect within the internal reflection element, Figure 2.6.

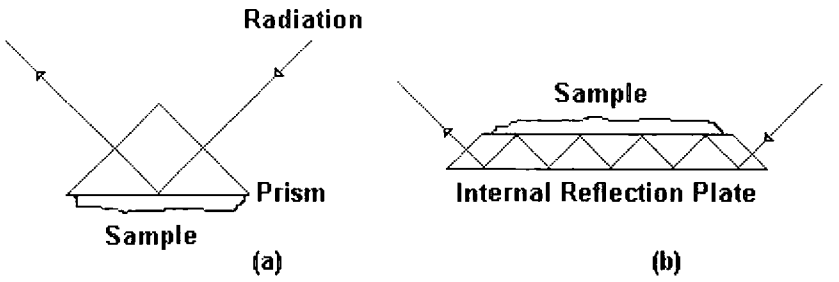

Figure 2.6: Optical diagrams of the internal reflection technique (a) Single reflection from prism, (b) Multiple-reflection method from plate.

Total internal reflection is where all radiation is reflected back into the dense medium. At each reflection, an evanescent electric field *(E)* is generated and its intensity decays exponentially with distance *(z)*. It can persist beyond the interface into the rare medium.

$$E = E_\rho e^{-z/d_\rho} \qquad \textbf{(2.10)}$$

Where E_o is the intensity of the incident radiation and d_p, the depth of penetration, represents the distance at which the evanescent wave drops to 1/e times the intensity at the surface.

The intensity of the reflected light at each reflection point will be reduced or "attenuated" by the presence of infrared absorbing material in the rare medium. The surface sensitivity of ATR results from the addition of a number of small absorbances from each reflection.

The spectrum for internally reflected radiation is analogous to the conventional spectrum for absorbed infrared radiation for a substance. The

infrared band intensities are equivalent to a penetration of a few microns into the sample and are independent of sample thickness beyond a certain minimum. The depth of penetration can be calculated using Equation 2.11:

$$d_p = \frac{\lambda}{2\pi n_1 \sqrt{(\sin^2\theta - n_{21}^2)}} \qquad (2.11)$$

Where λ is the wavelength of the light (the depth of penetration is a function of wavelength), n_1 is the refractive index of the ATR crystal (this is independent of wavelength), n_2 is the refractive index of the rare medium (this value is a function of wavelength), θ is the angle of incidence and n_{21} is the ratio of the refractive indexes of the rare medium to the dense medium[25].

2.2.4.2: Reflection Absorption Infrared Spectroscopy (RAIRS)

Infrared vibrations of surface-bound molecules can be studied by shining infrared light on to the surface. Hence, an infrared spectrum of light reflected from the surface will show absorption peaks which are characteristic of the molecule and its method of bonding to the surface. This is the basis of the RAIRS technique. Vibrations can only be detected if the vibration is perpendicular to the surface.

With RAIRS, a beam of infrared radiation is reflected off a polished surface at grazing incidence, maximizing the electric field[26]. Molecules near the interface can absorb some of this IR radiation, but only if the dipole moment for the transition is perpendicular to the plane of the surface. Radiation polarized parallel to the surface plane has a near zero electric field near the interface. Thus, an IR absorption spectrum for adsorbed species can be acquired, yielding molecular identity information. At the same time, information on the molecular orientation can be obtainable due to this "surface selection rule"[27].

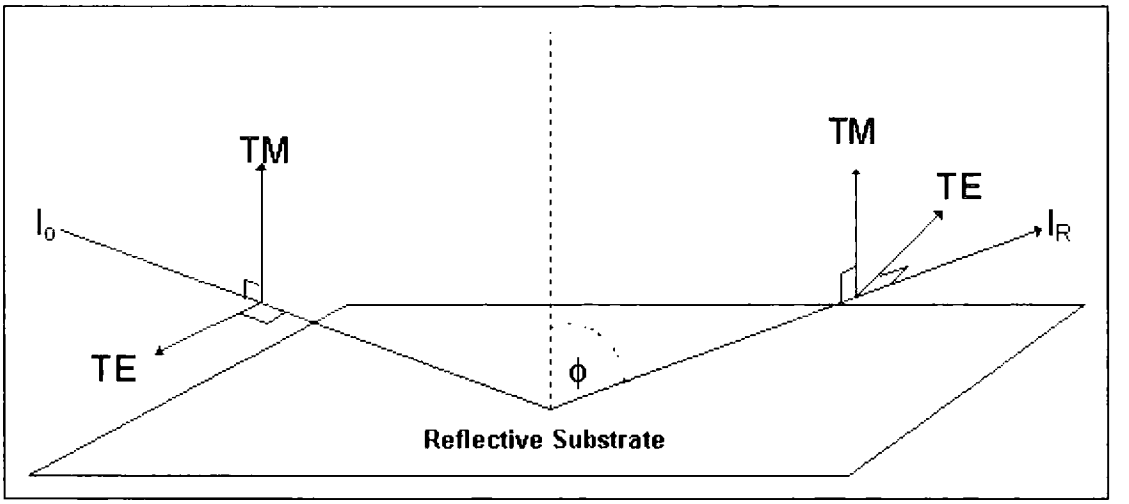

Figure 2.6: Optical configuration of the RAIRS experiment.

Figure 2.6 shows infrared radiation directed at the grazing angle, Φ and reflected at the substrate surface. Upon reflection the incident light I_0 is inverted and the net electric field is zero parallel to the surface (TE) and doubled perpendicular to it (TM) (the Surface Selection Rule). Using this optical configuration, it is possible to obtain structural and orientational information on very thin layers[28].

2.2.4.3: Potassium Bromide Disc Method

A suitable way of obtaining FTIR spectra of small of volumes of liquid is the potassium bromide disc method. The discs are formed by pressing KBr powder in an evacuated die under high pressure. The resulting discs are transparent and if a small amount of liquid is "sandwiched" between two discs, excellent spectra can be obtained. The advantage of using KBr discs is that they do not have absorption bands above 400 cm^{-1}, resulting in no interference.

2.3: Scanning Electron Microscopy[29]

The scanning electron microscope generates a beam of electrons in a vacuum. These electrons are emitted from a cathode and accelerated by passage through electrical fields[30]. The beam is collimated by electromagnetic condensor lenses, focused by an objective lens and scanned across the surface of the sample by electromagnetic deflection coils. The primary imaging method is by collecting secondary electrons that are released by the sample. The secondary electrons are detected by a scintillation material that produces flashes of light from the electrons. The light flashes are subsequently detected and amplified by a photomultiplier tube. By correlating the sample scan position with the resulting signal, an image can be formed.

The scanning electron microscope (SEM) has a large depth of field, which allows a large amount of the sample to be in focus at one time. The SEM also produces images of high resolution, which means that closely spaced features can be examined at a high magnification. Preparation of the samples is relatively easy since most SEMs only require the sample to conduct electricity - hence some samples often have to be covered with a 10 nm-thick layer of gold. The combination of higher magnification, larger depth of focus, greater resolution, and ease of sample observation makes the SEM one of the most heavily used instruments in research. The size and shape of the apparent source, beam acceleration and current are the primary determining factors in the performance and resolution of a scanning electron microscope.

The electron gun in a scanning electron microscope is the source for the electron beam used to probe the sample[31]. Electrons are emitted from a cathode, consisting of either tungsten or lanthanum hexaboride and the beam accelerated towards the anode, focused to a fine probe and scanned over the sample, ionizing it and producing secondary electrons, Figure 2.7.

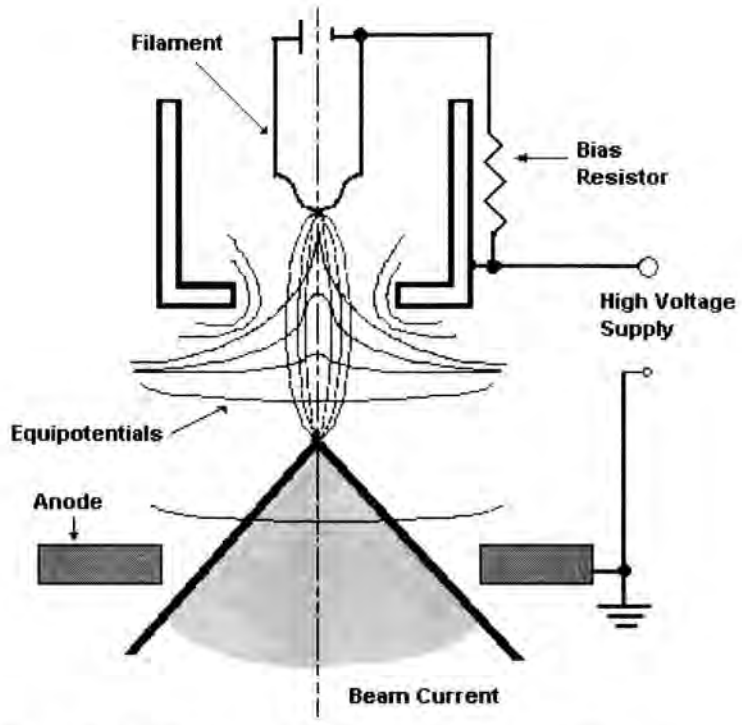

Figure 2.7: Schematic of an electron gun used in SEM.

Secondary electrons are specimen electrons that obtain energy by inelastic collisions with beam electrons. They are defined as electrons emitted from the specimen with energy less than 50 eV. The secondary electrons are predominantly produced by the interactions between energetic beam electrons and weakly bonded conduction-band electrons in metals or the valence electrons of insulators and semiconductors. There is a significant difference between the amounts of energy contained by beam electrons compared to the specimen electrons. This can result in only a small amount of kinetic energy being transferred to the secondary electrons.

Secondary electrons are collected by a detector, converted to a voltage, and amplified. The amplified voltage is applied to the grid of the cathode ray tube (CRT) and causes the intensity of the spot of light to change. The image consists of thousands of spots of varying intensity on the face of a CRT that correspond to the topography of the sample. Hence the image is built up point-by-point.

When an electron beam strikes a sample, a signal can also be generated from back-scattered electrons. This is the elastic scattering of primary electrons and it occurs between the electron and a nucleus within the specimen being analysed. This is essentially Rutherford scattering and it can be detected to build up an image, yielding topographical information of a sample.

2.4 : Surface Plasmon Resonance

Surface plasmon resonance (SPR) reflectivity measurements are surface-sensitive, spectroscopic methods that can be used to characterize the thickness and refraction index of thin organic and biopolymer films at metal (Au, Ag, Cu) surfaces[32]. Surface plasmon resonance spectroscopy has become widely used in the fields of chemistry and biochemistry to characterize biological surfaces and to monitor binding events. The success of these SPR measurements is primarily due to three factors:

- The kinetics of biomolecular interactions can be measured in real time;
- The adsorption of molecules to the surface can be monitored;
- SPR has a high degree of surface sensitivity that allows weakly bound interactions to be monitored in the presence of excess solution species.

SPR spectroscopy can be used to monitor such events as antibody-antigen binding, DNA hybridization, and protein-DNA interactions. SPR works by the following principle. If monochromatic, polarized light is emitted onto an interface, there is no refraction as incident light is completely reflected[33]. However, the electromagnetic component penetrates a short distance (in the order of nanometres) into the medium and an evanescent wave is generated. If the interface is coated with a thin layer of metal, the intensity of reflected light is reduced and there is a resonance energy transfer between the evanescent wave and surface plasmons. These resonance conditions are governed by the species absorbed on the metal film.

The precise angle of incidence at which this occurs is determined by the refractive index of the species grafted to the metal surface. If binding occurs to the immobilised target; the local refractive index changes. This leads to a change in the SPR angle, which can be monitored in real-time by detecting changes in the intensity of the reflected light, hence producing a sensorgram.

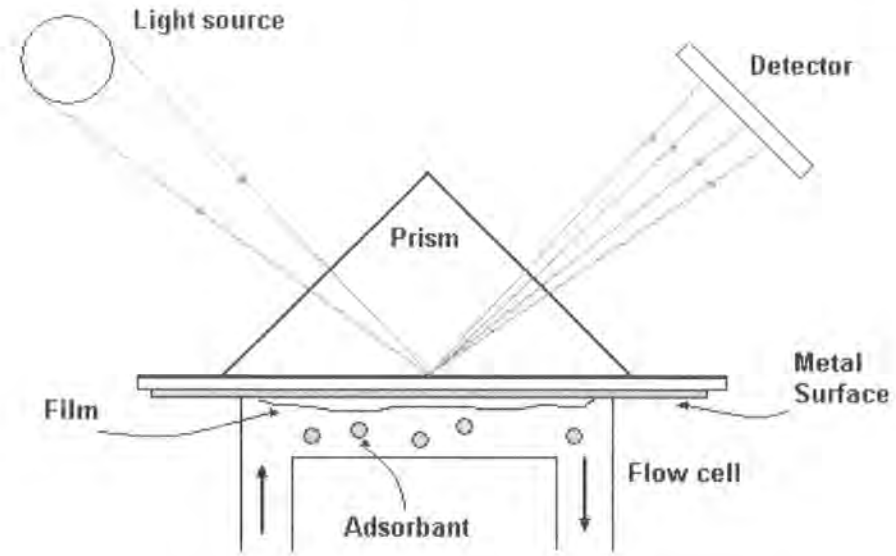

Figure 2.8: Schematic of a surface plasmon resonance detection unit.

The rates of change of the SPR signal can be analysed to yield apparent rate constants for the association and dissociation phases of the reaction. The ratio of these values gives the apparent equilibrium constant and hence the affinity. The magnitude of the change in SPR signal is directly proportional to the mass of material being immobilised, allowing the reaction to be quantified. This method is highly sensitive as signals are easily obtained from sub-microgram quantities of adsorbant. Since the SPR signal depends only on binding to the immobilised template, it is also possible to study binding events from molecules in extracts, i.e. it is not necessary to have highly purified components. SPR analysis is hence a versatile way to detect and quantify the presence of a biopolymer[34] on a chemically modified gold surface by this change in the local index of refraction that occurs upon adsorption.

2.5 Reflectometry

Reflectometry is a non-destructive technique, which is commonly used in the semiconductor and thin film magnetic head industries to measure film thickness. Reflectometry measures the ratio of the incident light's intensity to that of the reflected light at wavelengths over the UV-visible region, obtaining optical constants, n and k which describe how light propagates through a film, n being the refractive index and k the extinction coefficient of a layer. The refractive index can be described as the ratio of the speed of light in a vacuum to the speed of light in the material and the extinction coefficient a measure of how much light the material absorbs.

As the UV light meets an interface, it will be both reflected and refracted. The amount of reflected light depends on the number of interfaces the light meets i.e. the number of layers present and hence the sum of the individual reflections[35]. The reflections may add constructively or destructively, depending upon the phase relationship of the reflected beams. This relationship is determined by the difference in optical path length of the reflections, which is directly related to film thickness, d. Reflections are in phase and interfere constructively when

$$2nd = i\lambda \qquad \textbf{(2.12)}$$

Where i is an integer and λ = wavelength of light. Reflections are out of phase and interfere destructively when

$$2nd = (i + \frac{1}{2})\lambda \qquad \textbf{(2.13)}$$

The amplitude and wavelength of the reflectance of a thin film is determined as well as the optical constants and other properties such as interfacial roughness and film thickness. It is not possible to solve for n and k at each wavelength individually when more than one interface is present and therefore mathematical models which can describe n and k over a range of wavelengths are required. Film thickness (d) is calculated by minimizing the differences between measured and model-generated data using the Cauchy material model, which is a material model for polymers and dielectrics where k is approximately zero.

The reflectance curve calculated by the model differs from the measured experimental data because the wavelengths and amplitudes do not match. The wavelength of the oscillations is dependent on layer thickness whereas the amplitude is representative of the contrast between the refractive index of the layer and the substrate. Vertical positioning of the transmitted light curve gives information about the absorption in the layers and substrate.

An iterative algorithm such as that developed by Levenberg-Marquadt can then be used to minimize the mean square error, which is a measure of the quality of the match between measured and model-calculated data. The algorithm is used to calculate a theoretical curve for the transmittance and reflectance of the sample and then compare it to the measured data on a point-by-point basis to measure this dimensionless quantity. This operates until the measured and calculated data match, yielding the value of film thickness, d, as a parameter. The Levenberg-Marquadt method is an efficient solution to the problem of non-linear curve fitting and is most commonly used for simple analyses.

2.6: Contact angle Analysis

A designated volume of liquid is deposited onto a sample's surface using a syringe, a digital photo is subsequently taken of the droplet on the surface by a video camera at a preset magnification and from this the contact angle can be measured.

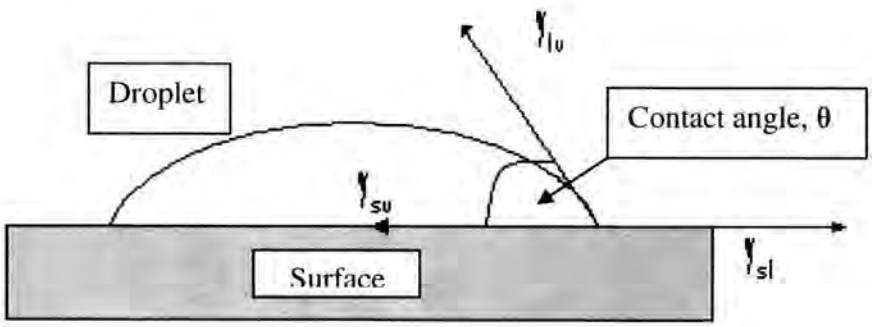

Figure 2.9 Contact angle of a droplet of liquid placed on a substrate's surface

When a drop of liquid is placed on a surface, Figure 2.9, if there is no spreading of the droplet, the liquid-vapour interface will form a finite angle (θ) with an assumed planar solid surface. The contact angle is essentially the balance of the opposing forces of cohesion of the liquid molecules and adhesion of the liquid to the surface[36]. The relationship between surface tension, γ, and the contact angle can be described by Young's equation:

$$\gamma_{sv} - \gamma_{sl} = \gamma_{lv} \cos\theta \qquad \textbf{(2.14)}$$

Where:

γ_{sv} = surface tension at the solid-vapour phase

γ_{sl} = surface tension at the solid-liquid phase

γ_{lv} = surface tension at the liquid-vapour phase

This equation is best fitted to an ideal situation in which there is a homogeneous surface, perfectly flat, that remains unperturbed by the liquid and its vapour. However deviations can occur due to factors such as surface roughness.

This method of analysis is especially useful when investigating the hydrophobicity of a surface i.e. when the droplet placed on the substrate is deionized water.

2.7: Fluorescence Microscopy

Fluorescence microscopy is a method commonly used in cell biology to detect structures, molecules or proteins[37, 38]. Fluorescent molecules absorb light at one wavelength and emit light at different, longer wavelength. When fluorescent molecules absorb a specific absorption wavelength for an electron in a given orbital, the electron rises to a higher energy level, an excited state. Electrons in this state are unstable and will return to the ground state, releasing energy in the process in the form of light and heat.

This emission of energy is fluorescence and because some energy is lost as heat, the emitted light contains less energy and therefore is of a longer wavelength than the absorbed or excitation light.

In fluorescence microscopy, a cell or molecule is tagged with a dye and the sample illuminated with filtered light at the absorbing wavelength; the light emitted from the dye is viewed through a filter that allows only the emitted wavelength to be seen. The dye glows brightly against a dark background because only the emitted wavelength is allowed to reach the eyepieces or camera port of the microscope. Most microscopes are designed using epi-illumination, where excitation light goes through the objective lens and illuminates the object. Light emitted from the specimen is collected by the same objective lens.

Among the common fluorescence dyes are fluorescein, which emits green light when exited with blue light and rhodamine, which emits a deep red fluorescence when excited by green-yellow light. Fluorescence microscopes are

frequently equipped with three fluorescent filter cubes, each containing specific barrier filters and a beam-splitting mirror, Figure 2.10.

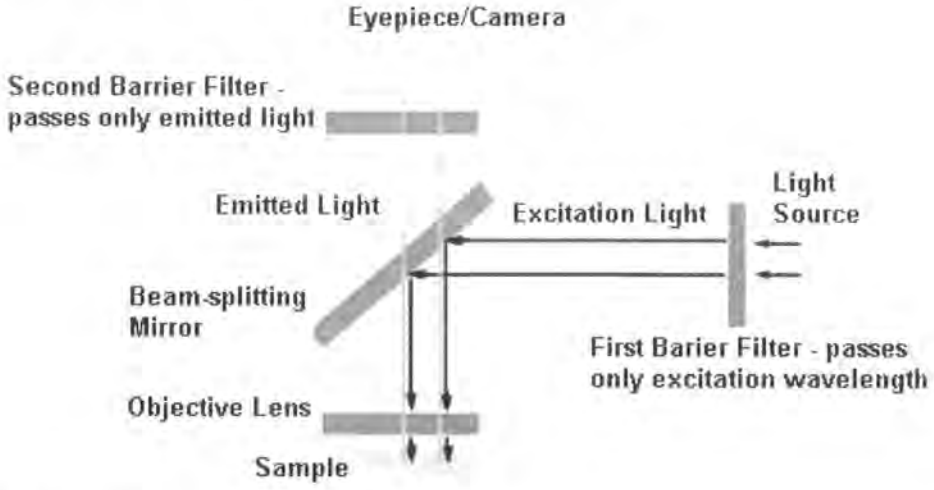

Figure 2.10: schematic of a fluorescence microscope.

2.8 References

[1] Briggs, D.; Sean, M. P. *Practical Surface Analysis*, Wiley, New York, **1990**.

[2] Jenkin, J. G.; Leckey, R. C. G.; Liesegang, J., *J. Electron Spectrosc.*, 12, **1977**, 1.

[3] Briggs, D.; Sean, M. P. *Practical Surface Analysis*, Wiley, New York, **1990,** 206.

[4] Walls, J. M.; *Methods of Surface Analysis*, Camb. Univ. Press, Cambridge, **1989**.

[5] Turner, N. H.; Schreifels, J. A., *Anal. Chem.*, 64, **1992**, 502.

[6] Wertheim, G. K., *J. Franklin Institute*, 298, **1974**, 289.

[7] Brisk, M. A.; Baker, A. D., *J. Electron. Spectrosc.*, 7, **1975**, 197.

[8] Kriele, J.; Munzel, N.; Schulz, R.; Schweig, A., *Chem. Phys. Lett.*, 108, **1984**, 609.

[9] Clark, D. T.; Dilks, A., *J. Polym. Sci. Polym. Chem. Ed.*, 14, **1976**, 533.

[10] Jenkin, J. G.; Leckey, R. C. G.; Liesegang, J., *J Electron Spectrosc.*, 14, **1978**, 477.

[11] Siegbahn, K.; Nordling, C.; Fahlman, A.; Nordberg, R.; Hamrin, K.; Hedman, J.; Johansson, G.; Berkmrsk, T.; Karlsson, S.E.; Ligren, I.; Lindberg, B., *Atomic, Molecular and Solid State Structure Studied by Means of Electron Spectroscopy,* Almqvist and Wiksells; Uppsala, **1967**.

[12] Garbassi, F.; Morra, M.; Occhiello, E., *Polymer Surfaces*, Wiley, New York, **1994**.

[13] Sabbatini, L.; Zambini, P. G.; *Surface Characterization of Advanced Polymers*, VCH, **1993**.

[14] Briggs, D.; Sean, M.P. *Practical Surface Analysis*, Wiley, New York, **1990**.

[15] Moulder, J. F.; Stickle, W. F.; Sobol, P. E.; Bomben, K. D., *Handbook of X-ray Photolectron Spectroscopy*, Perkin Elmer, Minnesota, **1992**.

[16] Beamson, G.; Briggs, D; *High Resolution XPS of Organic Polymers*, Wiley, New York, **1992**.

[17] Griffiths, P.R.; de Haseth, J.A. *Fourier Transform Infrared Spectrometry*. Wiley, New York. **1986**.

[18] Banwell, C.N. *Fundamentals or Molecular Spectroscopy*, McGraw Hill, London, **1983**.

[19] Colthup, N. B.; Daly, L. H.; Wiberley, S. E., *Introduction to Infrared and Raman Spectroscopy*, Academic Press Inc., London, **1990**.

[20] Griffiths, P. R., *Chemical Infrared Fourier Transform Spectroscopy*, Wiley, New York, **1975**.

[21] Christy, A. A.; Ozaki, Y.; Gregariou, V. G., *Modern Fourier Transform Infrared Spectroscopy,* Elsevier, **2001**.

[22] Ferraro, J. R.; Basile, L. J., *Fourier Transform Infrared Spectroscopy: Techniques Using Fourier Transform Interferometry,* Academic Press, **1982**.

[23] Griffiths, P. R.; De Haseth, J. A., *Fourier Transform Infrared Spectrometry*, Wiley, New York, **1986**.

[24] Fahrenfort, *J.; Spectrochim. Acta*, 17, **1961**, 698.

[25] Harrick, N. J. *Internal Reflection Spectroscopy*, Wiley, New York, **1967**.

[26] Hayden, B. E.; *Methods of Surface Characterisation*, Plenum Press, **1987**, Vol 4.

[27] Greenler, R. G., *J. Chem. Phys.*, 44, **1966**, 301.

[28] Suetaka, W., *Surface Infrared and Raman Spectroscopy*: Methods and Applications, Plenum Press, **1995**.

[29] Flegler, S L., *Scanning and Transmission Electron Microscopy: An Introduction*, Oxford University Press Inc, USA, **1997**.

[30] Lafferty, J. M., *J. Appl. Phys.*, 22, **1951**, 299-309.

[31] Flegler, S. L.; Heckman, J. W., Klomparens, K. L. *Scanning and Transmission Electron Microscopy: An Introduction*, Oxford University Press, **1993**.

[32] Daniels, P.; Deacon, J.; Eddowes, M.; Pedley, D., *Sensors and Actuators*, 15, **1988**, 11.

[33] Brockman, J.M.; Corn, R.M. *Ann. Rev. Phys. Chem.*, 51, **2000**.

[34] Lukosz, W., *Biosensors and Bioelectronics*, 6, **1991**, 215-225, 41.

[35] Tabet, F. M.; McGahan, W. A. *Thin Solid Films*, **2000,** 370, 122.

[23] Mittal K. L., *Contact angle, Wettability and Adhesion*, VSP, Utrecht, **1993**.

[37] Rost, F. W. D., *Fluorescence Microscopy*, Cambridge University Press, **1995**.

[38] Taylor, D., L.; Wang, Y. L., *Fluorescence Microscopy of Living Cells in Culture: Quantitative Fluorescence Microscopy - Imaging and Spectroscopy,* Academic Press, New York, **1990**.

Chapter 3: A Substrate-independent, Single-step Method for Thermo-responsive Coatings

3.1 Introduction

An intelligent polymer is one that exhibits a sharp physical change in response to external stimuli[1, 2, 3] e.g. pH, temperature and exposure to ultra violet light or an electric charge. Poly(n-isopropylacrylamide) (PNIPAAm) is one such polymer due to the physical change it undergoes with temperature.

The increased interest in PNIPAAm is mainly due to its fully reversible lower critical solution temperature (LCST) which lies between room temperature (~ 20 °C) and body temperature (37 °C); the value of the LCST for PNIPAAm is generally considered in the range of 31 - 32 °C[4]. Table 3.1 details LCST values for a range of polymers.

Polymer	LCST in Water (°C)
Poly(n-isopropylacrylamide), PNIPAAm	32
Poly(vinyl methyl ether), PVME	40
Poly(propylene glycol), PPG	50
Poly(ethylene glycol), PEG	120
Poly(vinyl alcohol), PVA	125
Methylcellulose, MC	80
Poly(methacrylic acid), PMAA	75
Poly(vinyl pyrrolidinone), PVP	160

Table 3.1: Lower critical solution temperatures of various polymers in water

In an aqueous solution below the LCST, PNIPAAm is an expanding structure[5] with a random coil configuration. Hydrogen bonding occurs between the polar groups and water molecules, leading to dissolution of the polymer. However

above the LCST, PNIPAAm is a shrinking structure[5], collapsing into a globular conformation[6] and hydrophobic reactions dominate, resulting in precipitation of the polymer in water. The formation of hydrogen bonds between the N-H and C=O in PNIPAAm chains and the surrounding water is controlled by very small changes in temperature, giving rise to the remarkable hydration-dehydration change that occurs[7, 8]. The LCST is hence a result of the entropy gain for the dehydration of the amide moieties with temperature increase. At high temperatures, a PNIPAAm surface can be considered as an alkane-like surface of packed propyl groups. Below the LCST, it can be considered as water and amide groups mixed at the interface[9, 10].

The hydrophilicity of PNIPAAm has been studied by measuring the water contact angle on a PNIPAAm surface. At room temperature (20 - 25°C), below the LCST, contact angle has been measured to be 45.4°[11] and 42°[12] whereas at body temperature (37°C), above the LCST, water contact angle is around 90°.

Due to its thermo-responsive properties, which affect its affinity to proteins and cells, PNIPAAm can be exploited in some of the following fields; separation[13, 14], controlled release of drugs[15, 16, 17], cell culture[18] and cell structure substrates to control attachment and detachment of cells, hence tissue engineering[19, 20, 21]. The affinity of surface coatings to the adsorption of proteins and cells is discussed in detail in Chapter 7.

The regulation of cell functions by biomaterials is an important technique for the engineering of tissue. In addition to cell attachment and cell shape, cell detachment is also regulated by biomaterials, e.g. by a thermo-responsive polymer where cells can be recovered by lowering temperature[22, 23, 24]. PNIPAAm surfaces are commonly exploited in this field due to the fact that tissue can be engineered at body temperature (37 °C) and then subsequently detached by allowing the substrate to rapidly hydrate when it is cooled.

The principal existing application of PNIPAAm in tissue engineering is as a component of three-dimensional scaffolds of polymer matrices which can successfully mimic the in vivo environment of an extra-cellular matrix (ECM). This is a common approach to repair damaged or diseased tissue and organs because the tissue can be regenerated both in vivo and in vitro. Cells are seeded into the matrices and the 3-D structures guide the cell's organization

and development into tissues and organs[25]. Matrices of this type have been simulated using collagen and polylactic acid[26].

Previous work has shown injectable semi-interpenetrating networks (IPN) of PNIPAAm and AAc hydrogels can be used to tailor matrices that serve as functional scaffolds in applications of tissue engineering[27]. Hydrogels of PNIPAAm and polyacrylic acid (PAAc) have hindrances in interacting with the biological environment at the molecular level. Hence these IPNs have to be coupled with peptides found in the natural ECM macromolecules to ensure compatibility with the in-vitro environment[28, 29].

The phase behaviour of PNIPAAm chains and hydrogels can be manipulated by the addition of other monomers. Copolymerization of PNIPAAm with another monomer can control the LCST over a broad temperature range, due to the effect it has on hydrophobicity. The more hydrophobic the monomer used for copolymerization, the lower the LCST. NIPAAm has been successfully copolymerized with isocyanate[30] and acrylic acid[22, 31, 32, 33] which is a hydrophilic monomer. The LCST has been found to increase as high as 38 °C (above body temperature) and this is attributable to the fact that the AAc functionality hinders dehydration of the PNIPAAm chains and acts to expand the collapsing polymer structure. PNIPAAm coupled with azoaniline hydrochloride can decrease the LCST to as low as 17 °C[34].

Various methods have been employed to generate surfaces of PNIPAAm to investigate its phase changes with temperature and its compatibility with biomaterials. PNIPAAm has been successfully deposited onto polystyrene using electron beam irradiation fitted with a mask to form a pattern[11, 35]. It was found that cells migrated into the PNIPAAm regions at 37 °C but not at room temperature (20 °C) - the cells started to spread when the LCST was reached. PNIPAAm surfaces can be prepared by irradiating polyethylene films with argon and then submersing in a solution of NIPAAm[5], by atom transfer free radical [36, 37] photo-initiated polymerization [38, 39, 40] and free radical polymerization by surface retention of persulfate[41] and dialkylazene initiators[28, 29, 42].

Surfaces of PNIPAAm on silicon wafers have been successfully generated using plasma polymerization. To obtain a large enough vapour pressure to generate a plasma, the NIPAAm monomer must be heated to

around 50 °C. PNIPAAm was deposited[43] via a continuous wave plasma at 120 W, lowered stepwise to 1 W to obtain a functionalised coating, which was characterised with XPS and FTIR spectroscopy. The FTIR results show a good retention of functional groups using this method. Analysis for the adsorption of proteins showed that the PNIPAAm films had an appreciable resistance protein adsorption at 20 °C and adsorption increased by a factor of ten when heated to 37 °C. However when the films were cooled back to 20 °C, the protein adsorption that had occurred at higher temperatures was found to be irreversible[44, 45].

3.2 Aims

Pulsed plasma polymerization will be deployed to generate a PNIPAAm layer on a variety of substrates, Scheme 3.1. Due to conventional chemistry processes occurring during "plasma off" periods, a high retention of functional groups and control of film properties should result.

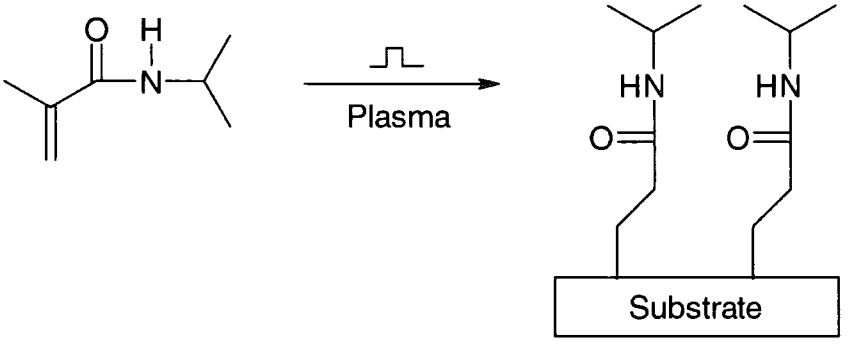

Scheme 3.1: Pulsed plasma polymerization of n-isopropylacrylamide.

It is the abundance of functional groups that is responsible for the non-fouling properties of PNIPAAm below its phase transition temperature. A lesser degree of cross-linking compared to continuous wave methods can allow PNIPAAm chains to alter conformation with greater efficiency when the lower critical solution temperature is surpassed. This should result in a noticeable improvement in the previously developed continuous wave method due to the reduced heat load on the reactor and increased efficiency of the process. The

reduction in cross-linking will aid structural retention, which could, in turn allow the fully reversible adsorption of proteins with temperature.

These films can be characterized and hydrophilicity investigated by monitoring water contact angle. Compatibility with proteins and hence cells with varying temperature can be investigated with surface plasmon resonance and by observation of the behaviour of fluoroscein-tagged proteins using fluorescence microscopy.

3.3 Experimental

3.3.1 Pulsed Plasma Polymerization of n-isopropylacrylamide

n-isopropylacrylamide (NIPAAm) (97 % purity, Aldrich) was loaded into a sealable glass tube, followed by further purification using several freeze-pump-thaw cycles. Pulsed plasma polymerization of the monomer was carried out in a cylindrical glass reactor (4.5 cm diameter, 460 cm^3 volume, 2 x 10^{-3} mbar base pressure, leak rate 1.4 x 10^{-9} mol/s) enclosed in an aluminium container and surrounded by a copper coil (4 mm diameter, 10 turns, located 15 cm away from the precursor inlet). The chamber was evacuated using a 30 L min^{-1} rotary pump attached to a liquid nitrogen cold trap, whilst monitoring the system pressure with a Pirani gauge. All fittings were grease-free. The output impedance of a 13.56 MHz radio frequency (RF) power supply was matched to the partially ionised gas load using an L-C network. During pulsed plasma deposition, the RF source was triggered by a signal generator and the pulse shape monitored with an oscilloscope (Tektronix Instruments). The power supply and pulse generator were custom built.

The steel container encasing the plasma chamber was internally lined with insulating material (Dalfratex) and fitted with an internal halogen lamp and thermostat. The monomer and chamber were heated to 50 °C, allowing monomer vapour pressure to rise to a level where plasma polymerization could occur.

Prior to each deposition, the apparatus was cleaned by scrubbing with detergent, rinsing in propan-2-ol, and then oven drying. At this stage the reactor was reassembled and evacuated to base pressure. Further cleaning

entailed running a continuous wave air plasma at 0.2 mbar and 40 W lasting 30 min. Next, silicon wafers, gold SPR chips or polytetrafluoroethylene strips (1.0 cm x 1.5 cm) were inserted into the centre of the reactor and the system pumped back to base pressure. NIPAAm vapour was introduced into the chamber at a pressure of 0.15 mbar for 5 min prior to plasma ignition. Film deposition conditions corresponded to a 35 W continuous wave burst varied from 20 - 100 μs (t_{on}), followed by an off-period (t_{off}) set at 2000 μs. Hence peak power set by the power supply and pulse generator was in the range of 0.35 W to 1.75 W, although actual power supplied to the plasma would be significantly less than this. Power density (power per unit volume) used for the deposition of PNIPAAm under these conditions was estimated to be in the range of 10 - 50 W/g depending on the duty cycle used. After the deposition, the RF generator and halogen lamp were switched off and the monomer allowed to purge through the system for a further 5 min. Finally the chamber was evacuated to base pressure and vented to atmospheric pressure.

3.3.2 Characterization of Poly(n-isopropylacrylamide) Films

Contact angle analysis on the pulsed plasma polymer NIPAAm films were carried out using a VCA2500XE video contact angle system (ASE Products), where 2.0 μl drops of deionized water were placed onto the surface and contact angles measured. Contact angle measurements were carried out at room temperature (20 °C) and at 40 °C where the sample was mounted onto a heated glass plate and temperature monitored with a thermocouple.

Plasma polymer film thicknesses were measured using a spectrophotometer nkd-6000 (Aquila Instruments Ltd). The transmittance-reflectance curves (350-1000 nm wavelength range) were fitted to a Cauchy material model using a modified Levenburg-Marquardt algorithm[46].

Chemical characterization of the deposited films was undertaken by X-ray photoelectron spectroscopy (XPS) using a VG ESCALAB II electron spectrometer equipped with an unmonochromated Mg $K_{\alpha 1,2}$ X-ray source (1253.6 eV) and a concentric hemispherical analyser. Photoemitted electrons were collected at a take-off angle of 30° from the substrate normal, with electron detection in the constant analyser energy mode (CAE, pass energy =

20 eV). The XPS spectra were referenced to the C(1s) peak at 285.0 eV and fitted with a linear background and equal full-width-at-half-maximum (fwhm) Gaussian components using Marquardt minimisation computer software[47].

Surface infrared spectroscopy was performed using a Perkin Elmer Spectrum One FTIR spectrometer equipped with a liquid nitrogen cooled MCT detector operating at 4 cm^{-1} resolution over the 700-4000 cm^{-1} range. The instrument was fitted with a reflection-absorption spectroscopy accessory (RAIRS) and a KRS-5 p-polariser with the reflection angle set to 66°.

3.3.3 Analysis with Surface Plasmon Resonance

For surface plasmon resonance (SPR) studies, NIPAAm films were deposited onto Biacore Sensor Chip Au (Biacore, Uppsala, Sweden). The substrates containing the poly-NIPAAm film were mounted in an SPR cartridge and placed inside a Biacore 1000 instrument for analysis. Adsorption of protein to the films was determined at temperatures of 25 °C and 36 °C.

The SPR protocol used for measuring the adsorption of proteins is as follows: i) flowing a solution of sodium dodecyl sulphate (+99% Sigma) (40 mM in buffer solution) over the surface for 3 mins and then rinsing with buffer solution for 10 min; ii) flowing buffer solution for 2 min, subsequently substituting the flow with protein solution (1 mg/ml in buffer) for 30 min; iii) allowing buffer solution to flow over the surface for an additional 10 min.

Flow rates employed for all experiments were 10 µl/min. The buffer solution comprised 0.01 M HEPES (4-(2-hydroxyethyl)-1-piperazinethanesulfonic acid), pH 7.4, 0.15 NaCl, 3 mM ethylenediaminetetraacetic acid, 0.005 % polyoxyethylenesorbitan surfactant. The two proteins used were fibrinogen (from bovine plasma) (Sigma) and lysozyme (from egg white), (Sigma).

After analyses of the film were complete, the chips were submersed for 30 min in a solution of 3 parts 99% sulphuric acid and 1 part 37% hydrogen peroxide (Aldrich) – "piranha solution" to allow complete removal of the polymer films.

3.3.4 Analysis with Fluorescence Microscopy

The fluorescent protein deployed in fluorescence microscopy experiments was fluoroscein isothiocyanate-labelled bovine serum albumin (FITC-BSA) (Fluka), 0.5 mg/ml in HBS-EP buffer[48]. Fluroscein isocyanate has an excitation wavelength of 495 nm and an emission wavelength of 520 nm.

Samples were soaked in FITC-BSA solution at two temperatures: 40 °C and 20 °C, and subsequently viewed with a fluorescence microscope. Background fluorescence counts for both ppNIPAAm and PTFE were recorded in order to accurately determine the level of fluorescence arising from the FITC-BSA.

The fluorescence images were recorded using an Olympus IX-71 inverted microscope equipped with a mercury lamp for UV-vis excitation. The excitation light was selected using a band-pass filter (UG-1) and reflected off a dichroic mirror (Comar Instruments, 475-BK shortwave reflecting) into the samples via a 10x lens (Olympus UPLFL). The fluorescence image was passed thorough a 520 nm cut off filter (Comar Instruments) and imaged using a slow-readout, cooled CCD camera (Starlight-Xpress HX-916), producing 650 x 500 pixel image which was transferred to a PC for analysis and archiving.

3.4 Results and Discussion

3.4.1 Analysis of Water Contact Angle

Varying the pulse duty cycle during the plasma deposition affects the hydrophobicity and hence water contact angle of the pulsed plasma polymerized n-isopropylacrylamide (ppNIPAAm) films. Duty cycle was adjusted until the films were as hydrophilic as possible without film removal at room temperature i.e. water contact angle is at a minimum, Figure 3.1. If the plasma "on time" is too low, the water droplet removes the film. A duty cycle of 60 μs on, 2000 μs off yields the lowest value of water contact angle (44°) without the ppNIPAAm film washing off. At this duty cycle, the balance of cross-linking and structural retention is such that the films are sufficiently hydrophilic yet robust. When the film temperature is raised to 40 °C, contact

angle is measured as 81°, exhibiting the change in properties of ppNIPAAm films with temperature.

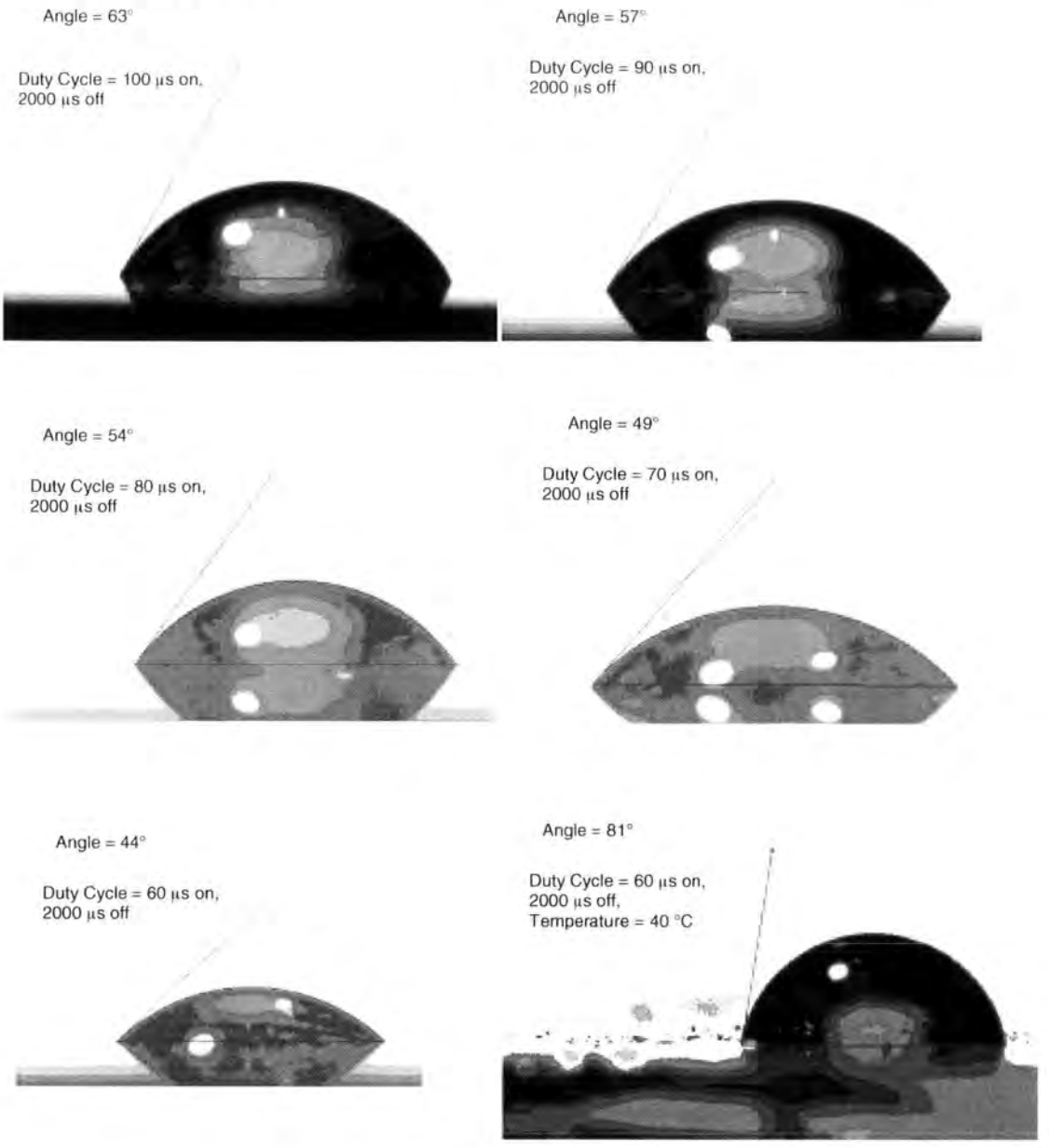

Figure 3.1: Variation of water contact angle on ppNIPAAm surfaces with varying pulse duty cycle and temperature (temperature = 20 °C, unless stated)

3.4.2 Analysis with X-ray Photolectron Spectroscopy

The stoichiometry of n-isopropylacrylamide pulsed plasma polymer (ppNIPAAM) films coincides with theoretical values, Table 3.2. Peak fitting of the high resolution C(1s) envelope reveals four different carbon environments, Figure 3.2; hydrocarbon (C_xH_y = 285.0 eV), carbon adjacent to a carbonyl group (C-C=O) = 285.70 eV) carbon attached to nitrogen (C-N = 285.95 eV) and carbon doubly bonded to oxygen within an amide group (N-C=O = 288.2 eV). The absence of any Si(2p) signals verifies homogeneous films of thickness greater than 2-5 nm.

Table 3.2: Elemental analysis of ppNIPAAm by XPS.

NIPAAm	Stoichiometry	%C	%O	%N	%Si
60/2000 µs Pulse duty cycle	Theoretical	75	12.5	12.5	0
	Experimental	74 ± 1	12 ± 1	14 ± 1	0

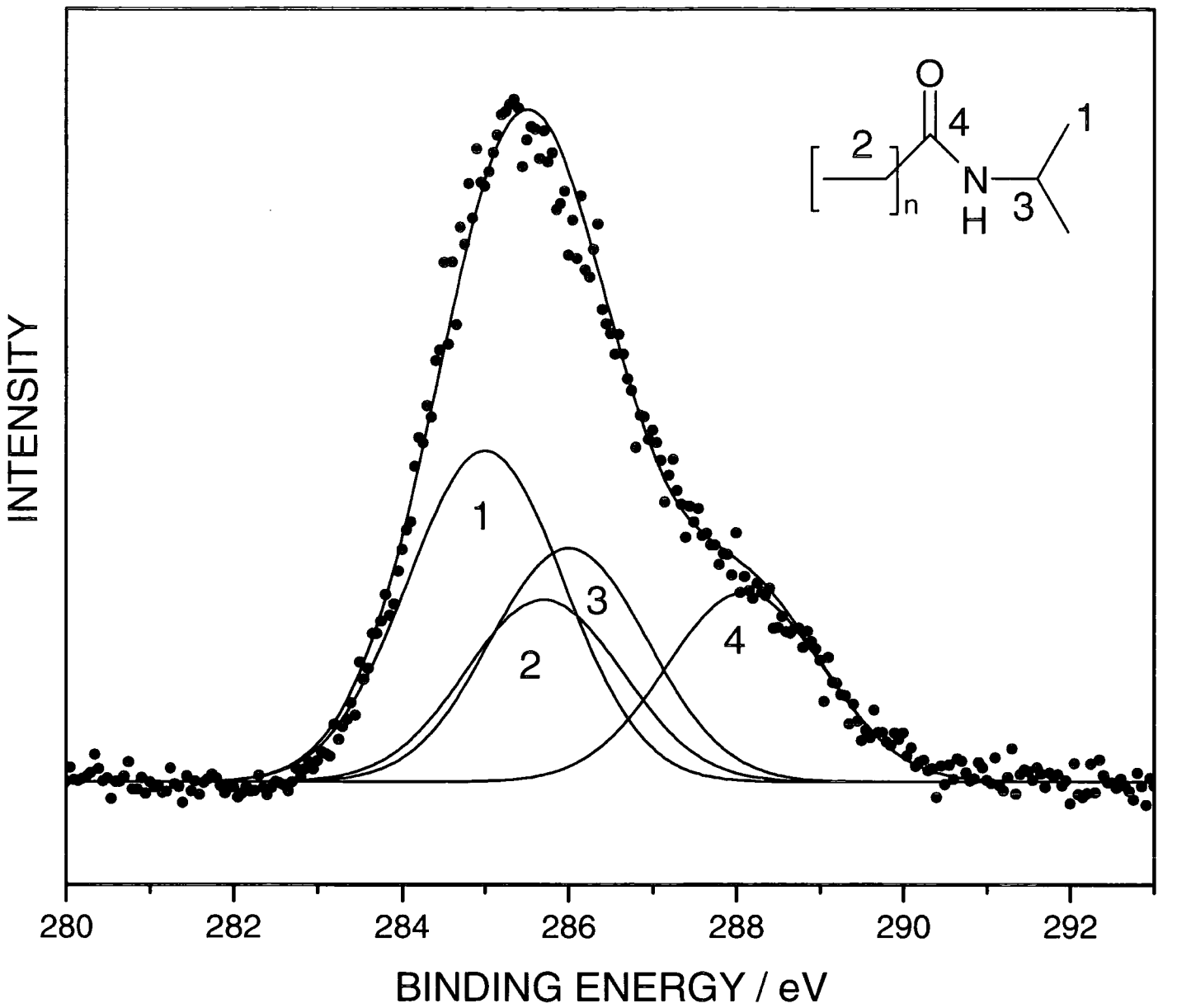

Figure 3.2: XPS C(1s) Envelope of pulsed plasma polymerized n-isopropylacrylamide.

3.4.3 Analysis with Fourier Transform Infrared Spectroscopy

Structural retention of ppNIPAAm layers on silicon is also authenticated using RAIRS, which detects characteristic absorptions such as the N-H stretch at 3300 cm^{-1} (A), the amide I stretch at 1660 cm^{-1} (C) and the amide II stretch at 1540 cm^{-1} (E), Figure 3.3(a) and (b), Table 3.3. Absence of the C=C stretch at 1630 cm^{-1} (D) in (b) corroborates NIPAAm polymerization.

Table 3.3: FTIR peak assignments for ppNIPAAm and NIPAAm monomer.

FTIR Absorption Peak	**Designation**	**ppNIPAAm**	**NIPAAm monomer**
A: 3300 cm^{-1}	N-H stretch	*	*
B: 2987-2833 cm^{-1}	CH_2 antisymmetric stretch	*	*
C: 1668-1641 cm^{-1}	Amide C=O stretch	*	*
D: 1630-1620 cm^{-1}	C=C double bond stretch		*
E: 1540cm^{-1}	Amide II stretch	*	*
F: 1475-1407 cm^{-1}	CH_2 scissor deformation	*	*

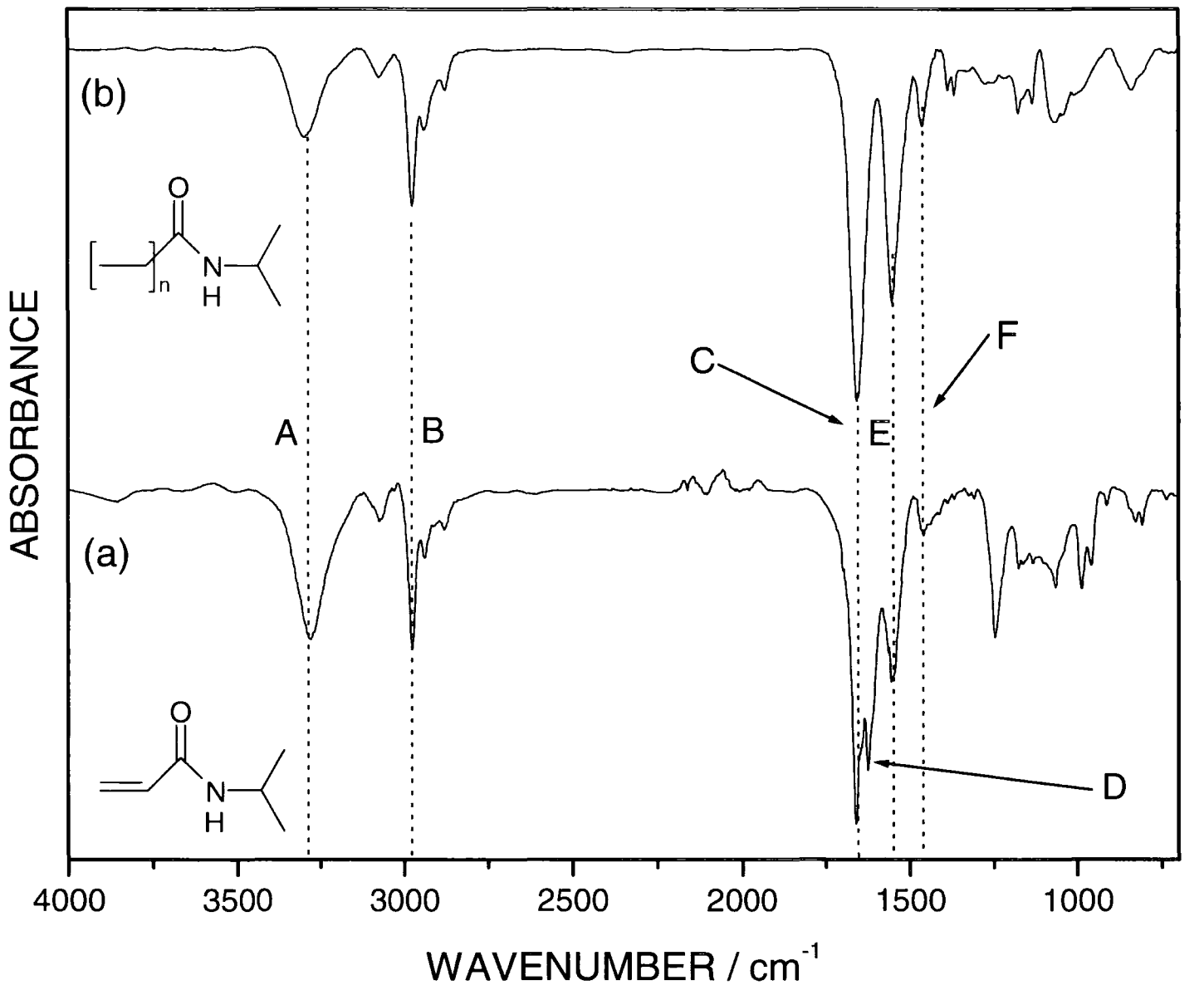

Figure 3.3: FTIR spectra of (a) n-isopropylacrylamide monomer, (b) pulsed plasma polymerized n-isopropylacrylamide.

3.4.4 Analysis with Surface Plasmon Resonance

In surface plasmon resonance, the refractive index of the medium being analyzed governs whether an evanescent wave can be produced. This is crucial for protein adsorption measurements to be carried out and requires film thicknesses on gold chips to be in the order of 20 - 30 nm. If the pulse duty cycle used is 60 µs on, 2000 µs off and power is set to 35 W, a plasma deposition time of 2 minutes yields ppNIPAAm film thicknesses of 25 nm as measured by reflectometry.

Figures 3.4, 3.5 and Table 3.4 detail the adsorption of fibrinogen and lysozyme on ppNIPAAm films. In the case of fibrinogen, an increase in adsorption of approximately tenfold is observed when the temperature of the films is increased from 25 °C (below the LCST) to 36 °C (above the LCST). In the case of lysozyme, the adsorption increased by a factor of approximately seven. Adsorption of both proteins at 36 °C is found to be fully reversible.

Table 3.4: SPR measurements of protein adsorption to ppNIPAAm surface with varying temperature.

Temperature	**Fibrinogen Adsorption (arbitrary units)**	**Lysozyme Adsorption (arbitrary units)**
25 °C	188 ± 110	28 ± 15
36 °C	1831 ± 295	183 ± 125

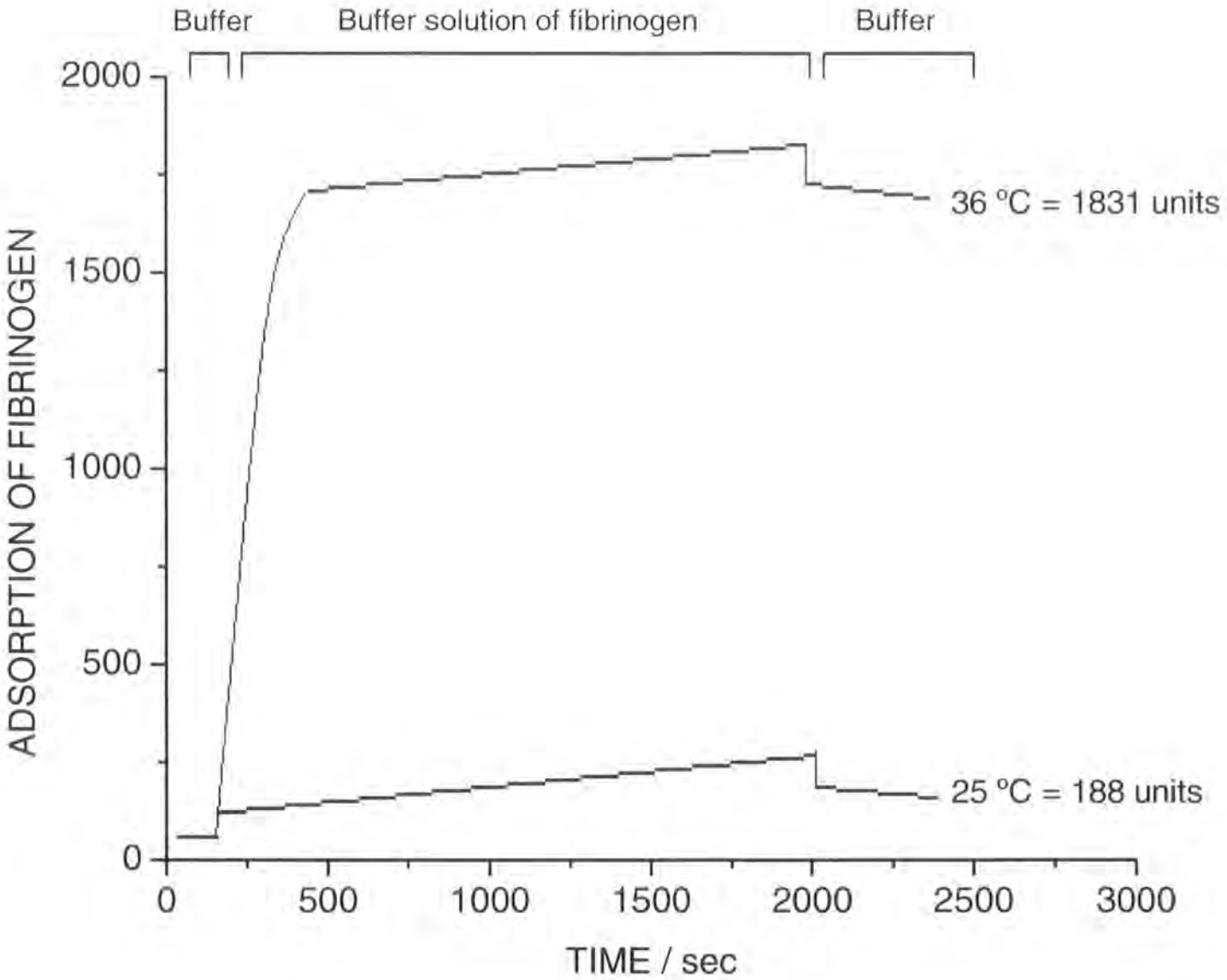

Figure 3.4: Diagram illustrating relative adsorption of fibrinogen to ppNIPAAm films at different temperatures determined by SPR (adsorption measured in arbitrary units).

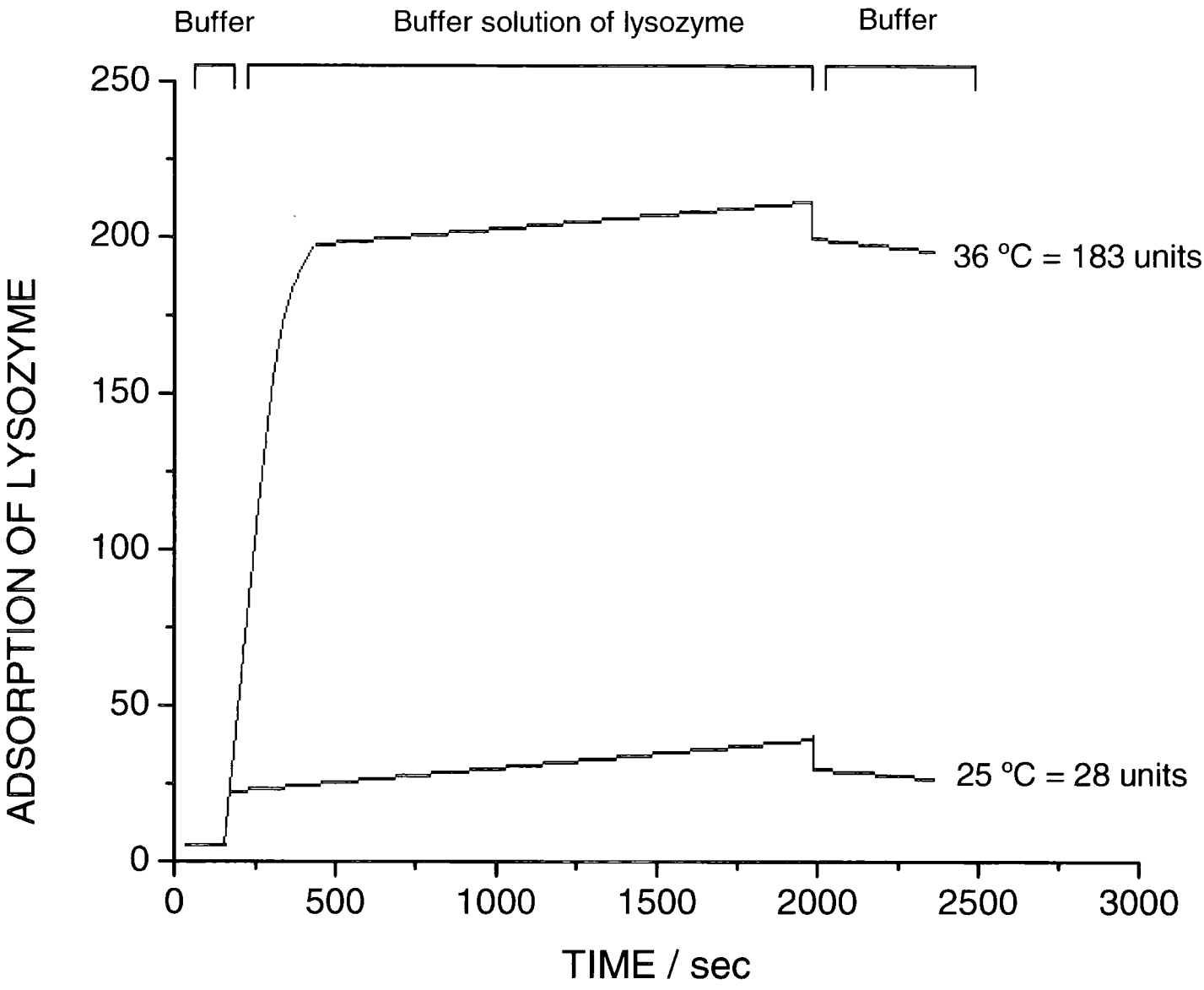

Figure 3.5: Diagram illustrating relative adsorption of lysozyme to ppNIPAAm films at different temperatures determined by SPR (adsorption measured in arbitrary units).

3.4.5 Analysis with Fluorescence Microscopy

Figure 3.6 displays a fluorescence image of ppNIPAAm arrays on a PTFE chip (100 μm squares separated by 20 μm) at 40 °C. The pulsed plasma polymerized n-isopropylacrylamide regions are found to exhibit a similar degree of fluorescence to the hydrophobic PTFE regions.

Figure 3.7 corresponds to the ppNIPAAm arrays at room temperature (20 °C). The contrast in fluorescence between the ppNIPAAm and PTFE regions is significantly more pronounced when the sample is cooled below the lower critical solution temperature of ppNIPAAm (32 °C).

Background fluorescence levels are measured to be 2,200. Fluorescence of PTFE and ppNIPAAm before exposure to FITC-BSA are found to be 5,000 and 6,000 arbitrary units respectively. Table 3.5 details levels of fluorescence measured within the various regions of the sample at differing temperatures. As found with surface plasmon resonance, adsorption of proteins at 40 °C is reversible. When the sample is cooled to 20 °C, fluorescence and hence protein adsorption is reduced by a factor of 7.5, which is relatively consistent with values obtained by SPR. The affinity of ppNIPAAm to different protein structures may vary, resulting in differences in adsorption measurements when a different adsorbate is used[29] e.g. albumin and fibrinogen. The affinity for protein adsorption of PTFE is found not to vary noticeably with temperature.

Table 3.5: Adsorption of FITC-BSA to PTFE-ppNIPPAAm array determined by fluorescence microscopy.

Mean Fluorescence (counts)		
	Squares (ppNIPAAm)	**Gaps (PTFE)**
Total Background Fluorescence	8,200	7,200
40 °C sample following exposure to FITC-BSA	29,850	34,044
minus background fluorescence	*21,650*	*26844*
20 °C sample following exposure to FITC-BSA	11,100	32,705
minus background fluorescence	*2,900*	*25,505*

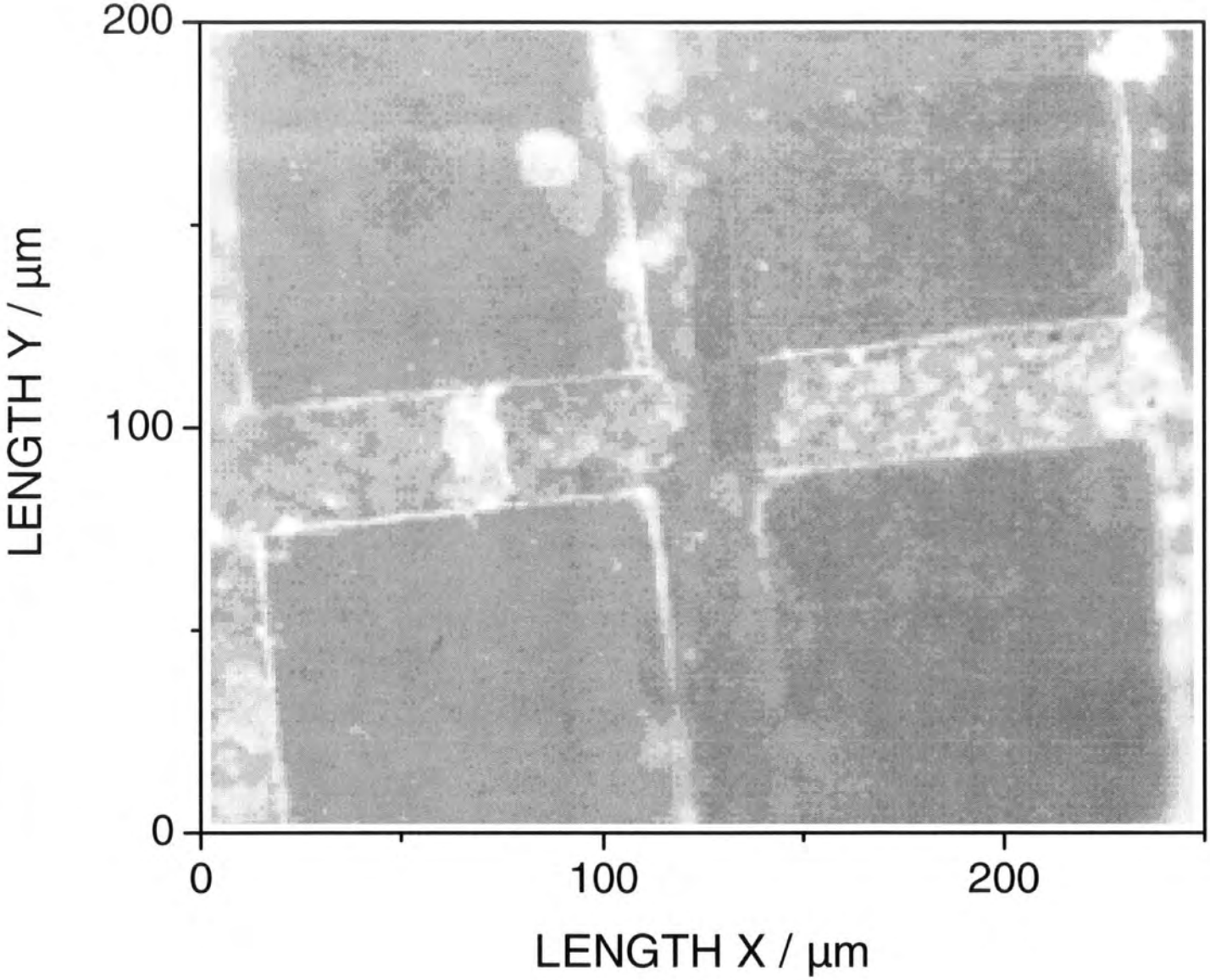

Figure 3.6: Fluorescence image of ppNIPAAm array reacted with FITC-BSA at 40 °C.

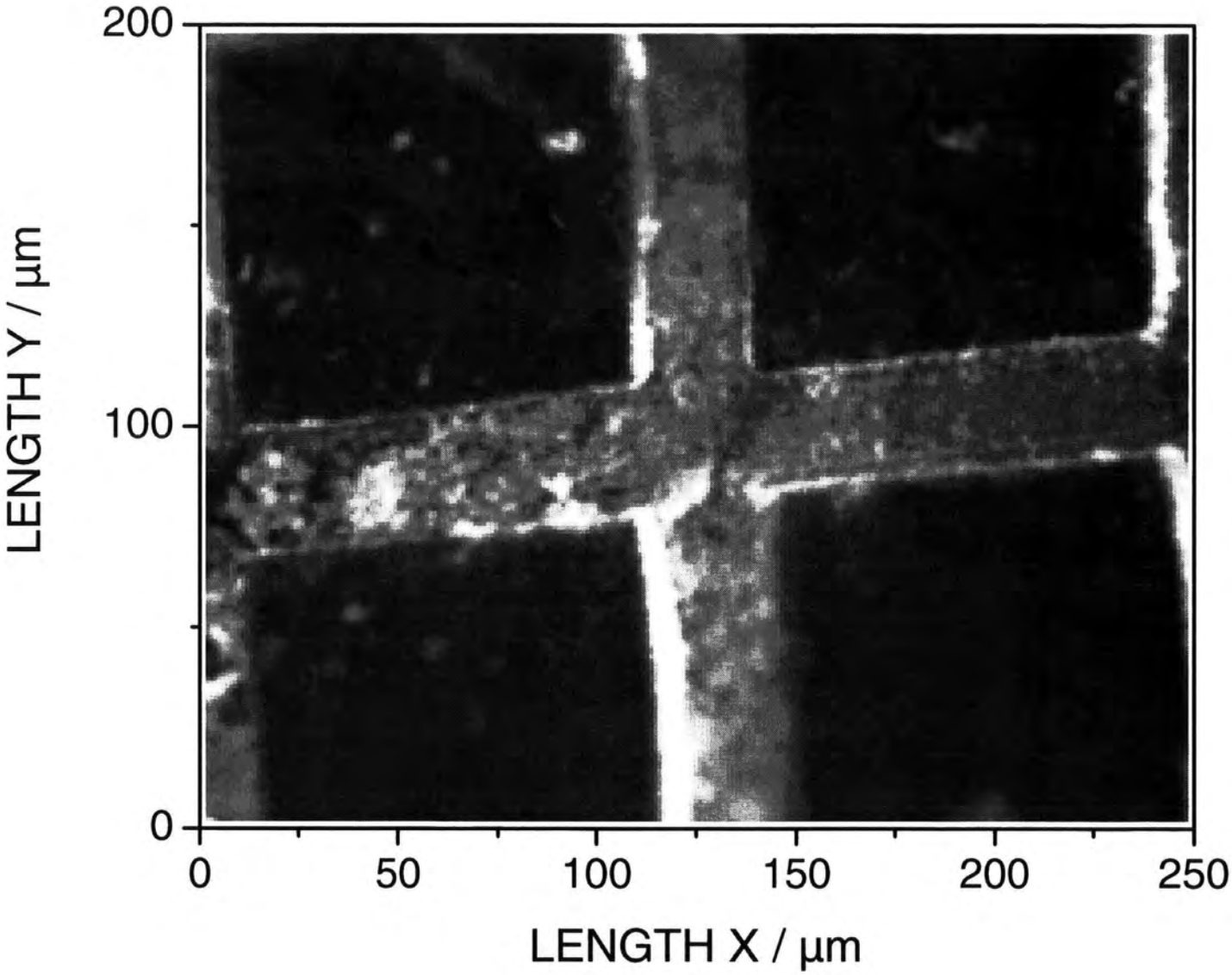

Figure 3.7: Fluorescence image of ppNIPAAm array reacted with FITC-BSA at 20 °C.

The fully reversible adsorption of proteins with temperature is a marked improvement on existing continuous wave methodologies. It is a consequence of a significant reduction in cross-linking within the ppNIPAAm structure, resulting in an increased degree of freedom of the polymer chains. This in turn, permits change in chain conformation to occur more effectively with temperature. The inherent response of pulsed plasma polymerized NIPAAm films leads to little or no trapping of protein molecules within the polymer matrix upon cooling to below the LCST.

This single step procedure has a strong potential for applications such as tissue engineering. Cells (which essentially consist of proteins) can be cultured on ppNIPAAm-coated surfaces at body temperature, preceding their removal which can be achieved by simply cooling the substrate to room temperature[22-24].

3.5 Conclusions

A substrate-independent, one step process for the deposition of well-defined, thermally responsive poly(n-isopropylacrylamide) films has been developed and successfully utilised as a "smart polymer" surface.

This has been a noticeable improvement on the existing continuous wave protocol due to the high level of structural retention, which has resulted in the fully reversible adsorption of proteins with temperature, which had not been achievable with previously deployed plasma deposition methods.

The apparent high level of control in protein affinity of these films with changing temperature along with a simplistic preparation process exemplifies their suitability in the cell culture and tissue engineering industries.

3.6 References

[1] Saunders, B. R.; Vincent, B., *Adv. Colloid Interface Sci.*, 80, **1999**, 1.

[2] Badiger, M. V.; Lele, A. K.; Bhalerao, V. S.; Varghese, S.; Mashelkar, R. A., *J. Chem. Phys.*, 109, **1998**, 1175.

[3] Chen, G. H.; Hoffman, A. S., *Nature*, 373, **1995**, 49.

[4] Heskins, M.; Guillet, J.E.; James, E., *J. Macromol. Sci., Chem.*, A2, **1968**, 1441.

[5] Snowden, M.; Murray, M.; Chowdry, B., *Chem. Ind.*, 15, **1996**, 531.

[6] Schild, H.G., *Prog. Polym. Sci.*, 17, **1992**, 163.

[7] Plate, N. A.; Lebedeva, T. L.; Valuev, L. I., *Polym. J.*, 31, **1999**, 21.

[8] Jeong, B.; Kim, S. W.; Bae, Y.H., *Adv. Drug. Deliv. Rev.*, 54, **2002**, 37.

[9] Huang, J.; Wang, X.; Chen, X.; Yu, X., *J. Appl. Polym. Sci.*, 89, **2003**, 3180.

[10] Plunkett, M. A.; Wang, Z.; Rutland, M. W.; Johannsmann, D., *Langmuir*, 19, **2003**, 6837.

[11] Kwon, O. H.; Kikuchi, A.; Yamato, M; Okano, T., *J. Biomed. Mater. Res.*, 50, **2000,** 81.

[12] Zhang, J.; Pelton, R.; Deng, Y., *Langmuir*, 11, **1995**, 2301.

[13] Chen, J.P.; Hoffman, A.S., *Biomaterials*, 11, **1990**, 631.

[14] Yoshida, R.; Uchida, K.; Kaneko, Y.; Sakai, K.; Kikuchi, A.; Sakurai, Y.; Okano, T., *Nature*, 374, **1995**, 240.

[15] Bae, Y. H.; Okano, T.; Kim, S. W.; *J. Polym. Sci. B.*, 28, **1990**, 923.

[16] Yoshida, R.; Sakai, K.; Okano, T.; Sakurai, Y., *Adv. Drug. Deliv. Rev.*, 11, **1993**, 85.

[17] Inoue, T.; Chen, G. H.; Hoffman, A. S.; Nakamae, K.; *J. Bioact. Compat. Polym.* 13, **1998**, 50.

[18] Aoki, T.; Nagao, Y.; Terada, E.; Sanui, K.; Ogata, N.; Yamada, N.; Sakurai, Y.; Kataoka, K.; Okano, T., *J. Biomater. Sci., Polym. Ed.*, 7, **1995**, 539.

[19] von Recum, H. A.; Kim, S. W.; Kikuchi, A.; Okuhara, M.; Sakuria, Y.; Okano, T., *J. Biomed. Mater. Res.*, 40, **1998**, 631.

[20] von Recum, H. A.; Kikuchi, A.; Okuhara, M.; Sakuria, Y.; Okano, T.; Kim, S. W., *J. Biomater. Sci. Polym.*, 9, **1998**, 1241.

[21] Yamoto, M.; Utsi=umi, M.; Kushida, A.; Konno, C.; Kikuchi, A.; Okano, T., *Tissue Eng.*, 7, **2001**, 473.

[22] Takezawa, T.; Mori, Y.; Yoshizato, K.; *Biotechnology*, 8, **1990**, 254.

[23] Yamada, N.; Okano, T.; Sakai, H.; Karikusa, F.; Sawasaki, Y.; Sakurai, Y., *Makromol. Chem. Rapid Commun.*, 11, **1990**, 571.

[24] Chen, G.; Ito, Y.; Imanishi, Y., *Biotechnol., Bioeng.*,53, 1997, 339.

[25] Stile, R. A.; Burghardt, W. R.; Healy, K.E., *Macromolecules*, 32, **1999**, 7370.

[26] Ellis, D. L.; Yannas, I. V., *Biomaterials*, 17, **1996**, 291.

[27] Stile, R. A.; Healy, K.E., *Biomacromolecules*, 3, **2002**, 591.

[28] Schmaljohann, D.; Oswald, J.; Jorgensen, B.; Nitschke, M.; Beyerlein, D.; Werner, C., *Polym. Mater. Sci. Eng.*, 89, **2003**, 255.

[29] Schmaljohann, D.; Oswald, J.; Jorgensen, B.; Nitschke, M.; Beyerlein, D.; Werner, C., *Biomacromolecules*, 4, **2003**, 1733.

[30] Hirata, I.; Okazaki, M.; Iwata, H., *Polymer*, 45, **2004**, 5569.

[31] Ito, Y.; Chen, G.; Guan, Y.; Imanishi, Y. *Langmuir*, 13, **1997**, 2756.

[32] Serizawa, T.; Matsukuma, D.; Nanameki, K.; Uemura, M.; Kurusu, F.; Akashi, M., *Macromolecules*, 37, **2004**, 6531.

[33] Liu, H.; Ito, Y., *J. Biomed. Mater. Res.*, 67, **2003**, 1424.

[34] Chen, G.; Imanishi, Y.; Ito, Y., *J. Biomed. Mater. Res.*, 42, **1998**, 38.

[35] Yamato, M.; Konno, C.; Utsumi, M.; Kikuchi, A.; Okano, T., *Biomaterials*, 23, **2002**, 561.

[36] Cunliffe, D.; Peters, V.; Smith, J. R.; Alexander, C., *Langmuir*, 19, **2003**, 2888.

[37] Balamurugan, S.; Mendez, S.; O'Brien, M.J.; Lopez, G.P., *Langmuir*, 19(7), **2003**, 2545.

[38] Harmon, M. E.; Jakob, T. A. M.; Frank, C., *Macromolecules*, 35, **2002**, 5999.

[39] Liang, L.; Feng, X.; Liu, J.; Fryxell, G. E., *Macromolecules*, 31, **1998**, 7845.

[40] Ohya, S.; Nakayama, Y.; Matsuda, T., *Biomacromolecules*, 2, **2001**, 856.

[41] Saitoh, T.; Sekino, A.; Hiraide, M., *Chem. Lett.*, 37, **2004**, 912.

[42] Ista, L. K.; Mendez, S.; Perez-Luna, V. H.; Lopez, G. P., *Langmuir*, 17, **2001**, 2552.

[43] Pan, Y. V.; Wesley, R. A.; Ratner, B. D. *Biomacromolecules*, 2, **2001**, 32.

[44] Ratner, B. D.; Cheng, X.; Wang, Y, Hanein, Y.; Bohringer, K. F., *Polymer Preprints,* 44, **2003**, 198.

[45] Cheng, X.; Wang, Y.; Hanein, Y.; Bohringer, K. F.; Ratner, B. D., J. Biomed. Mater. Res., 70, 2004, 159.

[46] Tabet, F. M.; McGahan, W.A.; *Thin Solid Films*, **2000**, 370, 122.

[47] Ninomiya, K.; Himai, Y.; Momose, A; Aoki, S.; Suzuki, K., *J. Vac. Sci. Technol.*, 9, 1991, 1244.

[48] Sharma, S.; Johnson, R. W.; Desai, T. A., *Appl. Surf. Sci.*, 206, **2003**, 218.

Chapter 4: Surface-initiated Aqueous-Phase Free Radical Polymerization of Acrylates and Acrylamides

4.1 Introduction

Free radical polymerization utilising initiators such as benzoyl peroxide[1] and azobisbutyronitrile[2, 3] (AIBN) has been extensively used to polymerize a wide range of vinyl monomers such as styrene[4], ethylene[5] and various acrylates[6, 7].

4.1.1 Mechanism of Free Radical-initiated Polymerization

Radical polymerization proceeds as according to the mechanism outlined in Scheme 4.1 where AIBN is employed as the initiator.

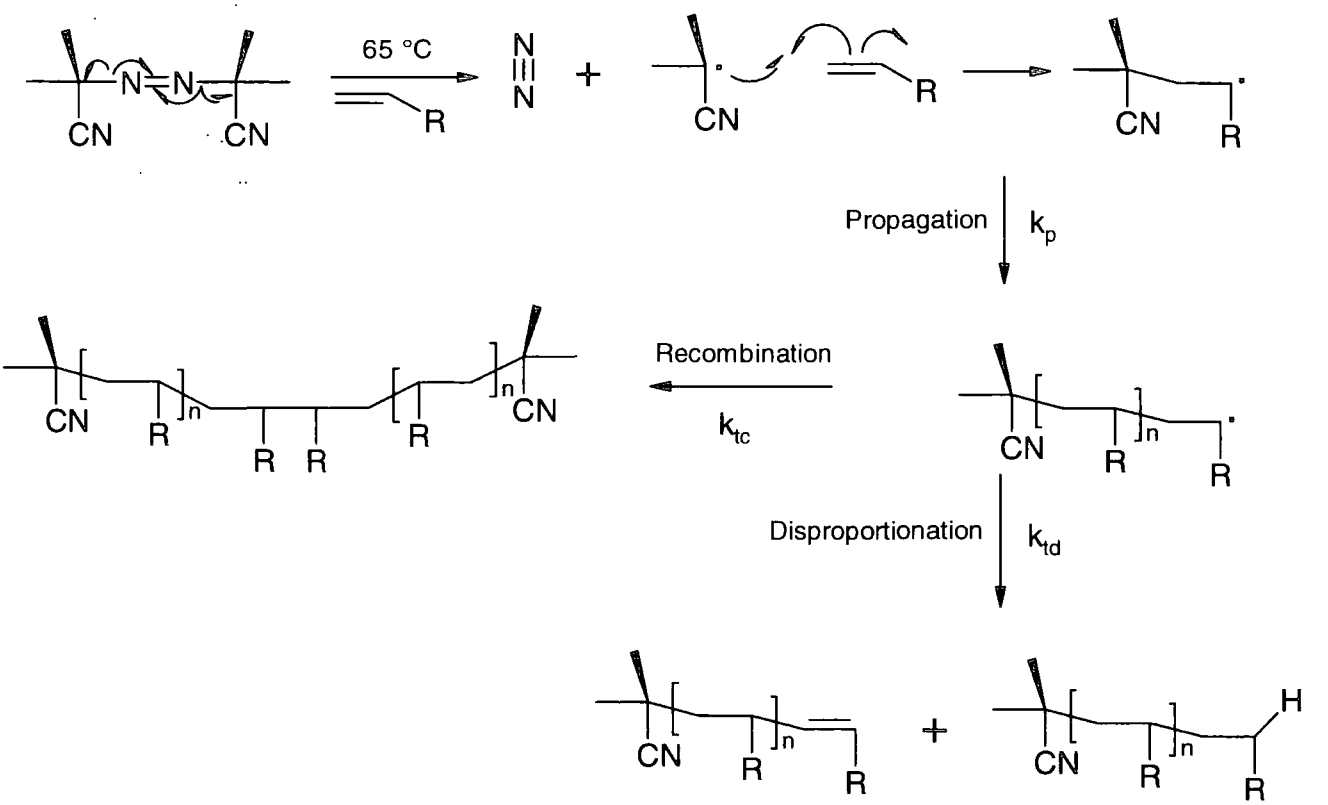

Scheme 4.1: Mechanism of free radical polymerization

Initiation and termination give rise to structural units that differ to those that constitute the bulk of the polymer chain. However when expressed as a weight fraction of the total material, they appear insignificant.

The major virtue of radical polymerization is that it can be undertaken under relatively undemanding conditions, exhibiting a tolerance to trace impurities. Additionally, high molecular weight polymers can be produced without having to remove stabilizers found in commercially available monomers and polymerization can proceed in aqueous media.

The propagation step in radical polymerization is very fast, for example propagation rate, k_p for styrene[8] is 2000 $Lmol^{-1}s^{-1}$. Rate of chain termination, k_{tc}, which can occur by the recombination of radicals is also very rapid[9]; $k_{tc} \sim 10^7$ $Lmol^{-1}s^{-1}$. Disproportionation, where a hydrogen atom is transferred between chains can also terminate chain growth[10]. Rate of polymer chain growth by free-radical polymerization can be described by Figure 4.1.

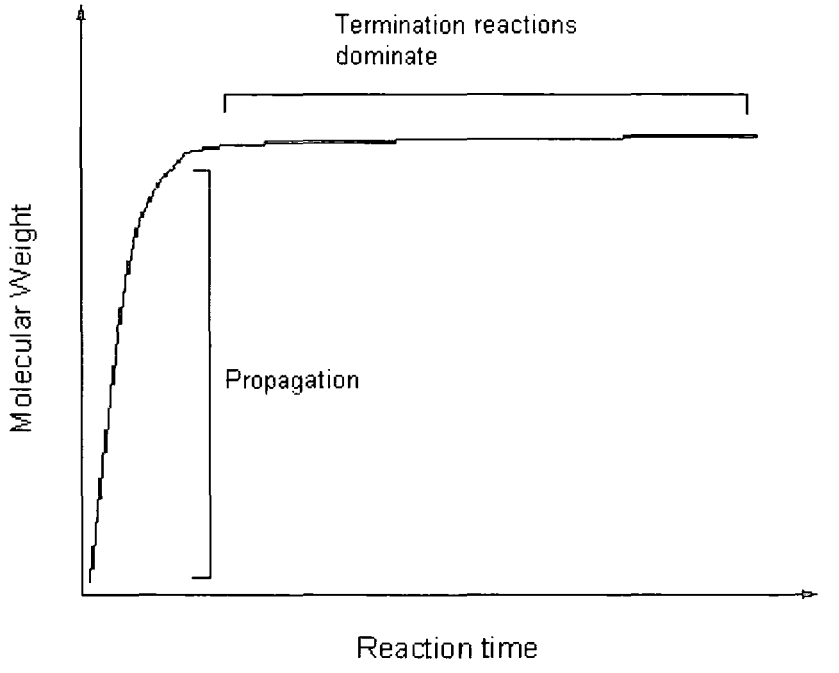

Figure 4.1: Molecular weight of polymer chains with reaction time.

Hence attaining a target molecular weight for polymer chains can be problematic due to the fact that chain termination reactions dominate as reaction time increases.

One notable complication in free radical polymerization is chain transfer. This can be described as a reaction between a propagating radical and a non radical constituent to produce a dead polymer chain and a radical capable of propagating a new chain, Scheme 4.2.

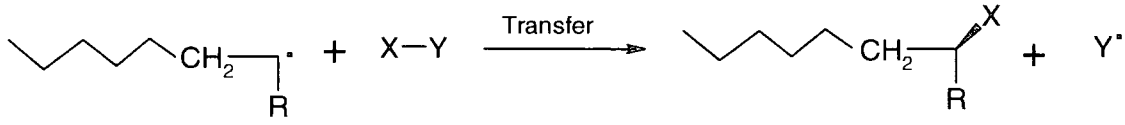

Scheme 4.2: Chain transfer during radical polymerization

Dialkyldiazene initiators such as AIBN are widely deployed in radical polymerization due to the fact they decompose into free radical groups at comparatively low temperatures (60-70 °C)[11]and have a low tendency towards chain transfer. Most dialkyldiazene initiators are symmetrical and generally tertiary with functionalities such as a cyano group to stabilize the incipient radical[12, 13, 14]. The proportion of useful radicals generated from AIBN is typically 50 - 70% in media of low viscosity (i.e. low conversion polymerizations). The main cause of inefficiency is the loss of radicals through self-reaction[15].

Molecular oxygen can present a hindrance towards free radical polymerization[16]. Media are usually thoroughly purged with inert gas such as nitrogen or outgassed to remove molecular oxygen present prior to polymerization. If these measures are not taken, oxygen can become involved in and complicate initiation processes. In the case of AIBN, the cyanoisopropyl radical reacts with molecular oxygen to form an alkyl-peroxy radical[17]. This is then able to abstract hydrogen from monomers or polymers to form potentially reactive hydroperoxides and new species that can themselves initiate polymerization, cause chain transfer and hence further complications, Scheme 4.3.

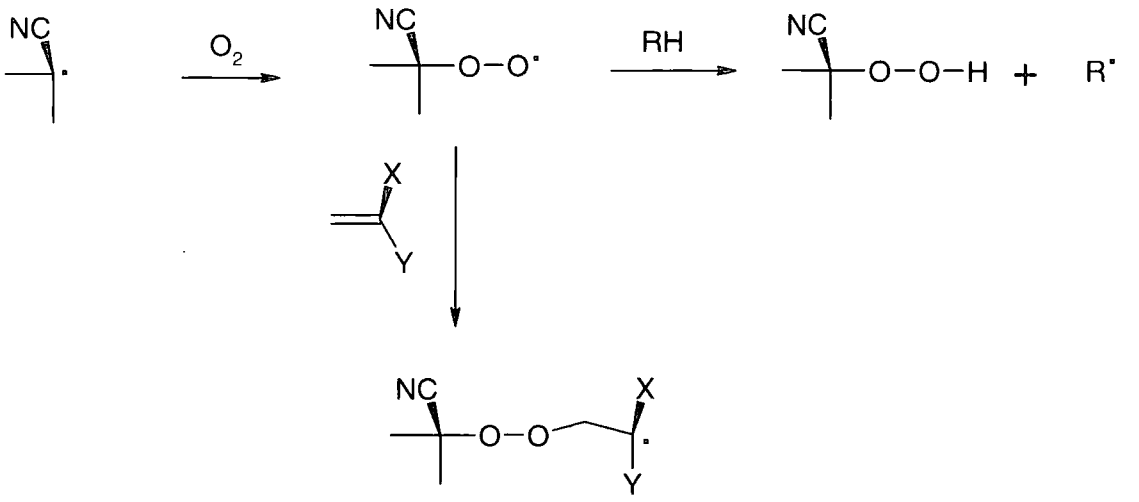

Scheme 4.3: The effects of molecular oxygen on radical polymerization.

4.1.2 Free Radical-initiated Polymerization from Surfaces

Free radical initiators, namely AIBN analogues, have been successfully adhered to surfaces by a variety of methods. These include the formation of self assembled monolayers (SAMs) on gold with carboxylic acid functionalities[18] that can be subsequently activated with Woodward's reagent[19] or pentafluorophenol[20] to permit attachment of 2,2'-azobis(2-amidinopropane) hydrochloride. Further strategies include azo initiators functionalized with acid groups such as 4,4-azobis(4-cyano-pentanoic acid) and 4,4-azobis(4-cyanovaleric acid) that can be grafted to surface-confined amino or halogen moieties tailored to silica substrates[21, 22, 23], carbon[24], polypeptide microcapsules[25], monolithic polymer discs[26, 27] and plasma-activated polyamide[28].

Surface properties such as wetting, biocompatibility and adhesion can be easily controlled from modification by surface-grafted polymers. Polymeric films of this nature have been extensively employed for applications such as food packaging, microelectronic components[29, 30] and biocompatible coatings[31, 32].

4.2 Aims

The objectives underlying this work are the surface attachment of a free radical initiator followed by surface-initiated radical polymerization. By employing pulsed plasma polymerization of glycidyl methacrylate (GMA) and its reactivity towards amines, an amine-terminated AIBN analogue such as 2,2'-azobis(2-amidinopropane) can be grafted to a substrate surface in two reaction steps, Scheme 4.4. This improves on previously described methods that require additional reaction steps and are limited by substrate-specific chemistries.

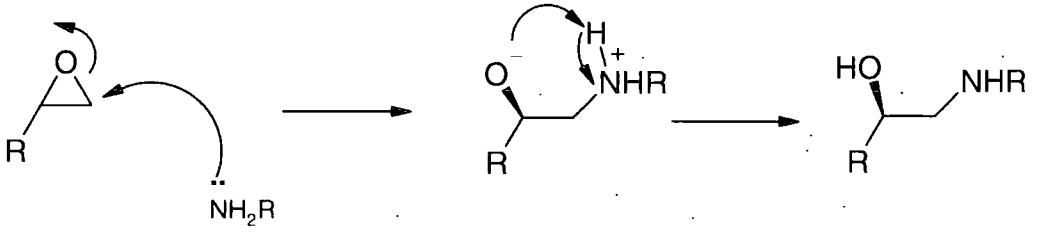

Scheme 4.4: Reaction mechanism for amination of epoxides.

Surface-initiated free radical polymerization of monomers such as acrylates and acrylamides can then be undertaken in aqueous media, Scheme 4.5. This method can be employed to generate arrays of grafted polymer chains, exemplifying the versatility of this method for a variety of applications.

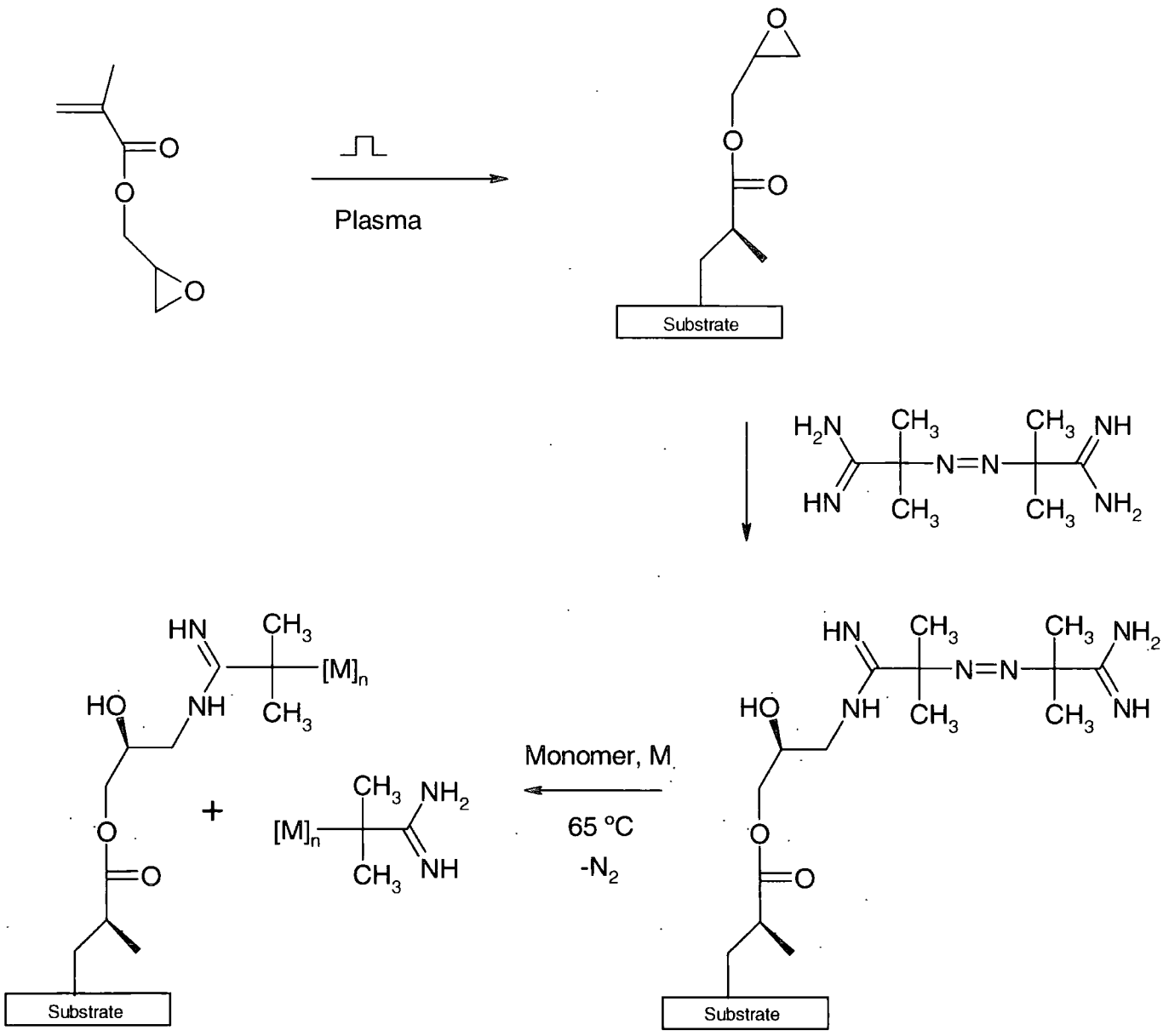

Scheme 4.5: Surface retention of poly(glycidyl methacrylate) followed by functionalization with amine-terminated azo-initiator and subsequent free radical polymerization.

4.3 Experimental

4.3.1 Preparation of Initiator Surface

Glycidyl methacrylate (97% purity, Aldrich) was loaded into a sealable glass tube, followed by further purification using several freeze-pump-thaw cycles to remove adsorbed gases. Pulsed plasma polymerization of the precursor was undertaken in a cylindrical glass reactor (4.5 cm diameter, 460 cm^3 volume, 2 x 10^{-3} mbar base pressure, leak rate 1.4 x 10^{-9} mol/s) enclosed in a Faraday cage and surrounded by a copper coil (4 mm diameter, 10 turns, located 15 cm away from the precursor inlet). The chamber was evacuated using a 30 L min^{-1} rotary pump attached to a liquid nitrogen cold trap, whilst monitoring the system pressure with a Pirani gauge. All fittings were grease-free. The output impedance of a 13.56 MHz radio frequency (RF) power supply was matched to the partially ionised gas load using an L-C network. During pulsed plasma deposition, the RF source was triggered by a signal generator and the pulse shape monitored with an oscilloscope.

Prior to each deposition, the apparatus was cleaned by scrubbing with detergent, rinsing in propan-2-ol, and then oven drying. At this stage the reactor was reassembled and evacuated to base pressure. Further cleaning entailed running a continuous wave air plasma at 0.2 mbar and 40 W lasting 30 min. Next, silicon wafers or polytetrafluoroethylene strips (1.0 cm x 1.5 cm) were inserted into the centre of the reactor and the system pumped back to base pressure. Glycidyl methacrylate vapour was introduced into the chamber at a pressure of 0.15 mbar for 5 min prior to plasma ignition. Film deposition conditions corresponded to a 20 W continuous wave bursts lasting 20 μs (t_{on}), followed by an off-period (t_{off}) set at 20,000 μs[33]. After the deposition, the RF generator was switched off and the monomer allowed to purge through the system for a further 5 min. Finally the chamber was evacuated to base pressure and vented to atmospheric pressure.

The pulsed plasma polymerized glycidyl methacrylate (ppGMA) coated substrates were immersed in a 0.1 M aqueous solution of 2,2'-azobis(2-

amidinopropane) hydrochloride (VAzo) (99%, Aldrich), 3.0 M sodium chloride (99.9%, Sigma) and 0.5 M sodium citrate dehydrate (99%, Aldrich) (pH adjusted to 4.5 with citric acid monohydrate (99%, Aldrich)) for 16 hours before being washed in deionized water and dried in a stream of nitrogen.

4.3.2 Free Radical Polymerization

The ppGMA-VAzo films were submersed in a 1.0 M aqueous solution of either n-isopropylacrylamide (NIPAAm), (98% Aldrich) or methylmethacrylate (99%, Aldrich), outgassed using several freeze thaw cycles to remove oxygen and heated at 65 °C for 16 hours in a silicone oil bath. The films were then removed and washed in deionized water.

Control experiments involved attempting free radical polymerization of n-isopropylacrylamide with pulsed plasma polymerized GMA films minus VAzo functionalization.

Film characterization was undertaken with X-ray photoelectron spectroscopy, Fourier transform infrared spectroscopy and reflectometry procedures in accordance with those outlined in chapter 3.

4.3.3 Formation of Poly(n-isopropylacrylamide) Arrays

Arrays of free radical polymerized NIPAAm were formed by plasma depositing GMA through a nickel grid (200 mesh, 200 μm holes separated by 20 μm) embossed onto 1.0 x 1.0 cm squares of polytetrafluoroethylene (PTFE). This was followed by the removal of the grid and submersion of the ppGMA-coated PTFE squares in the aqueous VAzo solution. After washing in deionized water, the VAzo-derivatized PTFE squares were subjected to free radical polymerization of NIPAAm.

The arrays were tested for thermal response and protein adsorption by immersion in a solution of fluoroscein isothiocyanate-labelled bovine serum albumin (FITC-BSA) (Fluka), 0.5 mg/ml in HBS-EP buffer at temperatures of 20 °C and 40 °C. The films were subsequently rinsed in a buffer solution of the

corresponding temperature and viewed with fluorescence microscopy (see chapter 3 for specifications).

4.4 Results and Discussion

4.4.1 Analysis with X-ray Photoelectron Spectroscopy.

Elemental composition of pulsed plasma polymerized glycidyl methacrylate (ppGMA) determined by XPS, coincides with theoretical values, Table 4.1. The high resolution XPS C(1s) envelope of ppGMA, Figure 4.2(a), exhibits five different carbon environments: carbon bonded to hydrogen (C_xH_y = 285.0 eV), carbon adjoining a carbonyl group (C-C=O = 285.7 eV), carbon bonded to oxygen (C-O = 286.45 eV), carbon in an epoxide group (binding energy = 287.2 eV) and carbon within a carbonyl group (C=O = 289.1 eV)[34]. Absence of any Si(2p) signals authenticates homogeneous films of thickness greater than 2-5 nm.

Stoichiometric analysis of ppGMA reacted with 2,2'-azobis(2-amidinopropane) hydrochloride (VAzo) shows that approximately 25% of the epoxide groups within a 2-5 nm penetration depth had reacted with amine groups, thus tailoring the free radical initiator to the surface, Table 4.1.

Elemental analysis of the poly(n-isopropylacrylamide) (PNIPAAm) films is in good agreement with the theoretical values. Four carbon environments are observed with XPS: carbon bonded to hydrogen (C_xH_y = 285.0 eV), carbon adjacent to a carbonyl group (C-C=O = 285.7 eV), carbon bonded to nitrogen (C-N = 285.95 eV) and carbonyl carbon within an amide group (C=O = 288.2 eV), Figure 4.2b.

Stoichiometry measurements of the poly(methylmethacrylate) (PMMA) layer corroborate predicted values, Table 4.1. The absence of a nitrogen signal indicates a homogeneous film of PMMA polymer chains within a 2-5 nm penetration depth. The XPS C(1s) envelope details four different carbon environments characteristic of PMMA: carbon bonded to hydrogen (C_xH_y = 285.0 eV), carbon adjacent to a carbonyl group (C-C=O = 285.7 eV), carbon bonded to

oxygen (C-0 = 286.45 eV) and carbonyl carbon within an ester group, (N-C=O = 289.1 eV), Figure 2.2c.

Table 4.1: Elemental composition of ppGMA, ppGMA-VAzo and polymer films determined by XPS.

Surface Coating		**%C**	**%O**	**%N**
ppGMA	Theoretical	70	30	-
	Experimental	70	30	-
ppGMA-VAzo	Theoretical (assuming 100% of ppGMA reacts with VAzo)	62.5	12.5	25
	Experimental	63	25	12
Free radical-polymerized n-isopropylacrylamide	Theoretical	75	12.5	12.5
	Experimental	74	13	13
Free radical-polymerized methylmethacrylate	Theoretical	72	28	0
	Experimental	73	27	<0.1

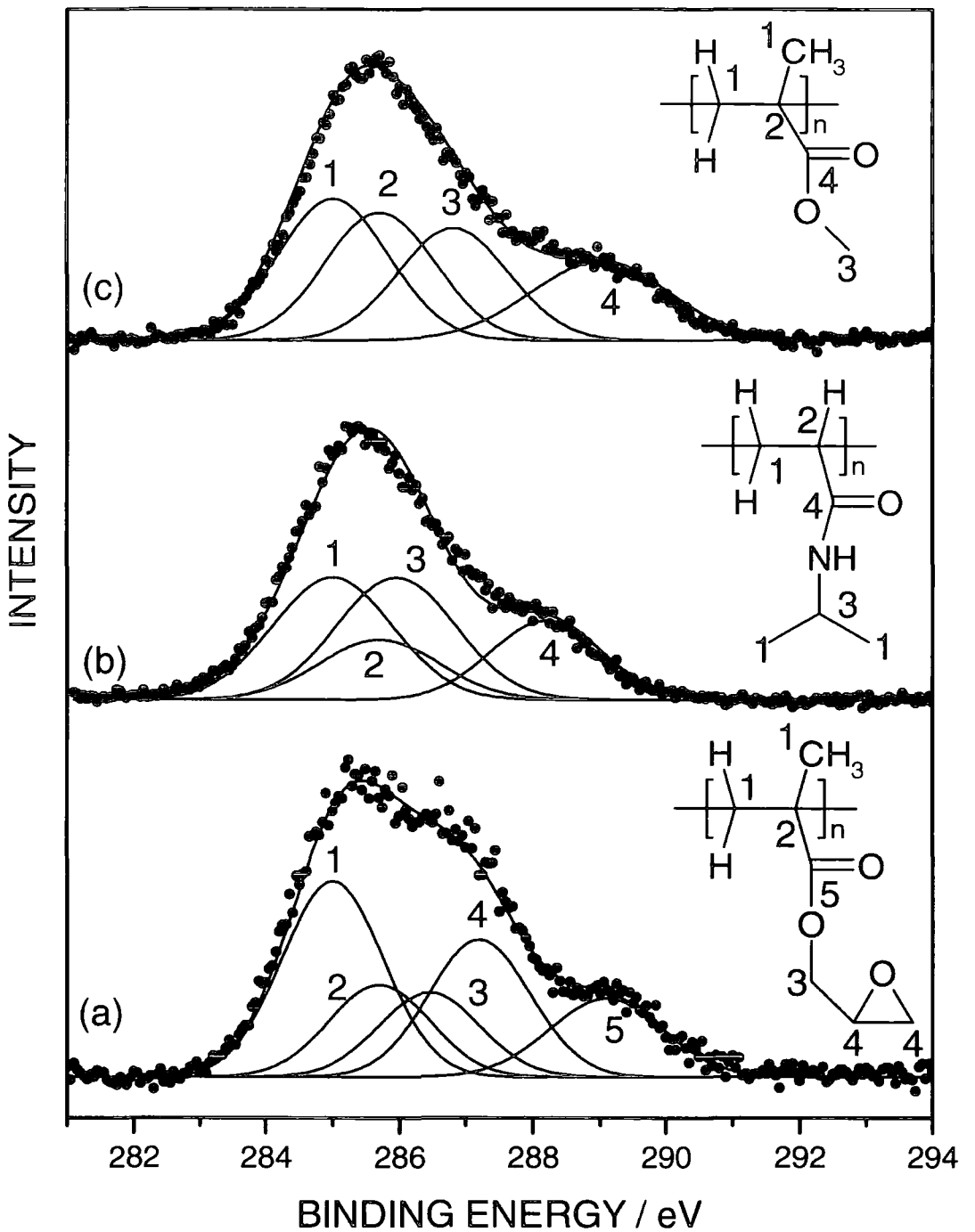

Figure 4.2: XPS C(1s) envelope of (a) pulsed plasma polymerized glycidyl methacrylate, (b) free radical-polymerized n-isopropylacrylamide, (c) free radical-polymerized methylmethacrylate.

4.4.2 Analysis with Fourier Transform Infrared Spectroscopy.

FTIR spectra authenticate structural retention of poly(glycidyl methacrylate) functionalities in the pulsed plasma polymer layer by the detection of signature absorptions such as epoxide stretches at 840 and 908 cm^{-1} and the carbonyl stretch at 1730 cm^{-1}, Table 4.2, Figure 4.3 (a) and (b). Absence of the C=C stretch at 1630 cm^{-1} confirms that polymerization has occurred. Structural retention of 2,2'-azobis(2-amidinopropane) is also corroborated by the presence of amine stretches at 3300 cm^{-1} and 1600 cm^{-1} and the C-N stretch at 1670 cm^{-1}, Figure 4.3 (c) and (d).

Further analysis with FTIR-RAIRS verifies the growth of PNIPAAm chains. The characteristic amide bands at 1680 cm^{-1} and 1540 cm^{-1} are observed in addition to the carbonyl peak at 1730 cm^{-1}, representative of the ppGMA layer, Figure 4.4 (e) and (f). Due to obvious structural similarities, FTIR-RAIRS cannot effectively distinguish between the pulsed plasma polymerized PGMA layer and the PMMA polymer chains, due to many of the signature peaks being shared by both polymers, Figure 4.4 (g) and (h). The presence of PMMA chains was corroborated by analysis with XPS and by a significant increase in film thickness (+ 70 nm) following polymerization.

Control experiments reveal no structural retention of poly(n-isopropylacrylamide) or discernible increase in film thickness, verifying the VAzo functionality is responsible for polymer chain growth from the surface.

Table 4.2: FTIR peak assignments.

Designation	GMA	ppGMA	ppGMA-VAzo	VAzo	NIPAAm	ppGMA-VAzo-NIPAAm	MMA	ppGMA-VAzo-MMA
A: N-H stretch, 3250 - 3300 cm^{-1}			*	*	*	*		*
B: CH_2 stretch, 2930 cm^{-1}	*	*	*		*	*	*	*
C: C=O ester stretch, 1730 cm^{-1}	*	*	*			*	*	*
D: C=N stretch, 1660 cm^{-1}			*	*				
E: Amide C=O stretch, 1680 cm^{-1}					*	*		
F: C=C stretch, 1630 cm^{-1}	*				*		*	
G: NH_2 deformation, 1600 cm^{-1}			*	*				
H: Amide (II) stretch, 1540 cm^{-1}					*	*		
I: Epoxide ring breathing, 1253 cm^{-1}	*	*	*			*		*
J: Epoxide antisymmetric stretch, 908 cm^{-1}	*	*	*			*		*
K: Epoxide symmetric stretch stretch, 840 cm^{-1}	*	*	*			*		*

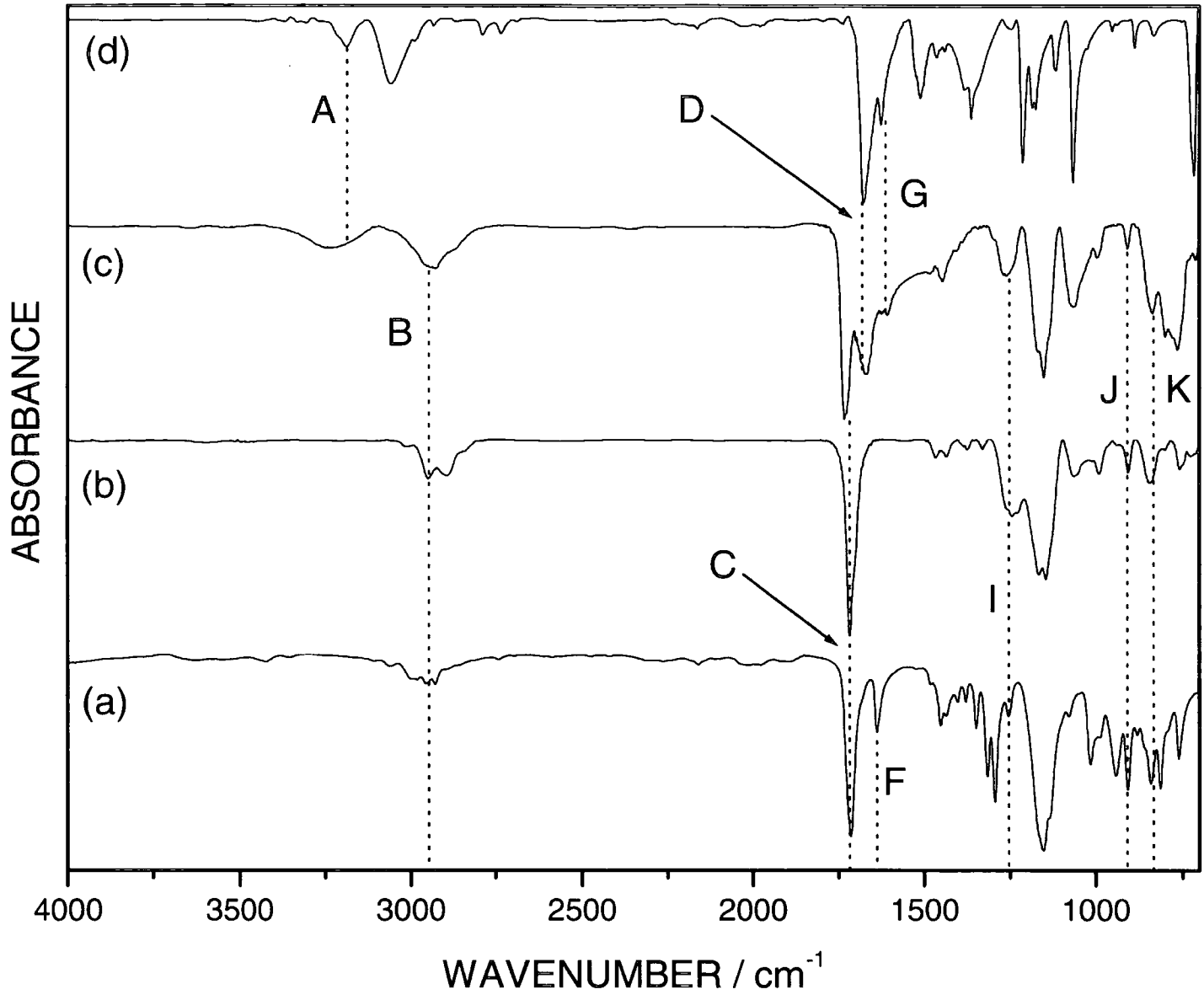

Figure 4.3: FTIR spectra of (a) glycidylmethacrylate monomer, (b) pulsed plasma-polymerized glycidyl methacrylate, (c) pulsed plasma-polymerized glycidyl methacrylate reacted with 2,2'-azobis(2-amidinopropane) hydrochloride, (d) 2,2'-azobis(2-amidinopropane) hydrochloride.

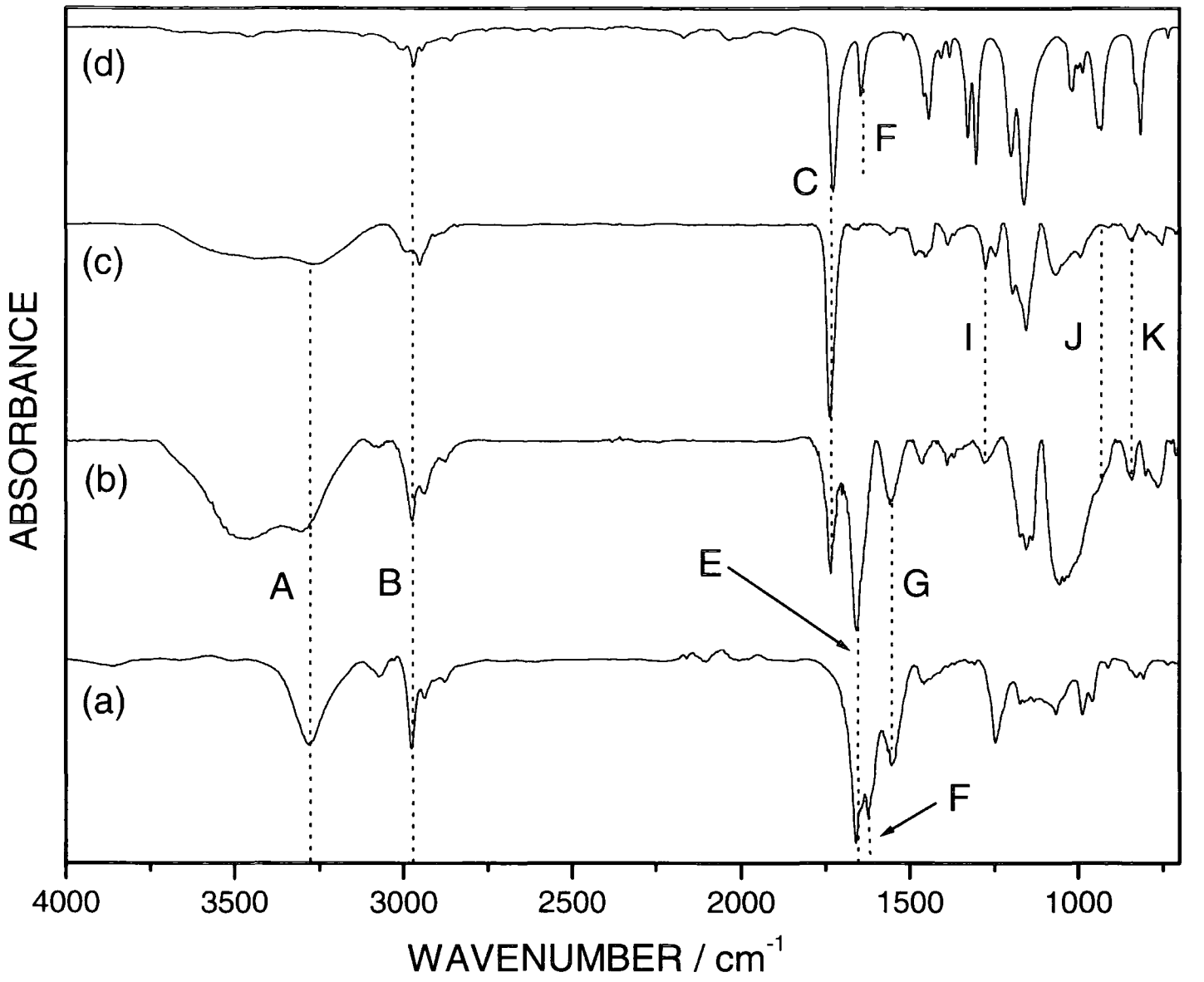

Figure 4.4: FTIR spectra of (a) n-isopropylacrylamide monomer, (b) free radical-polymerized n-isopropylacrylamide, (c) free radical-polymerized methylmethacrylate, (d) methylmethacrylate monomer.

4.4.3 Analysis of PNIPAAm films with Fluorescence Microscopy

The versatility of this method of surface-induced polymerization can be demonstrated by the formation of microscopic arrays of well-defined polymers. Figure 4.5 displays a fluorescence image of ppNIPAAm squares on PTFE strips (100 μm squares separated by 10 μm) at 20 °C. Due to the inherent resistance to adsorption of proteins exhibited by both PNIPAAm (below lower critical solution temperature) and the inertness of PTFE, the fluorescence signal is most pronounced around the edges of the PNIPAAm squares. This is attributable to residual traces of exposed ppGMA, which has a greater affinity to protein adsorption. Figure 4.6 corresponds to the PNIPAAm arrays at 40 °C. When heated above the lower critical solution temperature (32 °C), PNIPAAm becomes susceptible to protein adsorption (Chapters 3 and 7) and hence fluorescence can now be clearly observed in these regions.

Background fluorescence levels for the PNIPAAm squares and the PTFE gaps were measured to be 9,500 and 7,000 arbitrary units respectively. Table 4.3 details levels of fluorescence measured within the various regions of the sample at differing temperatures. It can be seen that the fluorescence and hence adsorption of FITC-BSA protein within ppNIPAAm regions is a factor of 6 – 7 times higher at 40 °C than at 20 °C, which is in excellent agreement with values determined for pulsed plasma polymerized NIPAAm, Chapter 3. Adsorption of FITC-BSA for PTFE is observed not to vary noticeably with temperature, verifying its relative inertness.

Table 4.3: Adsorption of FITC-BSA to PNIPPAAm array using fluorescence microscopy.

	Mean Fluorescence (counts)	
	Squares (PNIPAAm)	**Gaps (PTFE)**
Background Fluorescence	9,500	7,000
20 °C sample	12,390	10,360
minus background fluorescence	*2,890*	*3,360*
40 °C sample	28,240	10,725
minus background fluorescence	*19,240*	*3,725*

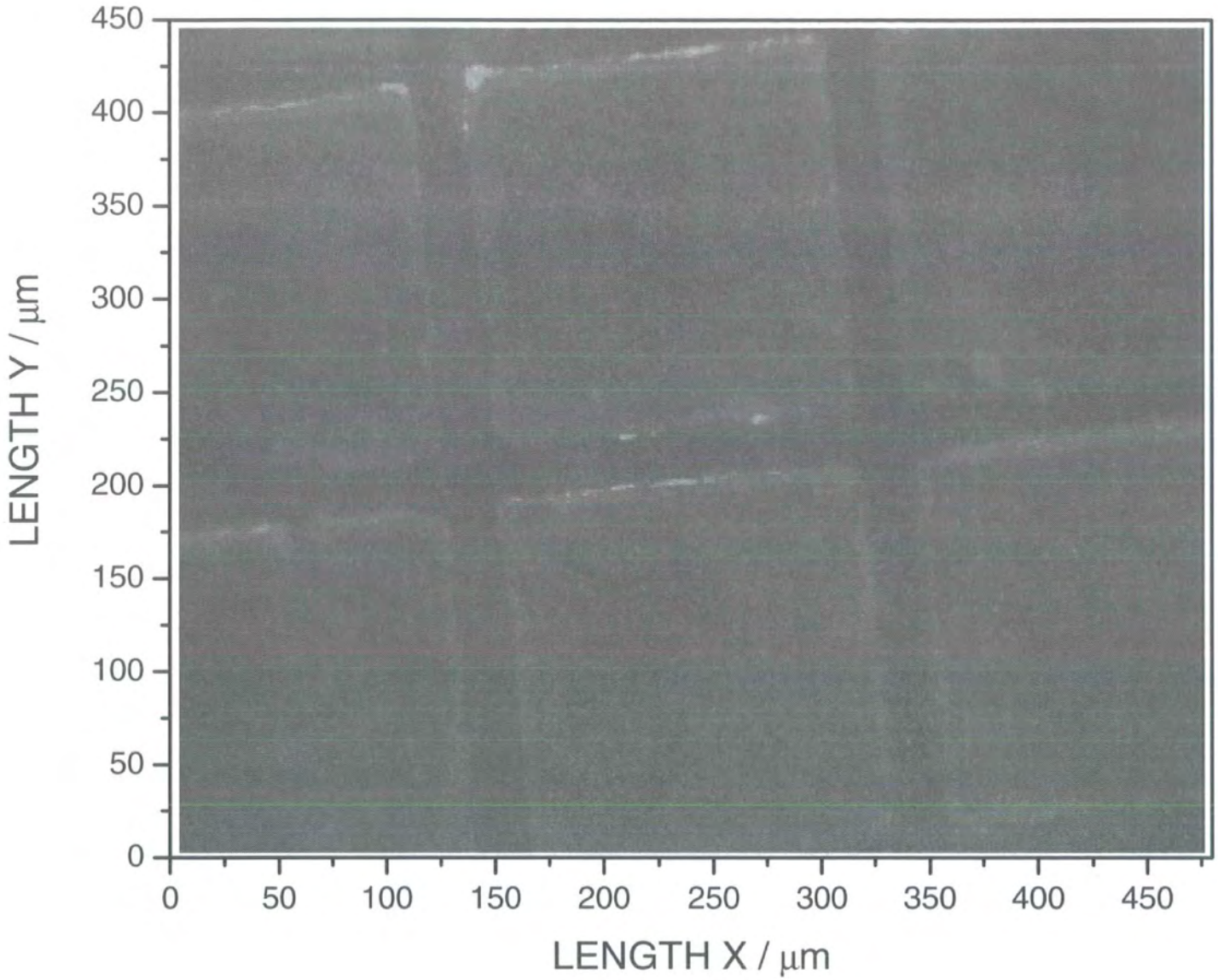

Figure 4.5: Fluorescence image of PNIPAAm array at 20 °C following exposure to FITC-BSA.

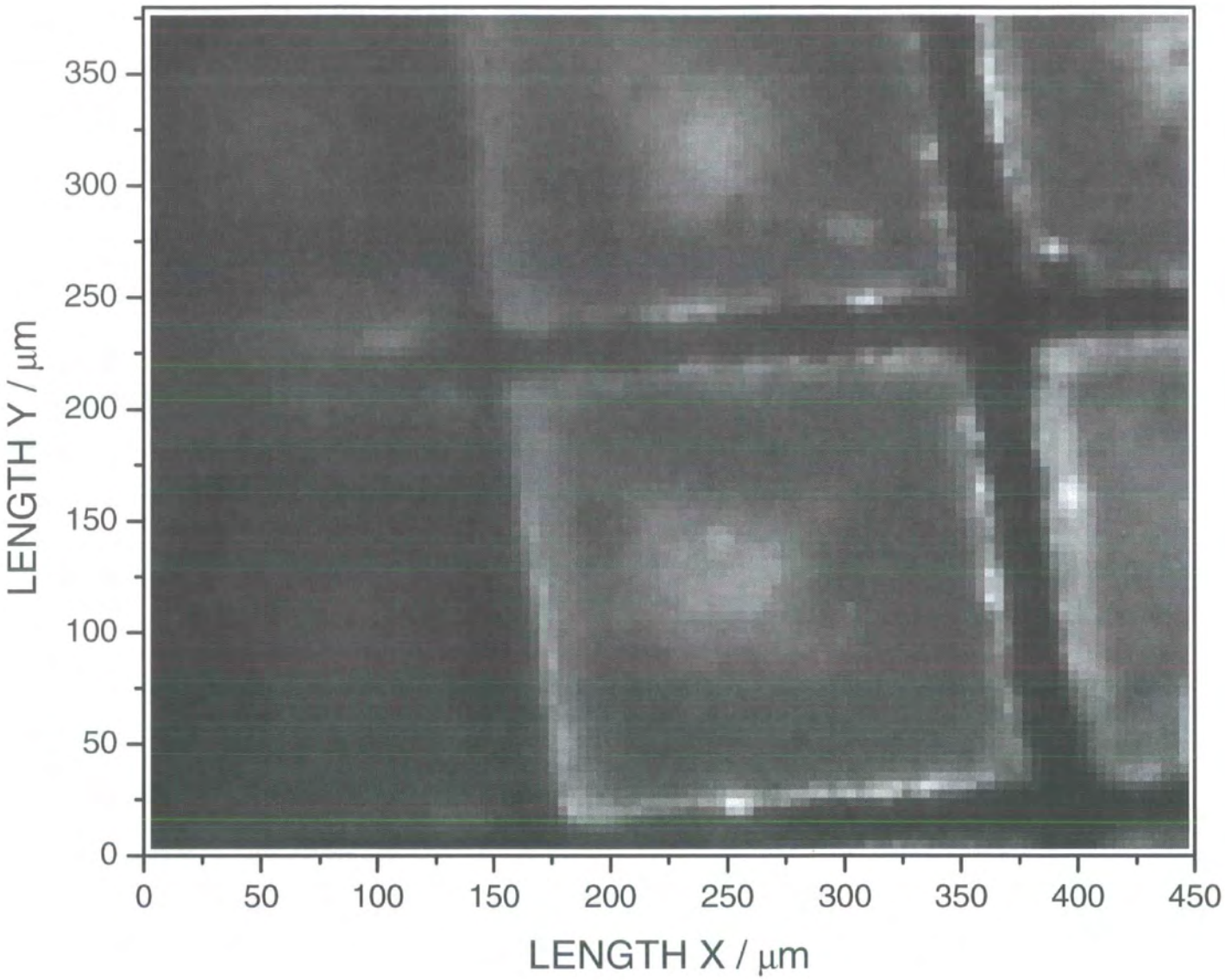

Figure 4.6: Fluorescence image of PNIPAAm array at 40 °C following exposure to FITC-BSA.

Reflectometry measurements show that films thicknesses increased from ~ 100 nm to ~ 160 - 180 nm when PMMA or PNIPAAm chains are grown from ppGMA-VAzo films. This is found to not vary noticeably with reaction time, suggesting only a very limited degree of control over polymer chain molecular weight as expressed by Figure 4.1. Polymerization in solution is also observed in both cases, which is consistent with the reaction mechanism in Scheme 4.5 where one of the radical species produced can dissociate from the surface and induce polymerization.

The thermal response of poly(n-isopropylacrylamide) films is further verified by water contact angle measurements. At 20 °C, contact angle is found to be 48° ±1. When heated on a glass plate at 40 °C, water contact angle of the films increases to 86° ±2. This change in hydrophobicity is representative of the change in conformation of the PNIPAAm chains when the lower critical solution temperature of 32 °C is surpassed (see Chapter 3).

The production of thin, well-defined polymer films and thermo-responsive, biocompatible polymer microarrays has highlighted the potential of this technique for applications such as the controlled delivery of drugs[35, 36] and the culturing of cells[37].

4.5 Conclusions

A substrate-independent, two-step method for generating surface-bound free radical initiating groups has been developed via pulsed plasma polymerization of glycidyl methacrylate followed by reaction with an amine-terminated dialkyldiazene. Polymer chains of methylmethacrylate and n-isopropylacrylamide have been successfully grown from these surfaces in aqueous conditions.

Analysis with X-ray photoelectron spectroscopy and infrared spectroscopy has corroborated a high retention of functional groups within these polymer films. Further analysis with fluorescence microscopy has authenticated the formation of microscopic arrays and the thermo-responsive properties of poly(n-isopropylacrylamide).

4.6 References

[1] Okamura, S.; Motoyama, T., *J. Polym. Sci.*, 17, **1955**, 428.

[2] Imoto, M.; Otsu, T.; Ota, T.; Takatsugi, H.; Matsuda, M., *J. Polym. Sci.*, 22, **1956**, 137.

[3] May, J. A.; Smith, W. B., *J. Phys. Chem.*, 72, **1968**, 2993.

[4] Vanhook, J. P.; Tonolsky, A. V., *J. Polym. Sci.*, 33, **1958**, 429.

[5] Kodama, S.; Matushima, Y.; Ueyoshi, A., *J. Polym. Sci.*, 41, **1959**, 83.

[6] Indictor, M.; Mogolesk, P.; Jaffe, H., *J. Polym. Sci., Polym. Chem.*, 5, **1967**, 1107.

[7] Gaylord, N. G.; Maiti, S., *J. Polym. Sci., Pol.. Lett.*, 10, **1972**, 35.

[8] Scamehorn, J. F.; Timm, D. C., *J. Polym. Sci., Polym. Chem.*, 13, **1975**, 1241.

[9] Ng, S. C.; Chee, K. K., *J. Polym. Sci., Polym. Chem.*, 20, **1982**, 409.

[10] Hatada, K.; Kitayama, T.; Matsuda, E., *Polym. J.*, 17, **1985**, 985.

[11] Engel, P. S.; *Chem. Rev.*, 80, **1980**, 99.

[12] Barbe, W.; Ruckhardt, C., *Makromol. Chem.*, 184, **1983**, 1235.

[13] Krstina, J.; Moad, G.; Willing, R. I.; Danek, S. K.; Kelly, D. P.; Jones, S. L.; Solomon, D. H., *Eur. Polym. J.*, 29, **193**, 379.

[14] Talat-Erben, M.; Bywater, S. J., *J. Am. Chem. Soc.*, 77, **1954**, 3712.

[15] Moad, G.; Rizzardo, E.; Solomon, D. H.; Johns, S. R.; Willing, I. R., *Makromol. Chem., Rapid. Commun.*, 5, **1984**, 793.

[16] Maillard, B.; Ingold, K. U.; Scaiano, J. C., *J. Am. Chem. Soc.*, 97, **1975**, 335.

[17] Bevington, J. C.; Troth, H. G., *Trans. Faraday Soc.*, 58, **1962**, 186.

[18] Roux, S.; Duwez, A. S.; Demoustier-Champagne, S., *Langmuir*, 19, **2003**, 306.

[19] Ista, L. K.; Mendez, S.; Perez-Luna, V. H.; Lopez, G. P., *Langmuir*, 17, **2001**, 2552.

[20] Hyun, J.; Chilkoti, A., *Macromolecules*, 34, **2001**, 5644.

[21] Bekku, H.; Katsuki, K.; Usui, H.; Patton, D.; Locklin, J.; Advincula, R.., *Polym. Preprint.*, 45, **2004**, 812.

[22] Konradi, R.; Ruhe, J., *Polym. Preprint.*, 44, **2003**, 546.

[23] Abadie, M. J. M.; Popa, M.; Zaharia-Arnautu, M.; Bulacovschi, V.; Popa, A. A.; *Eur. Polym. J.*, 36, **2000**, 571.

[24] Tsubokawa, N.; Koshiba, M., *J. Macromol. Sci.*, A34, **1997**, 2509.

[25] Kidchob, T.; Kimura, S.; Imanishi, Y., *J. Controlled Release*, 50, **1998**, 205.

[26] Tripp, J. A.; Svec, F.; Frechet, J. M. J., *J. Comb. Chem.*, 3, **2001**, 216.

[27] Tripp, J. A.; Svec, F.; Frechet, J. M. J., *J. Comb. Chem.*, 3, **2001**, 604.

[28] Motornov, M.; Minko, S.; Nitschke, M.; GrundKe, K.; Stamm, M., *Polym. Mat. Sci. Eng.*, 88, **2003**, 264.

[29] Husemann, M.; Morrison, M.; Benoit, D.; Frommer, J.; Mate, C. M.; Hingsberg, W. D.; Hedrick, J. L.; Hawker, C. J., *J. Am. Chem. Soc.*, 122, **2000**, 1844.

[30] Husemann, M.; Malmstrom, E. E.; McNamara, M.; Mate, Mercerreyes, D.; Benoit, D.; Hedrick, J. L.; Mansky, P.; Huang, E.; Russell, T. P.; Hawker, C. J., *Macromolecules*, 32, **1999**, 1424.

[31] Nakayama, Y.; Matsuda, T., *Macromolecules*, 29, **1996**, 8622.

[32] Nakayama, Y.; Matsuda, T., *Langmuir*, 15, **1999**, 5560.

[33] Tarducci, C.; Kinmond, E, J.; Badyal, J. P. S.; Brewer, S. A.; Willis, C., *Chem. Mater.*, 12, **2000**, 1884.

[34] Beamson, G.; Briggs, D; *High Resolution XPS of Organic Polymers*, Wiley, New York, **1992.**

[35] Bae, Y. H.; Okano, T.; Kim, S. W.; *J. Polym. Sci. B.*, 28, **1990**, 923.

[36] Yoshida, R.; Sakai, K.; Okano, T.; Sakurai, Y., *Adv. Drug. Deliv. Rev.*, 11, **1993**, 85.

[37] Aoki, T.; Nagao, Y.; Terada, E.; Sanui, K.; Ogata, N.; Yamada, N.; Sakurai, Y.; Kataoka, K.; Okano, T., *J. Biomater. Sci., Polym. Ed.*, 7, **1995**, 539.

Chapter 5: Electrodeless Deposition of Transition Metals onto Pulsed Plasma Polymer Films

5.1 Introduction

Electrodeless metal deposition is a process where metal ions in solution are chemically reduced to the metal at the substrate surface[1]. This process has been successfully employed for the metallization of non-conducting substrates such as plastics and ceramics in the electronic and automotive industries and the metal plating of substrates with complex shapes[2, 3, 4].

Further applications for electrodeless deposition of metals are in porous electrodes[5]. These electrodes require three-dimensional structures with a large surface area and micro-porosity[6]. One such substrate suitable for this application is Teflon (polytetrafluoroethylene), which is a high-temperature thermoplastic used for insulation. Teflon possesses many desirable properties such as thermal stability and a low dielectric constant. However it is chemically inactive and exhibits poor adhesion qualities, but if pre-treated with boiling hydrochloric acid and subsequently submersed in a palladium catalyst solution, C-F-Pd bonds are formed.

Advances in the microelectronics industry have resulted in copper and nickel rapidly replacing the more commonly used aluminium in multilevel metallization processes. These metals have a lower susceptibility to electromigration and a lower resistance-capacitance delay than aluminium. The metallization of substrates using electrodeless methods is simplistic, selective and economical as well as requiring low processing temperatures.

Palladium is one of the most commonly used catalysts for electrodeless plating[1, 7]. However, it cannot be chemisorbed to most inert substrates without prior sensitization of the surface with a tin compound such as $SnCl_2$.

5.1.1: Existing Methods of Electrodeless Metal Deposition

Recently developed methods include the selective binding of palladium catalysts to surface-bound ligands[8] such as self-assembled monolayers of amine groups tailored to silicon using silane linkages[5], making the surface amenable to electrodeless deposition of metals[9].

Patterning on the substrate is attainable by various methods including x-rays, ion beams and electron beams which destroy the ligating ability of regions of the substrate[10, 11].

To successfully generate arrays of nickel and copper deposition, one strategy that has been successfully used is the deposition of chloromethyl styrene groups[12, 13, 14]. Aromatic based films are excellent for patterning due to the fact that they readily absorb ultra-violet light (UV). The functional groups of chloromethyl styrene are radiation-sensitive[15] causing it to rapidly lose a hydrogen chloride molecule at low exposure doses of UV (~50 mJ/cm^2). This would allow oxidation of the chloromethyl groups to aldehydes[16]. If a mask is used, only exposed regions of the chloromethyl styrene film will be oxidized by radiation.

Areas within the chloromethyl styrene film not oxidised by UV are able to entrap pyridine groups[13]. Pyridine can only be entrapped in the non-oxidised regions because the carboxylate product hinders ligand insertion due to increased hydrophilicity and steric effects. A Palladium (II) catalyst can then be attached to the nitrogen atoms within the pyridine molecules, allowing subsequent metal deposition.

Another recently-developed strategy is to reductively aminate the oxidised aldehyde regions, hence forming NH_2 groups that can permit attachment of a Pd(II) catalyst. The advantages of this reaction are that it can be done in aqueous solutions and at ambient conditions. If the selective in-situ reduction is carried out using $NaBH_3CN$, imines are irreversibly trapped as aliphatic amines[17]. Hence reductive amination of benzaldehyde groups (as formed in oxidation of chloromethyl styrene with UV radiation) will yield amine-functionalized benzene rings which can be used for selective electrodeless metal deposition.

5.1.2 Electrodeless Metal Deposition Baths

In 1946, Brenner and Riddell found that deposition of Nickel occurred when no external current was applied[18]. The nickel deposition was not only dependant on chemical reduction, but also on a catalytic surface. Once initiated, the nickel deposit was itself catalytic; hence this process was described as 'the autocatalytic chemical reduction of metal ions to form a metal deposit '– 'electrodeless[19]'.

This led to electrodeless plating, which is very important for finishing steel, copper, plastics and many materials. It is also widely used in the electronics industry. The advantages of electrodeless plating over electrolytic plating include the following:

- Allows uniform deposits over irregular surfaces
- Direct plating on non-conductors
- Deposits are less porous and more corrosion resistant
- Deposition can occur on isolated metal areas

Nickel-phosphorous, nickel-boron and copper deposition systems are the techniques most commonly used. The main advantage of electrodeless deposition is deposit uniformity, which can be achieved on irregular surfaces such as threads and complex-shaped parts. Uniform deposits on small holes, crevices and tube interiors are virtually impossible with the electrolytic plating technique. Electrodeless nickel and copper are commonly deposited on non-conductors as a conductive base for subsequent electrolytic plating. They are both employed for electroplated plastic products that will be subjected to prolonged, corrosive environmental exposure. Electrodeless nickel and copper are also used for the functional plating of plastics for the purpose of controlling electromagnetic interference e.g. in computer packages[20]. Thicker coatings of electrodeless copper have been employed in printed circuit boards for many years. Other electrodeless baths currently available include cobalt, tin, gold and silver.

5.1.3 Nickel-Boron Electrodeless Bath

Nickel-boron alloys have been successfully employed in the food-processing, automotive, aircraft and petroleum industries[21, 22].

It has been found that certain reagents have the ability to dramatically increase nickel deposition rates. These are referred to as exaltants[23] and can also provide beneficial complexing and buffer action[24]. The ratio of reducing agents, in this case boranes, and nickel salts is also important as this can affect the optimum deposition rate and properties of the resulting alloy e.g. wear resistance and hardness. Trace amounts of catalytic poisons[25] are also added to stabilise the bath and prevent spontaneous decomposition that can result in a black powder and hence a useless solution. Existing nickel-boron baths therefore consist of chelates, exaltants, buffers, stabilisers as well as dimethylaminoborane and the necessary nickel salts, operating at pH values of 5 to 11. The deposited nickel-boron alloy (Ni-B) contains around 0.1 up to 5 % (by weight) boron which is co-deposited[26]. Deposits that contain around 0.5 % boron exhibit properties very similar to that of pure nickel such as electrical properties and melting point (~ 1450 °C)[27].

The proposed mechanism for Ni-B deposition is as follows[28]:

$$(CH_3)_2NBH_2 + H_2O \longrightarrow (CH_3)_2NBHO^- + 2H^+ + H^- \quad \textbf{(1)}$$

The hydride ion on the catalytic surface can react with available nickel ions by electron transfer to produce a nickel deposit and hydrogen gas evolution

$$2H^- + Ni^{2+} \longrightarrow Ni^0 + H_2 \quad \textbf{(2)}$$

Hence the overall reaction is:

$$2(CH_3)_2NBH_2 + 2H_2O + Ni^{2+} \longrightarrow Ni^0 + H_2 + 4H^+ + 2(CH_3)_2NBHO^- \quad \textbf{(3)}$$

2 gram-moles of dimethylaminoborane can theoretically produce 1 gram atomic weight of nickel.

5.1.4 Copper Electrodeless Bath

This bath was first developed for plated-through-hole printed circuit boards. The first copper baths utilised the autocatalytic chemical reduction of copper from alkaline copper tartrate baths with formaldehyde as the reducing agent[29]. Copper baths have a limited life because cuprous oxide particles form spontaneously in solution, acting as catalytic nuclei for the formation of precipitous copper powder, leading to rapid decomposition of the bath.

Baths can be stabilised by bubbling through air, hence oxidising the cuprous oxide, preventing the formation of the destabilizing catalytic nuclei. Other reagents such as thiourea [30], cyanide [31] and divalent sulphur compounds[32] are also effective stabilisers.

Formaldehyde reduction capability increases with alkalinity, hence baths are normally operated at a pH above 12. Complexing agents prevent cupric hydroxide precipitation. They are crucial because they affect bath stability, decomposition rates and quality of copper deposits. Tartrates, alkanoamines and ethylenediaminetetraacetic acid can be used as complexing agents.

Theoretically, for each gram atomic weight of copper plated electrodelessly on a catalytic surface, at least 2 moles of formaldehyde and 4 moles of sodium hydroxide are consumed and 1 mole of hydrogen is evolved:

$$Cu^{2+} + 2HCHO + 4OH^- \longrightarrow Cu^0 + H_2 + 2HCOO^- + 2H_2O \quad \textbf{(4)}$$

There will be, in reality, more formaldehyde and hydroxide consumed due to disproportionation into methanol and formate. The actual mechanism may involve hydride transfer from formaldehyde at the catalytic surface, similar to the Ni-B bath[13].

5.2 Aims

The objective of this work is to improve on existing methods of metal deposition onto surfaces via the pulsed plasma polymerization of nitrogen-containing precursors, which allows the development of a substrate independent, solventless method for generating sites that are amenable to Pd(II) attachment. Hence if a monomer such as 4-vinylaniline is pulsed plasma polymerized onto substrates such as silicon wafers, sheets of polytetrafluoroethylene (PTFE) or polystyrene beads; functionalized surfaces with amine moieties can be generated in one reaction step. A Pd (II) catalyst can then be tailored to surface-confined amine groups permitting subsequent deposition of copper and nickel via suitable electrodeless baths. Microscopic arrays of deposited metals can be achieved by embossing substrates with a grid prior to the plasma deposition step.

5.3: Experimental

5.3.1: Pulsed Plasma Polymerization of 4-Vinylaniline

The formation of plasma polymers on surfaces was carried out according to the procedures outlined in Chapter 4. The pulse duty cycle used in the deposition of 4-vinylaniline (98% purity, Aldrich) was 100 μs on, 4000 μs off with peak power set to 20 W. This pulse duty cycle has been successfully exploited previously for depositions involving precursors containing aromatic ring groups. Polystyrene beads were coated using a plasma chamber rotated by motors at approx 20 rpm to ensure maximum exposure of the beads' surface area to the plasma. Depositions were performed at room temperature (20 °C).

5.3.2: Attachment of a Palladium Catalyst

Pulsed plasma polymerized 4-vinylaniline (pp4VAni) coated silicon wafers were submersed in an aqueous catalyst solution containing 0.01 M palladium chloride (99%, Aldrich), 3.0 M sodium chloride (99.9%, Sigma) and 0.5 M sodium citrate dehydrate (99%, Aldrich) (pH adjusted to 4.5 with citric acid

monohydrate (99%, Aldrich)) for 2 hours and before being washed in deionised water for 1 hour.

5.3.3: Electrodeless Deposition of Selected Metals

The pp4VAni-Pd films were then immersed for 30 minutes in an aqueous solution consisting of 1.5% by weight copper sulphate pentahydrate (98%, Fluka), 7% sodium potassium tartrate (98%, Aldrich), 1% sodium hydroxide (98%, Fluka) and 50% formaldehyde (37% in water, Aldrich) to allow the formation of a layer of copper metal.

For the electrodeless deposition of nickel; pp4VAni-coated substrates were submersed in an EL468 Nickel Bath (Shipley), containing nickel sulphate, dimethylaminoborane and active components for 30 minutes.

Control experiments entailed immersion of pp4VAni films in the metal baths without derivatization with the palladium catalyst.

5.3.4: Formation of Metal Arrays

A brass grid comprising of 500 μm holes separated by 1 mm was embossed onto 2.0 cm squares of polytetrafluoroethylene (PTFE). This was followed by a 10 minute deposition of 4-vinylaniline onto the substrate as previously described. The grid was subsequently removed and the substrates treated as outlined in section 5.3.2. This was followed by immersion in either the nickel or copper sulphate baths for 30 minutes. The arrays were viewed with a multi-step optical microscope (Spectrum One, Perkin Elmer) fitted with a x 20 magnification lens and a 5,000 μm image obtained with a 100 μm step resolution.

5.3.5: Formation of Metal-coated Beads

The versatility of this methodology was demonstrated by coating polystyrene beads (80 μm diameter, Biosearch Technologies One) with a pulsed plasma polymerized 4-vinylaniline layer and subsequently treating with palladium catalyst before submersion in the nickel bath for 30 minutes. The nickel-coated microspheres were then washed in deionized water and sprinkled on top of a thin layer of molten thermoplastic adhesive (Tempfix, Agar Scientific)

which had been spread onto an aluminium plate (1 x 1 cm). Cooling to room temperature allowed immobilization of the beads into the adhesive surface. Thin slices were taken off the top of the exposed polymer microspheres by mounting the plate onto a cryogenic microtome to reveal cross-sections. Throughout the cutting procedure, the temperature of the substrate holder and knife was kept below -20 °C whilst the surrounding chamber temperature was maintained at -90 °C. Following a 10 nm coating of gold, the nickel layer enveloping the beads could be viewed by utilising scanning electron microscopy (Cambridge Instruments, model S240).

5.4: Results and Discussion

5.4.1: Pulsed Plasma Polymerization of 4-vinylaniline

Analysis with XPS shows that stoichiometric measurements of pp4VAni are in excellent agreement with theoretical values, Table 5.1. The high resolution XPS C(1s) envelope exhibits 3 carbon environments, carbon within an aromatic ring bonded to hydrogen (binding energy = 284.75 eV), carbon within a hydrocarbon group (285.0 eV) and carbon adjoined to nitrogen (285.95 eV), Figure 5.1. The π-π^* shake up peak can be observed at 291.5 eV, hence corroborating structural retention of aromatic groups. The N(1s) binding energy of 4-vinylaniline is measured to be 398 eV.

Table 5.1: Stoichiometries of pulsed plasma polymerized 4-vinylaniline (pp4VAni), pp4VAni-$Pd(II)Cl_2$, pp4VAni-$Pd(II)Cl_2$-copper and pp4VAni-$Pd(II)Cl_2$-nickel found by XPS.

Surface Coating		**% C**	**% N**	**% O**	**% Cl**	**% Pd**	**%Metal** (estimated sensitivity factors)	**%B**
pp4VAni	Theoretical	89	11	0	-	-	-	-
	Experimental	89 ± 1	11 ± 1	Trace	-	-	-	-
pp4VAni-$Pd(II)Cl_2$	Experimental	64	8	22	4	2	-	-
pp4VAni-$Pd(II)Cl_2$ copper	Experimental	50	3	34	Trace	Trace	13	-
pp4VAni-$Pd(II)Cl_2$ nickel	Experimental	25	Trace	39	Trace	Trace	36	Trace

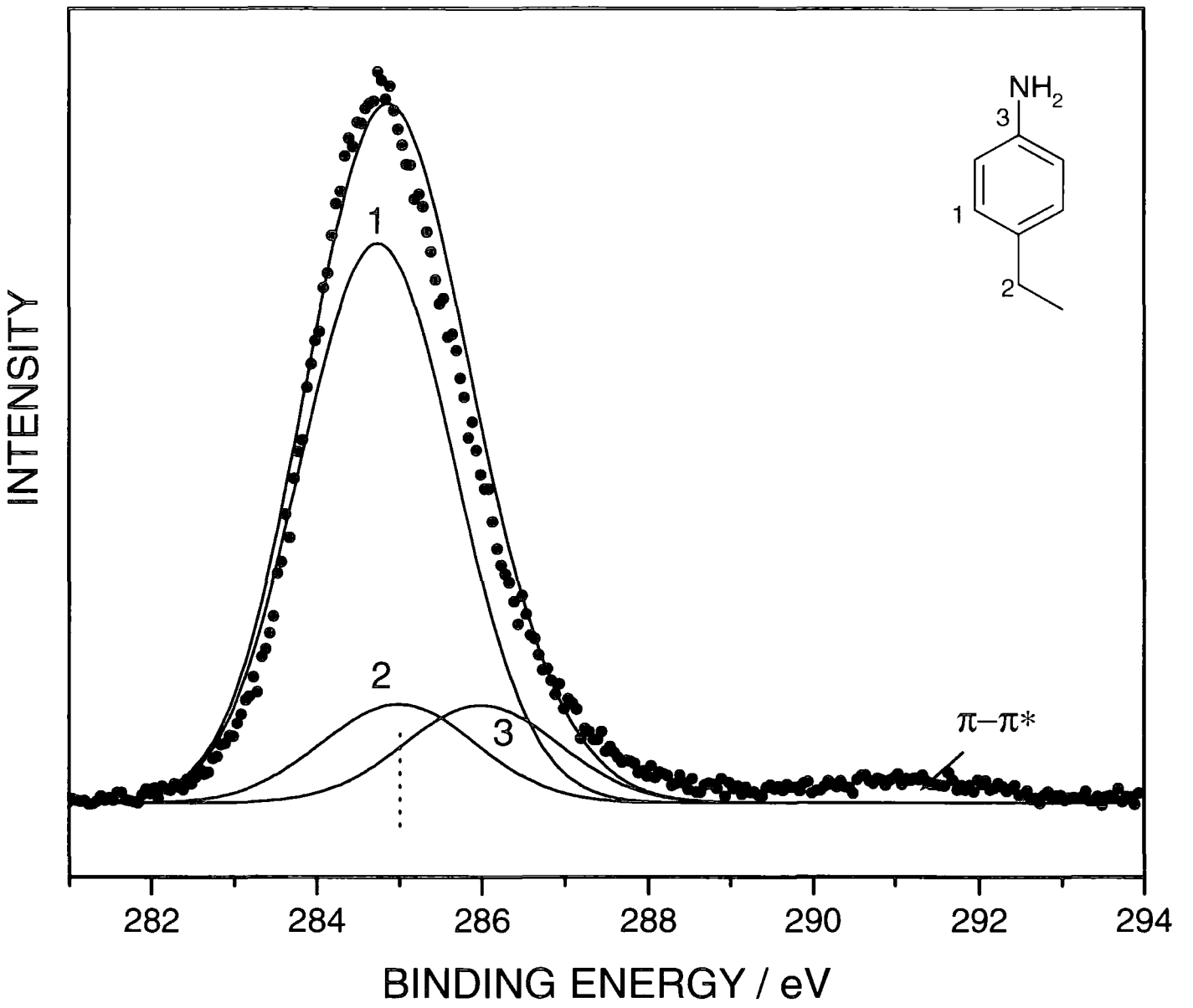

Figure 5.1: XPS C(1s) spectra of pulsed plasma polymerized 4-vinylaniline.

Figure 5.2 details the FTIR spectra of 4-vinylaniline monomer and the plasma polymer films. The peaks at 3435 (A), 3360 cm^{-1} (B) and 1620 cm^{-1} (E2), which are representative of amine stretches are found to be prevalent in both spectra along with aromatic stretches at 1603 cm^{-1} (E3) and 1520 cm^{-1} (F), authenticating the presence of 4-vinylaniline, Table 5.2. Peaks E1, E2 and E3 are situated in such close proximity that it is not possible to distinguish

between them. Hence they are represented by a combination of peaks, Figure 5.2(a). A decrease in width and intensity relative to aromatic peak (F) is observed in Figure 5.2(b) due to an absence of the C=C stretch at 1630 cm^{-1} (E1) following pulsed plasma polymerization of 4-vinylaniline.

Table 5.2: FTIR peak assignments for 4-vinylaniline monomer and pulsed plasma polymer.

Designation	**4-vinylaniline monomer**	**4-vinylaniline plasma polymer**
A: Antisymmetric amine stretch, 3435 cm^{-1}	*	*
B: Symmetric amine stretch, 3360 cm^{-1}	*	*
C: CH_2 in-phase stretch, 2992 cm^{-1}	*	*
D: Aromatic ring stretch, 2921 cm^{-1}	*	*
E1: C=C stretch, 1630 cm^{-1}	*	
E2: NH_2 scissor stretch, 1620 cm^{-1}	*	*
E3: Para-substituted benzene stretch, 1603 cm^{-1}	*	*
F: Para-substituted benzene stretch, 1520 cm^{-1}	*	*
G: Aromatic C-N stretch, 1173 cm^{-1}	*	*

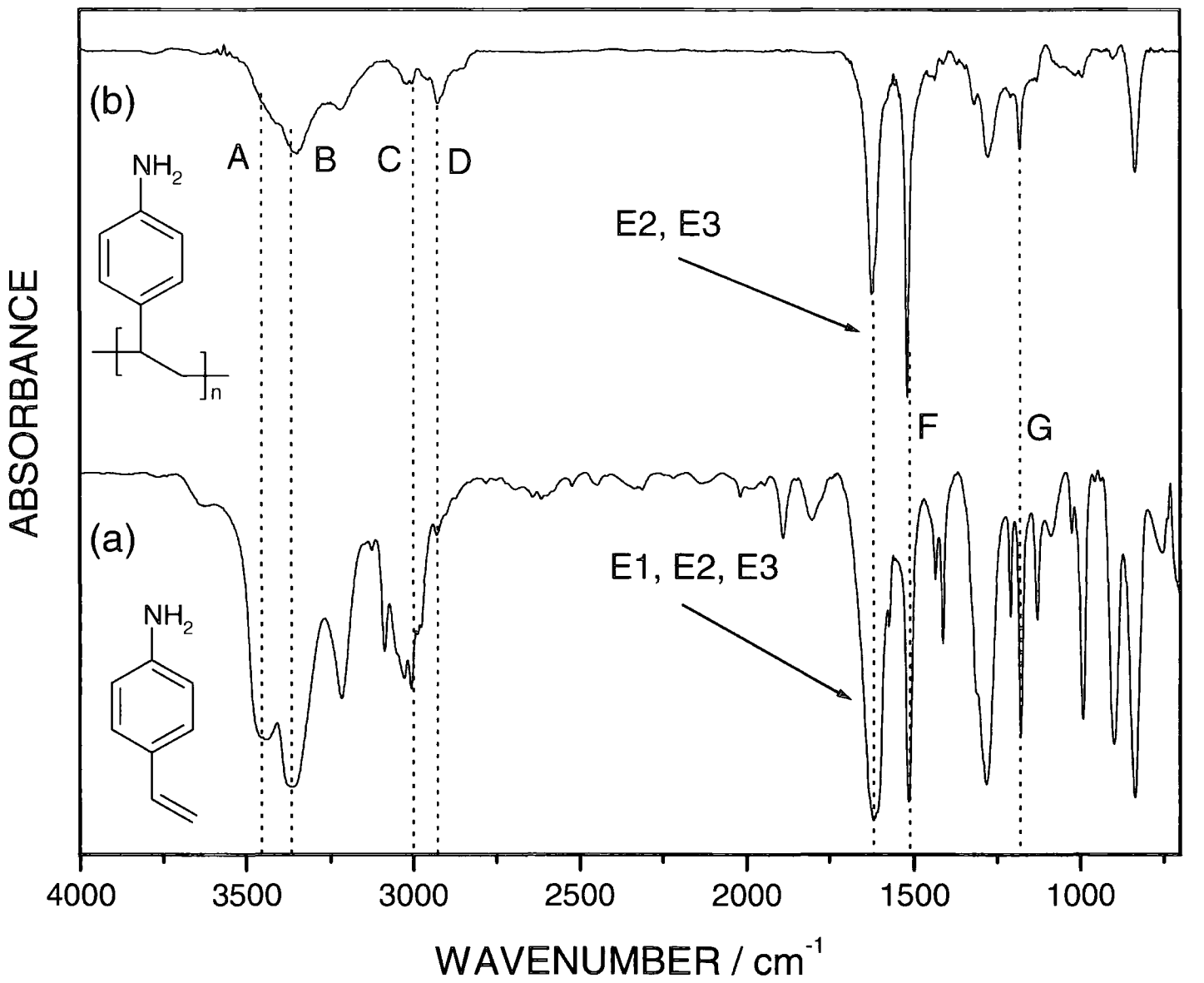

Figure 5.2: FTIR spectra of (a) 4-vinylaniline monomer, (b) 4-vinylaniline pulsed plasma polymer.

Deposition rate of 4-vinylaniline using parameters outlined in 5.3.1 is 10 nm per minute, as determined by reflectometry.

5.4.2: Attachment of a Palladium Catalyst

Figure 5.3(b), the XPS scan of pp4VAni films reacted with $PdCl_2$ verifies the presence of both chlorine (2p binding energy = 200 eV) and palladium (3d = 350 eV) additional to carbon and nitrogen. Stoichiometric analysis shows chlorine and palladium in a 2:1 ratio as expected. A comparison between the relative amounts of palladium to nitrogen shows that approximately 20 % of the amine groups within the penetration depth (2 – 5 nm) of the 4-vinylaniline films have formed stable Lewis acid-base interactions with the palladium chloride catalyst, Table 5.1. Binding energy of N(1s) is found to have increased to from 398 to 403 eV following reaction of pp4VAni with Palladium.

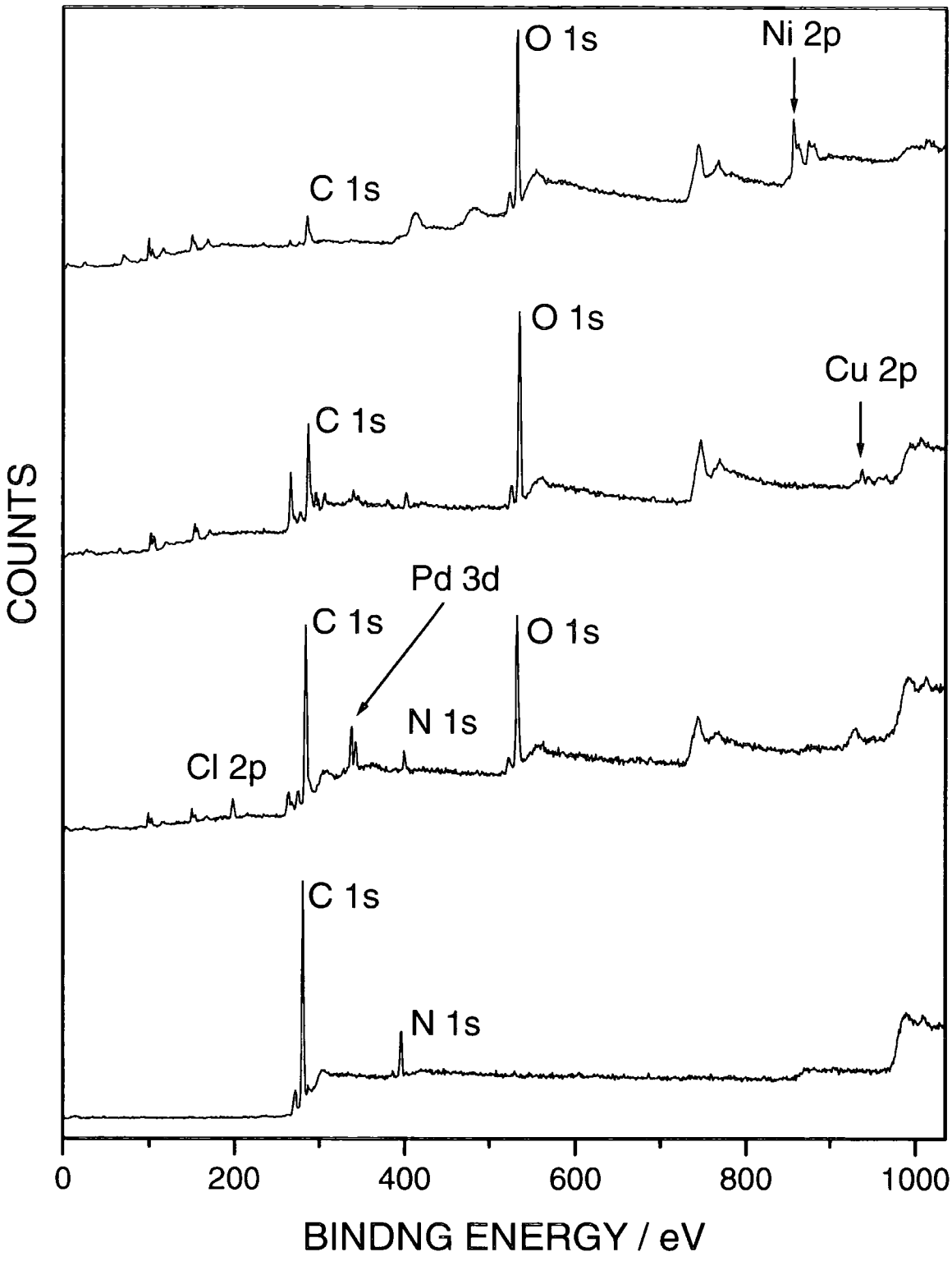

Figure 5.3: XPS wide scan of (a) 4-vinylaniline pulsed plasma polymer (b) 4-vinylaniline pulsed plasma polymer reacted with Palladium chloride solution after washing, (c) pp4VAni-Pd(II)Cl_2 films reacted in copper sulphate bath after washing, (d) pp4VAni-Pd(II)Cl_2 films reacted in Shipley EL468 nickel bath after washing.

5.4.3: Electrodeless Deposition of Selected Metals

Atomic copper formation from reacting pp4VAni-Pd(II)Cl_2 films with a copper sulphate bath in the presence of formaldehyde is easily observed with the naked eye. The XPS scan of the copper layer, Figure 5.3(c), details the Cu 2p 1/2 peak at binding energy 930 eV confirming the presence of copper metal. Stoichiometric analysis reveals the presence of carbon and nitrogen, which are indicative of the pp4VAni film below the copper layer, Table 5.2. An appreciable amount of adsorbed oxygen is also present at the surface.

Regarding deposition of nickel, the formation of atomic metal upon the substrate surface is visible. The presence of nickel is authenticated by XPS, Table 5.1 and Figure 5.3(d), which details the Ni 2p peak at 870 eV. As in the case of copper deposition; carbon and nitrogen and oxygen are detected by XPS.

Control experiments reveal no metallization at the surface, proving the presence of the palladium catalyst is vital for electrodeless deposition of metals to occur.

5.4.4: Formation of Metal Arrays

Figures 5.4 and 5.5 show arrays of electrodelessly deposited copper and nickel respectively. Metal deposition occurs only within regions coated with pp4VAni.

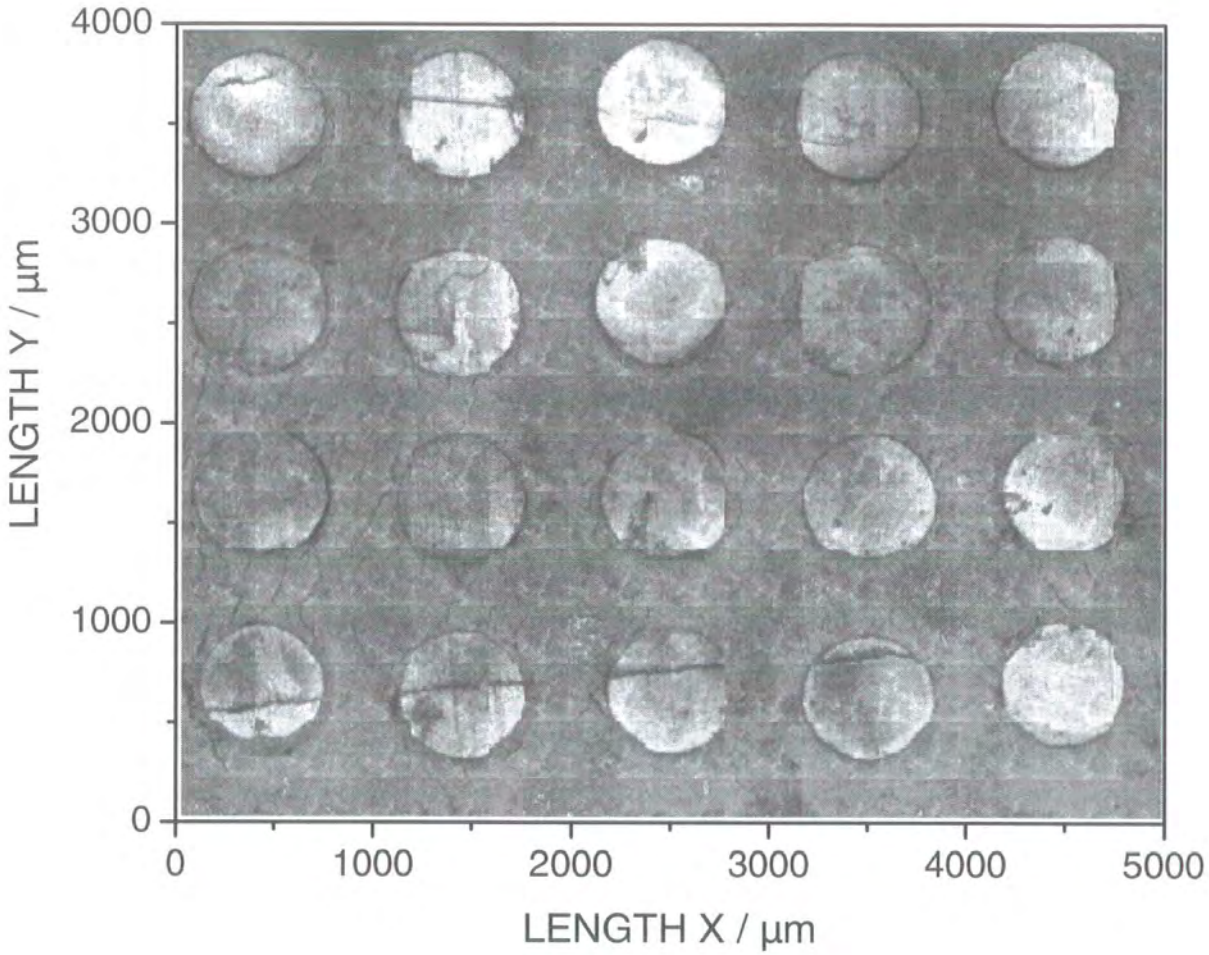

Figure 5.4: Array of electrodelessly-deposited copper onto PTFE.

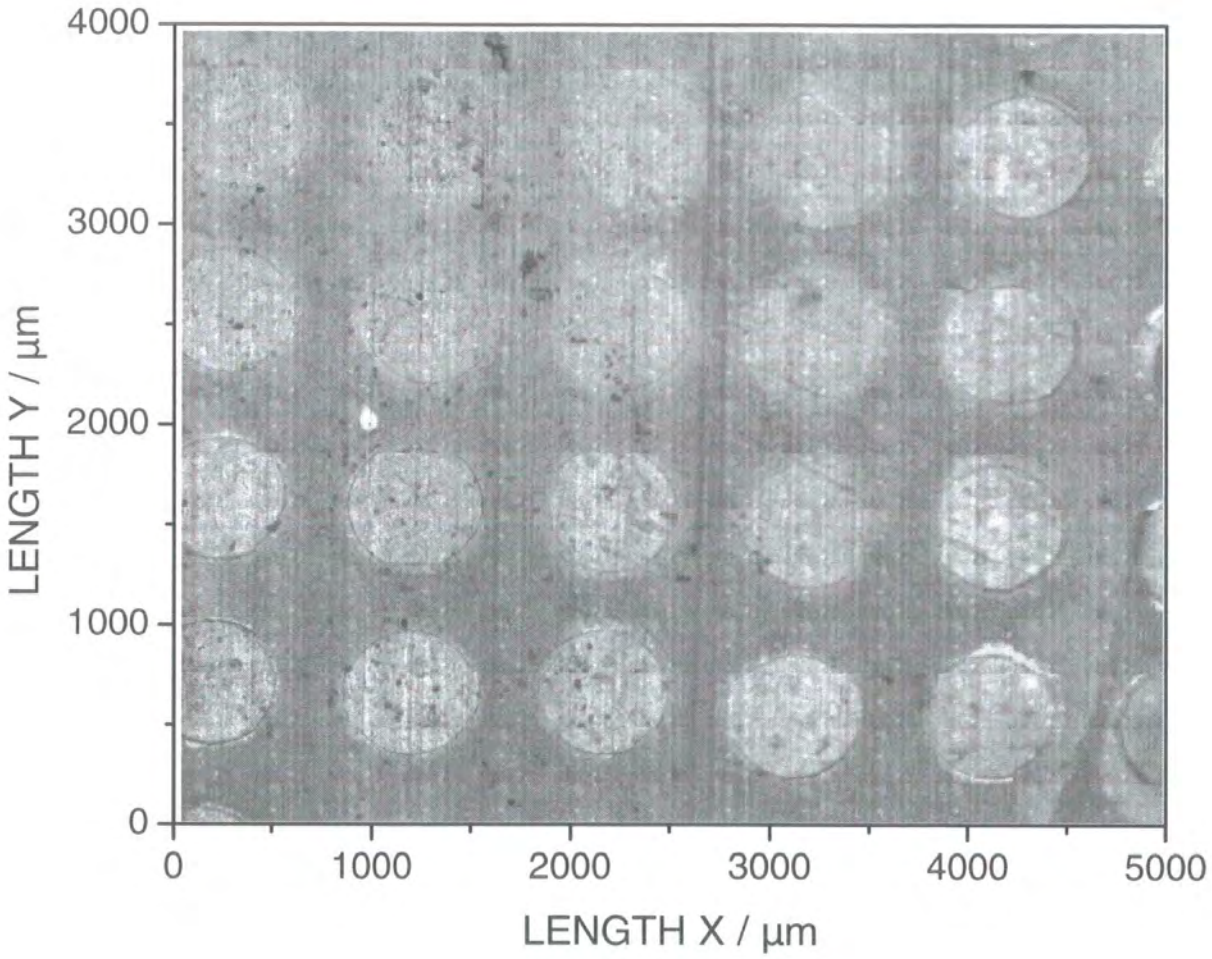

Figure 5.5: Array of electrodelessly-deposited nickel onto PTFE.

5.4.5: Formation of Metal-coated Beads

Figure 5.6 details a scanning electron microscopy cross-section of an polystyrene microsphere (80 μm diameter) coated with 100 nm pulsed plasma polymerized 4-vinylaniline, which was followed by treatment with the Pd(II) catalyst and 30 minutes exposure to the nickel bath. The resulting nickel layer surrounding the bead is approximately 6 μm thick. (Note that the size of the cross-section is dependent upon the depth at which the polymer bed was sliced).

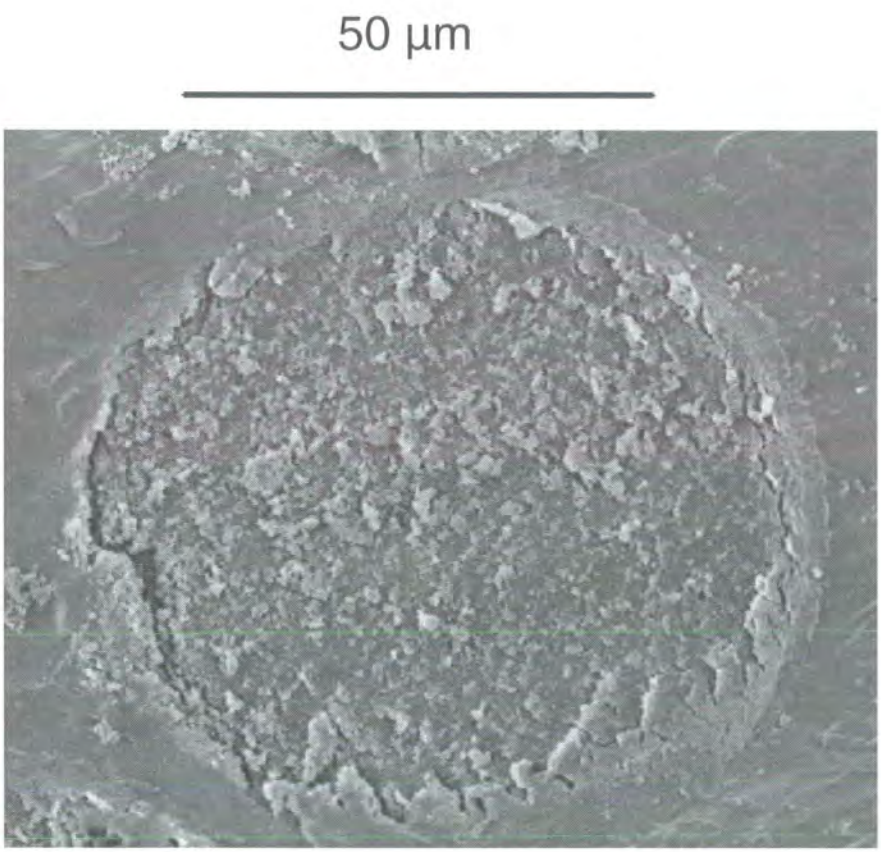

Figure 5.6: SEM cross section of microscopic bead coated with 6 μm layer of nickel.

4-vinylaniline has been successfully deposited onto a variety of substrates by pulsed plasma polymerization for the first time. Analysis with XPS, FTIR and reflectometry has verified excellent structural retention of functional groups and a high level of film controllability.

The electronegative nitrogen in the amine groups can attract Pd(II) ions from an acid solution and can impart its lone pair of electrons to the adsorbed

Pd ions[33]. This results in Pd atoms being complexed to the nitrogen atoms, indicated by an increase in N(1s) binding energy, as previously observed.

Metal ions from the bath e.g. Ni(II) can then complex with palladium on the surface[34]. This is then followed by reduction of the metal by the reducing agent present in the bath e.g. DMAB in nickel baths. Hence the metal is reduced at the substrates surface giving rise to electrodeless metal deposition, Figure 5.7.

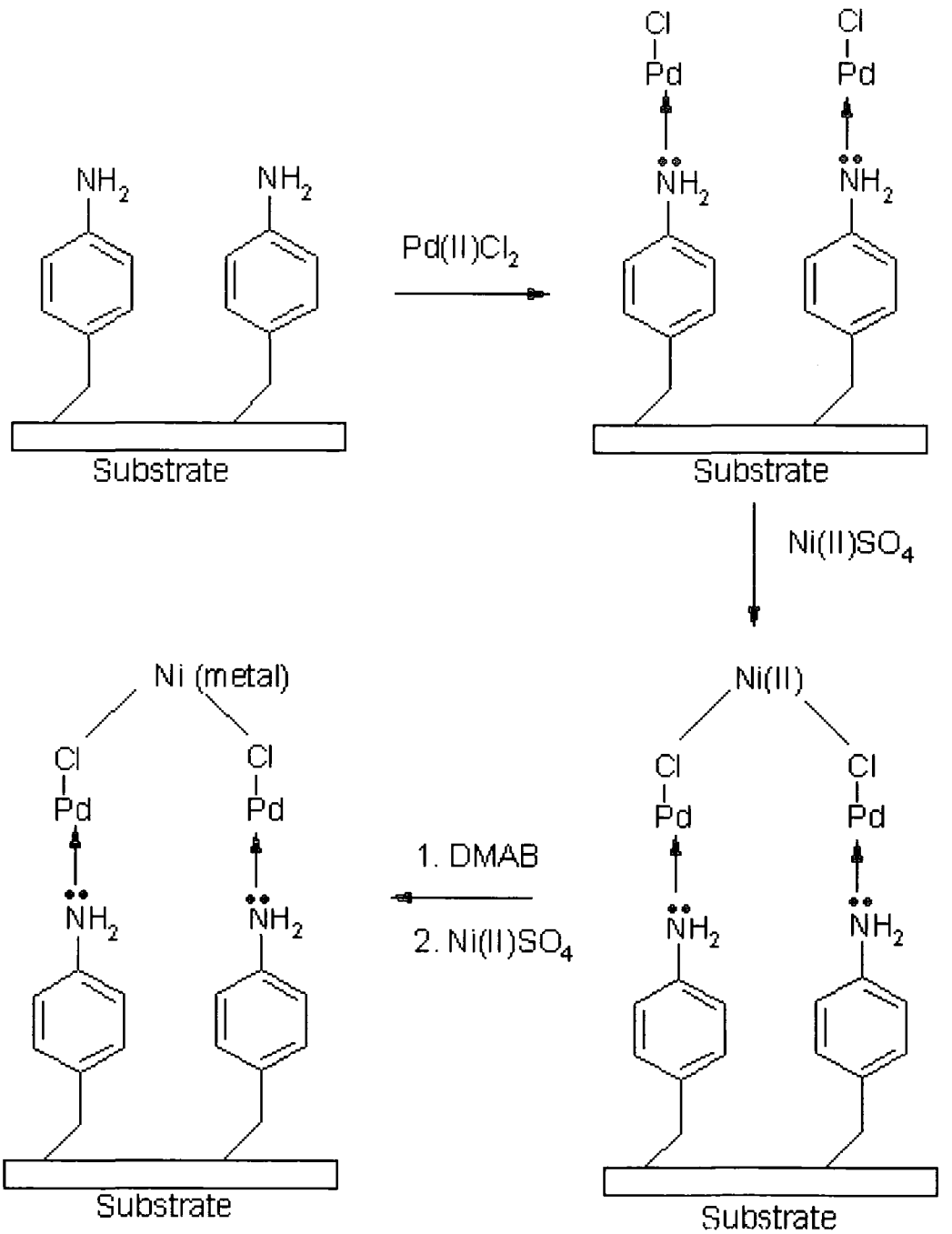

Figure 5.7: Mechanism of electrodeless deposition of nickel onto Pd(II)-treated pp4VAni.

Both metals deployed in this work have been successfully deposited onto Pd(II)-treated arrays and microscopic beads. This demonstrates the wide scale applicability of this method due to the controllability of metal deposition to the 500 μm range and the fact that complex shapes can be coated effectively. This methodology has also reduced the number of reaction steps existing in current methods as palladium catalyst can be adhered to a surface in just two reaction steps as opposed to five[12-15], utilising minimum quantities of reagents.

5.5 Conclusions

It has been shown that both nickel and copper can be deposited by an electrodeless substrate-independent method via a three-step method using pulsed plasma polymers of 4-vinylaniline. This has been a marked improvement on existing methods that require additional reaction steps due to restrictions arising from substrate specifications. The approach employed here is substrate independent and not hindered by substrate geometry.

The successful deposition of arrays and the coating of complex shapes using this technique highlight its important potential for use in the electronic circuit industry.

5.6 References

[1] Shipley, C. R., *Plating Surf. Finish*, 71, **1984**, 92.

[2] Stremdoerfer, G.; Wang, Y.; Nguyen, D.; Clechet, P.; Martin, J. R., *J. Electrochem. Soc.*, 140, **1993**, 2022.

[3] Stremdoerfer, G.; Calais, C.; Martin, J. R.; Clechet, P.; Nguyen, D., *J. Electrochem. Soc.*, 137, **1990**, 835.

[4] Stremdoerfer, G.; Perrot, H.; Martin, J. R.; Clechet, P., *J. Electrochem. Soc.*, 135, **1988**, 2881.

[5] Yamasaki, N.; Korablova, I. R.; Korablov, S. F., *Mater. Letts.*, 58, **2004**, 768.

[6] Sotiropoulos, S.; Brown, I. J.; Akay, G.; Lester, E., *Mater. Letts.,* 35, **1998**, 383.

[7] Dressick, W. J.; Kondracki, L.M.; Chen, M.; Brandow, S. L.; Matijevic, E.; Calvert, J. M; *Colloids and Surfaces A*, 108, **1996**, 101.

[8] Dressick, W. J.; Dulcey, C. S.; Georger, J. R.; Calvert, J. M., *Chem. Mater.*, 5, **1993**, 148.

[9] Potochnik, S. J.; Pehrsson, P. E.; Hsu, D. S. Y.; Calvert J. M., *Langmuir*, 11, **1995**, 1841.

[10] Dulcey, C. S.; Georger, J. H.; Krauthamer, V.; Stenger, D. A.; Fare, T. L.; Calvert J. M., *Science*, 252, **1991**, 551.

[11] Marrian, C. R. K.; Perkins, F. K.; Brandow, S. L.; Koloski, T. S.; Dobisz, E. A.; Calvert, J. M., *Appl. Phys. Lett.*, 64, **1994**, 390.

[12] Brandow, S. L.; Chen, M. S.; Aggarwal, R.; Dulcey, C. S.; Calvert, J. M.; Dressick, W. J., *Langmuir*, 15, **1999**, 5429.

[13] Brandow, S. L.; Chen, M. S.; Fertig, S. J.; Chrisey, L. A.; Dulcey, C. S.; Dressick, W. J., *Chem. Eur. J.*, 7, **2001**, 4495.

[14] Dressick, W. J.; Chen, M. S.; Brandow, S. L.; *J. Am. Chem. Soc.*, 122, **2000**, 982.

[15] Dressick, W. J.; Calvert, J. M., *Jpn. J. Appl. Phys.*, 32, **1993**, 5829.

[16] Doppelt, P.; Stelzle, M., *Microelectron Eng.* 33, **1997**, 15.

[17] Borsch, R. F.; Bernstein, M. D.; Durst, H. D., *J. Am. Chem. Soc.*, 93, **1971**, 2897.

[18] Brenner, A.; Riddell, G. E., *Proc. AES,* 33, **1946**, 23.

[19] Brenner, A.; Riddell, G. E., *Proc. AES,* 34, **1947**, 156.

[20] Lordi, G. A., *Plating*, 54, **1967**, 382.

[21] Baudrand, D. W., *Plat. Surf. Finish,* 70, **1983**, 24.

[22] Duncan, R. N., *Products Finish*, 46, **1982**, 46.

[23] Gutzeit, G.; Ramirez, E. J., *U.S. Patent 2,658,842,* **1953.**

[24] Gutzeit, G.; Krieg, A., *U.S. Patent 2,658,841,* **1953.**

[25] Talmey, P.; Gutzeit, G., *U.S. Patent 2,782,273,* **1956.**

[26] Cooper, W. J.; Renforth, J. C.; Varga, R. J.; Weber, A. E., *Electrodeless Plating with Amine Boranes*, Callery Chem. Co., Callery, PA 16024, **1968.**

[27] Gawrilov, G. G.; *Chemical (Electrodeless Nickel Plating,* Portcullis Press Ltd., Surrey, **1979.**

[28] Lukes, R. M., *Plating*, 51, **1964**, 969.

[29] Cahill, A. E., *AES Proc*, 44, **1957**, 130.

[30] Saito, M., *Prod. Finish*, 31, **1967**, 7.

[31] Zeblisky, R. J.; McCormack, J. F.; Williamson, J. D.; Scheble, F. W., *U.S. Patent 3,095,309*, **1963** .

[32] Scheble, F. W,; Zeblisky, R. J.; McCormack, J. F.; Williamson, J. D., *U.S. Patent 3,361,58*, **1968.**

[33] Yang, G. H.; Kang, E. T.; Neoh, K. G.; Zhang, Y.; Tan, K. L., *Langmuir*, 17, **2001**, 211.

[34] Jackson, R. L., *J. Electrochem Soc.*, 137, **1990**, 95.

Chapter 6: Growth of Block Copolymers onto Solid Surfaces Using Iniferter Photopolymerization

6.1 Introduction

The modification of surfaces by the attachment of polymers is a very versatile and efficient method of controlling surface chemistry and properties such as biocompatibility, wetting, adhesion and friction. Chemical bonding between layers enhances the polymeric layer with greater environmental and chemical stability over a range of conditions e.g. pH, temperature and resistance to solvents. Polymeric coatings such as these are useful in printing and food packaging and in the development of microdevices and microelectronics applications[1, 2, 3] chemical separations[4], microelectronics and biomaterials where surfaces need to be cell-adhesive or anti-coagulant to prevent biocolloidal adsorptions in biomedical applications[5, 6, 7, 8]. Surface design in biomaterials is vital to whether bio-applications would be accepted by the human body's defence mechanisms.

Several methods exist for the coating of a substrate with a polymeric layer. These include: *Physisorption* (e.g. by spin-coating) where non-covalent adsorption of a preformed polymer occurs onto a surface; these systems lack robustness due to relatively weak adsorption forces. *Grafting to* is an alternative approach where a preformed polymer is attached to the substrate via chemical binding; however grafting density and layer thickness tend to be low due to diffusional and steric limitations at the interface. Finally there is *Grafting From* where polymer chains grow off surface-immobilized initiator groups; in this case the aforementioned drawbacks can be avoided.

Methods of attaching monolayers of initiating groups with high grafting densities to surfaces include alkoxysilanes on glass[9], silica particles[10], and silicon[11, 12, 13]. For polymerization to be initiated by the surface, the monolayer is treated with an initiating group that can generate radical species such as trapped polymers and peroxide groups. Radical formation from these groups can be obtained by γ–ray radiation[7, 12], plasma glow discharge[14] and ozone gas treatments[15].

Conventional free radical polymerization from solid surfaces does however have a significant drawback, which is related to the propensity of the propagating free radical chain end to undergo a variety of different termination reactions. This leads to a non-linear increase in macromolecular weight with conversion and prohibits the preparation of block copolymers. The aforementioned hindrances can be circumvented by use of iniferter polymerization[16].

The iniferter technique is a quasi-living polymerization method based on the formation of a reactive radical (the *ini*tiator) and a more stable counter-radical which acts as a trans*fer* agent and a *ter*minating species, hence the term *iniferter*[17]. Normally photochemically driven, iniferter polymerization has unique behaviour. The advantages offered by this technique include i) linear increase of molecular weight with monomer conversion, resulting in the steady growth of a uniform polymeric layer ii) a wide range of monomers can be polymerized using this method such as acrylates, methacrylates, acrylonitrile, acrylamides and styrenes. iii) block copolymers can be formed by reinitiating polymerization in the presence of a different monomer[7].

Photoiniferter-mediated polymerizations have been used extensively since their initial discovery. The ability to produce well-defined block and graft polymers combined with the ability to incorporate different chemistries within the same macromolecule has led to further utilization of photoiniferters for "grafting from" polymeric surfaces.

Once a photoiniferter group has been generated, it can be used to polymerize monomers via a quasi-living radical polymerization method. It was found that the number of iniferter groups per polymer chain remained constant[17].

6.1.1 Mechanism of Iniferter Polymerization

The most commonly used and versatile photoiniferter is the diethyldithiocarbamate molecule, which contains bonds which cleave when exposed to UV radiation. When cleaved, two radicals are formed; a relatively unreactive diethyldithiocarbamyl radical and a more reactive carbon radical, which readily initiates monomer polymerization. For instance benzyl diethyldithiocarbamate, once irradiated with UV, forms a reactive benzyl

radical and a diethyldithiocarbamyl radical[16, 17]. This less reactive dithiocarbamyl (DC) moiety under suitable conditions will terminate with propagating polymer chains, which had been initiated by the more reactive benzyl radical. Hence the DC groups are reformed as terminal groups on the polymer chains, where they can redissociate by further adsorption of a photon; hence further exposure to UV[16], Scheme 6.1

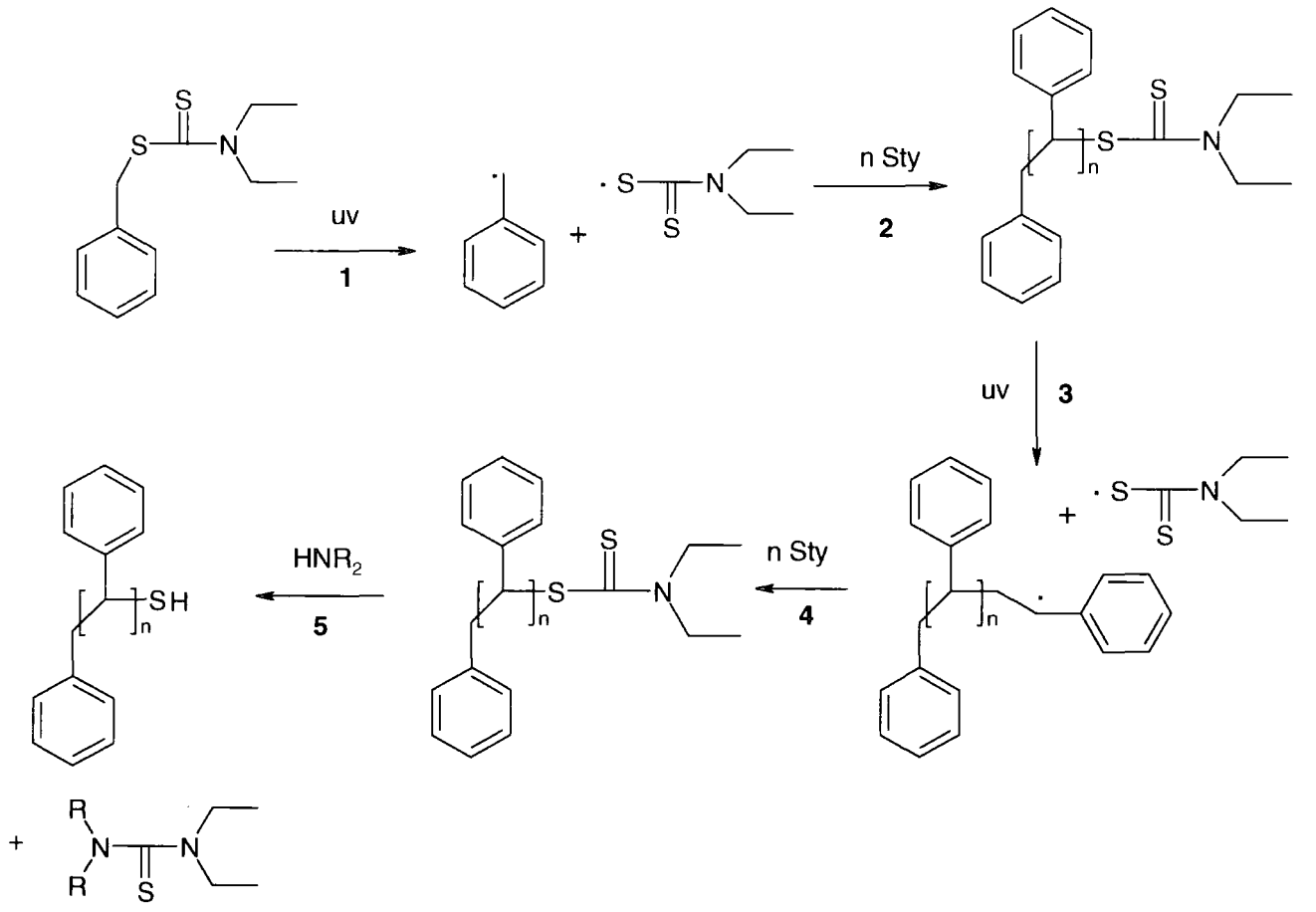

Scheme 6.1: Mechanism of quasi-living iniferter polymerization of styrene (Sty) using benzyldiethyldithiocarbamate[17, 18].

In this bi-radical mechanism, the relatively fast first step is the dissociation of benzyl-DC to produce the reactive carbon radical; the initiating group and the comparatively stable DC radical; the terminating group. Step 2 is the initiation and resulting propagation of the polystyrene chain followed by termination with the DC radical. Step 3 is the dissociation of the DC radical allowing the polymer chain to propagate further in the presence of ultra violet light and

additional monomer, hence permitting a longer polymer chain or the production of a block-copolymer if monomers are switched.

Additional monomer units can be inserted into the chains before termination re-occurs, making chain length proportional to irradiation time, light intensity and monomer concentration, step 4. Polymerization will only occur during irradiation time and in irradiated areas. After photopolymerization has completed, photoiniferter groups will remain at the polymer chain ends, until removal by the addition of a dialkylamine[19], step 5.

Polymerization that is induced by ultraviolet light (UV) is a beneficial method for surface modification. Reasons for this include; a high concentration of active species is produced between the substrate and the monomer, allowing a high degree of polymerization to take place; the process is also economical, energy efficient and relatively simple to carry out. Furthermore graft polymerization can be initiated without the need for modification by other living radical initiators[11, 20]. In the case of iniferter polymerization, the preparation and handling of samples is easier than in the case of atom transfer radical polymerization where inorganic salts form at the surface, requiring extra purification stages if the surface is to be characterized between polymerization steps[2].

The temperature in which the polymerization is carried out affects molecular weight and conversion of monomer. The initiation rate is the same for all temperatures because it is photochemically controlled, but propagation rate increases with temperature. Molecular weight will hence increase, but the number of polymer chains will remain the same. Different wavelengths of light have also been discovered to affect monomer conversion[21].

The iniferter method is very versatile and has successfully polymerized or block-copolymerized the following monomers: methyl methacrylate[11, 19, 22, 23] methyl acrylate, styrene[11, 13, 24], poly(ethylene glycol) methacrylate and dimethacrylate[11, 24, 25], hydroxyethyl methacrylate[24], dimethylacrylamide[11, 25, 25], acrylonitrile[16], methylacrylonitrile[16, 17] and n-isopropylacrylamide[26], [27], [28].

It has been found that monomer conversion is proportional to concentration of iniferter groups present, which was confirmed by calculating the graft efficiency and conversion[21]. Additionally the presence of higher concentrations of iniferter was found to suppress chain transfer. Chain

transfer causes a decrease in graft efficiency because it can lead to branching and cross-linking[22].

Other features of true living systems such as a low polydispersity index and a high control over molecular weight cannot be attained by this method due to the fact that the counter dithiocarbamyl radical has a tendency to initiate polymerization. One primary requirement of a mediating radical in true living systems is that it undergoes reversible termination of a polymer chain end without acting as an initiating species[29].

6.1.2 Iniferter Polymerization from Surfaces

Photoinitiated polymerization has been previously carried out on a variety of surfaces which include glass[6, 9], silicon[3] and cellulose [30] where chloromethylphenyl groups have been attached to the surface via a siloxane linkage and subjected to a further reaction with sodium diethyldithiocarbamate (NaDC). Polymer chains have also been grafted from Merrifield resin where DC has been tailored to the surface by reaction with the chlorine end groups[31]. Other methods include segmented polyurethane films which have been pre-treated with carbon tetrachloride and chloromethyl ether[32, 33] and DC-derivatized polystyrene films that comprise chloromethylstyrene groups copolymerized with styrene and reacted with NaDC[8, 11, 25].

This photo-initiated method has proved to be problematic for monolayers of initiator deposited onto gold by thiol terminated groups due to the fact that the thiol-gold bond has proved to be unstable to UV radiation[34, 35]. The methods outlined above require substrate-specific chemistries and multiple reaction steps to attain adequate surface retention of iniferter groups.

6.2 Aims

Diethyldithiocarbamate groups can be grafted to a surface by reacting sodium diethylthiocarbamate with a surface-bound halogenoalkane group such as benzyl chloride.

Plasma polymers can be deposited onto a surface in one simple step without the necessity of solvents or surface pre-treatment. Hence a surface coated with a layer of pulsed plasma polymerized 4-vinylbenzyl chloride can act as a suitable anchor for iniferter groups, Scheme 6.2.

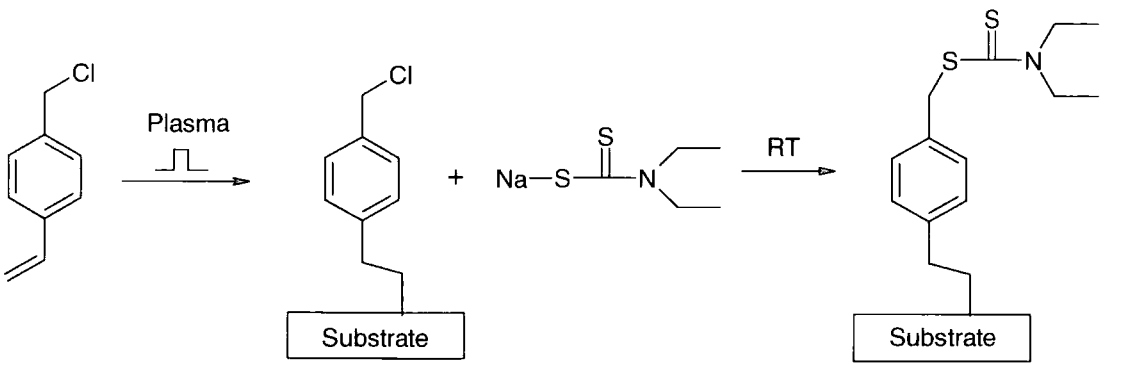

Scheme 6.2: Formation of surface-bound iniferter groups from plasma polymers.

The objectives behind this work are the surface retention of halogen-containing moieties via pulsed plasma polymerization followed by functionalization with dithiocarbamate initiating groups. These surfaces can then be employed to generate grafted polymeric films and subsequent block copolymers.

6.3 Experimental

6.3.1 Preparation of Iniferter Surfaces

4-vinylbenzyl chloride (97% purity, Aldrich) or 2-bromoethylacrylate (+98% purity, ABCR) was pulsed plasma polymerized onto silicon wafers at room temperature (20 °C) employing the same apparatus and protocol outlined in Chapter 4. Pulse duty cycles were set to 100 µs on, 4000 µs off and 20 µs on, 10,000 µs off for 4-vinylbenzyl chloride and 2-bromoethylacrylate respectively. Peak power was set to 20 W for both precursors.

Initiator functionalized surfaces were prepared by placing the plasma polymer coated silicon substrates into a glass tube containing a 22 mM solution of sodium diethyldithiocarbamate (99%, Aldrich) in ethanol at room temperature for a period of 24 hours. The wafers were subsequently removed and rinsed in ethanol.

6.3.2 Iniferter Polymerization

Iniferter-functionalised wafers were placed in a glass tube containing 0.5 M methyl methacrylate or styrene (99%, Aldrich) mixed with 3 cm^3 of methanol and outgassed with several freeze thaw cycles to remove absorbed oxygen. The system was subsequently positioned 10 cm away from a HgXe lamp (Oriel Instruments) to be irradiated with UV light, intensity set to 50 mW/cm^2 for predetermined time intervals. The grafted polymer brush films were then removed from solution and rinsed in methanol.

In order to differentiate between the molecular structure of the respective layers by infrared spectroscopy, 4-vinylbenzyl chloride-dithiocarbamate initiator films were used in the case of methylmethacrylate monomer whilst 2-bromoethylacrylate-dithiocarbamate films initiated the polymerization of styrene.

Chemical characterization of all films was achieved by X-ray photoelectron spectroscopy (XPS) and Fourier Transform Infrared Spectroscopy (FTIR) procedures as outlined in Chapter 3.

Silicon wafers functionalised with dithiocarbamate were irradiated in both methylmethacrylate and styrene solutions for varying time intervals to observe

how polymer layer thickness varied with UV irradiation time. A control experiment was carried out where 2-bromoethylacrylate-coated wafers minus dithiocarbamate functionalization were placed in a styrene solution, irradiated at varying time intervals and analysed as before to verify that the presence of the dithiocarbamate groups was responsible for the bulk growth of the polymer layer. Film thicknesses were obtained by taking cross sections of the silicon wafers, followed by a 10 nm coating of gold and analysis with scanning electron microscopy (Cambridge Instruments, S240).

6.3.3 Quasi-Living Polymerization

To verify quasi-living polymerization, block copolymer brushes of iniferter photo-polymerized polymethylmethacrylate-polystyrene were produced by photo-polymerizing an initial layer of PMMA onto functionalized wafers of dithiocarbamate; 15 minutes irradiation time, followed by washing in methanol and further photo-polymerization of styrene at varying time intervals (15 to 90 minutes). Monomer concentration in both instances was 0.2 M to permit the production of thinner films that could be analysed effectively with reflectometry.

6.4 Results and discussion

6.4.1 4-vinylbenzyl chloride Pulsed Plasma Polymer – Dithiocarbamate

XPS characterization of the deposited pulsed plasma polymerized 4-vinylbenzyl chloride layer indicates that the film stoichiometry is in close agreement with the predicted theoretical values, Table 6.1. The corresponding high resolution C(1s) XPS spectrum is consistent with indicated the presence of three types of carbon environment[36]: aromatic carbon bonded to hydrogen (binding energy = 284.75 eV), carbon bonded to carbon or hydrogen (285.0 eV), and carbon bonded to a chlorine atom (287.05 eV), Figure 6.1(a). A π- π * shake-up satellite representative of the surface retention of aromatic groups can be observed at 291.5 eV. Absence of any Si(2p) signal from the silicon substrate confirms complete coverage by the plasma polymer layer, Table 6.1.

Elemental analysis following reaction of sodium diethyldithiocarbamate with the 4-vinylbenzyl chloride pulsed plasma polymer layer shows that a small amount of chlorine remains following the reaction. Approximately 50% of the pulsed plasma polymerized 4-vinylbenzyl chloride groups present within a ~2 nm penetration depth of the surface have reacted to yield pulsed plasma 4-vinylbenzyl chloride - diethyldithiocarbamate iniferter groups. The C(1s) spectrum of polymethylmethacrylate photochemically grown from this surface can be fitted to four different carbon environments: carbon singly bonded to hydrogen (285.0 eV), carbon adjacent to the ester carbon, (285.7 eV), carbon singly bonded to oxygen (286.45 eV) and the ester carbon (289.1 eV); Figure 6.1(b). Stoichiometric analysis indicates good agreement between the predicted and measured elemental percentages, Table 6.1. In fact only trace amounts of sulphur and nitrogen (from iniferter groups located at the polymethylmethacrylate chain ends) are present.

Table 6.1: XPS stoichiometries of pulsed plasma polymerized 4-vinylbenzyl chloride (ppVBC), 2-bromoethylacrylate (ppBEA), iniferter films (DC) and photo-polymerized polymethylmethacrylate (PMMA) and polystyrene (PS).

Wafer Coating		**%C**	**%O**	**%S**	**%N**	**%Cl**	**%Br**
ppVBC	Theoretical	90	0	-	-	10	-
	Experimental	89 ± 1	<0.1	-	-	11 ± 1	-
ppBEA	Theoretical	63	25	-	-	-	12
	Experimental	65	24	-	-	-	11
ppVBC-DC	Theoretical	82	0	12	6	0	-
	Experimental	87	<0.1	7	3	3	-
ppBEA-DC	Theoretical	67	13	13	7	-	0
	Experimental	65 ± 3	15 ± 1.5	12 ± 1.5	5	-	3 ± 0.5
Photopolymerized PMMA	Theoretical	72	28	Trace	Trace	0	-
	Experimental	74	26	<0.1	<0.1	0	-
Photopolymerized PS	Theoretical	100	0	Trace	Trace	-	Trace
	Experimental	100	<0.1	<0.1	<0.1	-	<0.1

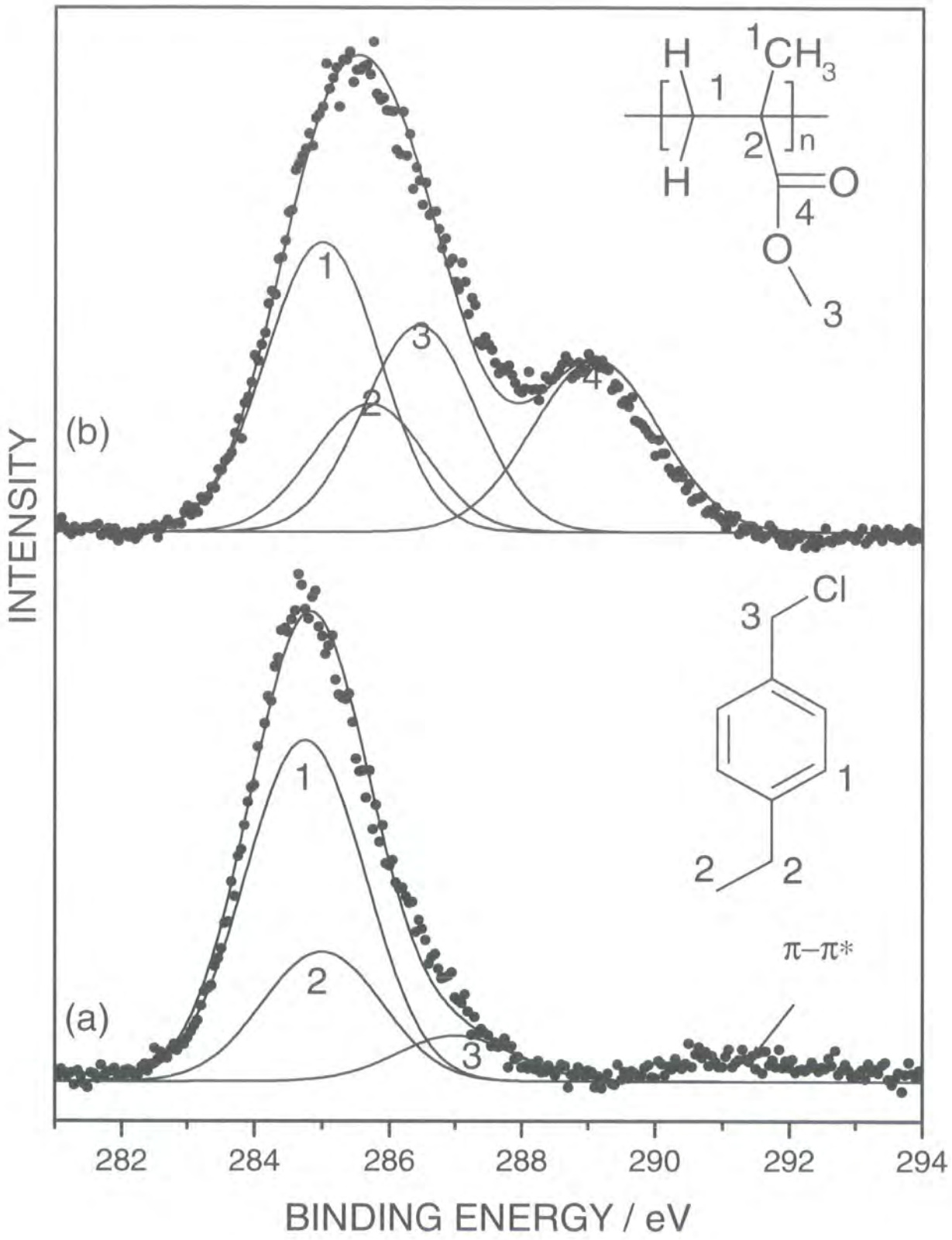

Figure 6.1: XPS C(1s) Envelopes of (a) pulsed plasma polymerized 4-vinylbenzyl chloride, (b) photopolymerized polymethylmethacrylate.

The Fourier transform infrared spectra of the pulsed plasma polymerized 4-vinylbenzyl chloride layer displays a loss of the vinyl carbon-carbon double bond stretch at 1630 cm^{-1} (B), Figure 6.2(b) and Table 6.2. Whilst the para-substituted benzene ring stretches at 1603 cm^{-1} (C) and 1495 cm^{-1} (D) remain intact. These observations are indicative of conventional polymerization occurring during the pulsed plasma duty cycle off-period.

Reaction of sodium diethyl dithiocarbamate with the 4-vinylbenzyl chloride pulsed plasma polymer film indicates the presence of two new peaks at 1270 cm^{-1} (F) and 1205 cm^{-1} (G), which correspond to the C=S and C-N stretches in S=C-N of dithiocarbamate respectively, Figure 6.2(c). Iniferter photopolymerization of methylmethacrylate gives rise to the C=O ester stretch at 1730 cm^{-1} (A) thereby confirming the formation of polymethylmethacrylate on the plasma polymer surface when compared with sourced PMMA (1 x 10^6 MW), Figures 6.2(d) and (e).

Table 6.2: FTIR Peak assignments for plasma polymers, iniferter films, photopolymerized and sourced PMMA and PS.

Designation	**VBC monomer**	**ppVBC**	**VBC-DC**	**VBC-DC-PMMA**	**Sourced PMMA**	**BEA monomer**	**ppBEA**	**BEA-DC**	**BEA-DC-STY**	**Sourced PS**
A: C=O ester stretch, 1730cm^{-1}				*	*	*	*	*	*	
B: C=C stretch, 1630cm^{-1}	*					*				
C: Para-substituted aromatic ring stretch, 1603cm^{-1}	*	*	*	*					*	*
D: Para-substituted aromatic ring stretch, 1495cm^{-1}	*	*	*	*					*	*
E: CH_2 symmetric stretch, 1452cm^{-1}	*	*	*	*	*	*	*	*	*	*
F: C-N stretch (in S=C-N), 1270cm^{-1}			*					*		
G: C=S stretch, 1205cm^{-1}			*					*		

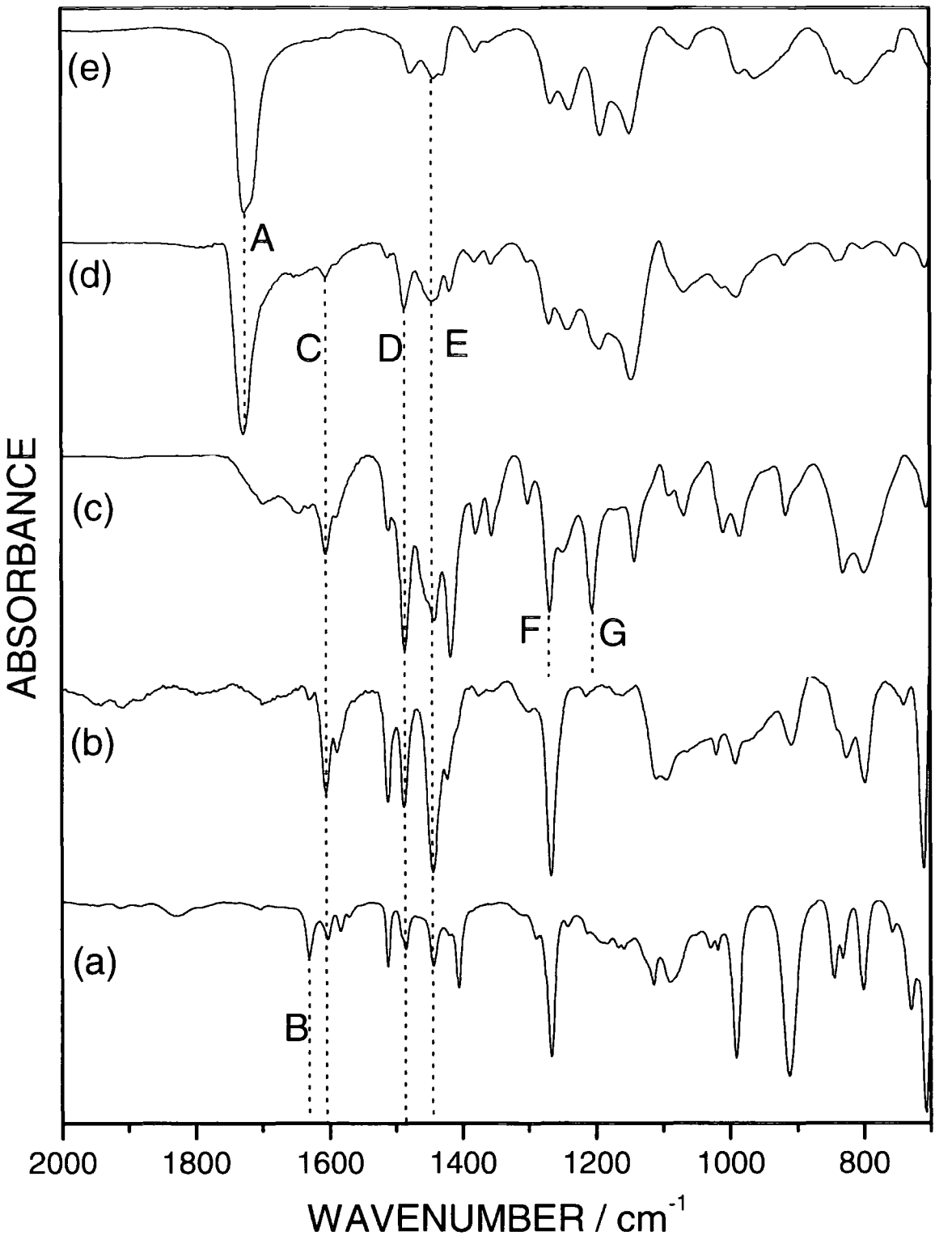

Figure 6.2: FTIR spectra of: (a) 4-vinylbenzyl chloride monomer; (b) pulsed plasma polymerized 4-vinylbenzyl chloride, (c) pulsed plasma polymerized 4-vinylbenzyl chloride functionalized with dithiocarbamate, and (d) photopolymerized polymethylmethacrylate, (e) sourced polymethylmethacrylate.

6.4.2 2-bromoethylacrylate Pulsed Plasma Polymer - Dithiocarbamate

The high resolution C(1s) XPS spectrum of the 2-bromoethylacrylate pulsed plasma polymer layer can be fitted to five carbon environments[30]: carbon singly bonded to hydrogen (binding energy = 285.0 eV), carbon adjoining an ester carbon (285.7 eV), carbon bonded to a bromine atom (285.75 eV), carbon singly bonded to oxygen (286.45 eV) and the ester carbon (289.1 eV), Figure 6.3(a). The film stoichiometry is in good agreement with the theoretical values, Table 6.1. Absence of Si(2p) signals corroborates complete coverage of the silicon wafer by the plasma polymer.

Stoichiometric analysis following reaction with sodium diethyldithiocarbamate shows that approximately 60% of the bromine atoms had reacted within the ~2 nm sampling depth to produce 2-bromoethylacrylate pulsed plasma polymer - diethyldithiocarbamate iniferter groups. The C(1s) spectrum following iniferter polymerization of styrene displays prominent hydrocarbon environments (284.75 and 285.0 eV) and its associated π- π * shake-up satellite, Figure 6.3(b). Stoichiometric analysis shows only trace amounts of sulphur and nitrogen (from dithiocarbamate groups present at the polystyrene chain ends).

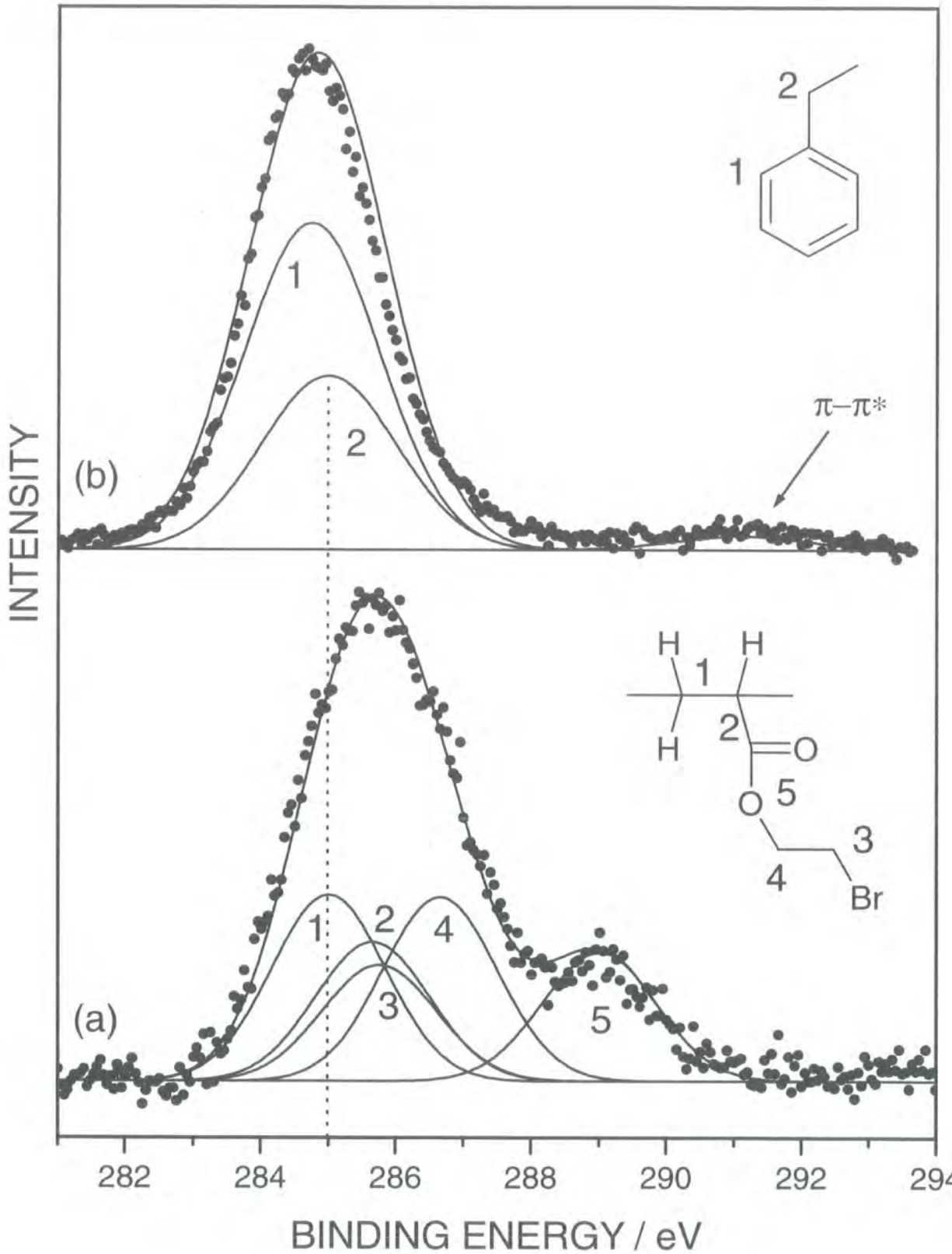

Figure 6.3: XPS C(1s) envelopes of: (a) pulsed plasma polymerized 2-bromoethylacrylate, and (b) photopolymerized polystyrene.

The infrared spectrum of 2-bromoethylacrylate monomer, Figure 6.4(a) contains a characteristic carbonyl stretch at 1730 cm^{-1} (A) and a C=C double bond stretch at 1630 cm^{-1} (B), Table 6.2. The carbonyl stretch is still evident following pulsed plasma polymerization of 2-bromoethylacrylate onto a silicon substrate, whilst the alkene stretch (B) has disappeared, thereby authenticating structural retention and polymerization, Figure 6.4(b).

Reaction with sodium diethyldithiocarbamate yields two signature peaks at 1270 cm^{-1} (F) and 1205 cm^{-1} (G), corresponding to the dithiocarbamate C=S and C-N (in S=C-N) stretches respectively, Figure 6.4(c). Iniferter photopolymerization of styrene gives rise to the emergence of aromatic ring stretches at 1603 (C) and 1495 cm^{-1} (D) attributable to polystyrene chain growth at the surface, Figures 6.4(d) and (e).

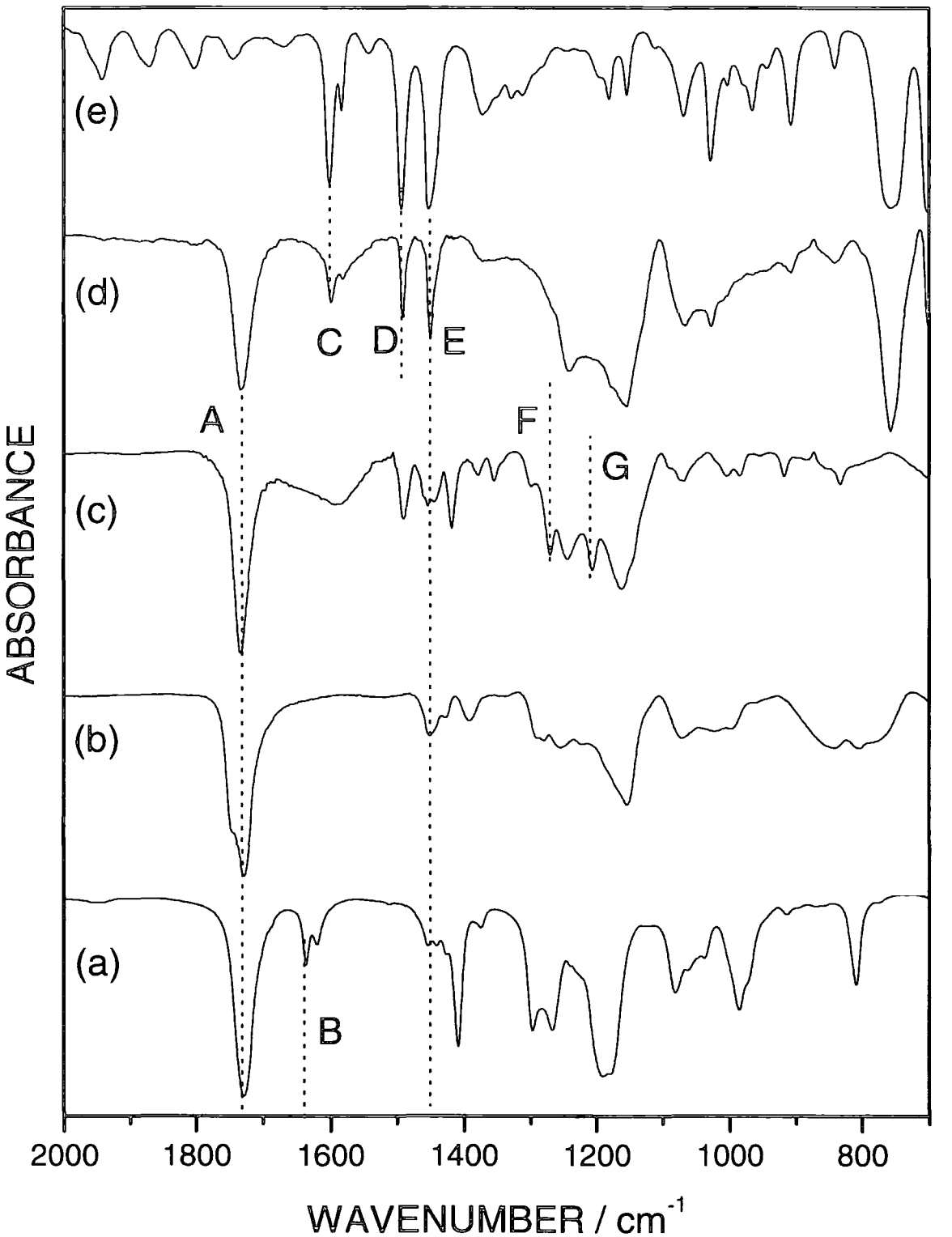

Figure 6.4: FTIR spectra of (a) 2-bromoethylacrylate monomer, (b) pulsed plasma polymerized 2-bromoethylacrylate, (c) pulsed plasma polymerized 2-bromoethylacrylate functionalized with dithiocarbamate, (d) photopolymerized polystyrene, (e) sourced polystyrene.

A high surface retention of iniferter groups has been achieved with greater simplicity and in a reduced number of reaction steps in comparison to existing methodologies[3, 6, 8, 9, 11, 25, 30-32]. These treated surfaces have been effectively deployed for photo-polymerization of acrylates and styrenes.

6.4.3 Quasi-living Polymerization

Scanning electron microscopy of a cross-section of 2-bromoethylacrylate pulsed plasma polymer layer indicates a swelling from 650 nm to ~800 nm following 24-hours of reaction with sodium diethyldithiocarbamate solution. Subsequent iniferter photo-polymerization gives rise to polystyrene film thickness of ~ 3 μm after 3 hours UV irradiation, Figure 6.5. The respective dithiocarbamate functionalised silicon wafers were irradiated in methylmethacrylate/styrene solutions for varying time intervals in order to follow how polymer layer thickness varied with UV irradiation time, Figures 6.6(a) and (b) and a linear correlation was measured by SEM. Differences in the increase of layer thickness versus UV irradiation time for photopolymerized methylmethacrylate and styrene can be ascribed to differing propagation rates.

Pseudo-living polymerization of this nature does not yield the same low polydispersity indices associated with conventional living polymerization, but the thickness of the bulk polymer layer is found to increase linearly with irradiation time.

Control experiments entailed repeating the solution phase UV polymerization using plasma polymer coated silicon wafers minus dithiocarbamate functionalization, Figure 6.6(c). These confirm the absence of polymer film growth.

To confirm pseudo-living polymerization, a block copolymer of polymethylmethacrylate-polystyrene was grown from dithiocarbamate-functionalised wafers, Figure 6.7. Bulk layer thickness of the second polymer layer (polystyrene) is found to increase linearly with respect to irradiation time, confirming the first polymer layer (polymethylmethacrylate) remains photochemically active following its removal from the initial polymerization mixture.

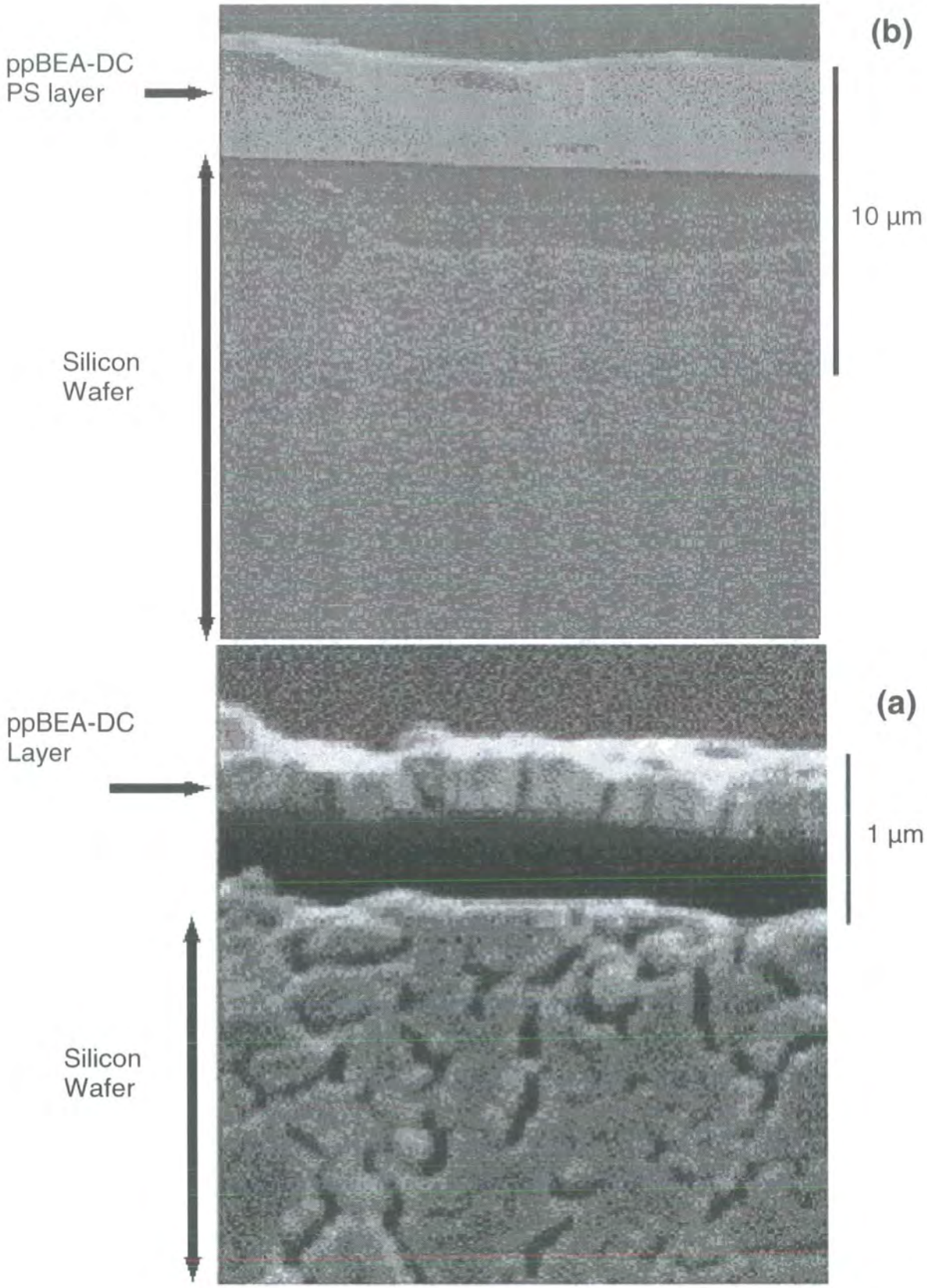

Figure 6.5: SEM micrograph of cross-section showing underlying silicon wafer coated with (a) ~800 nm layer dithiocarbamate-functionalised pulsed plasma 2-bromoethylacrylate; and (b) ~3 µm thick layer containing 800 nm dithiocarbamate-functionalised pulsed plasma 2-bromoethylacrylate and photopolymerized polystyrene after 3 hours UV irradiation.

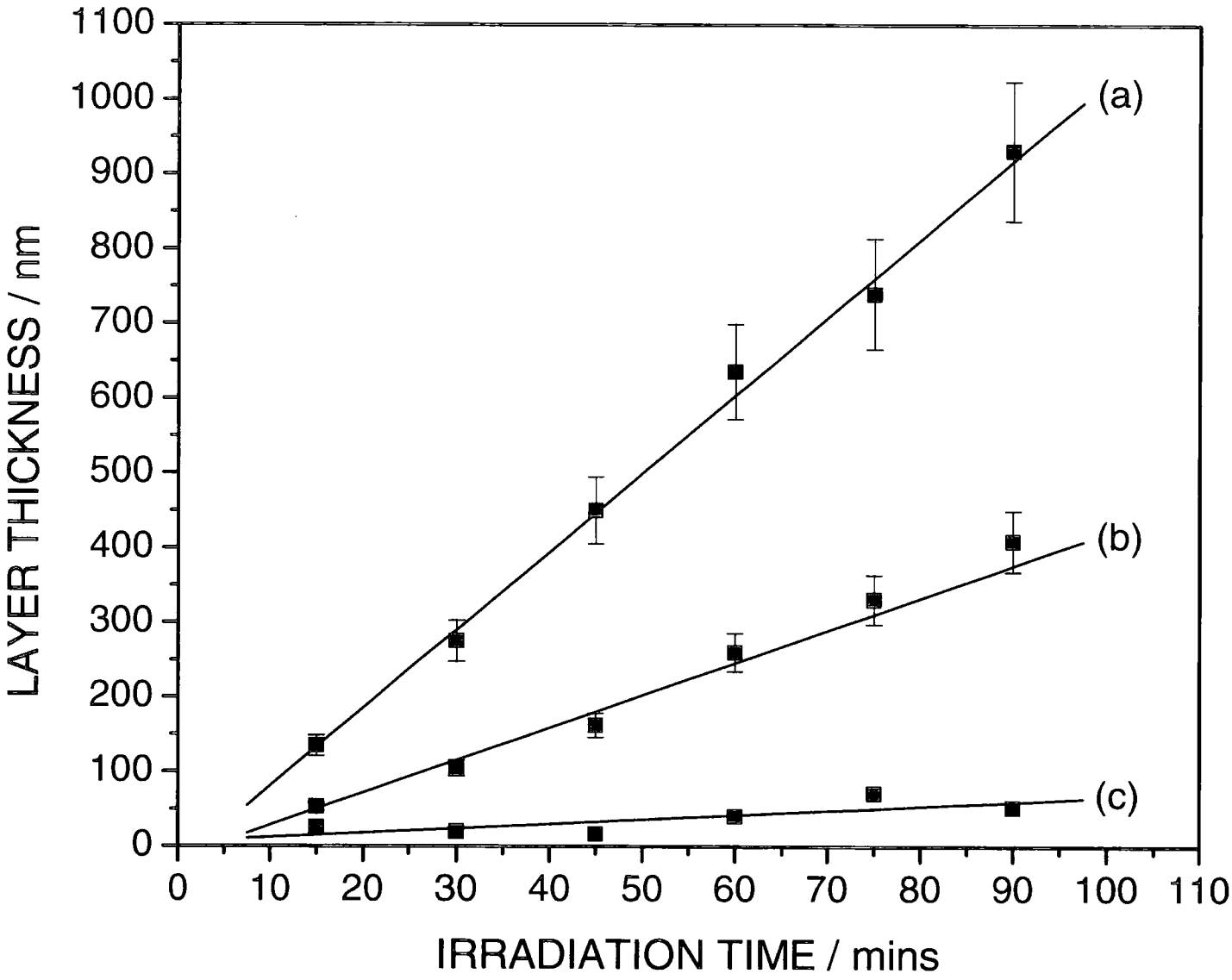

Figure 6.6: Time variation of: (a) iniferter photopolymerized polymethylmethacrylate layer thickness (± 10%) grown from dithiocarbamate-functionalized pulsed plasma 4-vinylbenzyl chloride (b) iniferter photopolymerized polystyrene layer thickness (± 10%) grown from dithiocarbamate-functionalized pulsed plasma 2-bromoethylacrylate; and (c) repeat of (b) in the absence of dithiocarbamate derivatization of the 2-bromoethylacrylate pulsed polymer layer.

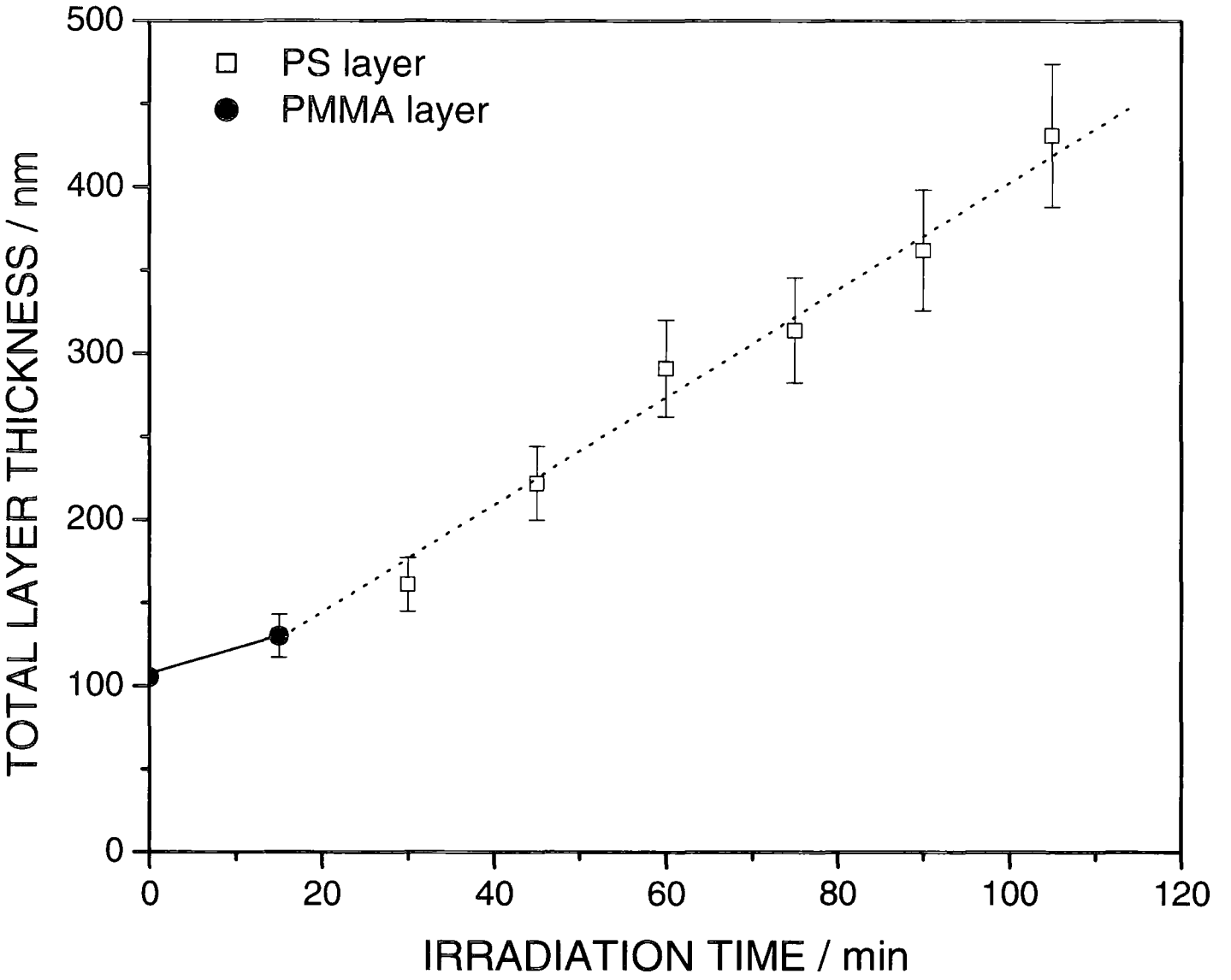

Figure 6.7: Layer thickness (± 10%) of polymethylmethacrylate-polystyrene block copolymer grown from iniferter films with respect to UV irradiation time.

6.5 Conclusions

A general method has been devised for the growth of block copolymer brushes onto solid surfaces at room temperature using iniferter photopolymerization. This entails pulsed plasma deposition of halogen-containing thin films which are then derivatized to form dithiocarbamate initiator sites. Quasi-living polymer brushes of polymethylmethacrylate and polystyrene have been successfully grown off these surfaces by iniferter photopolymerization, leading to subsequent block copolymerization. This technique has improved on previous methods because the number of reaction stages has been minimized and there are no restrictions imposed by the substrate.

6.6 References

[1] Husemann, M.; Morrison, M.; Benoit, D.; Frommer, J.; Mate, C. M.; Hingsberg, W. D.; Hedrick, J. L.; Hawker, C. J., *J. Am. Chem. Soc.*, 122, **2000**, 1844.

[2] Husemann, M.; Malmstrom, E. E.; McNamara, M.; Mate, Mercerreyes, D.; Benoit, D.; Hedrick, J. L.; Mansky, P.; Huang, E.; Russell, T. P.; Hawker, C. J., *Macromolecules*, 32, **1999**, 1424.

[3] Shah, R. R.; Mercerreyes, D.; Husemann, M.; Rees, I.; Abbott, N. L.; Hawker, C. J.; Hedrick, J. L., *Macromolecules*, 33, **2000**, 597.

[4] Huang, X. Y.; Doneski, L. J.; Wirth, M. J., *CHEMTECH*, **1998**, 19.

[5] Higashi, J.; Nakayama, Y.; Marchant, R. E.; Matsuda, T., *Langmuir*, 15, **1999**, 2080.

[6] Lee, H. J.; Nakayama, Y.; Matsuda, T., *Macromolecules*, 32, **1999**, 6989.

[7] Nakayama, Y.; Matsuda, T., *Macromolecules*, 29, **1996**, 8622.

[8] Nakayama, Y.; Matsuda, T., *Langmuir*, 15, **1999**, 5560.

[9] Matsuda, T.; Kaneko, M.; Ge, S. R., *Biomaterials*, 24, **2003**, 4507.

[10] Bai, J.; Qiu, K. Y.; Wei, Y., *Polymer International*, 52, **2003**, 853.

[11] De Boer, B.; Hadziioannou, G., *Macromolecules*, *33*, **2000**, 345.

[12] Nakayama, Y.; Matsuda, T., *Macromolecules*, *32*, **1999**, 5405.

[13] Ward, J. H.; Bashir, R.; Peppas, N. A., *J. Biomed. Mater. Res.*, 56, **2001**, 351.

[14] Wang, P.; Tan, K. L.; Kang, E. T., *J. Biomater. Sci., Polym. Ed.*, 11, **2000**, 169.

[15] Kwon, O. H.; Nho, Y. C.; Park, K. D.; Kim, Y. H., *J. Appl. Polym. Sci.*, 71, **1999**, 631.

[16] Otsu, T.; Yoshida, M.; *Macromol. Chem. Rapid Commun.*, 3, **1982**, 127.

[17] Otsu, T.; Yoshida, M.; Tazaki, T., *Macromol. Chem. Rapid Commun.*, 3, **1982**, 13.

[18] Otsu, T.; Yamashita, K.; and Tsuda, K., *Macromolecules*, 19, **1986**, 287.

[19] Ajayaghosh, A.: Das, S., *J. Appl. Polym. Sci.*, 45, **1992**, 1617.

[20] Luo, N.; Hutchison, B.; Anseth, K. S.; Bowman, C. N., *J. Polym. Sci.*, 40, **2002**, 1885.

[21] Otsu, T.; Matsunaga, T.; Doi, T.; Matsumoto, A.; *Eur. Polym. J.*, 31, **1995**, 67.

[22] Ajayaghosh, A.: Das, S., *J. Appl. Polym. Sci.*, 45, **1992**, 1617.

[23] Luo, N.; Hutchison, B.; Anseth, K. S.; Bowman, C. N., *Macromolecules*, 35, **2002**, 2487.

[24] Nakayama, Y.; Hirano, Y.; Goto, K.; Matsuda, T., *Biomaterials*, 20, **1999**, 963.

[25] Nakayama, Y.; Sudo, M.; Uchida, K.; Matsuda, T., *Langmuir*, 18, **2002**, 2601.

[26] Harmon, M. E.; Jakob, T. A. M.; Frank, C., *Macromolecules*, 35, **2002**, 5999.

[27] Liang, L.; Feng, X.; Liu, J.; Fryxell, G. E., *Macromolecules*, 31, **1998**, 7845.

[28] Ohya, S.; Nakayama, Y.; Matsuda, T., *Biomacromolecules*, 2, **2001**, 856.

[29] Hawker, C. J.; Bosman, A. W.; Harth, E., *Chem. Rev.*, 101, **2001**, 3661.

[30] Hattori, K.; Hiwatari, M.; Iiyama, C, ; Yoshimi, Y.; Kohori, F.; Sakai, K.; Piletsky, S. A.,
J. Membrane Sci., 233, **2004**, 169.

[31] Ruckert, B.; Hall, A. J.; Sellergren, B., *J. Mater. Chem.,* 12, **2002**, 2275.

[32] Lee, H. J.; Matsuda, T., *J. Biomed. Mater. Res.,* 47, **1999**, 564.

[33] Magoshi, T.; Ziani-Cherif, H.; Ohya, S.; Nakayama, Y.; Matsuda, T., *Langmuir*, 18, **2002**, 4862.

[34] Van der Wegte, E.W.; Hadziioannou, G., *Langmuir*, 13, **1997**, 4357.

[35] Werts, M. P.; Van der Wegte, E.W.; Hadziioannou, G., *Langmuir*, 13, **1997**, 4939.

[36] Beamson, G.; Briggs, D; *High Resolution XPS of Organic Polymers*, Wiley, New York, **1992.**

Chapter 7: A Substrate Independent Method for the Formation of Protein-resistant Surfaces

7.1 Introduction

Surfaces that are resistant to protein adsorption find an important role in preventing an extensive variety of problems such as (a) irritation arising from the adhesion of bacteria to contact lenses, (b) thrombosis resulting from adsorption of proteins onto intravenous medical devices such as catheters[1, 2], and (c) contamination of packaged food by micro-organisms which can lead to the production of a biofilm[3]. These surface coatings are biocompatible in the sense that they do not degrade after long term exposure to proteins and cells[4, 5, 6]. Existing applications for these protein-inert surfaces include sensors, implanted devices e.g. heart pacemakers[7], contact lenses[8, 9] and drug-delivery systems[10].

When a protein approaches a surface, it can interact by electrostatic forces, Van der Waals forces[11] and hydrogen bonds. Extensive studies[12, 13, 14] have demonstrated that in order for a molecule to be resistant to proteins, it must exhibit the following properties:

(1)	*The molecule must be hydrophilic*
(2)	*The molecule must contain a group that is a hydrogen bond acceptor (reduce H-Bond interactions)*
(3)	*The molecule must not be a hydrogen bond donor*
(4)	*The molecule must be of neutral electronic charge (to reduce electrostatic interactions)*

Systems previously employed to resist protein adsorption include polyvinylalcohol; adsorbed from an aqueous solution onto a polystyrene matrix, which has shown strong resistance to albumin[15]. Polysaccharides physisorbed onto polyethylene[16] or pyrolytic carbon-coated graphite[17] also exhibit a strong resistance to human plasma. Polyurethanes have been widely used as coatings for biomedical devices particularly in catheters[18].

One of the most widely researched molecules for protein resistance is poly(ethylene glycol) (PEG)[19, 20, 21]. It has been suggested that the hydrated PEG chains compress out of the PEG layer as protein molecules approach[11]. Dehydration of the PEG chains is a thermodynamically unfavourable process, resulting in steric repulsion, and hence repulsion of the protein. It is this factor which makes PEG so inert to the adsorption of proteins.

PEG is used in many existing bioapplications as a coating with non-fouling properties towards proteins and cells[22, 23]. PEG, being a polyether, is very hydrophilic, neutrally charged and a hydrogen bond acceptor. Its main disadvantage is that it oxidises in air quite readily or when in contact with transition metals[24, 25, 26].

PEG coatings have been formed by various physical and chemical methods. For example it can form copolymeric micelles with lactic acid[27] and lysine[28, 29] and can be attached to negatively-charged transition metal oxides e.g. TiO_2, Nb_2O_5 and Ta_2O_5 via positively charged amino groups. PEG has also been attached to chlorine-functionalised silicon by hydroxyl linkages[30]. Tri-block copolymers of poly(ethylene glycol) and poly(propylene glycol) immobilized on polymer interfaces such as polystyrene[31] have exhibited a high resistance to human serum albumin.

The most influential studies[12] have been carried out on different self-assembled monolayers grafted to a gold surface via thiol linkages. Inertness to fibrinogen and lysozyme adsorption using surface plasmon resonance (SPR) is well documented. The aforementioned examples are suitable plasma-proteins that adsorb to the surface in entirely opposing chemical interactions. Fibrinogen is a large protein that adsorbs readily onto hydrophobic and positively charged surfaces and has a particular affinity for adhesion to mammalian cells[32]. Lysozyme is an antibacterial defence found in tears and saliva. Compared to fibrinogen, it adsorbs to negatively-charged surfaces and is a relatively small protein.

Self-assembled monolayers (SAMS) that contain derivatives of PEG and other polyethers have, as expected a high resistance to protein adsorption due to their highly hydrophilic nature[33, 34]. Polymeric chains of glycine are also found to be reasonably resistant. However when the N-H bonds of glycine are converted to $N\text{-}CH_3$ (glysine $\rightarrow$ sarcosine groups)[14], protein resistance is

found to increase due to the significant reduction in hydrogen bond donor groups. Sarcosine polymers are hydrophilic and proficient hydrogen bond acceptors, giving rise to high degree of inertness to protein adsorption.

Self-assembled monolayers that contain large quantities of hydrocarbons or fluorinated hydrocarbons such as $-HN(CH_2)_nCH_3$ and $-HNCH_2(CF_2)_nCF_3$ show little resistance to the adsorption of both proteins, which coincides with the theory that proteins readily adsorb onto hydrophobic species[35].

Polyethylenimine (linear and branched) can be attached to an anhydride SAM[12]. Many secondary amine groups remain, but they can be acylated by reacting with acetyl chloride or anhydride-terminated PEG chains, converting the hydrogen bond donor amine to hydrogen bond-accepting amide groups. Tests with SPR found that the mixed SAM of amines acylated by acetyl chloride exhibit the same degree of resistance to protein adsorption as amine SAMS capped with anhydride-terminated poly(ethylene glycol).

Further research[13] has demonstrated the self-assembled monolayers formed from a 1:1 mixture of positively and negatively charged thiols, terminated in oligomers of tripolypropylene sulfoxide and quarternary ammonium groups are comparable with PEG in their ability to block protein adsorption with the added advantage that that they do not oxidise as readily in air. Singularly charged (either positive or negative) SAMS adsorbed nearly a full monolayer of fibrinogen and lysozyme. This evidence supports the theory that electrically neutral species are more resistant to the adsorption of proteins and cells.

7.2 Aims

To manufacture protein resistant surfaces from plasma polymers, maleic anhydride (MA) can be deposited by pulsed-plasma discharge onto substrates such as silicon wafers[36], polystyrene, polytetrafluoroethylene and gold and functionalized with protein-resistant moieties via amination of the anhydride groups, forming an amic acid. In the case of primary amines, if heat (~120 °C) is then applied, a water molecule is lost and the anhydride ring closes, forming a cyclic imide[37].

For example, an amine-terminated PEG chain can be grafted to a pulsed plasma polymer layer of MA and subsequently imidized. Linear polyethylenimine (LPEI) can also be tailored to the surface, but as it comprises secondary amine groups, imidization cannot occur. All excess amine groups can be subsequently acylated by reaction with acetyl chloride.

The aim of this research is to prepare protein-resistant surfaces from plasma polymers of maleic anhydride onto substrates including silicon and gold for characterization by XPS, FTIR, water contact angle and film thickness measurements and to assess the protein resistance of such surfaces to fibrinogen and lysozyme by surface plasmon resonance studies.

7.3 Experimental

7.3.1 Pulsed Plasma Polymerization of Maleic Anhydride

Maleic anhydride (99% purity, Aldrich) was plasma deposited according to the protocol described in Chapter 4. Plasmachemical conditions corresponded to a 10 W continuous wave burst lasting 20 μs (t_{on}), followed by an off-period (t_{off}) set at 1200 μs and a deposition duration of 5 minutes. The peak power of the plasma here is very low (0.16 W) in order to minimise fragmentation of the monomer. The films were deposited onto silicon wafers and gold SPR chips (Biacore) (~ 1.0 x 1.0 cm), Scheme 7.1.

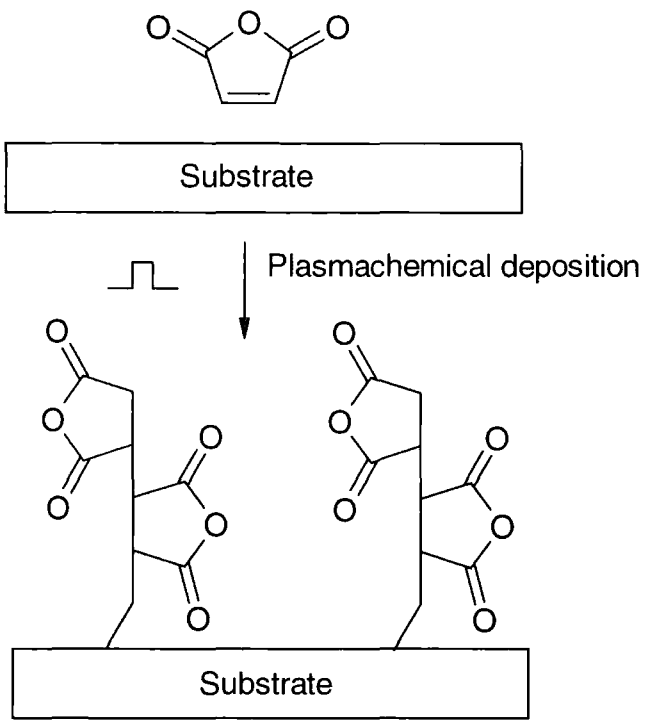

Scheme 7.1: Pulsed plasma polymerization of maleic anhydride onto substrate surface.

7.3.2 Grafting of Poly(ethylene glycol) to Maleic Anhydride Pulsed Plasma Polymer

Pulsed plasma deposited maleic anhydride coated wafers were immersed in 0.2% solution of amine-terminated poly(ethylene glycol) $(CH_2CH_2O)_n$ (M_n ~ 5400, Shearwater Polymers) in 5 ml toluene (Aldrich), (purified by several freeze thaw cycles to remove adsorbed gases) and heated at 40 °C for 24 hours, under vacuum. The wafers were removed from the reaction mixture, washed in toluene before being heated at 120 °C in an oven for 1 hour to allow imidization to occur, Scheme 7.2.

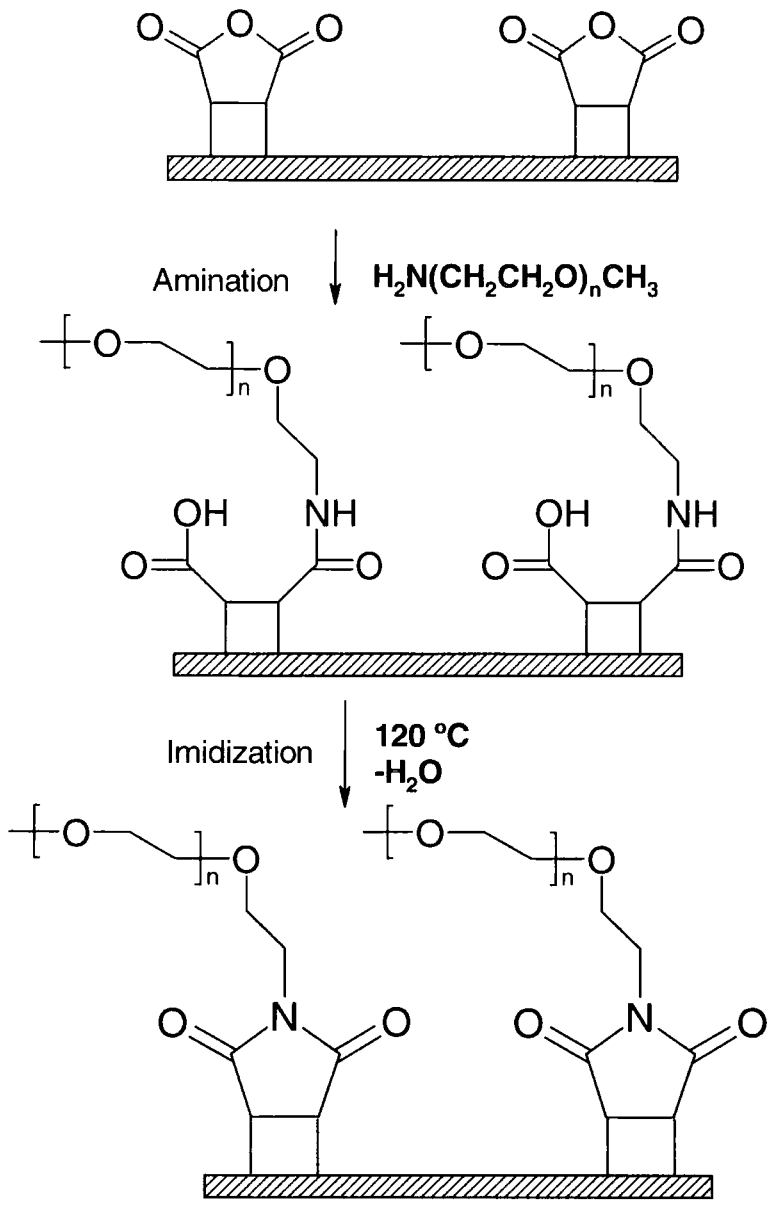

Scheme 7.2: Attachment of nPEG to ppMA layer followed by imidization.

7.3.3 Grafting of Polyethylenimine to Maleic Anhydride Pulsed Plasma Polymer

Linear polyethylenimine (LPEI), (M_n ~ 600, Aldrich) was dissolved in n-methylpyrrolidinone (NMP) (99%, Aldrich) (1:10 w/w). Plasma deposited MA coated silicon wafers were then immersed in the LPEI/NMP mixture for 24 hours and subsequently rinsed in NMP. Acylation of the remaining amine groups in the polymer was achieved by submersing the wafer for 2 hours in a solution of 0.3 mM acetyl chloride (99%, Aldrich), 0.3 mM triethylamine (99%, Aldrich) and dichloromethane (99%, Fluka) at 35 °C, Scheme 7.3.

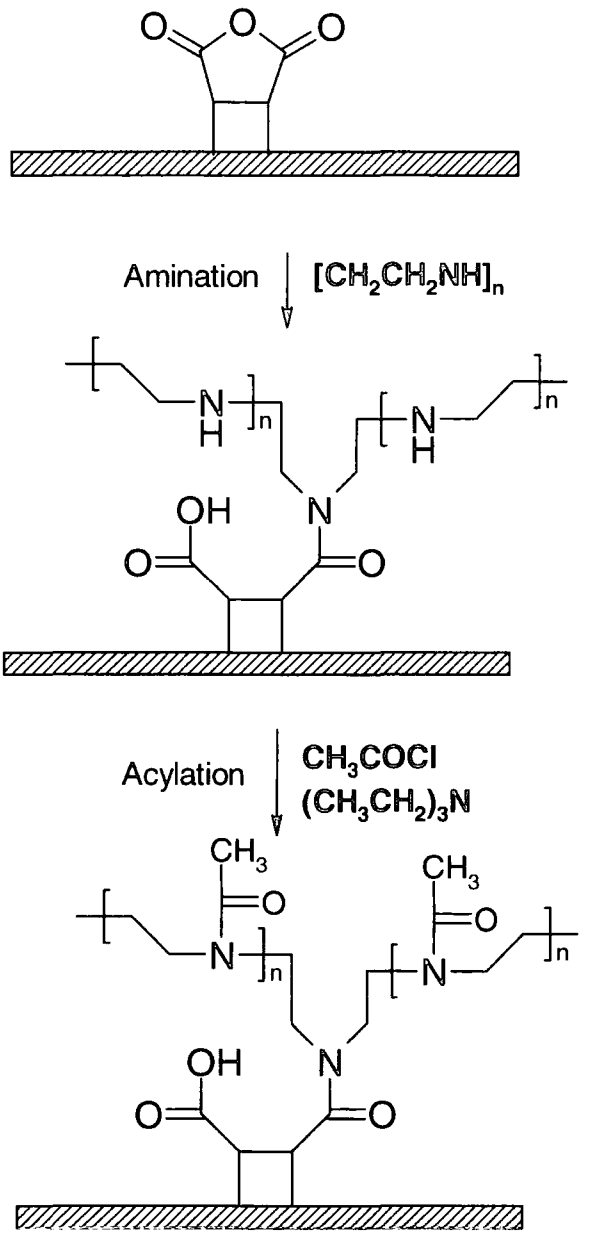

Figure 7.3: Attachment of LPEI to ppMA followed by acylation with acetyl chloride.

7.3.4 Preparation of a Control Surface

The standard control surface used in this experiment with which to compare values of protein adsorption is low molecular weight polyisobutylene $[CH_2\text{-}C(CH_3)_2]_n$ (Aldrich) (concentration, 0.2% by mass in toluene) which was spin-coated (30 sec, 2000 rpm) onto a gold SPR chip, (20 nm thickness).

7.3.5 Methods of Analysis

Plasma polymer film thicknesses were measured using reflectometry. Chemical characterization of the deposited films was performed using the same XPS and FTIR procedures outlined in Chapter 3.

Contact angle analysis on all pulsed plasma polymer-derivatized substrates was carried out using a VCA2500XE (ASE Products), where 2.0 µl drops of deionized water were placed onto the surface and the contact angles measured with the video contact angle system.

For surface plasmon resonance (SPR) studies, the tailored films were deposited onto Biacore Sensor Chip Au (Biacore, Uppsala, Sweden). The coated substrates were mounted in an SPR cartridge and placed inside a Biacore 1000 instrument for analysis. Adsorption of protein to the films was determined at a temperature of 25 °C.

The SPR protocol used for measuring the adsorption of proteins is as follows: i) flowing a solution of sodium dodecyl sulphate (+99%, Sigma) (40 mM in buffer solution) over the surface for 3 mins and then rinsing with buffer solution for 10 min; ii) flowing buffer solution for 2 min, subsequently substituting the flow with protein solution (1 mg/ml in buffer) for 30 min; iii) allowing buffer solution to flow over the surface for an additional 10 min.

The flow rate used for all experiments was 10 µl/min. The buffer solution used was HBS-EP (Biacore) consisting of 0.01 M HEPES (4-(2-hydroxyethyl)-1-piperazinethanesulfonic acid), pH 7.4, 0.15 sodium chloride, 3 mM ethylenediaminetetraacetic acid and 0.005% polyoxyethylenesorbitan surfactant. Two proteins were used, fibrinogen (from bovine plasma) (Sigma) and lysozyme (from egg white), (Sigma).

7.4 Results and Discussion

7.4.1 Analysis with X-ray Photoelectron Spectroscopy

XPS shows that the stoichiometry of the pulsed plasma maleic anhydride (ppMA) layer is in close agreement with the theoretical values, Table 7.1. Peak fitting of the high resolution C(1s) envelope reveals that there are five carbon environments present[36], Figure 7.1(a): hydrocarbon (C_xH_y = 285.0 eV), carboxyl (O-C=O ~289.2 eV), carbon adjacent to anhydride group (O=C-C-C = 285.7 eV), carbon singularly bonded to oxygen (C-O = 286.45 eV) and carbon doubly bonded to oxygen (C=O = 288.2 eV). The absence of any substrate Si(2p) signals verifies homogeneous films of thickness greater than 2-5 nm.

The stoichiometry of the ppMA-nPEG coating is found by XPS to be in agreement with predicted values, Table 7.1. The XPS C(1s) envelope identifies only one C(1s) peak at 286.45 eV[38], which is indicative of carbon singly bonded to oxygen, Figure 7.1(b). It is difficult to observe any discernable differences in the FTIR and XPS spectra once the sample has been heated to convert amic acid groups to imides due to the 2 – 5 nm analysis depth of XPS and the relative length of the nPEG chains (~ 110 repeat units).

Elemental concentrations of the ppMA-LPEI layer before acylation are consistent with predicted values, Table 7.1. The XPS C(1s) envelope, Figure 7.2(b), shows one carbon peak at 285.95 eV which corresponds to carbon adjoining an amine group.

Stoichiometry of the MA-LPEI (acylated) layer measured by XPS was in good agreement with theoretical values, Table 7.1, suggesting a high proportion of secondary amine groups within 2 – 5 nm of the surface depth have been successfully acylated. Analysis of the C(1s) envelope, figure 7.2(c), shows that there are three different carbon environments present in the MA-LPEI (acylated) layer as opposed to just one before the acylation reaction: carbon adjacent to a carbonyl group (C-C=O = 285.7 eV), carbon bonded to nitrogen (binding energy = 285.95 eV) and carbon in an amide group (N-C=O = 288.2 eV).

Table 7.1: Stoichiometric analysis of MA, MA-nPEG (imide), MA-LPEI and MA-LPEI (acylated)

Wafer coating		**%C**	**%O**	**%N**
MA	Theoretical	58	42	0
	Experimental	62	38	0
MA-nPEG (imide)	Theoretical	67	33	0
	Experimental	70	30	<0.1
MA-LPEI	Theoretical	67	0	33
	Experimental	68	<0.1	32
MA-LPEI (acylated)	Theoretical	66	17	17
	Experimental	66 ± 1	16 ± 1	18 ± 1

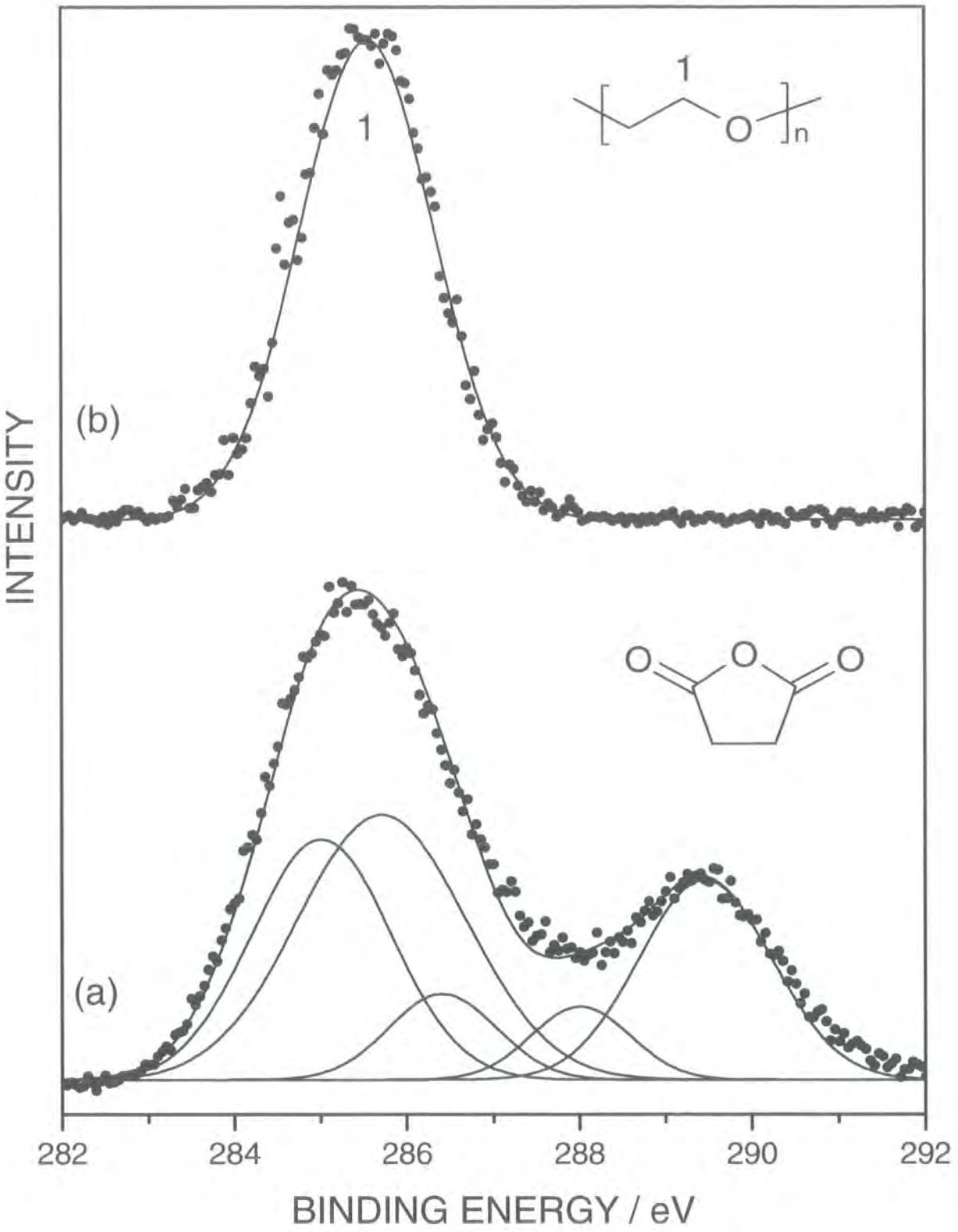

Figure 7.1: XPS C(1s) envelope of (a) pulsed plasma polymerized maleic anhydride, (b) amine-terminated poly(ethylene glycol) grafted to pulsed plasma polymerized maleic anhydride.

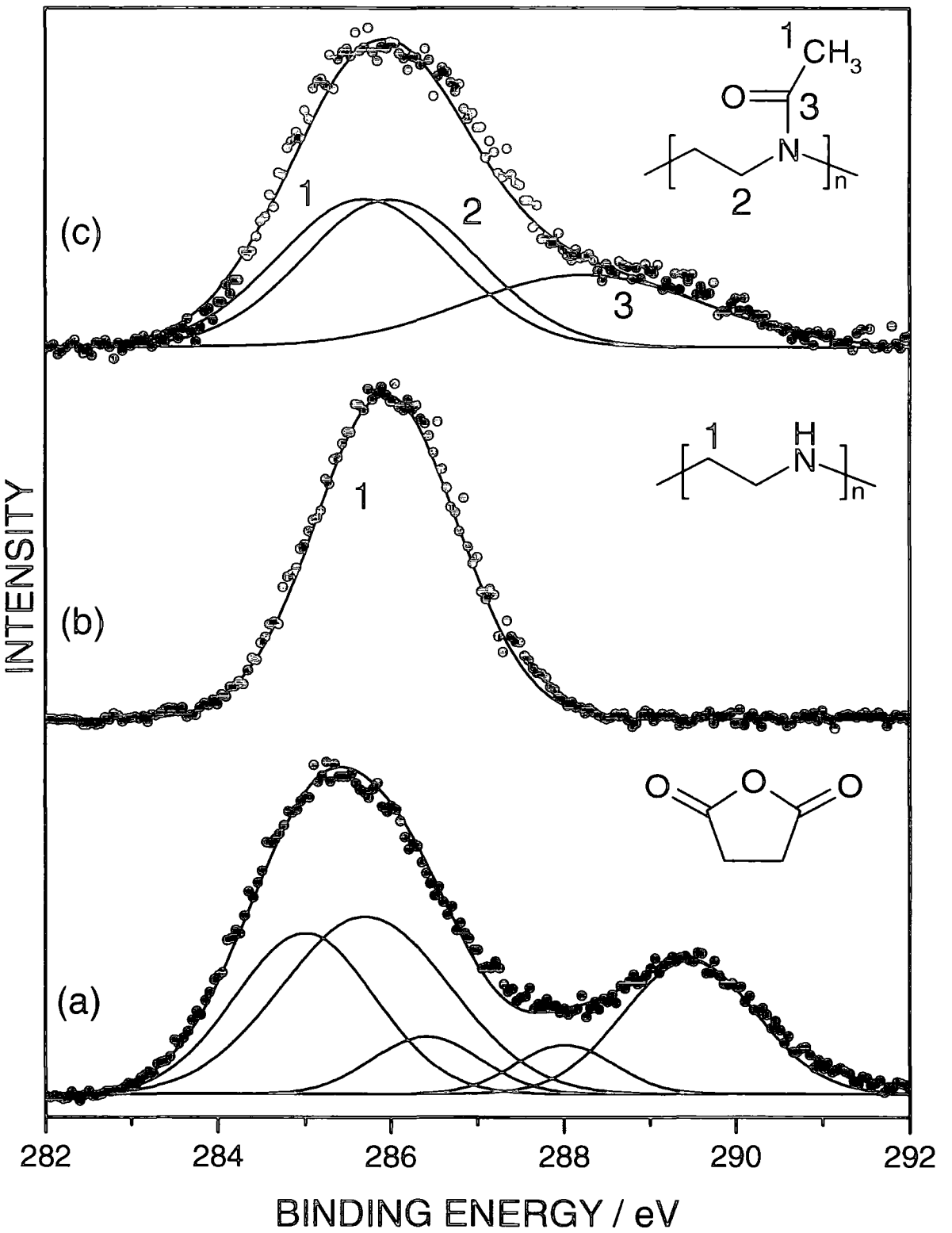

Figure 7.2: XPS C(1s) envelope of (a) pulsed plasma polymerized maleic anhydride, (b) linear polyethylenimine grafted to pulsed plasma polymerized maleic anhydride, (c) linear polyethylenimine grafted to pulsed plasma polymerized maleic anhydride following acylation.

7.4.2 Analysis with Fourier Transfer Infrared Spectroscopy.

The detection of characteristic infrared absorptions such as the asymmetric C=O stretch (C) at 1868 cm^{-1} and the symmetric C=O (D) anhydride stretch at 1800 cm^{-1} confirms structural retention of maleic anhydride functionalities within the pulsed plasma polymer layer, Figure 7.3(a), Table 7.2.

Analysis with FTIR-RAIRS verifies that the amine-terminated poly(ethylene glycol) (nPEG) polymer has been successfully grafted to the plasma polymerized maleic anhydride layer, Table 7.2, Figure 7.3. Signature vibrations of poly(ethylene glycol) such as the CH_2 antisymmetric stretch at 2926 cm^{-1} (B) and the C-O-C symmetric stretch at 855 cm^{-1} (I) can be observed in both the nPEG spectra and ppMA-nPEG spectra Figure 7.3(b) and (c). A carboxylic acid peak at 1740 cm^{-1} (E) can be observed after imidization. This can be attributed to hydrolysis of a proportion of the maleic anhydride groups

The FTIR peak at 1660 cm^{-1} (F), representative of an amide carbonyl stretch, corroborates the formation of an amide bond, Figure 7.4(b). This suggests linear polyethylenimine (LPEI) has been successfully grafted to the pulsed plasma polymerized maleic anhydride film (ppMA). This is further confirmed by an abundance of peaks in the 3280-3350 cm^{-1} (A) region, which corresponds to N-H stretching within secondary amine groups. A carbonyl stretch at 1740 cm^{-1} (E) can be detected, confirming the presence of amic acid groups.

Once the ppMA-LPEI has been reacted with acetyl chloride (MA-LPEI (acylated)), the amine peak present at 3280 cm^{-1} in figure 7.4 (a) and (b) is not evident in 7.4 (c), indicating that a high percentage of amine groups have reacted with acetyl chloride to form amide groups. The intensity of the amide C=O peak (F) relative to anhydride peak (D) has also increased, corroborating the acylation reaction.

Due to the fact that FTIR-RAIRS detects infrared vibrations within the layer as a whole, peaks (C) and (D) are present in Figures 7.3(b), 7.4(b) and 7.4(c), indicating unreacted maleic anhydride functionalities situated beneath the nPEG, LPEI and LPEI (acylated) layers respectively.

Table 7.2: FTIR peak assignments.

Designation	MA	nPEG	MA-nPEG (imide)	LPEI	MA-LPEI	MA-LPEI (acylated)
A: Amine N-H stretch, 3350 - 3250 cm^{-1}				*	*	
B: CH_2 antisymmetric stretch, 2987-2833 cm^{-1}		*	*	*	*	*
C: Antisymmetric anhydride C=O stretch, 1860 cm^{-1}	*		*		*	*
D: Symmetric anhydride C=O stretch, 1800 cm^{-1}	*		*		*	*
E: Carboxylic acid C=O stretch, 1740 cm^{-1}			*		*	*
F: Amide C=O stretch, 1668-1641 cm^{-1}					*	*
G: CH_2 scissor deformation, 1452 cm^{-1}		*	*	*	*	*
H: C-O-C antisymmetric stretch, 1140 cm^{-1}		*	*			
I: C-O-C symmetric stretch, 855 cm^{-1}		*	*			

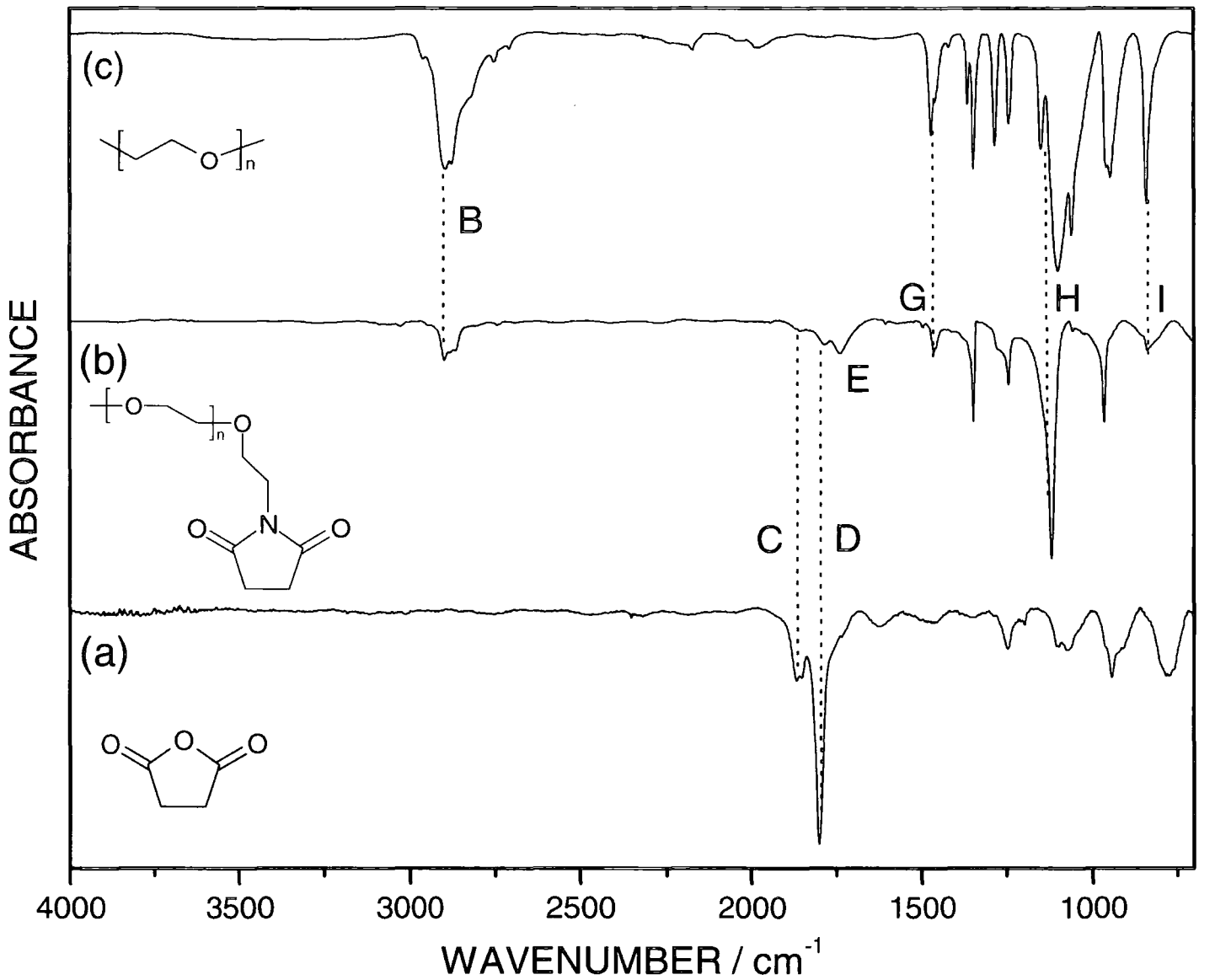

Figure 7.3: FTIR spectrum of (a) pulsed plasma polymerized maleic anhydride, (b) amine-terminated poly(ethylene glycol) grafted to plasma polymerized maleic anhydride, (c) amine-terminated poly(ethylene glycol).

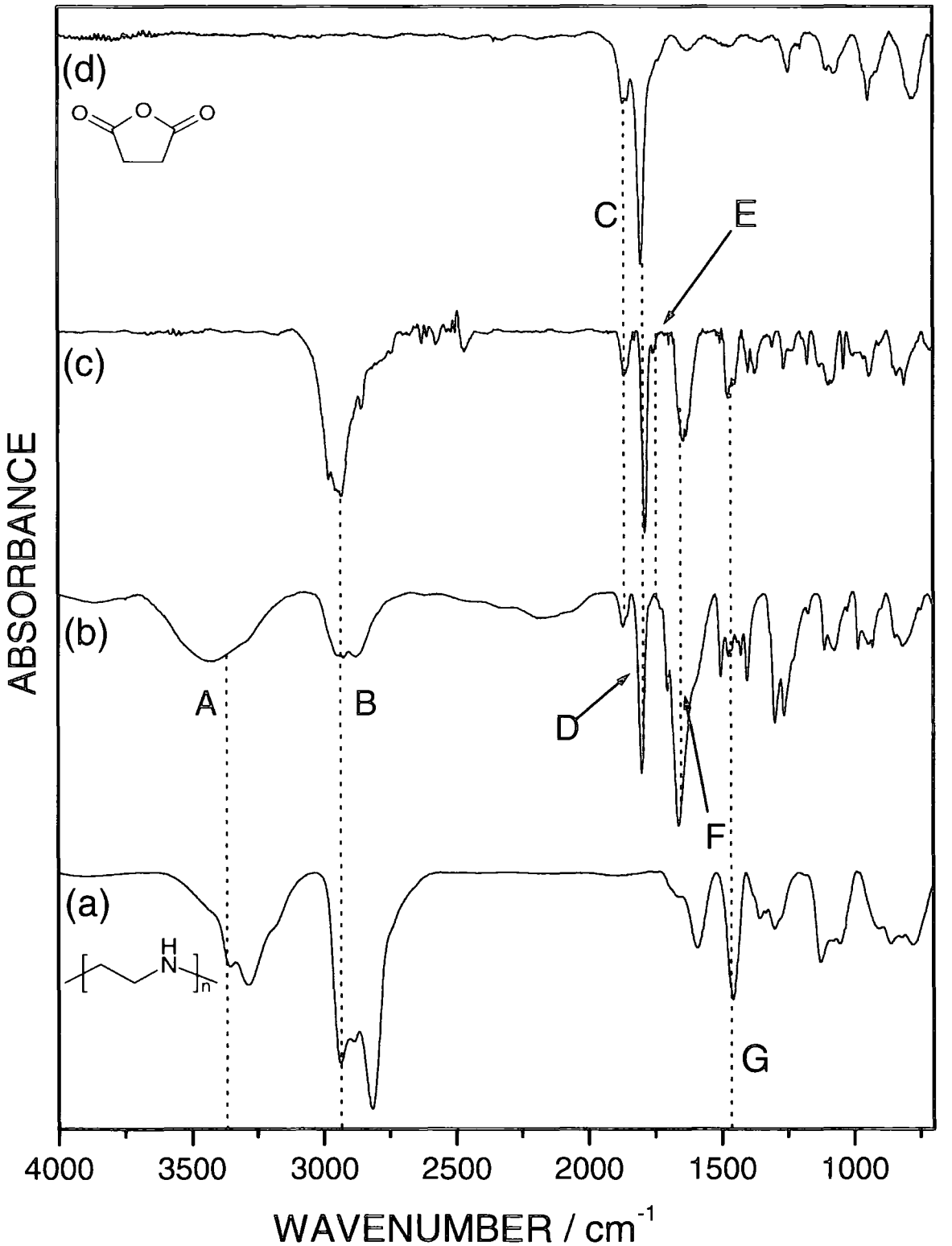

Figure 7.4: FTIR spectra of (a) linear polyethylenimine, (b) linear polyethylenimine grafted to pulsed plasma polymerized maleic anhydride, (c) linear polyethylenimine grafted to pulsed plasma polymerized maleic anhydride (following reaction between amine groups and acetyl chloride), (d) pulsed plasma polymerized maleic anhydride.

Table 7.3: Water contact angles of tailored surfaces.

Surface Coating	Water Contact Angle
ppMA-nPEG (imide)	34 ° (± 1)
ppMA-LPEI (acylated)	29 ° (± 0.5)
Poly(isobutylene)	96 ° (± 1)
ppMA	Totally wettable - hydrolysis

7.4.3 Analysis by Surface Plasmon Resonance.

Figure 7.5 details adsorption measurements obtained for each surface analysed. Adsorption measurements are in arbitrary units. In order to gain an insight into the degree of protein resistance of a surface, adsorption values obtained are compared with that of a hydrocarbon standard surface; in this case polyisobutylene, which has adsorption levels of 3092 and 1426 arbitrary units for fibrinogen and lysozyme respectively. In general, the resistance to fibrinogen is higher than that of lysozyme for all analysed films.

The pulsed plasma polymerized maleic anhydride films exhibit least resistance to both proteins due to the hydrolysis (ascribed to water present in the buffer solution) of maleic anhydride to carboxylic acid groups. The film has become a source of hydrogen bond donors and hence is susceptible to protein adhesion[14]. Hydrolysed maleic anhydride surfaces are negatively charged and hence have a particularly high affinity for lysozyme.

All derivatized pulsed plasma polymerized maleic anhydride films show a higher resistance to both proteins than the standard. The order of increasing protein resistance is: *ppMA < Standard < ppMA-nPEG < ppMA-nPEG (imide) < ppMA-LPEI (acylated)* for fibrinogen and *ppMA < ppMA-nPEG < Standard < ppMA-nPEG (imide) < ppMA-LPEI (acylated)* in the case of lysozyme.

Surface plasmon resonance measurements show that pulsed plasma polymerized maleic anhydride – imidized poly(ethylene glycol) films are resistant to the adsorption of fibrinogen but have only a sparing resistance to lysozyme. This marked difference is attributable to a significant proportion of

the maleic anhydride remaining unreacted due to steric hindrance cause by the comparatively large polyether chains (110 repeat units). This was previously indicated by FTIR analysis. Lysozyme, the smaller of the two proteins (20% the size of fibrinogen), is able to permeate into any gaps between the nPEG chains and be adsorbed by underlying areas of hydrolysed ppMA, giving rise to a higher degree of adsorption.

Fibrinogen is not adsorbed to the same extent as lysozyme and its increased size results in it not being able to penetrate the nPEG layer to the same extent as lysozyme, giving rise to a moderate value of resistance. Due to the relative length of the polyether chains, imidization of the ppMA-nPEG layer has no discernable affect on the protein resistance of the surface.

For both proteins employed, the pulsed plasma polymerized maleic anhydride – acylated linear polyethylenimine coating exhibits at least double the protein resistance to its nearest comparison. This is further verified by the fact that the ppMA-LPEI (acylated) coating was found to have the greatest hydrophilicity without the film washing off, Table 7.3.

The FTIR spectra displays anhydride absorptions suggesting that some maleic anhydride has not reacted, but due to the relatively low molecular weight of the polymer chains (~600) compared to that of nPEG (~5,400) there will be less steric hindrance and hence a large proportion of the anhydride groups at the interface reacting with secondary amine groups situated on the polymer chain. Shorter chains also result in there being fewer defects in the surface coverage of LPEI and hence protein permeation is circumvented due to resistance of the amide moieties arising from acylation of secondary amine groups[12].

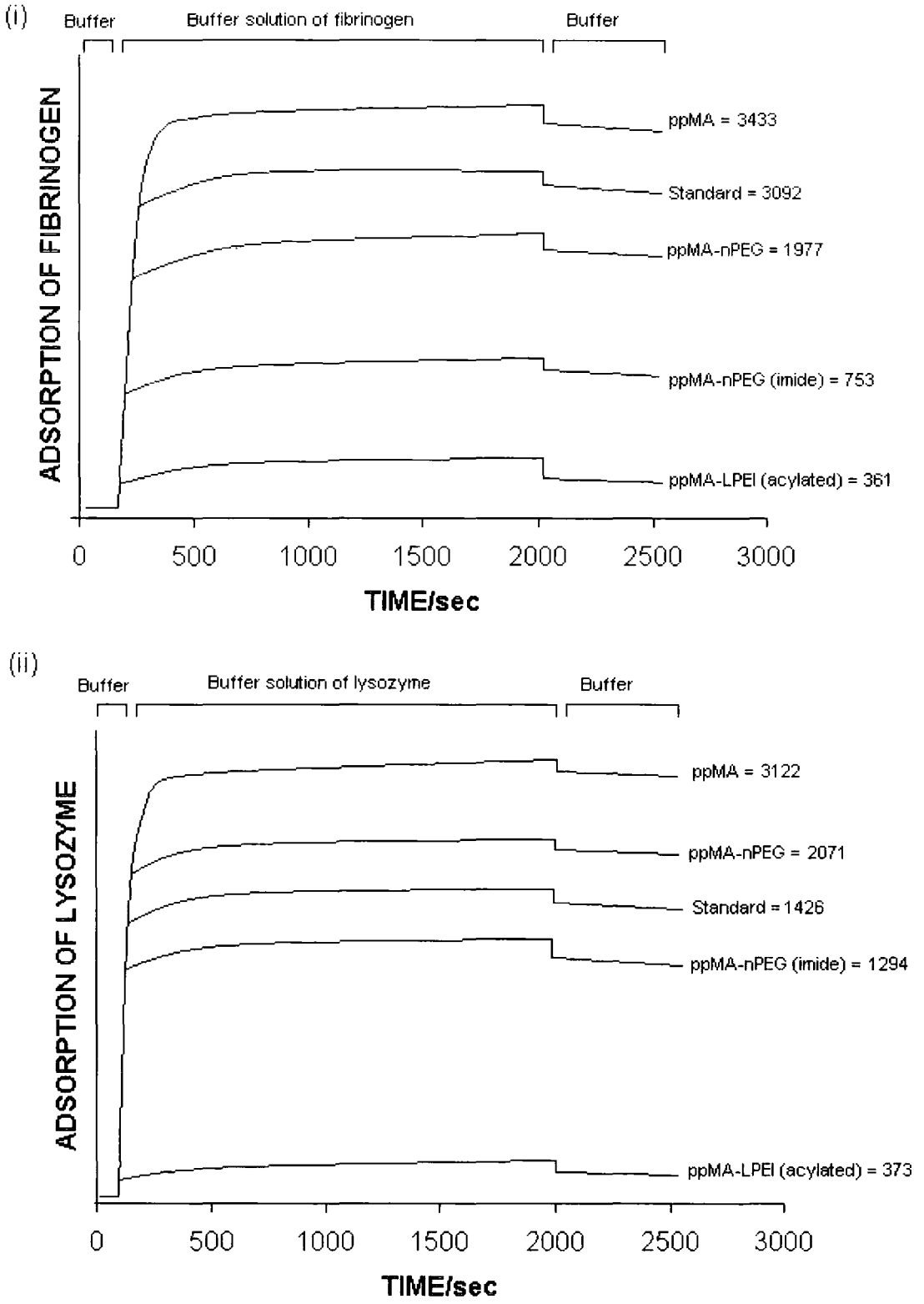

Figure 7.5: Diagram illustrating relative adsorption of (i) fibrinogen and (ii) lysozyme onto derivatized surfaces. Adsorption is measured in arbitrary units.

7.4.4 Pulsed Plasma Polymerization of Maleic Anhydride

The deposition of pulsed plasma polymers and hence the generation of surface-confined functional groups is important because it is not restricted by substrate-specific chemistries. Hence coatings of this nature can be deposited in a single step, independent of substrate type and geometry.

In this instance, the retention of anhydride groups permits further derivatization via amination reactions, allowing additional functionalities to be tailored to the surface, which can then be manipulated further to manufacture coatings that are resistant to the adsorption of proteins.

7.4.5 n-Poly(ethylene glycol)

Attaching nPEG polymer chains to the pulsed plasma polymerized maleic anhydride layer involved the use as toluene as the solvent. Whereas n-methyl pyrrolodinone could be used effectively for LPEI experiments, nPEG was found not to dissolve. Being a polyether, nPEG dissolved readily in polar solvents such as water but the disadvantage of this was that the maleic anhydride films are hydrolysed and the desired reaction involving the anhydride groups and the amine group terminating the n-PEG polymer chain cannot take place. Hence the nPEG polymer was dissolved in toluene at 40 °C and the ppMA-coated substrates immersed in the reaction mixture.

7.4.6 Linear Polyethylenimine

Unlike nPEG, when LPEI reacts with maleic anhydride, it is not possible to convert the amic acid groups to imide groups due to the fact that LPEI consists of secondary amine groups.

The grafting of LPEI to plasma polymerized maleic anhydride films results in the surface retention of hydrogen bond donor groups, which contribute to protein adsorption[14]. A very high proportion of these amine groups can however be acylated to amides with acetyl chloride as confirmed by the absence of amine peaks in the FTIR spectra and the presence of two additional carbon environments detected by XPS. In order for this reaction to proceed to completion, a base; in this case an equivalent of triethylamine was added to the reaction mixture. In this aminolysis reaction[39], acid chlorides

such as acetyl chloride react rapidly with amines to give amides with high yields, Scheme 7.4.

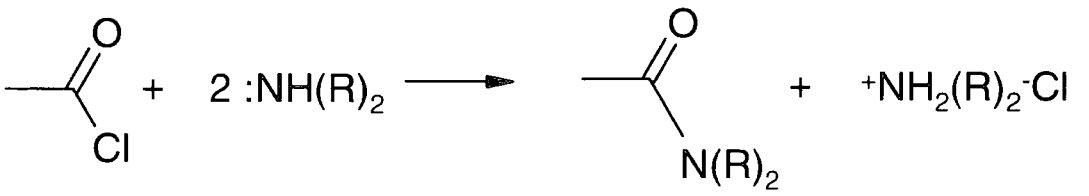

Scheme 7.4: The acylation of secondary amines.

Since the reaction produces hydrochloric acid, two equivalents of the amine must be used; one reacts with the acetyl chloride, the other with the hydrochloric acid to form an ammonium salt. A base such as triethylamine can be used to react with the HCl.

These coatings were found not to possess the same degree of resistance to adsorption of smaller proteins exhibited by films produced by other researchers[12-14]. However the methodology used to manufacture them is considerably more simplistic, economical and not restricted by substrate e.g. as in the case of thiol-gold linkages.

Results obtained here do suggest these derivatized surfaces; in particular acylated LPEI-functionalized films have potential for applications where the non-adhesion of larger proteins and cells (which are essentially structures that consist of proteins) is required. For instance in forensic testing it is imperative to hinder contamination by bacteria. Any resistant coatings deployed for these purposes would need to be versatile, and cost-effective to produce. Surfaces coated with pulsed plasma polymerized maleic anhydride functionalized with acylated linear polyethylenimine meet these criteria.

7.5 Conclusions

Surface coatings consisting of pulsed plasma polymerized maleic anhydride subsequently derivatized with an amine-terminated molecule have been successfully produced and characterized. Tests to show protein-resistant properties of these surfaces have yielded mixed results. However this substrate-independent, economical technique has produced films of acylated

polyethylenimine that exhibit high levels of resistance to the adsorption of larger proteins and cells, thus highlighting future potential of this methodology for applications within forensic testing to prohibit contamination from cells and bacteria due to its relative simplicity in comparison to the self-assembled monolayer approach.

7.6 References

[1] Jenney, C. R.; Anderson, J. M., *J. Biomed. Mater. Res.,* 44, **1999**, 206.

[2] Tseng, Y. C.; Park, K., *J. Biomed. Mater. Res.,* 26, **1992**, 373.

[3] Cunliffe, D.; Smart, C. A.; Vulfson, E. N., *Appl, Environ. Microbiol.* 65, **1999**, 4995.

[4] Sawney, A. S.; Hubble, J. A., *Biomaterials,* 13, **1992**, 863.

[5] Ishihara, K.; Nakabayashi, N.; Nishida, K.; Sakakida, M.; Shichiri, M., *CHEMTECH,* 23, **1993**, 19.

[6] Hocker, H.; Klee, D.; *Macromol. Symp.,* 102, **1996**, 421.

[7] Stelzle, M.; Wagner, R.; Nisch, W.; Jagermann, W.; Frohlich, R.; Schaldach, M., *Biosensors and Bioelectronics*, 12, **1997**, 853.

[8] Castillo, E. J.; Koenig, J. L.; Anderson, J. M.; Lo, J., *Biomaterials,* 6, **1985**, 338.

[9] Ou, S. H.; Ishida, H.; Lando, J. B., *J. Polym. Sci., Part B., Polym. Phys.,* 29, **1991**, 67.

[10] Santini, J. T.; Cima, M. J.; Langer, R. *Nature,* 397, **1999**, 335.

[11] Jeon, S. I.; Lee, J. H.; Andrade, J. D.; De Gennes, P. G. *J. Colloid Interface Sci.,* 142, **1991**, 149.

[12] Chapman, R. C; Whitesides, G. M. *Langmuir,* 17, **2001**, 1225.

[13] Chapman, R. C; Whitesides, G. M. *Langmuir,* 17, **2001**, 2841.

[14] Chapman, R. C; Whitesides, G. M. *Langmuir,* 17, **2001**, 5605.

[15] Barrett, D. A.; Hartshorne, M. S; Hussain, M. A.; Shaw, P. N.; Davies, M. C.; *Anal. Chem.,* 73, **2001**, 5232.

[16] Marchant, R.E.; Yuan, S.; Szakalas-Gratzl, G. *J. Biomater. Sci.,* 6, **1994**, 549.

[17] Tweden, K; Marchant, R.E. *J. Appl. Biomater.,* 6, **1995**, 259.

[18] Reid, G.; Tiezser, C., *Cell. Mater.* 3, **1993**, 171.

[19] Lee, J.H.; Kopeckova, P.; Zhang, J.; Kopecek, J; Andrade, J.D. *Polym. Mater. Sci. Eng.,* 59, **1988**, 234.

[20] McPherson, T.; Kidane, A.; Szleifer, I.; Park, K., *Langmuir,* 14, **1998**, 176.

[21] Lee, J. H.; Kopeckova, P.; Kopecek. J.; Andrade, J. D., *Biomaterials*, 11, **1990**, 455.

[22] Deible, C. R.; Petrosko, P.; Johnson, P. C.; Beckman, E. J.; Russell, A. J.; Wagner, W. R., *Biomaterials,* 19, **1998**, 1885.

[23] Leckband, D.; Sheth, S.; Halperin, A., *J. Biomat. Sci. Polym.,* 10, **1999**, 1125.

[24] Hamburger, R.; Azaz, E.; Donbrow, M., *Pharm. Acta. Helv.,* 10, **1975**, 50, 10.

[25] Gerhardt, W.; Martens, C., *Z. Chem.,* 25, **1985**, 143.

[26] Crouzet, C.; Decker, C.; Marchal, J., *Makromol. Chem.,* 177, **1976**, 145.

[27] Textor, M.; Spencer, N. D. *Langmuir,* 18, **2002**, 252.

[28] Textor, M.; Spencer, N. D. *Langmuir,* 17, **2001**, 489.

[29] Textor, M.; Spencer, N. D. *J. Phys. Chem. B,* 104, **2000**, 3298.

[30] Bunker, W. L.; Guo, A. *Langmuir,* 17, **2001**, 7798.

[31] Saul, J. B.; Williams, P. M.; *Langmuir,* 15, **1999**, 5136.

[32] Feuerstein, I. A.; McClung, W. G.; Horbett, T. A., *J. Biomed. Mater. Res.*, 26, **1992**, 221.

[33] O' Connor, S. M.; Deanglis, A. P.; Gehrke, S. H.; Retzinger, G. S., *Biotechnol. Appl., Biochem.,* 31, **2000**, 185.

[34] Green, R. J.; Davies, M. C.; Roberts, C. J.; Tendler, S. J. B., *J. Biomed. Mater. Res.,* 42, **1998**, 165.

[35] Mrksich, M.; Sigal, G.B.; Whitesides, G.M. *Langmuir,* 11, **1995,** 4383.

[36] Ryan, M.E.; Hynes, A.M.; Badyal, J.P.S. *Chem. Mater.* 8, **1996,** 37.

[37] Evenson, S. A.; Fail, C. A.; Badyal, J. P. S.; *Chem Mater*, 12, **2000**, 3038.

[38] Beamson, G.; Briggs, D; *High Resolution XPS of Organic Polymers*, Wiley, New York, **1992**.

[39] McMurry, J., *Organic Chemistry; 3rd Edition*, Wadsworth, California, **1992**, 809.

Chapter 8: Substrate-Independent, Surface-confined Living Radical Polymerization

8.1 Introduction

Atom transfer radical polymerization (ATRP) is a recognised method for synthesizing polymer brushes with controlled molecular weight and narrow polydispersity indices[1, 2]. Typically this approach constitutes a multi-component system, involving monomer, initiator (with a transferable halogen atom), and a catalyst (e.g. the transition metal complex copper (I) bromide dipyridyl, $Cu(I)(bpy)_2Br$). The modus operandi for ATRP is that the catalyst participates in a halogen transfer cycle consisting of growing polymer chain deactivation and reactivation via reversible halogen atom transfer and abstraction respectively, Scheme 8.1.

$$R^{\bullet} + Cu(II)bpy_2Br_2 \rightleftharpoons R\text{-}Br + Cu(I)bpy_2Br$$

Scheme 8.1: Halogen transfer cycle for atom transfer radical polymerization.

Hence polymer chain growth can be described as "living" due to it remaining reactive so long as both catalyst and monomer continue to be present in the system. By maintaining the balance of equilibrium towards a low concentration of radicals, chain termination and transfer reactions are minimised. Thereby enabling all polymer chains to grow at the same rate to yield a narrow molecular weight distribution. Monomers which have been successfully polymerized by the ATRP technique include styrenes, acrylates, and acrylonitrile, all of which contain substituents capable of stabilizing propagating radicals (e.g. phenyl or carbonyl

groups)[3]. Classes of monomer not amenable to ATRP include alkyl substituted alkenes (due to their low intrinsic reactivity towards radical polymerization[3]).

Potential applications for polymers prepared by ATRP include chemical separations where an inert polymeric resin is required (e.g. the purification of biotechnological products[4]) and ion exchange columns (e.g. for the removal of toxic metal ions and radioactive materials[5]).

8.1.1 ATRP Initiators

The main purpose of the initiator is to determine the number of growing polymer chains and hence the final molecular weight. If transfer and termination of the chains is negligible and initiation is very fast, the number of growing chains is equal to the amount of initiator groups present. Alkyl halides are typically used as ATRP initiators and the polymerization rate is first order with respect to the alkyl halide concentration. In order to obtain well-defined chains with a narrow molecular weight distribution, the halide group must be able to migrate between the growing chain and the transition metal catalyst. Molecular weight control is highest if the halide group used is bromine or chlorine although iodine has been found to successfully polymerize styrenes and acrylates[6]. However iodine is light-sensitive and can form metal iodide complexes with the transition metal catalyst. Fluorine is an unsuitable choice of halide due to the fact that the carbon-fluorine bond is too strong for homolytic cleavage to occur.

Alkyl halides with activating substituents on the α-carbon such as aryl, carbonyl or alkyl groups can be employed as ATRP initiators. Some examples of initiators that have been successfully utilised to initiate ATRP are halogenated alkenes[7], benzylic halides[8], α-haloesters[9], α-haloketones[10], α-halonitriles[11] and sulfonyl halides[12]. A good ATRP initiator's initiation rate should be fast compared to its propagation rate.

8.1.2 ATRP Catalysts

The catalyst within ATRP determines the position of the atom transfer equilibrium. The transition metal catalyst must have two readily accessible oxidation states separated by one electron e.g. Cu(II) and Cu(I). The metal centre must also have an affinity for halogens. A good ATRP catalyst needs to be highly selective for the atom transfer process and must not participate in side reactions.

A wide range of transition metals have been employed for ATRP; these include molybdenum[13], rhenium[5], iron[14], rhodium (Wilkinson's catalyst)[15] and nickel[16]. Complexes of copper have been found to be some of the most versatile and cost effective ATRP catalysts, which have been successfully employed in the polymerization of styrenes, methacrylates, acrylamides and acrylonitrile[17, 18].

The ligands within an ATRP catalyst are crucial in making the catalyst soluble in the designated solvent used in the reaction as well as stabilizing the catalyst in different monomers and at different temperatures. They also assist in the one electron transfer process required for ATRP. Nitrogen bidentate ligands such as dipyridyl along with polytertiary amines and pyridyl imines are commonly deployed in copper-mediated ATRP[10]. Metals from groups 6-10 were found to be effective catalysts when used in conjunction with phosphorous based ligands such as triphenyl phosphine[5, 13-16].

8.1.3 ATRP Solvents and Conditions

Many different solvents have been used for ATRP for different monomers. These include benzene, toluene, dimethyl formamide, N-methyl pyrrolidinone, alcohols and water[19, 20, 21] amongst others. ATRP possesses an appreciable tolerance to a variety of functional groups. For example, various solvents employed in copper-mediated ATRP had no noticeable effect the control of polymerization[22].

Polymerization rate for ATRP has been found to increase with higher temperatures because of an increase in radical propagation and the atom transfer equilibrium constant. It has, however, been observed that chain transfer and side reactions have a greater chance of occurring at higher temperatures[23].

Catalyst solubility increases with temperature, but the disadvantage is the possibility of thermal decomposition of the catalyst[16]. The optimal temperature hence depends on the monomer, catalyst and the desired molecular weight. For example ATRP of methyl methacrylate using a copper catalyst can be carried out effectively at temperatures below 100 °C[24, 25, 26, 27]. Hence relatively low reaction temperatures and an extensive monomer scope are ATRP's particular advantages. However one notable limitation is that the catalyst needs to be removed from the system following the reaction.

8.1.4 ATRP from Surfaces

Another area gaining attention is the growth of polymer brushes onto solid surfaces by the ATRP technique. The underpinning reason being the high level of control attainable over interfacial properties such as adhesion, friction, resistance to corrosion, and wettability[28]. Normally this entails immobilization of the initiator onto a solid substrate followed by ATRP polymer growth off the surface. Initiator layers have been successfully created in the past from self-assembled monolayers (SAMs, derived from either thiol-gold[29, 30] or silane-coupling[31, 32, 33, 34] chemistries), hydrosilyl – terminated polysiloxane chains reacted with 2-bromoisobutyrylbromide[35], Wang resin[36] (crosslinked polystyrene functionalized with hydroxybenzyl alcohol groups which are subsequently reacted with 2-bromoisobutyrylbromide), bromopropionyl derivatized Latex,[37] surface bromination [38], electrografting [39], and cellulose fibres or carbon nanotubes [40, 41, 42] (where surface hydroxyl groups are reacted with 2-bromoisobutyrylbromide). It should be noted that each of the aforementioned examples of initiator generation employ substrate-specific chemistries and require several reaction steps.

Furthermore, self-assembled monolayers generally provide a relatively low concentration of initiating groups. This results in a necessity for a sufficient concentration of the Cu(II) deactivating complex to achieve a controlled equilibrium between dormant and active chains. The process can be described as a redox-initiated radical polymerization in the absence of this equilibrium[2, 43].

An adequate concentration of the Cu(II) complex can be rapidly attained by adding it to the system before commencement of the reaction[44] or by the addition of free initiator, which reacts with the Cu(I) species to produce the active radical required for propagation[45].

8.2 Aims

The aim underlying this work is to develop a substrate – independent route for preparing ATRP initiator layers, Scheme 8.2. This entails deposition of well-adhered halogen-containing initiator films by pulsed plasma polymerization. Clearly there are a number of distinct advantages associated with plasmachemical functionalization, these include the fact that this approach is quick (single step), solventless, energy efficient, and can be applied to a whole host of materials and complex geometries (e.g. microspheres, fibres, tubes, etc.[46]).

For the purposes of this investigation, halogen-containing monomers have been selected for pulsed plasma polymerization in order to provide initiator functionalised surfaces which are amenable to ATRP, e.g. Scheme 8.2. Due to a comparatively high density of initiating groups present at the surface following pulsed plasma deposition, controlled surface-confined polymerization will be attempted without the addition of sacrificial initiator or copper (II) bromide deactivating complex.

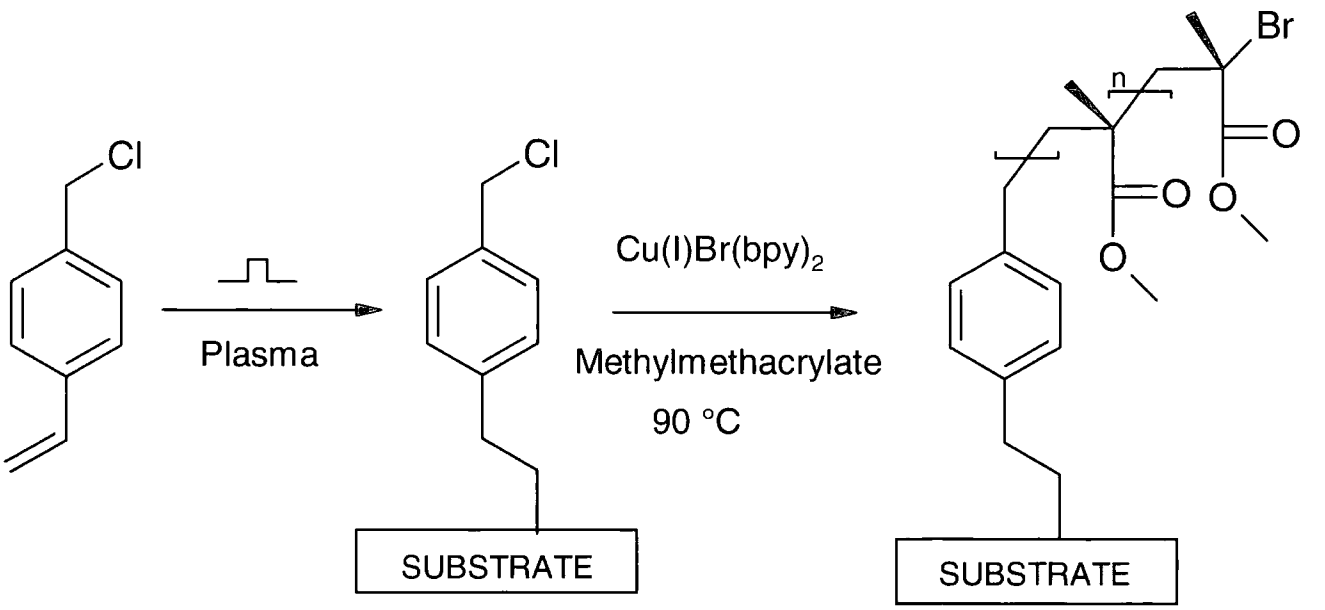

Scheme 8.2: Surface ATRP using pulsed plasma deposited chlorine-containing initiator layers.

8.3 Experimental

8.3.1 Preparation of Surface Initiator Layer

4-vinylbenzyl chloride (97% purity, Aldrich) or 2-bromoethylacrylate (98% purity, ABCR) was pulsed plasma polymerized onto silicon wafers and polytetrafluoroethylene strips at room temperature (20 °C) using the same apparatus and procedures outlined in Chapter 4. Pulse duty cycle was set to 100 μs on, 4000 μs off and 20 μs on, 10,000 μs off for 4-vinylbenzyl chloride and 2-bromoethylacrylate respectively. Peak power was set to 20 W for both precursors. The polystyrene beads were coated using the same apparatus as in Chapter 5.

8.3.2 Surface-confined Living Radical Polymerization

Atom transfer radical polymerization onto the pulsed plasma polymer coated silicon wafers entailed placing each substrate into a glass tube containing 0.01 M copper (I) bromide (98%, Aldrich), 0.03 M dipyridyl (99%, Aldrich), 0.2 M

methylmethacrylate (99%, Aldrich), glycidyl methacrylate (98%, Aldrich) or styrene (99%, Aldrich), and 3 ml of dimethyl formamide (99.9 %, Aldrich). The reaction tube was then immersed into an oil bath and maintained at 80°C for methylmethacrylate polymerizations, 50 °C for glycidyl methacrylate polymerizations and 120 °C for styrene polymerizations for varying time intervals. Upon cooling, the wafers were removed and any physisorbed impurities dislodged by continuous extraction in tetrahydrofuran solvent for 16 hours at 65 °C. Due to obvious structural similarities, resulting in difficulty in distinguishing between plasma polymer layers and ATRP polymers; 4-vinylbenzyl chloride films were not employed to polymerize styrene and 2-bromoethylacrylate films not used to polymerize acrylates.

Unequivocal proof that the halogen atoms present in the pulsed plasma polymer layer act as the initiation centres for atom transfer radical polymerization was obtained by running a control experiment feeding styrene instead of 4-vinylbenzyl chloride as the precursor during pulsed plasma polymerization. The same ATRP protocol as outlined above was followed thereafter.

The ATRP grafted polymethylmethacrylate, poly(glycidyl methacrylate) and polystyrene layers were characterized by XPS and FTIR techniques as previously described in Chapter 3. Film thickness measurements entailed cryogenic microtone cross-sectioning of the coated substrate (Leica model RM 2165) followed by metallization of 10 nm gold layer onto the surface and then scanning electron microscopy (SEM) analysis (Cambridge Instruments model S240). The living nature of these surfaces was exemplified by varying the polymerization time (1-8 hours) whilst measuring the polymer layer thickness using reflectometry. This entailed experiments where a lower concentration of methylmethacrylate (0.1 M) was added to the reaction mixture in order to yield thinner films (i.e. more accurately determinable by the reflectometry technique).

8.3.3 Polymer-grafted Microscopic Beads

The wide-scale applicability of this ATRP methodology was demonstrated by coating polystyrene beads (80 μm diameter, Biosearch Technologies One) with a

pulsed plasma polymerized 4-vinylbenzyl chloride layer and subsequently ATRP grafting polymethylmethacrylate (40 hours polymerization time). These polymer brush-functionalized microspheres were then sprinkled on top of a thin layer of molten thermoplastic adhesive (Tempfix, Agar Scientific) which had been spread onto an aluminium plate (1 x 1 cm). Cooling to room temperature immobilized these beads into the adhesive surface. Thin slices were taken off the top of the exposed polymer microspheres by mounting this plate onto a cryogenic microtone to reveal cross-sections. Throughout this cutting procedure, the temperature of the substrate holder and knife was kept below -20 °C whilst the surrounding chamber temperature was maintained at -90 °C. The polymethylmethacrylate layer thickness enveloping the beads was measured by scanning electron microscopy.

8.3.4 Microscopic Polymer Arrays

Micropatterned arrays of atom transfer radical polymerized glycidyl methacrylate (a reactive polymer amenable to derivatization[47]) were produced by embossing a nickel grid (Agar, 2000 mesh nickel corresponding to 7.5 μm square holes separated by 5 μm) into polytetrafluoroethylene (PTFE) slides (1.5 cm x 1.0 cm). The exposed PTFE pixels were activated by exposure to a 50 W argon plasma pre-treatment for 20 min followed by pulsed plasma polymerization of 4-vinylbenzyl chloride. The embossed grid was then lifted off the surface to leave behind well-defined pixels of ATRP initiator. ATRP polymerization entailed immersion of the microarray into a glass tube containing the catalyst solution employed previously and 0.2 M glycidyl methacrylate (the reactive pendant epoxide groups can be further derivatized with a fluorescent dye). Dissolved gases were removed by several freeze-pump-thaw cycles. Polymerization was carried out in an oil bath at 50 °C for 12 hours.

Next, the PTFE slides were removed, rinsed in dimethyl formamide, and the microarrays fluorescently tagged by reacting the glycidyl methacrylate polymer epoxide groups with a solution of cresyl violet perchlorate fluorescent dye (5 mg cresyl violet perchlorate per litre of de-ionized water) for 1 hour at room

temperature and washing in de-ionized water. A fluorescence microscope system (LABRAM, Tobin Yvon Ltd) was then used to map the functionalized ATRP microarray. This entailed focussing 590 nm wavelength light onto the sample surface through the microscope objective and collecting the corresponding fluorescence signal whilst simultaneously scanning the surface with a computerized x-y translation stage moving in 1.0 μm steps.

8.3.5 Block Copolymerization

Finally growth of an ATRP polystyrene-poly(glycidyl methacrylate) block copolymer was attempted by pulsed plasma deposition of 4-vinylbenzyl chloride followed by ATRP of styrene (0.1 M), with a polymerization time of 2 hours. The films were subjected to washing in DMF followed by ATRP of glycidyl methacrylate (0.1 M) at varying time intervals (1-6 hours) using the same reaction protocol outlined previously with the addition of copper (II) bromide (99%, Aldrich) (0.005 M). Film thicknesses were determined with reflectometry.

8.4 Results and Discussion

8.4.1 Analysis with X-ray Photoelectron Spectroscopy

XPS characterization of the deposited pulsed plasma polymerized 4-vinylbenzyl chloride and 2-bromoethylacrylate layers indicates that film stoichiometries are in close agreement with the predicted theoretical values for complete functional retention, Table 8.1. The corresponding high resolution C(1s) XPS spectra of the pulsed plasma 4-vinylbenzyl chloride layer indicates the presence of three types of carbon environment[48]: carbon bonded to hydrogen within an aromatic ring (binding energy = 284.75 eV), carbon bonded to carbon or hydrogen (285.0 eV), and carbon bonded to a chlorine atom 287.05 eV). An aromatic shake-up peak can also be observed at ~291.5 eV, Figure 8.1(a). Absence of any Si(2p) signal from the silicon substrate in both instances confirms complete coverage by the plasma polymer film, Table 8.1.

The C(1s) spectrum of the ATRP grafted polymethylmethacrylate layer is consistent with four different carbon environments: carbon singly bonded to hydrogen (285.0 eV), carbon adjacent to a carbonyl group (285.7 eV), carbon singly bonded to oxygen (286.45 eV), and the ester carbon (289.1 eV), Figure 8.1(b). In the case of poly(glycidyl methacrylate) five carbon environments are observed: carbon singly bonded to hydrogen (285.0 eV), carbon adjoining a carbonyl group (285.7 eV), carbon singly bonded to oxygen (286.45 eV), carbon within an epoxide group (287.2 eV) and the carbonyl carbon (289.1 eV), Figure 8.1(c).

The C(1s) spectrum of pulsed plasma polymerized 2-bromoethylacrylate exhibits five carbon environments: carbon bonded to hydrogen (285.0 eV), carbon adjoining a carbonyl group (285.7 eV), carbon bonded to bromine (285.75 eV) carbon singly bonded to oxygen (286.45 eV), and carbon within a carbonyl group (289.1 eV), Figure 8.2(a). In the instance of ATRP-polymerized polystyrene, two carbon environments are present; carbon bonded to hydrogen within an aromatic ring (284.75 eV) and carbon bonded to hydrogen (285.0 eV), Figure 8.2(b). The characteristic aromatic π-π^* shake-up satellite of polystyrene can be observed at ~291.5 eV.

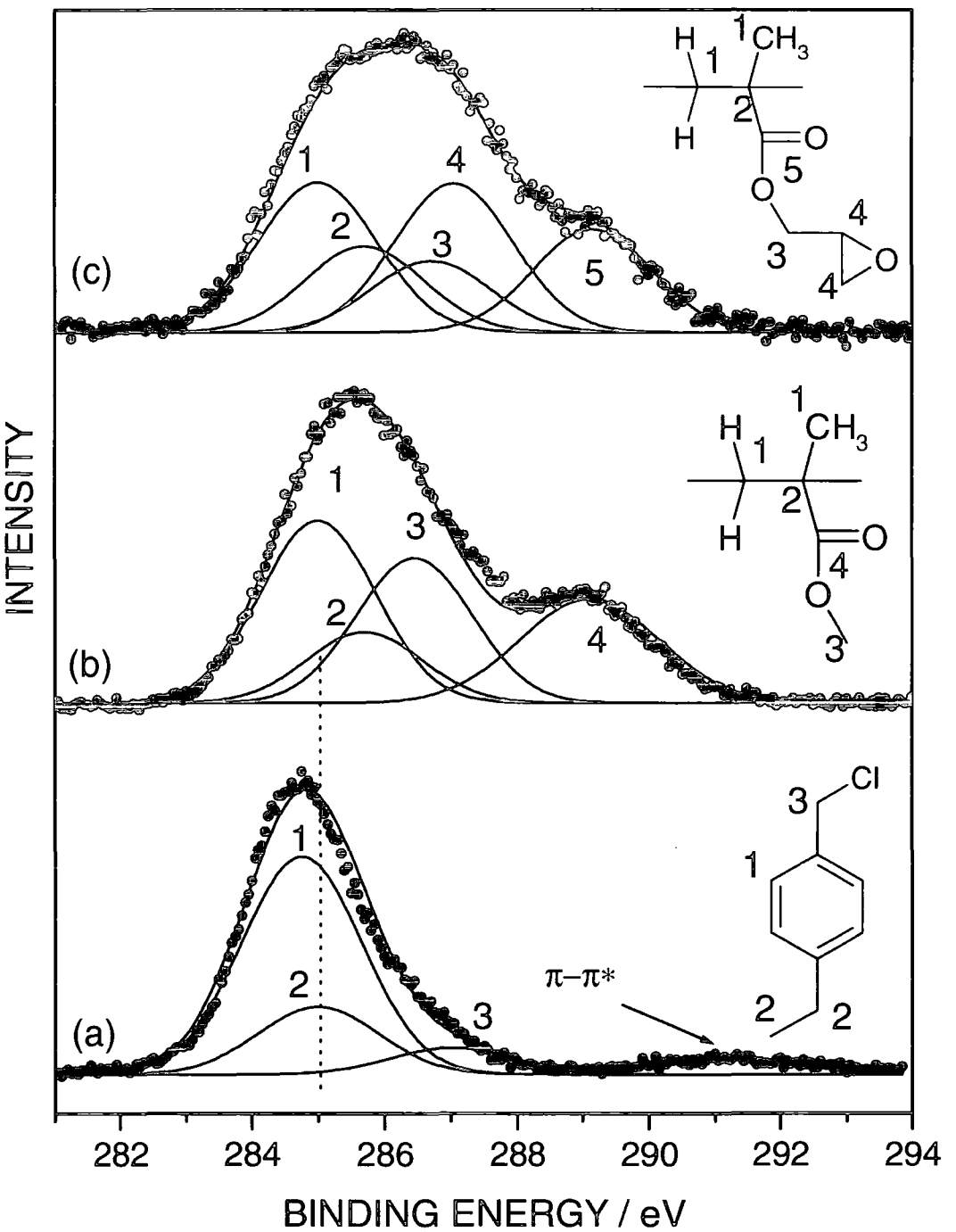

Figure 8.1: XPS C(1s) spectra of: (a) pulsed plasma polymerized 4-vinylbenzyl chloride, (b) ATRP grafted polymethylmethacrylate and (c) ATRP grafted poly(glycidyl methacrylate) onto a pulsed plasma polymerized 4-vinylbenzyl chloride layer.

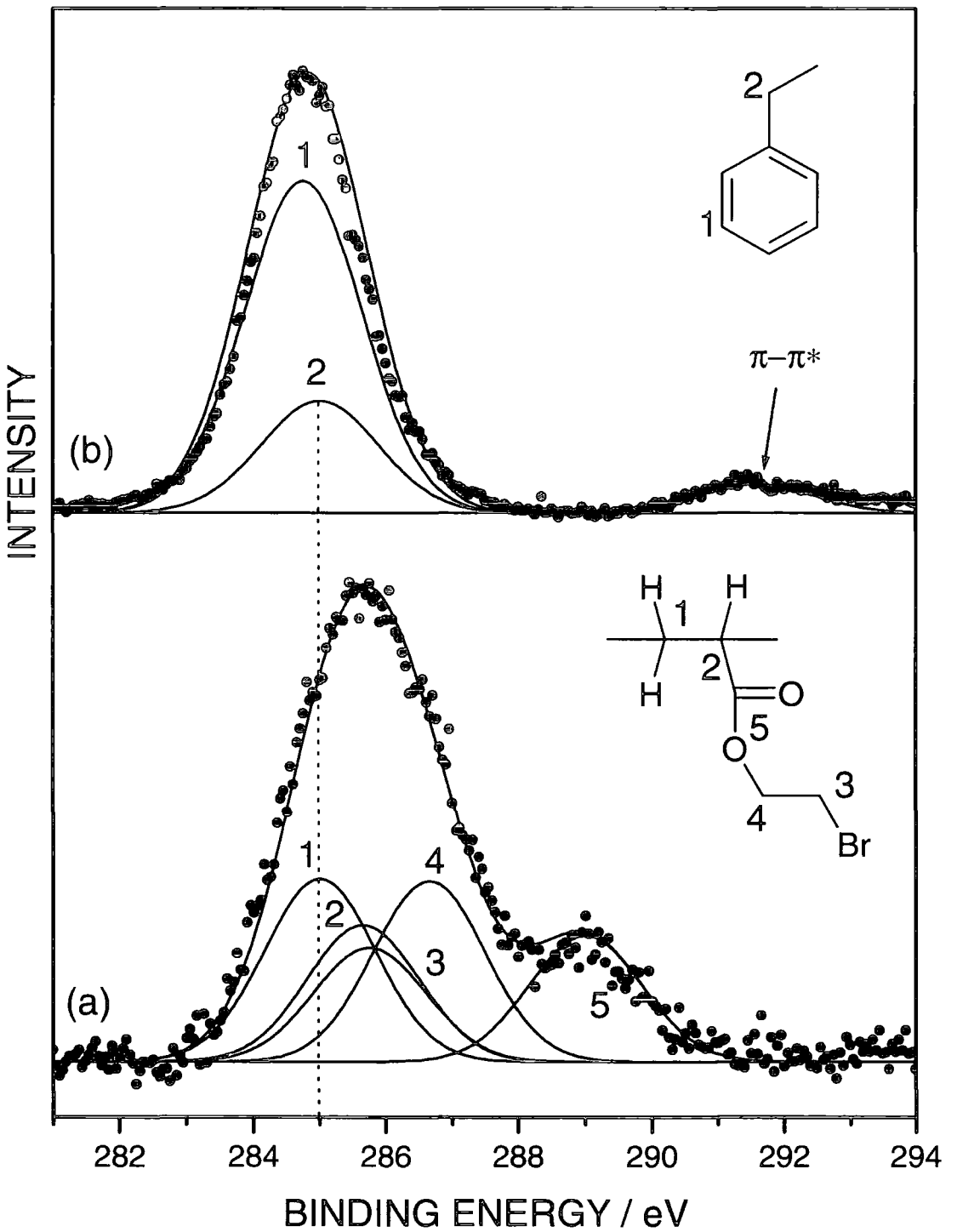

Figure 8.2: XPS C(1s) spectra of: (a) pulsed plasma polymerized 2-bromoethylacrylate, (b) ATRP grafted polystyrene onto a pulsed plasma polymerized 2-bromoethylacrylate layer.

XPS stoichiometric analysis provides additional evidence for the ATRP growth of polymethylmethacrylate, polystyrene and poly(glycidyl methacrylate) on the surface, Table 8.1.

Table 8.1: XPS stoichiometries of pulsed plasma polymerized vinylbenzyl chloride and 2-bromoethylacrylate (Plasma VBC and BEA), ATRP grafted polymethylmethacrylate (PMMA), ATRP grafted polystyrene (PS) and ATRP grafted poly(glycidyl methacrylate) (PGMA).

Substrate		**%C**	**%O**	**%Cl**	**%Br**	**%Si**
Plasma VBC	Theoretical	90	0	10	-	0
	Measured	89 ± 1	0	11 ± 1	-	0
Plasma BEA	Theoretical	63	25	-	12	0
	Measured	65	24	-	11	0
ATRP PMMA	Theoretical	72	28	Trace	-	0
	Measured	75 ± 2	25 ± 2	<0.1	-	0
ATRP PS	Theoretical	100	0	-	Trace	0
	Measured	100	0	-	<0.1	0
ATRP PGMA	Theoretical	70	30	Trace	-	0
	Measured	68	32	<0.1	-	0

8.4.2 Analysis with Fourier Transform Infrared Spectroscopy

Fourier transform infrared spectra of the pulsed plasma polymerized vinylbenzyl chloride layer displays a loss of the vinyl carbon-carbon double bond stretch at 1630 cm^{-1} (B), Table 8.2 and Figure 8.3. Whilst the para-substituted benzene ring stretches at 1603 cm^{-1} (C) and 1495 cm^{-1} (D) remain intact. These observations are demonstrative of conventional polymerization reaction pathways proceeding during the plasma duty cycle off-period. The marked similarity between the infrared spectra of commercially available polymethylmethacrylate (Aldrich, 1 x 10^6 MW) and ATRP grafted polymethylmethacrylate onto plasma polymerized vinylbenzyl chloride surfaces confirms that ATRP has taken place (e.g. the C=O ester stretch at 1730 cm^{-1} (A) is a signature peak of polymethylmethacrylate).

FTIR analysis of ATRP poly(glycidyl methacrylate) details a peak at 1730 cm^{-1} (A) representative of the carbonyl group and peaks at 908 cm^{-1} (I) and 840 cm^{-1} (J) corroborating structural retention of epoxide groups, Figure 8.4(e). Absence of a carbon double bond stretch at 1630 cm^{-1} (B) verifies polymerization of glycidyl methacrylate.

The infrared spectrum of 2-bromoethylacrylate monomer, Figure 8.4(a) contains a characteristic carbonyl stretch at 1730 cm^{-1} (A) and a C=C double bond stretch at 1630 cm^{-1} (B), Table 6.2. The carbonyl stretch is still evident following pulsed plasma polymerization of 2-bromoethylacrylate onto a silicon substrate, whilst the alkene stretch (B) can not be detected, thereby authenticating structural retention and polymerization, Figure 8.4(b). ATRP of styrene gives rise to the emergence of aromatic ring stretches at 1603 (C) and 1495 cm^{-1} (D) attributable to polymer chain growth at the surface, Figure 8.4(d), which displays a marked similarity to commercially available polystyrene, Figure 8.4(e).

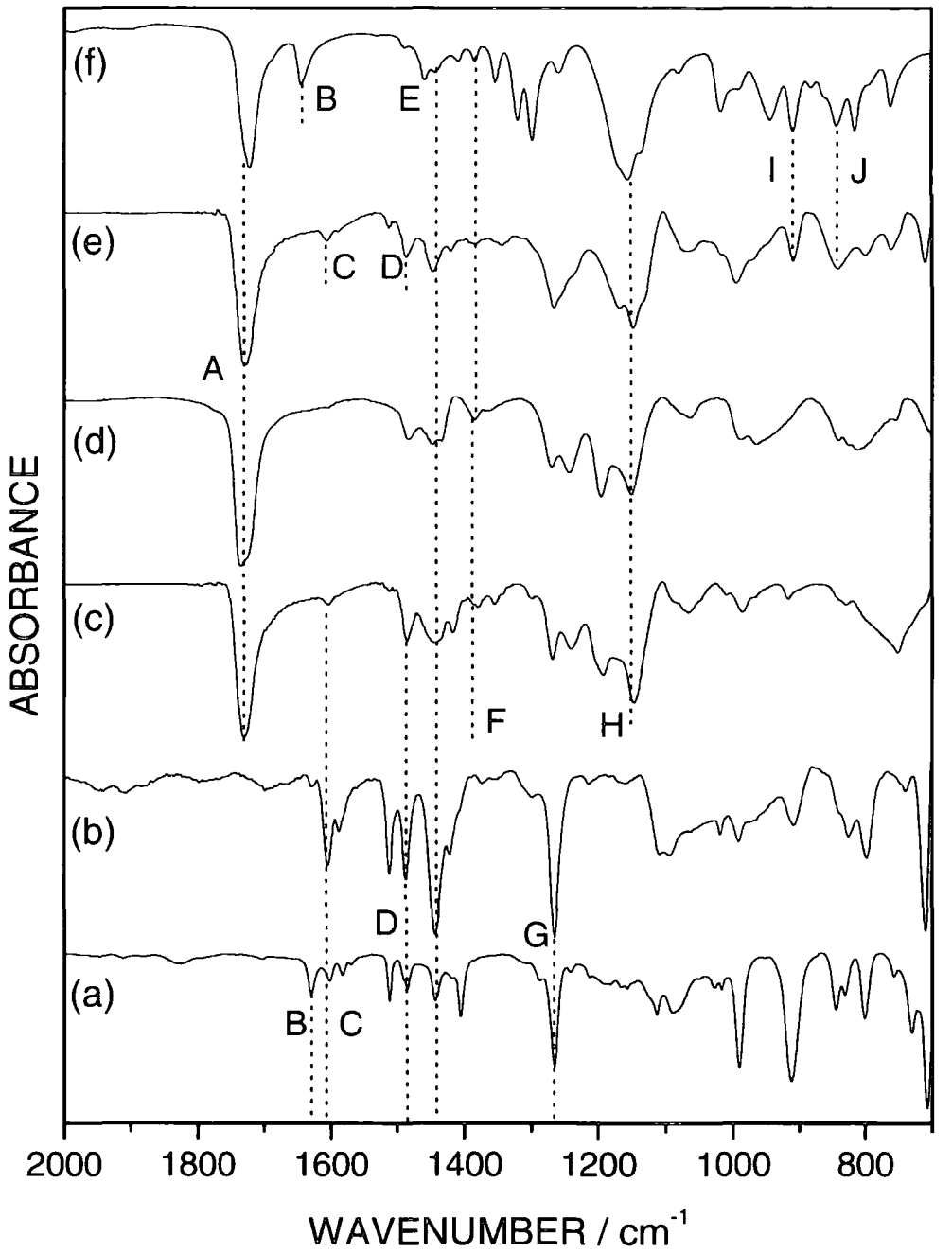

Figure 8.3: FTIR spectra of: (a) 4-vinylbenzyl chloride monomer; (b) pulsed plasma polymerized 4-vinylbenzyl chloride; (c) ATRP grafted polymethylmethacrylate onto pulsed plasma polymerized 4-vinylbenzyl chloride; (d) commercially available polymethylmethacrylate; (e) ATRP grafted poly(glycidyl methacrylate) onto pulsed plasma polymerized 4-vinylbenzyl chloride; and (f) glycidyl methacrylate monomer.

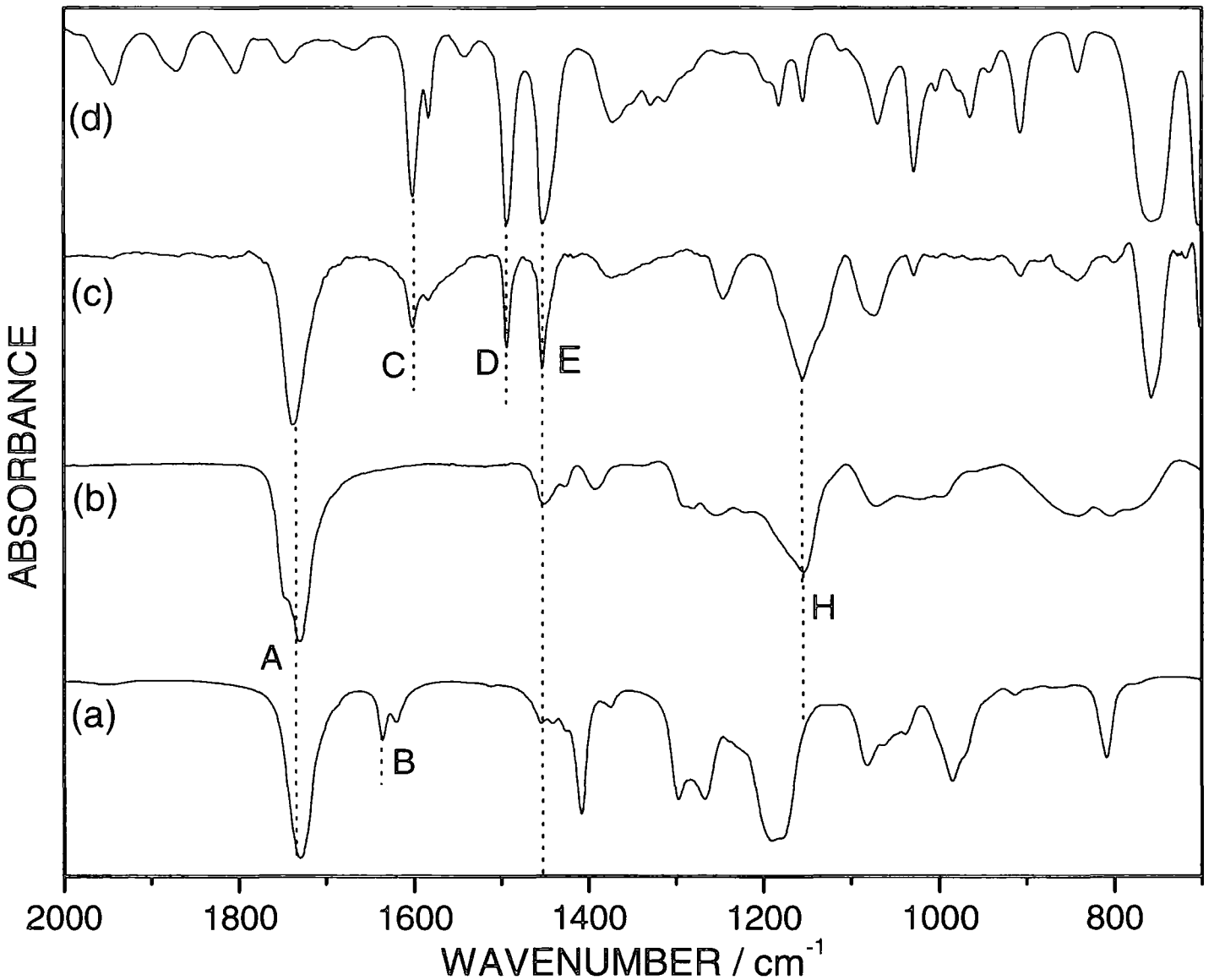

Figure 8.4: FTIR spectra of: (a) 2-bromoethylacrylate monomer; (b) pulsed plasma polymerized 2-bromoethylacrylate; (c) ATRP grafted polystyrene onto pulsed plasma polymerized 2-bromoethylacrylate; and (d) commercially available polystyrene.

Table 8.2: FTIR absorbance assignments for initiator precursors (VBC and BEA), pulsed plasma polymerized initiators (Plasma VBC, BEA), ATRP grafted polymer layers (ATRP PMMA, PS and PGMA), commercially sourced polymethylmethacrylate and polystyrene (sourced PMMA and PS) and glycidyl methacrylate monomer (GMA).

Vibration	**VBC**	**Plasma VBC**	**BEA**	**Plasma BEA**	**VBC-ATRP PMMA**	**Sourced PMMA**	**BEA-ATRP PS**	**Sourced PS**	**VBC-ATRP PGMA**	**GMA**
A: C=O stretch, 1730 cm^{-1}			*	*	*	*	*		*	*
B: C=C stretch, 1630 cm^{-1}	*		*							*
C: Aromatic ring stretch, 1603 cm^{-1}	*	*			*		*	*	*	
D: Aromatic ring stretch, 1490 cm^{-1}	*	*			*		*	*	*	
E: CH_2 symmetric stretch 1445 cm^{-1}	*	*	*	*	*	*	*	*	*	*
F: C-H (in CH_3 group) stretch, 1387 cm^{-1}					*	*			*	*
G: CH_2 wag (CH_2Cl), 1266 cm^{-1}	*	*								
H: C-O-C stretch, 1140 cm^{-1}			*	*	*	*	*		*	*
I: Epoxide antisymmetric stretch, 908 cm^{-1}									*	*
J: Epoxide symmetric stretch, 840 cm^{-1}									*	*

A control experiment employing a layer of pulsed plasma polymerized styrene was not found to undergo ATRP of methylmethacrylate, thereby highlighting the necessity of the halogen group for the initiator species as depicted in Scheme 8.1.

8.4.3 Analysis with Scanning Electron Microscopy

Cross-section analysis by scanning electron microscopy (SEM) of ATRP grafted polymethylmethacrylate onto plasma polymerized 4-vinylbenzyl chloride clearly shows the respective layers, Figure 8.5. In this case, the 700 nm thickness measured by SEM for the plasma polymer layer is consistent with the 650 nm value obtained by the reflectometry technique prior to the ATRP grafting of polymethylmethacrylate.

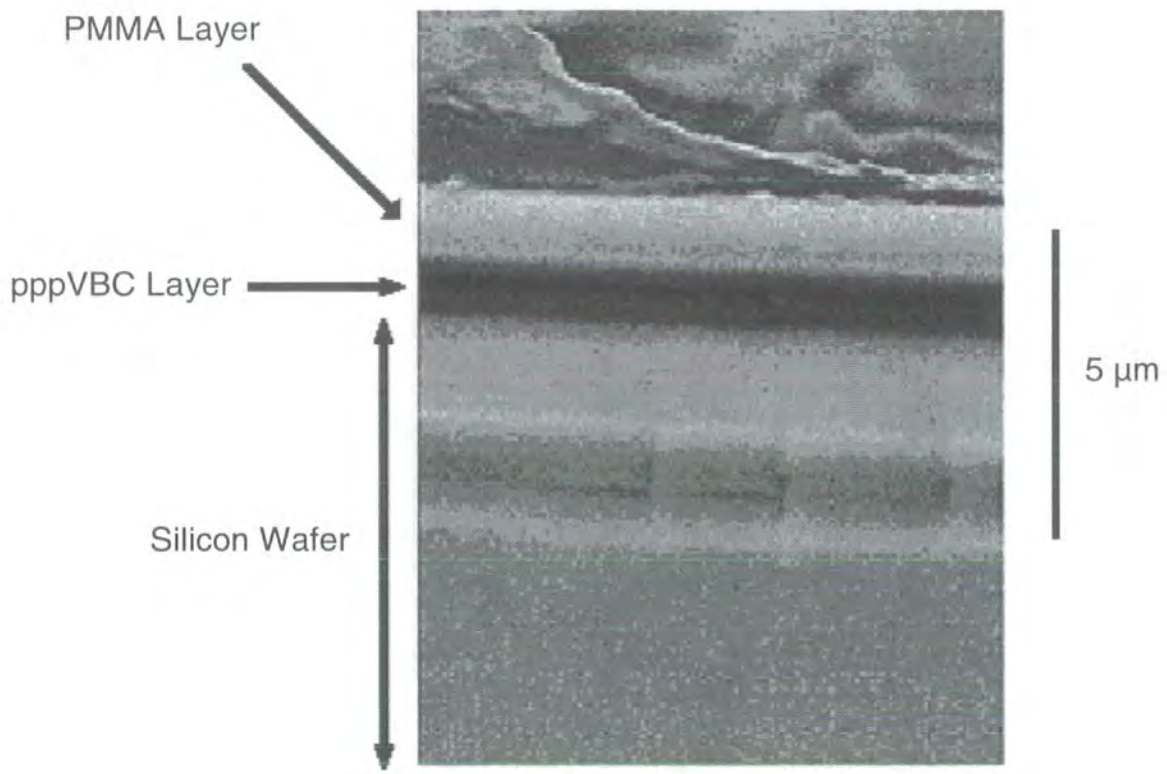

Figure 8.5: SEM micrograph of cross-section showing underlying silicon wafer, pulsed plasma polymerized vinylbenzyl chloride (pppVBC, 700 nm), and ATRP grafted polymethylmethacrylate layer (PMMA, 1.2 µm) (ATRP reaction time = 40 hours).

Similarly, SEM images of vinylbenzyl chloride pulsed plasma polymer coated 80 μm polystyrene microspheres which had then been subjected to ATRP clearly show the grafted polymethylmethacrylate layer, Figure 8.6.

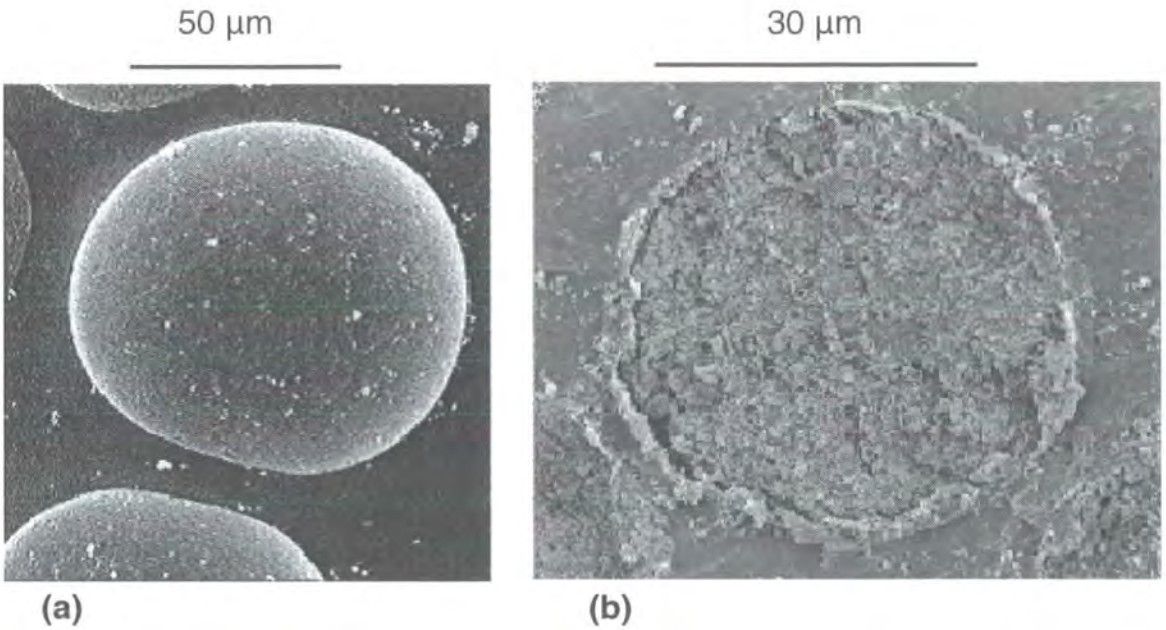

Figure 8.6: SEM cross-section of: (a) uncoated 80 μm polystyrene microsphere and (b) polystyrene microsphere coated with 200 nm pulsed plasma polymerized 4-vinylbenzyl chloride followed by ATRP grafting of polymethylmethacrylate (1.2 μm thickness). The size of the cross-section depends upon the depth at which the polymer bed has been sliced.

8.4.4 Living Radical Polymerization

In order to demonstrate the "living" nature of ATRP grafted polymethylmethacrylate films, reflectometry thickness measurements were undertaken on 150 nm thick vinylbenzyl chloride pulsed plasma polymer films as a function of different ATRP time intervals, Figure 8.7. The grafted polymethylmethacrylate layer thickness (hence the polymer's molecular weight) is found to increase linearly in proportion to reaction time, thereby proving that the ATRP process is living. Polymerization is found to occur only at the surface; polymerization in solution is not observed.

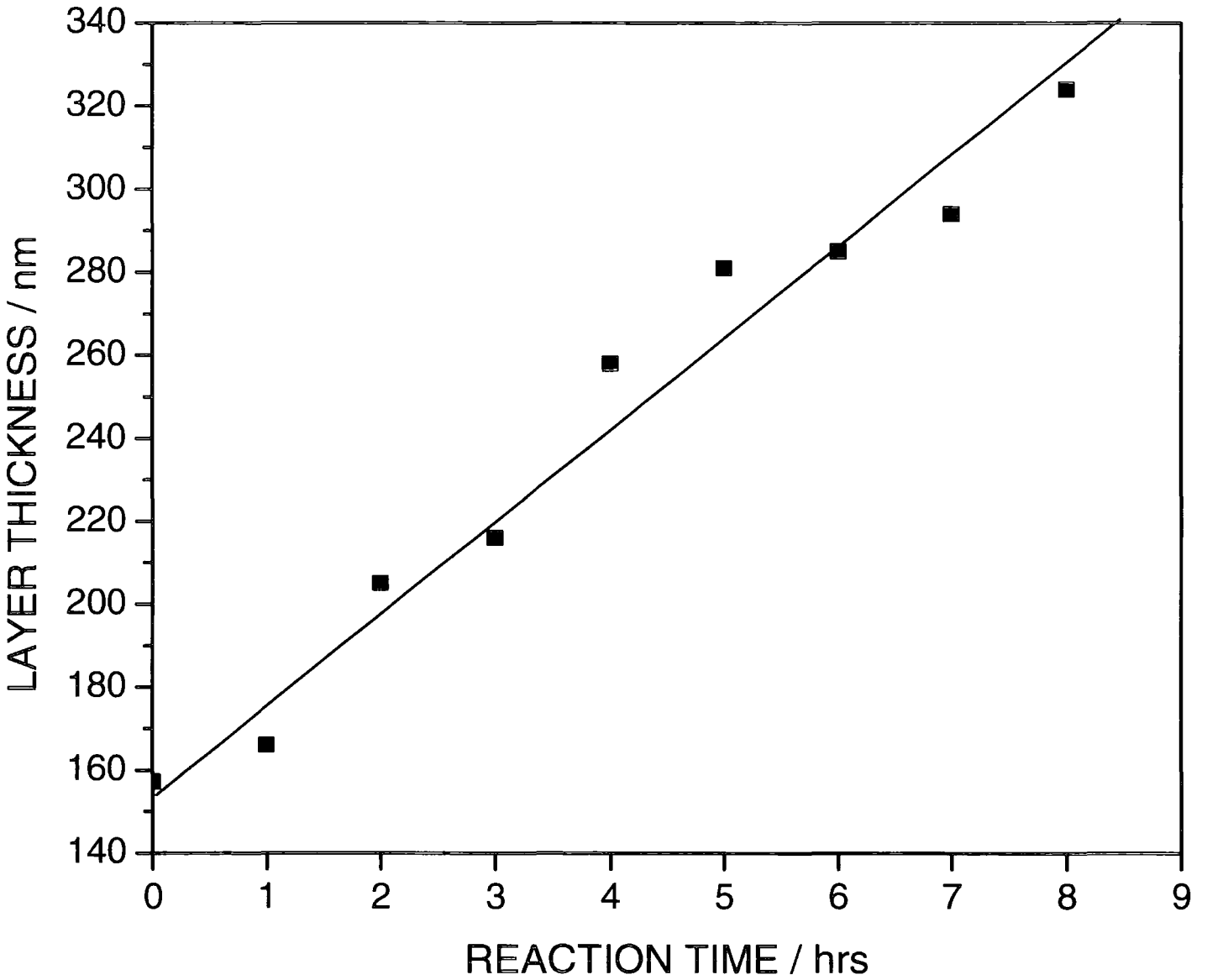

Figure 8.7: Variation of ATRP grafted polymethylmethacrylate layer thickness grown off 150 nm pulsed plasma polymerized 4-vinylbenzyl chloride versus ATRP reaction time.

8.4.5 ATRP Microarray

A pulsed plasma polymerized 4-vinylbenzyl chloride initiator microarray (squares of 7.5 μm width separated by 5 μm gaps) was deposited onto a PTFE substrate through an embossed metal grid. ATRP grafting of poly(glycidyl methacrylate) followed by reaction with aqueous cresyl violet perchlorate fluorescent dye solution confirms the wide-scale applicability of this approach. Clearly the pendant epoxide groups contained in the poly(glycidyl methacrylate) brushes are potentially suitable for a host of different derivatization chemistries.

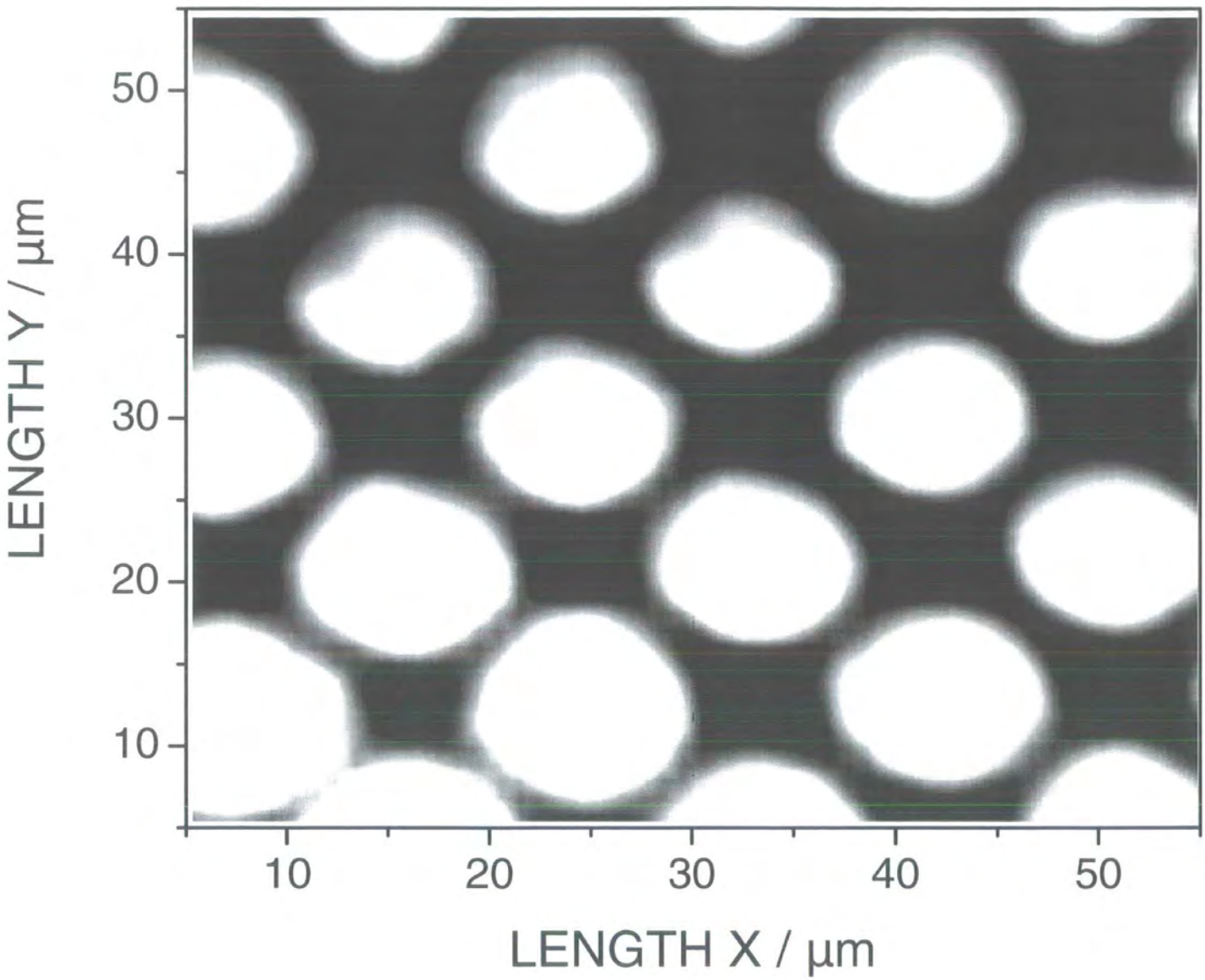

Figure 8.8: Fluorescence micrograph of 7.5 µm pixels of ATRP grafted poly(glycidyl methacrylate) onto pulsed plasma polymerized 4-vinylbenzyl chloride and then tagged using fluorescent cresyl violet perchlorate.

8.4.6 Formation of a Block Copolymer

One notable advantage of this methodology is that the addition of Cu(II) complex or sacrificial initiator is not required to attain linear, controlled growth of polymer chains for growth of an initial polymer layer onto plasma polymer surfaces. This can be attributable to the relatively high concentration of surface-bound initiating groups within the plasma polymer coating in comparison to previously employed self-assembled monolayers. However attempts to grow a second polymer layer of poly(glycidyl methacrylate) without additional deactivating species or sacrificial initiator exhibits an insufficient level of control on polymer chain growth, which can be ascribed to a now relatively low density of initiator groups situated on the chain ends of the pre-grafted ATRP polystyrene layer.

The addition of copper (II) bromide to the polymerization mixture prior to reaction commencement helps to ensure a sufficient retention of end group functionalities to initiate the second block copolymer[49]. It is also found to yield controlled linear growth of the second polymer layer with respect to reaction time, which could not be achieved in previous attempts, Figure 8.9. An excess of deactivating groups results in substantial suppression of chain termination and transfer, allowing polymer chains to grow at the same rate, yielding a high degree of control of molecular weight.

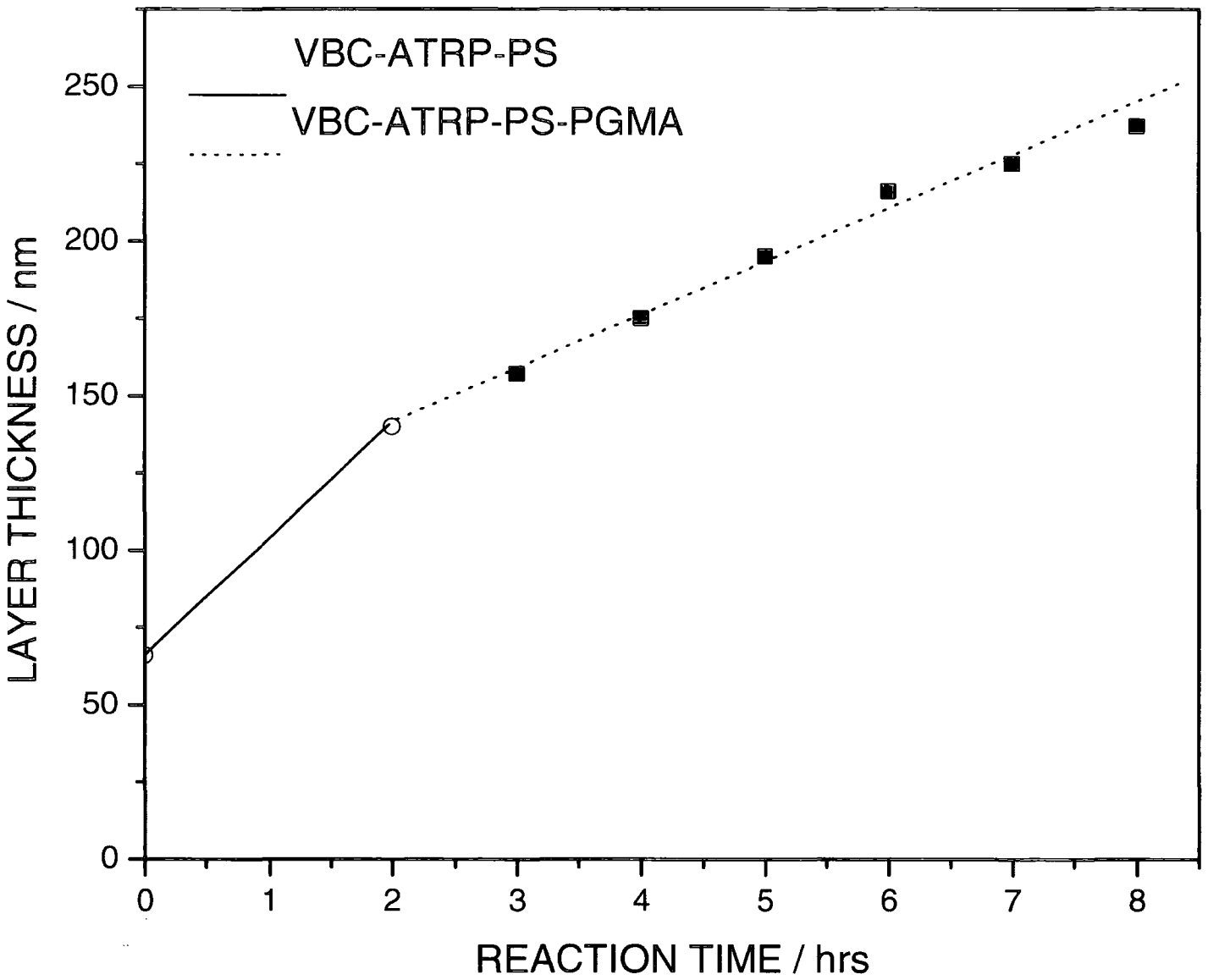

Figure 8.9: Variation of ATRP grafted polystyrene-poly(glycidyl methylmethacrylate) block copolymer layer thickness grown off 150 nm film of pulsed plasma polymerized 4-vinylbenzyl chloride versus ATRP reaction time.

The results obtained in this work have shown that ATRP grafting of polymer brushes in the aforementioned manner could quite easily be adapted for many applications, including novel adhesives, gas separation membranes [50], fillers [51], the immobilisation of biological molecules, biocompatible surfaces [52], and hybrid nanomaterials (e.g. coated magnetic nanoparticles[53]).

8.5 Conclusions

The synthesis of polymer brushes onto a range of different substrates and geometries has been demonstrated for the first time by the deployment of pulsed plasmachemical methods. This entails plasmachemical functionalization of solid surfaces with halogen containing initiator moieties followed by conventional ATRP growth of polymer brushes from these sites.

The versatility of this technique has been exemplified by the production of polymer-coated beads, derivatized polymer microarrays and block copolymers. The controlled, linear growth of an initial polymer layer has been made possible without the addition of sacrificial initiator or the $Cu(II)Br_2$ catalyst. These facets along with the minimisation of the number of reaction step required to generate a layer of initiator, demonstrate the clear advantages of this method over currently utilised approaches of surface-initiated living radical polymerization.

8.6 References

[1] Wang, J. S.; Matyjaszewski, K., *J. Am. Chem. Soc.*, 117, **1995**, 5614.

[2] Wang, J. S.; Matyjaszewski, K., *Macromolecules,* 28, **1995**, 7901

[3] Matyjaszewski, K. *Chem. Eur. J.*, 5, **1999**, 3095.

[4] Huang, X.; Doneski, L. J.; Wirth, M.J., *Chemtech*, 28, **1998**, 19.

[5] Sonmez, H. B.; Senkal, B. F.; Sherrington, D. C.; Bicak, N., *React. Funct. Polym.*, 55, **2003**, 1.

[6] Kotani, Y.; Kamigaito, M.; Sawamoto, M., *Macromolecules,* 32, **1999**, 2420.

[7] Kato, M..; Kamigaito, M.; Sawamoto, M.; Higashimura, T., *Macromolecules,* 28, **1995**, 1721.

[8] Matyjaszewski, K.; Wang, J.-L.; Grimaud, T.; Shipp, D. A., *Macromolecules*, 31, **1998**, 1527.

[9] Ando, T.; Kamigaito, M.; Sawamoto, M. *Tetrahedron*, 53, **1997**, 15445.

[10] Granel, C.; Dubois, P.; Minet, M.; Teyssie, P. ; Senninger, T.; Jerome, R., *Macromolecules,* 29, **1996**, 27.

[11] Matyjaszewski, K.; Jo, S. M.; Paik, H.-j.; Gaynor, S. G. *Macromolecules*, 30, **1997**, 6398.

[12] Percec, V.; Kim, H. J.; Barboiu, B. *Macromolecules*, 30, **1997**, 8526.

[13] Brandts, J.A.M.; van de Geijn, P.; van Fassen, E. E.; Boersma, J.; van Koten, G. *J. Organomet. Chem.*, 584, **1999**, 246.

[14] Ando, T.; Kamigaito, M.; Sawamoto, M. *Macromolecules,* 30, **1997**, 4507.

[15] Moineau, G.; Granel, C.; Dubois, P.; Minet, M.; Jerome, R.; Teyssie, P. *Macromolecules,* 31, **1998**, 542.

[16] Uegaki, H.; Kotani, Y.; Kamigaito, M.; Sawamoto, M. *Macromolecules,* 30, **1997**, 2249.

[17] Patten, T. E.; Matyjaszewski, K. *Adv. Mater.* 10, **1998**, 901.

[18] Patten, T. E.; Matyjaszewski, K. *Acc. Chem. Res.* 32, **1999**, 895.

[19] Jones, D. M.; Huck, W. T. S., *Adv. Mater.*, 13, **2001**, 1256.

[20] Wang, X. S.; Armes, S. P., *Macromolecules*, 33, **2000**, 6640.

[21] Wang, X. S.; Lascelles, R. A.; Jackson, R. A.; Armes, S. P., *Chem. Commun.*, 18, **1999**, 1817

[22] Matyjaszewski, K.; Patten, T. E.; Xia, J. *J. Am. Chem. Soc.*, 119, **1997**, 674.

[23] Matyjaszewski, K.; Davis, K.; Patten, T.E.; Wei, M. *Tetrahedron*, 53, **1997**, 15321.

[24] Kim, J. B.; Bruening, M. L.; Baker, G. L. *J. Am. Chem. Soc.*, 122, **2000**, 7616.

[25] Huang, W; Kim, J.B.; Bruening, M.L.; Baker, G.L. *Macromolecules*, 35, **2002**, 1175.

[26] Huang, W; Baker, G.L; Bruening, M.L. *Angew. Chem. Int. Ed.*, 40, **2001**, 1510.

[27] Shah, R.R.; Merreceyes, D.; Husemann, M.; Rees, I.; Abbott, N.L.; Hawker, C.J.; Hedrick, J.L. *Macromolecules*, 33, **2000**, 597.

[28] Hikita, M.; Tanaka, K.; Nakamura, T.; Kajiyama, T.; Takahara, A., *Langmuir,* 20, **2004**, 5304.

[29] Kim, J. B.; Bruening, M. L.; Baker, G. L., *Polym. Mater. Sci. Eng.,* 85, **2001**, 310.

[30] Jones, D. M.; Brown, A. A.; Huck, W. T. S.; *Langmuir*, 18, **2002**, 1265.

[31] Huang, X.; Wirth, M. J. *Macromolecules,* 32, **1999**, 1694.

[32] Edmondson, S.; Huck, W. T. S., *J. Mater. Chem.,* 14, **2004**, 730.

[33] Marutani, E.; Yamamoto, S.; Ninjbadgar, T.; Tsujii, Y.; Fukuda, T.; Takano, M., *Polymer,* 45, **2004**, 2231.

[34] Xiao, D.; Zhang, H.; Wirth, M. J., *Langmuir,* 18, **2002**, 9971.

[35] Miller, P. J.; Matyjaszewski, K., *Macromolecules*, 32, **1999**, 8760.

[36] Angot, S.; Ayres, N.; Bon, S. A. F.; Haddleton D. M., *Macromolecules*, 34, **2001**, 768.

[37] Guerrini, M. M.; Chateaux, B.; Vairn, J. P., *Macromol. Rapid Commun.*, 21, **2000**, 669.

[38] Desai, S. M.; Solanky, S. S.; Mandale, A. B.; Rathore, K.; Singh, R. P., *Polymer*, 44, **2003**, 7645.

[39] Claes, M.; Voccia, S.; Detrembleur, C.; Jerome, C.; Gilbert, B.; Leclere, P.; Geskin, V. M.; Gouttebaron, R.; Hecq, M.; Lazzaroni, R.; Jerome, R., *Macromolecules*, 36, **2003**, 5926.

[40] Kong, H.; Gao, C.; Yan, D., *J. Mater. Chem.*, 14, **2004**, 1401.

[41] Qin, S.; Qin, D.; Ford, W. T.; Resasco, D. E. ; Herrera, J. E., *J. Am. Chem. Soc.*, 126, **2004**, 170.

[42] Carlmark, A.; Malmstrom, E., *J Am. Chem. Soc.*, 124, **2002**, 900.

[43] Matyjaszewski, K.; Xia, J., *Chem. Rev.,* 101, **2001**, 2921.

[44] Matyjaszewski, K.; Miller, P. J.; Shukla, N.; Immaraporn, B.; Gelman, A.; Luokala, B. B.; Siclovan, T. M.; Kickelbick, G.; Vallant, T.; Hoffman, H.; Pakula, T., *Macromolecules,* 32, **1999**, 8716

[45] Ejaz, M.; Yamamoto, S.; Ohno, K., Tsujii, Y.; Fukuda, T., *Macromolecules*, 31, **1998**, 5934

[46] Lintz, H. K.; Murell, S. R.; Crawley, R. L.; Daukas, J. C., *J. Vac. Sci. Technol. A.*, 6, **1988**, 1869.

[47] McMurry, J., *Organic Chemistry 3rd Ed,* Wadsworth, California, **1992** , 680.

[48] Beamson, G.; Briggs, D; *High Resolution XPS of Organic Polymers*, Wiley, New York, **1992**.

[49] Kim, J.B.; Huang, W.; Bruening, M.L.; Baker, G.L. *Macromolecules*, 35, **2002**, 5410.

[50] Balachandra, A. M.; Baker, G. L.; Bruening, M. L., *J. Membrane Sci.,* 227, **2003**, 1.

[51] Liu, T.; Jia, S.; Kowalewski, T; Matyjaszewski, K.; Casado, P.; Belmont, J., *Langmuir* 19, **2003**, 6342.

[52] Huang, X.; Doneski, L. J.; Wirth, M. J., *Anal. Chem.*, 70, **1998**, 4023.

[53] Vestal, C.R.; Zhang, Z. J., *J. Am. Chem. Soc.*, 124, **2002**, 14312.

Chapter 9: General Conclusions

It has been shown in this work that a wide range of precursors can be successfully deposited onto a variety of substrates by pulsed plasma polymerization. These films can be further manipulated to fit an extensive range of desired applications, demonstrating the versatility of this technique in the treatment of surfaces.

Chapter three details a one-step, substrate independent route to a thermally responsive n-isopropylacrylamide coating. It also exemplifies that by varying pulse parameters and peak power of the plasma; it is possible to successfully deposit films that exhibit fully-reversible adsorption of proteins with changing temperature; a facet that can not be achieved with previous continuous wave methods. These films show excellent potential for the cell culture and tissue engineering industries due to the simplicity and efficiency of this process.

Chapters four and six outline methods of surface-initiated polymerization from pulsed plasma polymers. Following a pulsed plasma polymerization step, surfaces can be subsequently derivatized by reaction of the films in solution to incorporate a new functionality. In the case of free radical polymerization, a dialkyldiazene can be tailored to pulsed plasma polymerized glycidyl methacrylate, whereas for quasi-living photo-initiated polymerization, an *iniferter* group is attached to pulsed plasma polymerized halogen-containing monomers. Polymer chains of acrylates, acrylamides and styrenes can then be grafted from these treated substrates. These methods have provided a significant improvement to previously methods of surface polymerization due the fact that they are not restricted by substrate chemistries and are achievable in a minimum number of reaction stages.

Halogenated films utilised for photo-initiated polymerization can also be employed without further derivatization as initiators for surface-confined atom transfer radical polymerization. Atom transfer radical polymerization at surfaces is currently an extensively researched field where a variety of substrates and

strategies have been investigated. This method has yielded a surface layer of initiating groups in the just reaction step and the density of initiating groups present has effectively made one of the polymerization components redundant for growth of an initial polymer layer. This approach is not restricted by substrate or geometry and can be successfully deployed to generate microscopic arrays of polymer brushes and block copolymers, which have potential applications as ion exchange resins and gas separation membranes.

Additional uses for pulsed plasma polymers involve the functionalization of amine-containing films with a palladium catalyst, thus making the substrate amenable to electrodeless deposition of transition metals. Arrays of atomic copper and nickel are formed in a greatly reduced number of reaction steps compared to existing methodologies, highlighting the importance of this technique for the electronic circuit industry.

Lastly pulsed plasma polymer films of maleic anhydride can be derivatized with protein resistant groups such as acylated polyethylenimine providing a surface that prevents contamination from bacteria and cells because of its inherent non-fouling properties. This method was found to be most effective for the repulsion of larger biological species and is far more economical than previously-described self-assembled monolayer techniques, which incorporated gold substrates.

In most instances, experiments carried out during the course of this work have shown a marked improvement on existing methods of surface modification. For example many methodologies are restricted by substrate-specific chemistries such as the "thiols linked to gold" route and this has been overcome. Additionally, techniques developed in this research have significantly reduced the number of reaction steps and the amounts of reagents required to attain the desired result. The versatility of plasma deposition for a range of applications has been successfully demonstrated by this work.

9.1 Further Work

Recommendations for improvements and modifications for this work would include the following:

- Further demonstration of the suitability of ppNIPAAm films for tissue growth by the culturing of cells onto treated surfaces such as ppNIPAAm-coated Petri dishes.
- Enhanced control and understanding over the kinetics of the metal deposition process, leading to the ability to produce smaller arrays of metal i.e. below 500 μm.
- The acquisition of an nPEG molecule with only 4-5 repeat units, followed by attachment to pulsed plasma deposited poly(maleic anhydride) surfaces. This should result in few gaps between the polymer chains and hence a greater tendency to repel smaller protein molecules such as lysozyme.
- The acquisition and successful pulsed plasma polymerization of protein resistant monomers such as (polyethyleneglycol)methacrylate. Hence bio-inert surfaces could be achievable in one reaction stage.
- Providing a copper mesh with apertures smaller than 7.5 μm can be obtained, smaller arrays of polymer brushes could be generated by surface-initiated atom transfer radical polymer from plasmachemically-deposited initiating groups.